Spatial and Temporal Changes in Marine-terminating Glaciers on the Antarctic Peninsula since the 1940s

Alison Joan Cook

Submitted in fulfilment of the requirements for the Degree of Doctor of Philosophy

College of Science

Swansea University

November 2014

The candidate confirms that the work submitted is her own and that appropriate credit has been given where reference has been made to the work of others.

This copy has been supplied on the understanding that it is copyright material and that no quotation from the thesis may be published without proper acknowledgement.

DECLARATION

This work has not previously been accepted in substance for any degree and is not being concurrently submitted in candidature for any degree.

Signed ..... (candidate)

Date .....

STATEMENT 1

This thesis is the result of my own investigations, except where otherwise stated. Where correction services have been used, the extent and nature of the correction is clearly marked in a footnote(s).

Other sources are acknowledged by footnotes giving explicit references. A bibliography is appended.

Signed ..... (candidate)

Date .....

STATEMENT 2

I hereby give consent for my thesis, if accepted, to be available for photocopying and for inter-library loan, and for the title and summary to be made available to outside organisations.

Signed ..... (candidate)

Date .....

Abstract

The numerous glaciers on the Antarctic Peninsula are highly sensitive to environmental changes, with potential to make a significant contribution to sea-level rise, and yet they have been distinctly under studied. An absence of fundamental details on glacier characteristics and behaviour is due in part to the inaccessibility of the region. In this research, the production of a new topographic model and an inventory of 1590 glacier drainage basins between 63-70° S have enabled detailed analysis of these glaciers for the first time.

Area change measurements since the 1940s reveal that 90% of the 860 marine-terminating glaciers have retreated. Greatest glacier area loss has occurred in the north-east, primarily due to the demise of ice shelves. In the west, an increasing gradient of overall ice loss from north to south is observed, as well as a distinct region in the north-west where glaciers have remained stable. There are also clear trends over time, such as reduction in glacier retreat rates in the late 1980s, and acceleration in retreat since the late 1990s. These statistically significant trends indicate that there are external control factors currently outweighing local glaciological controls on glacier extent.

Analysis of atmospheric and ocean temperature data reveals that, to the west of the peninsula, patterns in ocean temperatures have a strong synchroneity with glacier area change. An increasing ocean temperature gradient from north to south, which strengthens with depth, is closely correlated with glacier front changes. Furthermore, a warming at mid ocean depths has occurred since the 1990s. This research suggests that although the atmosphere is rapidly warming, melt by the ocean is the primary cause of glacier retreat along the western peninsula. With persistent warm ocean temperatures, glacier retreat and associated mass loss is set to continue, leading to an increasing contribution to sea-level rise.

Acknowledgements

This project was funded by the AXA Research Fund. The AXA global financial protection group is interested in supporting risk-related climate research and I'm very grateful to them for the award that facilitated this research.

My supervisors Professor Tavi Murray and Professor Adrian Luckman within the Glaciology Group at Swansea University, and Professor David Vaughan at the British Antarctic Survey (BAS), have given me support throughout the project and I'd like to thank them very much for their valuable expertise and helpful advice.

I'm also extremely grateful to a number of scientists who were happy to contribute their data to this research. In particular, I'd like to thank Dr Paul Holland (BAS) for providing the ocean temperature data and for discussion of ideas. Thanks to Dr Nick Barrand (previously at BAS, now at Birmingham University) for providing temperature records and melt duration data, as well as DEMs for accuracy tests. Thanks to Dr J. Comiso (Cryospheric Sciences Laboratory, NASA) for providing his surface temperature gridded data and Dr J. Lenaerts (Institute for Marine and Atmospheric research, Utrecht University) for his modelled surface mass balance data. Credit is given to them where appropriate within the thesis. I'm also grateful to the USGS and BAS for permission to use the data that I produced during my involvement with the *Coastal-Change and Glaciological Maps of Antarctica* programme prior to the PhD.

I have had two fantastic work experience assistants who helped out with the some of the more laborious tasks in this project. Anna Weissenmayer spent 2 weeks in July 2011 digitising glacier fronts from recent satellite imagery, and Anneka France worked for 6 weeks in July/Aug 2012 editing the GIS database. I've also had invaluable emergency help with IT related issues from Steve Shaw.

Finally, I'd like to say thanks to the Swansea Glaciology Group as well as friends and colleagues at BAS for support and helpful discussions, and to friends and family who have spurred me on throughout the past four years!

Contents

Abstract ..... *v*

Acknowledgements ..... *vii*

Contents ..... *ix*

Tables ..... *xv*

Figures ..... *xvii*

Abbreviations ..... *xxi*

CHAPTER 1
INTRODUCTION AND AIMS

1.1 Motivation 1

1.2 Aims 3

1.3 Thesis structure 4

1.4 Published material 5

CHAPTER 2
THE ANTARCTIC PENINSULA ICE SHEET AND CLIMATE CHANGE

2.1 Introduction 7

2.2 Glaciology of the Antarctic Peninsula 8

2.2.1 History of the AP Cryosphere 10

2.2.1.1 The Last Glacial Maximum 10

2.2.1.2 The Cryosphere since the early Holocene 11

2.2.2 Mass balance of the APIS 15

2.2.2.1 Mass estimates 15

2.2.2.2 Sea-level rise 16

2.2.2.3 Surface mass balance 16

2.2.3 Ice Shelves and Glaciers on the AP 18

2.2.3.1 Ice shelves 18

2.2.3.2 Glaciers 24

2.3 Recent changes in the climate and ocean around the AP 32

2.3.1 Climate 32

2.3.1.1 Air Temperature 33

2.3.1.2 Surface melt 35

2.3.1.3 Sea-ice 37
2.3.1.4 Precipitation 38
2.3.2 Ocean 40
2.3.2.1 West Antarctic Peninsula 41
2.3.2.2 Weddell Sea Sector 44
2.3.3 Ocean-Atmosphere Interactions 45
2.4 Global glacier monitoring and applications to the AP 47
2.4.1 Mass balance monitoring 48
2.4.2 Glacier-length monitoring 49
2.5 Summary 51

CHAPTER 3
A NEW DIGITAL ELEVATION MODEL FOR ANTARCTIC PENINSULA GLACIOLOGY
3.1 Introduction 55
3.2 Digital Elevation Models for glaciological applications 56
3.3 High resolution gridded elevation datasets for the Antarctic Peninsula 59
3.4 ASTER GDEM: limitations and potential for use in the AP 62
3.5 DEM correction methodology 65
3.5.1 An alternative approach to ASTER GDEM correction 65
3.5.2 ASTER GDEM improvement procedure 67
3.6 Error analysis 71
3.6.1 Vertical accuracy 72
3.6.1.1 Absolute vertical accuracy 72
3.6.1.2 Vertical accuracy for corrected vs. uncorrected regions 76
3.6.1.3 Vertical accuracy according to slope 77
3.6.2 Horizontal accuracy 79
3.6.2.1 Horizontal accuracy based on GPS points and a photogrammetric DEM 80
3.6.2.2 Relative accuracy and consistency tests using SPIRIT DEMs 81
3.6.2.3 Horizontal differences from the Landsat Image Mosaic of Antarctica 83
3.6.3 Methodology errors 84
3.7 Summary 85

CHAPTER 4
GLACIER BASINS AND AREA CHANGE: DATA ACQUISITION AND ANALYSIS METHODS

4.1 Introduction 87
4.2 Glacier outlines 88
4.2.1 Current glacier inventory compilation methods 88
4.2.2 Glacier inventory challenges in the AP 89
4.2.3 Glacier basin delineation methodology 91
4.2.3.1 Principles of basin delineation 91
4.2.3.2 Coastline digitisation 93
4.2.3.3 Coastline sector criteria 94
4.2.3.4 Watershed delineation 95
4.3 Glacier attribution 98
4.3.1 Nominal glacier characteristics 98
4.3.2 Geometric and topographic characteristics 99
4.4 Glacier-change data 101
4.4.1 Glacier-change studies 102
4.4.2 Glacier-change data in the AP 103
4.4.3 AP Coastal-Change dataset revision 103
4.4.3.1 Georegistering the coastal-change dataset 104
4.4.3.2 Updating ice fronts post-2002 105
4.4.3.3 Joining ice fronts to glacier basins 106
4.4.3.4 Separation of dates into temporal intervals 107
4.4.3.5 ‘Multiple’ glacier basins and floating ice 108
4.5 Glacier-change analysis methods 113
4.5.1 Long-term glacier-change analysis methods in Greenland: case studies 114
4.5.1.1 Small sample, multiple observation periods 114
4.5.1.2 Large sample, minimal observation periods 115
4.5.1.3 Large sample, concurrent observation years 116
4.5.1.4 Large sample, multiple observation periods 117
4.5.2 AP glacier-change analysis: new methodologies 117
4.5.2.1 AP glacier-change analysis challenges 117
4.5.2.2 Absolute and relative area change calculations 120
4.5.2.3 Rates of change calculations 121

4.5.2.4 Area-change over length-change calculations 122
4.6 Further considerations 124
4.6.1 Uncertainty estimates 124
4.6.2 Annual glacier cycles 127
4.7 Summary 130

CHAPTER 5
GLACIER AREA CHANGES ON THE ANTARCTIC PENINSULA SINCE THE 1940S
5.1 Introduction 133
5.2 Glacier distribution and characteristics 133
5.2.1 All AP glacier basins 133
5.2.2 Marine-terminating glacier basins 142
5.3 Glacier changes 148
5.3.1 Overall change since earliest records 148
5.3.1.1 Overall absolute and relative change: correlations with glacier variables 150
5.3.1.2 Spatial distribution of overall change 152
5.3.2 Temporal patterns of change 155
5.3.2.1 Area differences relative to 2000-04 155
5.3.2.2 Rates of change 159
5.3.2.3 Significance of temporal trends 162
5.3.3 Spatial patterns of change 165
5.3.4 Correspondence with previous AP glacier-change study results 166
5.3.5 Spatial and temporal patterns: regional summary 168
5.4 Behavioural comparisons between glacier-types 171
5.5 Summary 175

CHAPTER 6
EXTERNAL CONTROLS ON GLACIER CHANGE ON THE ANTARCTIC PENINSULA
6.1 Introduction 179
6.1.1 Regional patterns of glacier change 179
6.1.2 Regional drivers of change 180
6.2 Atmospheric patterns 180
6.2.1 Station and AWS temperature records 181
6.2.2 Spatial patterns of melt 2000-09 185
6.2.3 Surface temperatures from AVHRR imagery, 1980-2008 189

6.2.3.1 Surface temperature data 189
6.2.3.2 Surface temperature spatial patterns 190
6.2.3.3 Surface temperature temporal patterns 193
6.2.4 Surface Mass Balance from modelled data, 1979 – 2010 196
6.2.5 Surface temperature and mass balance patterns 199
6.3 Ocean temperature patterns 200
6.3.1 Ocean temperature data 201
6.3.2 Bathymetry data 202
6.3.2.1 Wide-scale regional bathymetry 202
6.3.2.2 Bathymetry close to the coastline 203
6.3.2.3 Ice thickness at the ocean edge 206
6.3.2.4 Pressure melting point at ice fronts 208
6.3.3 Wide-scale regional ocean temperatures 208
6.3.3.1 Spatial ocean temperature patterns 208
6.3.3.2 Temporal ocean temperature patterns 213
6.3.3.3 Temperature differences between repeat measurements 221
6.3.4 Ocean temperatures close to the coast 223
6.4 Summary 225
6.4.1 Atmospheric patterns 225
6.4.2 Ocean temperature patterns 226
6.4.3 Differences between temperature patterns 227

CHAPTER 7
IDENTIFYING THE PRINCIPAL DRIVER OF GLACIER AREA CHANGES ON THE ANTARCTIC PENINSULA

7.1 Introduction 229
7.2 AP glacier area-change patterns 230
7.3 Local controls on frontal behaviour 232
7.4 Atmospheric controls on glacier area change 233
7.4.1 Spatial patterns 234
7.4.2 Temporal patterns 238
7.5 Ocean temperature controls on glacier area change 241
7.5.1 Wide-scale patterns in ocean temperature 241
7.5.2 Coastal bathymetry and near-shore ocean temperatures 243

7.5.3 Correlations between ocean temperature and overall glacier change 246
7.5.4 Temporal synchroneity of ocean temperature and glacier change rates 251
7.5.4.1 Western AP temporal patterns 251
7.5.4.2 Sample region temporal patterns 256
7.6 Glacier-Ocean interactions in the Antarctic Peninsula 257
7.6.1 Ice-Ocean interactions in West Antarctica 257
7.6.1.1 Amundsen Sea Embayment 257
7.6.1.2 Bellingshausen Sea 259
7.6.2 Ice-ocean interactions along the west Antarctic Peninsula 260
7.6.3 Causes of ocean warming in the west AP 262
7.6.4 Implications of a warming ocean 263
7.7 Summary 266

CHAPTER 8
SUMMARY AND CONCLUSIONS

8.1 Thesis summary 269
8.2 Conclusions 270
8.2.1 The new AP DEM and glacier drainage basins 270
8.2.2 Spatial and temporal patterns of glacier area change 272
8.2.3 Drivers of glacier area change 273
8.3 Suggestions for further work 275
8.3.1 Short-term trends 276
8.3.2 Individual glacier behaviour 276
8.3.3 Additional boundary conditions 277
8.3.4 Modelling future contribution to sea level 278

REFERENCES 279
APPENDIX – CHAPTER 1 297
APPENDIX – CHAPTER 2 299
APPENDIX – CHAPTER 3 303
APPENDIX – CHAPTER 4 307
APPENDIX – CHAPTER 5 319

N.B. Chapter and Section citations throughout the text are in green text to assist with navigation through the document. Similarly, Appendix citations are in purple text.

Tables

Table 2.1: Decadal area changes of ice shelves on the AP. 19

Table 3.1: Summary of dataset acronyms 72
Table 3.2: Mean elevation differences from ICESat across the new DEM. 74
Table 3.3: Comparisons between the new DEM and ASTER GDEM 77
Table 3.4: Mean elevation differences from ICESat in regions with real-surface slope < 30° 79
Table 3.5: New DEM absolute errors in the Ryder Bay region. 81
Table 3.6: New DEM relative errors 83
Table 3.7: New DEM consistency tests. 83
Table 3.8: New DEM horizontal differences from LIMA (in metres). 84

Table 4.1: Nominal categories and classification types. 98
Table 4.2: Ice front record counts per glacier basin 108
Table 4.3: Reliability ratings ice fronts within each 5-year interval. 126
Table 4.4: Intra-annual area change summary 129

Table 5.1: Number and percentages of glaciers in each size class, and sum total area 135
Table 5.2: Total glacier count and area coverage per glacier type 137
Table 5.3: Glacier count and area by degrees latitude. 141
Table 5.4: Correlations between glacier characteristics 145
Table 5.5: Correlations between overall change and selected glacier characteristics. 151
Table 5.6: Paired sample Student's t-test for glacier relative rates of change (% a^{-1}). 163

Table 6.1: Summary of temperature records obtained from Automatic Weather Stations and manned stations 184
Table 6.2: Glaciers with depth measurements available within 5 km, 2 km and 1 km. 205
Table 6.3: Glacier counts and percentages with bathymetric data at a range of depths 206
Table 6.4: Mean ocean temperatures at each depth (m), by east/west AP. 211

Table 6.5: Ocean temperature measurement counts. 214
Table 6.6: Ocean temperature trends for deep (>= 150 m) and shallow (< 150 m) waters. 216
Table 6.7: Ocean temperature data counts, by region, depth (in metres) and decade. 219
Table 6.8: Ocean temperature trends at each depth (m), by Region. 220
Table 6.9: Ocean temperature differences between 1990s-2000s, by depth (m). 222
Table 6.10: Glaciers with ocean temperature and bathymetry measurements within 5 km. 223
Table 6.11: Measurements vs. interpolated grids. 224

Table 7.1: Correlations between mean surface temperatures, MMD and glacier change. 238
Table 7.2: Correlations between ocean temperatures and glacier change rates. 250
Table 7.3: Same as Table 7.2, by Region. 251

Figures

Figure 1.1: Antarctica and an outline of the study location. 2

Figure 2.1: Antarctic Peninsula location map with key place names..... 9
Figure 2.2: The thermal limit of viability of ice shelves. 20
Figure 2.3: Spatial distribution of overall glacier length changes on the AP. 26
Figure 2.4: Glacier length change rates on the AP..... 27
Figure 2.5: AP glacier length changes rates by latitudinal regions. 28
Figure 2.6: Ocean circulation patterns surrounding the AP. 42

Figure 3.1: The surface texture of ASTER GDEM..... 62
Figure 3.2: ASTER GDEM stacking numbers. 64
Figure 3.3: Sample map illustrating ASTER GDEM improvement procedure. 68
Figure 3.4: The new 100-m DEM of the Antarctic Peninsula. 70
Figure 3.5: Edited region coverage. 73
Figure 3.6: Scatterplots of ICESat and the DEM elevation values. 75
Figure 3.7: DEM profiles along an ICESat track. 76
Figure 3.8: Graphs show DEM mean differences from ICESat..... 78
Figure 3.9: Horizontal offset sample region - Ryder Bay, Adelaide Island. 80
Figure 3.10: Map showing SPIRIT tiles used for relative accuracy tests. 82

Figure 4.1: Glacier drainage basin outlines. 97
Figure 4.2: Sample regions illustrating glacier basin outlines, centrelines and outlet widths. ... 100
Figure 4.3: Sample region showing historical glacier front positions..... 106
Figure 4.4: Location map showing all marine-terminating glacier basins. 111
Figure 4.5: Examples of multiple glacier basins. 112
Figure 4.6: Source data temporal distribution. 113
Figure 4.7: Time series plots for 4 sample glaciers. 119
Figure 4.8: Change-rates single glacier plot. 122

Figure 4.9: Intra-annual glacier front change. 128
Figure 4.10: Boxplot showing distribution of mean seasonal area change 129

Figure 5.1: Histogram showing distribution of AP glacier basin sizes. 134
Figure 5.2: Number and area coverage of all glacier systems on the AP, by glacier size class. . 135
Figure 5.3: Graphs summarising total glacier count and area coverage per glacier type: 136
Figure 5.4: Size class, Primary Classifications and Front types of all 1590 glaciers. 138
Figure 5.5: Reference map showing spatial boundaries 140
Figure 5.6: Number and area coverage of all glacier systems, binned by size class 140
Figure 5.7: Number and area coverage of all glacier systems, split by east/west and degrees latitude. 141
Figure 5.8: Glacier classes and elevation attributes 143
Figure 5.9: Scatter matrix for selected glacier attributes 144
Figure 5.10: Scatterplots for outlet and mountain glaciers. 146
Figure 5.11: Inter-dependence of characteristics: glacier slopes, surface length and size. 147
Figure 5.12: Aspect sectors 147
Figure 5.13: Summary map showing spatial distribution of overall advance/retreat. 149
Figure 5.14: Histograms showing overall change per glacier 150
Figure 5.15: Overall mean change according to Front type. 152
Figure 5.16: Spatial distributions of overall change in area from earliest to latest records..... 153
Figure 5.17: Overall area change by degrees latitude. 154
Figure 5.18: Box plots of glacier basin areas relative to the basin areas in 2000-04. 156
Figure 5.19: Up-scaled areas by 5-year time intervals since 1945. 158
Figure 5.20: Up-scaled areas for glaciers with records in 9 or more intervals (36 glaciers). 158
Figure 5.21: Rates of change for all glaciers across all intervals. 160
Figure 5.22: Latitudinal spread of data availability (stacked) per 5-year interval. 161
Figure 5.23: Maps plots showing the spatial distribution of area change rates (in $km^2\ a^{-1}$) over 5-year intervals, since 1955. 164
Figure 5.24: Glacier area changes compared to length changes from earlier coastal-change study by Cook *et al.* (2005). 167
Figure 5.25: Area-change rates by region (% a^{-1}). 169
Figure 5.26: Rates of change ($km^2\ a^{-1}$) for glaciers with contrasting characteristics. 172

Figure 6.1: Region definitions. 181
Figure 6.2: Station temperature records time series graphs 183
Figure 6.3: Annual Mean Melt Duration (in days) between 2000 and 2009. 187
Figure 6.4: Mean Melt Duration (MMD) close to glacier fronts, by degree latitude. 188
Figure 6.5: Mean Melt Duration (MMD) between 2000 and 2009, by region. 188
Figure 6.6: Mean Annual Surface Temperatures 1980-2008. 190
Figure 6.7: Seasonal average surface temperatures 1980-2008 (°C). 191
Figure 6.8: Surface temperatures by degrees latitude, for annual (a), winter (b) and summer (c) means between 1980 and 2008. 192
Figure 6.9: Mean Surface Temperatures (1980-2008) within 5 km of glacier fronts, by region. 193
Figure 6.10: Surface temperature anomalies, 1980-2008. 194
Figure 6.11: Mean surface temperatures (ST) by Region, in pentadal intervals. 195
Figure 6.12: Mean annual surface mass balance (SMB) between 1980 and 2009. 197
Figure 6.13: Mean pentadal surface mass balance anomalies from the mean (1980-2009). 198
Figure 6.14: IBCSO bathymetry data. 202
Figure 6.15: Glaciers with depth measurements available within 5 km, 2 km and 1 km 205
Figure 6.16: Ocean temperatures at specific depths. 209
Figure 6.17: Mean ocean temperatures at selected depths (m), by east/west AP. 211
Figure 6.18: Mean ocean temperatures at selected depths, by Regions. 212
Figure 6.19: Regional mean ocean temperatures by 5-year intervals. 213
Figure 6.20: Decadal ocean temperatures at 150 m depth. 217
Figure 6.21: Multi-dimensional plots showing mean temperature at specific depths over time. 218
Figure 6.22: Repeat temperature measurements between 1990s-2000s. 222
Figure 6.23: Mean ocean temperatures within 5 km of individual glacier fronts (west coast). .. 225

Figure 7.1: Mean melt durations and glacier retreat rates, by Region. 235
Figure 7.2: Mean surface temperatures and glacier retreat rates, by Region. 235
Figure 7.3: Mean melt duration classed by glacier change rates between 2000-09. 237
Figure 7.4: Mean surface temperatures classed by glacier change rates. 237
Figure 7.5: Temporal patterns for glacier change rates and surface temperatures. 240
Figure 7.6: Regional mean ocean temperatures. 242
Figure 7.7: Ocean temperatures and overall glacier change: spatial patterns. 244

Figure 7.8: Regional mean ocean temperatures, close to shore (west coast). 245
Figure 7.9: Mean ocean temperatures classed by glacier change rate. 247
Figure 7.10: Same as Figure 7.9, separated by depth. 248
Figure 7.11: Mean ocean temperatures classed by glacier change rate, for separate regions. 249
Figure 7.12: Same as Figure 7.11, for absolute area change rates (km^2 a^{-1})..... 250
Figure 7.13: Spatial distribution of glacier change rates in 1985-89 and 1995-99..... 253
Figure 7.14: Temporal patterns for glacier change rates and ocean temperatures. 254
Figure 7.15: Sample region – illustrating ocean temperature data spatial distribution. 256

Figure 8.1: Glaciers and bathymetry in Beascochea Bay (location shown on inset). 277

N.B. Figure and Table citations throughout the text are in red text to assist the reader with navigation through the document.

Abbreviations

ABS	Amundsen and Bellingshausen Seas
ACC	Antarctic Circumpolar Current
AIS	Antarctic Ice Sheet
ADD	Antarctic Digital Database
AP	Antarctic Peninsula
APCC	Antarctic Peninsula Coastal Current
APIS	Antarctic Peninsula Ice Sheet
ASAID	Antarctic Surface Accumulation and Ice Discharge (Project)
ASE	Amundsen Sea Embayment
ASTER	Advanced Spaceborne Thermal Emission and Reflection (Radiometer)
ATM	Automatic Thematic Mapper
AVHRR	Advanced Very High Resolution Radiometer
AWS	Automatic Weather Station
BEDMAP	Ice bed, surface and thickness datasets for Antarctica
BAS	British Antarctic Survey
BS	Bellingshausen Sea
CDW	Circumpolar Deep Water
CPT	Circumpolar Trough
DEM	Digital Elevation Model
DTM	Digital Terrain Model
ENSO	El Niño Southern Oscillation
ERA40	European Centre for Medium Range Forecasts Reanalysis (Data)
ERS	European Remote-sensing Satellite
GDEM	Global Digital Elevation Model
GHG	Greenhouse Gases
GIA	Glacial Isostatic Adjustment
GIS	Geographic Information System
GLAS	Geoscience Laser Altimeter System (ICESat)
GLIMS	Global Land Ice Measurements from Space
GRACE	Gravity Recovery and Climate Experiment (Satellite)
IBCSO	International Bathymetric Chart of the Southern Ocean

ICESat	Ice, Cloud and Land Elevation Satellite
IfAG	Institut für Angewendt Geodesie
IOM	Input Output Model
JRI	James Ross Island
LA	Laser Altimetry
LCC	Lambert Conformal Conic (Projection)
LGM	Last Glacial Maximum
LiDAR	Light Detection and Ranging
LIMA	Landsat Image Mosaic of Antarctica
MMD	Mean Melt Duartion
MODIS	Moderate Resolution Imaging Spectroradiometer
MSS	Multi-Spectral Scanner (Landsat)
NASA	National Aeronautics and Space Administration
NOAA	National Oceanic and Atmospheric Administration
NODC	National Oceanographic Data Center
NSIDC	National Snow and Ice Data Center
PDD	Positive Degree Day
QSCAT	QuikSCAT satellite (scatterometer data)
RA	Radar Altimetry
RACMO	Regional Atmospheric Climate Modelling
RAMP	Radarsat Antarctic Mapping Project
RGI	Randolph Glacier Inventory
RMSE	Root Mean Squared Error
RRR	Recent Rapid Regional (Warming)
SAR	Synthetic Aperture Radar
SAM	Southern Annular Mode
SAO	Semi-Annual Oscillation
SLE	Sea level equivalent
SMB	Surface Mass Balance
SOI	Southern Oscillation Index
SPIRIT	SPOT 5 stereoscopic survey of Polar Ice: Reference Images and Topographies
SPOT	Satellite Pour l'Observation de la Terre (Satellite)
SRTM	Shuttle Radar Topography Mission
SSI	South Shetland Islands

SST	Sea-surface temperature
ST	Surface temperature
THIR	Temperature Humidity infrared Radiometer
TM	Thematic Mapper (Landsat)
T_m	Pressure melting point of ice
USGS	United States Geological Survey
WAIS	West Antarctic Ice Sheet
wAP	Western Antarctic Peninsula
WGI	World Glacier Inventory
WGMS	World Glacier Monitoring Service
WOD	World Oceanographic Database
WS	Weddell Sea
WSM	Wide Swath Mode (SAR)

Chapter 1

Introduction and Aims

1.1 Motivation

The Antarctic Peninsula (AP) is described as an area of recent rapid regional warming, with air temperatures rising at rates six times the global average in the last few decades (Vaughan *et al.*, 2003). The AP Ice Sheet (APIS) is responding rapidly to this warming, with thinning and disintegration of ice shelves, the consequent acceleration of tributary glaciers and the retreat of glacier fronts (e.g. Shepherd *et al.*, 2003; Cook *et al.*, 2005; Pritchard & Vaughan, 2007). Furthermore, some of these events are unprecedented in the last 10,000 years (Domack *et al.*, 2005).

The most recent IPCC Report has stated that between 1901 and 2010, global mean sea level rose by a total of 0.19 m at a rate of ~1.7 mm a^{-1}, and between 1993 and 2010 the rate increased to ~3.2 mm a^{-1} (IPCC, 2013). By the end of the 21st century, it is projected to rise by 0.26-0.82 m. Mass loss from glaciers and ice caps around the globe has been a major contributor to this rise and this contribution is likely to increase over the next century (Gregory *et al.*, 2013). Some estimates have suggested that the AP region, which contains around 5-10 cm of global sea-level-rise potential, is one of the largest regional contributors to current sea-level rise (Pritchard & Vaughan 2007; Hock *et al.* 2009). However, the AP glaciers are not typically included in global estimates of sea-level rise, and changes in mass balance of most glaciers there have yet to be quantified. The harsh environment and inaccessibility means that few of the glaciers have been visited or studied in detail. The lack of glacier inventory and understanding of change over recent decades makes this a critical region for further study.

The APIS is very different from other parts of the Antarctic, consisting of numerous alpine-style glaciers flowing from a high (1400 - 2000 m a.s.l.) mountain plateau into ice shelves or through marine-terminating fronts, and surrounded by glacierized islands. This

study focuses on the region north of 70° S, where the mountain chain narrows and marine-terminating glaciers predominate along the west coast (Figure 1.1).

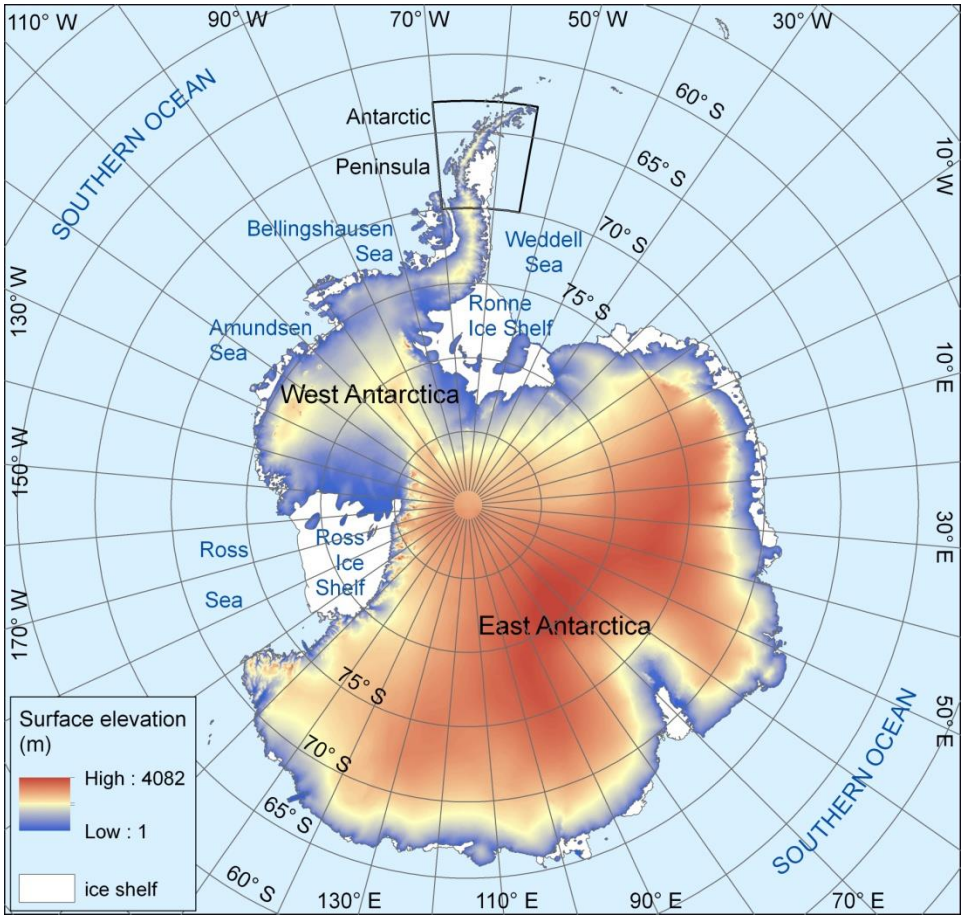

Figure 1.1: Antarctica and an outline of the study location.
The topography is from BEDMAP2 and the coastline is from the Antarctic Digital Database.

This region has a polar maritime climate and there is strong melt at low elevations in summer. Around one-third of the area lies within 200 m of sea level (Pritchard & Vaughan 2007), making the AP glaciers particularly vulnerable to temperature changes. Since records began in the 1950s, mean annual surface temperatures on the AP have risen rapidly, with all stations showing significant warming. While changes in precipitation and surface melt are important, tidewater glacier flow is sensitive also to changes in ocean temperatures (e.g. Holland *et al.*, 2008). There is evidence that the ocean around the AP has also warmed, with the near-surface ocean to the west warming by more than 1°C from 1951 to 1994 (Meredith & King 2005).

It is clear that the AP glaciers are highly sensitive to the warming trends, causing changes in their melt rates and dynamics and resulting in an increasing contribution to sea-level rise. However, neither the full extent of ice losses around the AP nor the degrees to which the climate or ocean conditions have driven these changes are known with any degree of certainty.

1.2 Aims

The main aim of this thesis is to advance knowledge on Antarctic Peninsula glaciers and determine the principal drivers of frontal change in recent decades. To achieve this it is necessary to establish their characteristics, to measure changes in their extent, to assess the spatial and temporal variability in these changes and understand the external controls on their behaviour. The ultimate objective is that these results will improve predictions in likely future changes of marine glaciers and their contribution to sea-level rise given particular climate scenarios.

A prerequisite for glacier-by-glacier mass balance studies is the definition of outlines for each individual ice mass. The remoteness and inaccessibility of the AP means that there is no comprehensive inventory and therefore data fundamental for glacier behavioural studies is missing. The glacier system is complex and therefore a high accuracy topographic model is required in order to delineate the individual glaciers. The initial aim of the project is therefore to produce a benchmark dataset on which further glacier analyses will be based. At the outset of the study, it became clear that there was no Digital Elevation Model (DEM) with the resolution and accuracy required and therefore the first part of the project is development of a suitable DEM. A chapter within the thesis is therefore centred on the DEM methodology and results since it is fundamental for the subsequent glacier analyses and valuable for future glaciological studies.

The specific aims are as follows:

- To produce a new DEM of the Antarctic Peninsula.
- To use the DEM to derive a comprehensive glacier inventory, including classification of glaciological features.

- To provide qualitative results on AP glacier types and their characteristics.
- To update existing historical ice front positions, and associate these with individual glacier drainage basins.
- To measure and quantify glacier area changes since the 1940s.
- To assess spatial and temporal patterns in glacier area changes.
- To quantify changes in the external controls on glacier change over the same time period.
- To determine the principal drivers of regional glacier area changes on the AP.

1.3 Thesis structure

Current knowledge on the APIS and its climate system is discussed in Chapter 2. The present state of the cryosphere must be understood in the context of longer-term trends, therefore a review of its history is given. The APIS consists of complex glacier dynamics and so understanding the mass balance of the system as a whole, as well as its ice shelf and glacier components, is also essential for the present study. A discussion of existing knowledge on the APIS highlights gaps in our understanding of glacier behaviour in the region. An overview of the climatic and oceanic setting and associated patterns of change is also given, since this is fundamental to determining how the glaciers may respond to future change. Finally, a number of global glacier studies are discussed with the purpose of identifying suitable methods to apply to this region.

As stated above, a key resource for distinguishing separate glaciers in such complex terrain is a DEM. Chapter 3 addresses the issue and outlines a new method to improve an existing DEM. This method can be applied to glacierized regions elsewhere for smoothing and correcting surface models. This chapter is therefore to be regarded as both methods and results for this distinct part of the thesis.

The methods used in producing a glacier inventory for the AP are explained in Chapter 4, along with a description of processes used to derive glacier characteristics and area-change measurements. A unique approach to analysing the glacier area changes is outlined, as well as an assessment of the accuracy of the results.

The new datasets are used initially to provide a descriptive overview of AP glaciers and their characteristics, which are presented in Chapter 5. This chapter goes on to quantify overall changes from the earliest to latest recorded positions for all glaciers. Wide-scale spatial patterns in these overall changes are identified. The glacier change-rates calculated across 5-year intervals are then analysed, revealing statistically significant regional trends.

The results in Chapter 6 are a quantification of atmospheric and oceanic temperatures changes that have occurred around the AP since the earliest available records. Previously unstudied surface temperature data and ocean temperature data are analysed here for the first time, and reveal distinct spatial and temporal patterns.

The results presented in Chapters 5 and 6 are discussed in Chapter 7, where the glacier area-change patterns are examined alongside the atmospheric and oceanic temperature patterns. The new findings are then discussed in the context of existing literature. The importance and implications of these findings are also highlighted.

Finally, Chapter 8 gives a summary and the conclusions from this thesis. This recaps the aims of the study, the principal findings from the research, and suggestions for further work that can build upon these findings.

1.4 Published material

A number of relevant papers on which I am author are referred to throughout the thesis. For clarity, the distinction is given here between those papers associated with related work undertaken prior to commencing the PhD in September 2010, and those that have been written and published from work undertaken during the PhD.

Relevant papers published prior to starting the PhD:

The present study arose from a joint project between the US Geological Survey (USGS) and British Antarctic Survey (BAS), '*Coastal-Change and Glaciological Maps of Antarctica*', in which historical ice front positions were digitised. This culminated with the delivery of a database and three hardcopy maps showing the changes (Ferrigno *et al.*,

2006, 2008, 2009) as well as a published paper on initial results (Cook *et al.*, 2005). The coastal positions were used in a review paper on ice shelf changes (Cook & Vaughan, 2010) and in other coastal research papers on which I am co-author (Peck *et al.*, 2010; Smith *et al.*, 2007).

Papers published from research undertaken during the PhD:

Two papers are based on direct output from this research:

- The new DEM methodology and results presented in Chapter 3 are published in Cook *et al.* (2012). I produced the results and led the writing and compilation of graphics and tables. Co-authors T. Murray, A. Luckman and D.G. Vaughan were involved in both discussion of content and manuscript editing, and N. Barrand provided DEMs for error analysis.

- A summary of the methods and results from Chapters 4 and 5 are published in Cook *et al.* (2014). I produced the results and led the writing and compilation of graphics and tables. Co-authors D. G. Vaughan, A. Luckman and T. Murray were involved in both discussion of ideas and manuscript editing.

The DEM and glacier drainage basin outlines have also been used in research by other scientists, resulting in joint authorship on the following papers: Barrand *et al.* (2013), Fretwell *et al.* (2013) and Scambos *et al.* (2014).

Contribution of glacier front position data to a world-wide glacier-change research project has also resulted in co-authorship on LeClercq *et al.* (2014).

The references to these papers are listed in Appendix – Chapter 1.

.

Chapter 2

The Antarctic Peninsula Ice Sheet and Climate Change

2.1 Introduction

The Antarctic Peninsula Ice Sheet (APIS) differs from the rest of the Antarctic continental ice sheet in that it is a narrow mountainous chain bounded to the east and west by ocean and it has a distinctive climatic regime. The nature of the topography is that in contrast to the large, low-sloping ice streams making up most of the continental fringe, there are numerous steep and heavily-crevassed mountain glaciers. Outlet glaciers drain to the east and west from the plateau of the APIS, and ice caps, mountain glaciers and piedmonts are prevalent along the margins and adjacent islands. These relatively small ice masses are crucial indicators of the variability of the regional climate system, and measuring their characteristics and behaviour would help improve our understanding of the glacial response to the rapidly changing climate both locally and for the system as a whole.

This chapter gives a review of current knowledge on the glaciology of the Antarctic Peninsula (AP), and the state of the cryosphere throughout recorded history. The complex mass balance processes occurring across the ice sheet are discussed. Factors influencing the mass balance of glaciers in this region include atmospheric temperatures, precipitation and ocean temperatures, and current knowledge on each of these variables is outlined here. Present knowledge highlights gaps in our understanding of glacier response to these environmental changes, and indicates the importance and urgency with which glacier changes must be analysed. Glaciers that are small in size relative to the continental-scale ice streams respond more rapidly to changes in controls on their behaviour and are therefore crucial indicators of the effect of climate change. The importance of close monitoring, and the best approach with which to do so, is also

discussed. Finally, previous glacier monitoring studies world-wide can indicate the best approach for studying glaciers in the Antarctic Peninsula and so relevant studies are reviewed here.

2.2 Glaciology of the Antarctic Peninsula

The Antarctic Peninsula is glaciologically complex because individual flow units are part of the much larger ice sheet system, making it difficult to distinguish boundaries between glaciers. Few of the glaciers on the AP have been studied in detail and there is no comprehensive inventory of all glacier outlines on both the mainland and islands, which makes glacier-by-glacier mass balance studies more challenging than in other glaciated regions around the world. Analyses of the ice sheet and of individual glaciers have been hindered by the scale and inaccessibility of the region, and glacier monitoring began significantly later than in other regions of the world simply due to the isolation and harshness of the environment.

The glaciers along the west coast between Trinity Peninsula in the north (~63° S) and George VI Sound in the south (~70° S) (Figure 2.1), are almost all marine-terminating; south of this glaciers flow into ice shelves. Along the east coast, the glaciers north of ~66° S are primarily marine-terminating; further south they feed the Larsen C Ice Shelf. Definitions of the extent of the AP vary but since the primary focus for glacier area change is the marine-terminating glaciers, the boundary chosen for this study is 63° to 70° S and 55° to 70° W. The area of this region (including islands but excluding ice shelves) is ~98 000 km^2, which is approximately 0.7 % of the area of the continent, and more than 96% of this area is ice-covered.

Glaciers throughout the Antarctic Peninsula have undergone extensive change in recent decades (e.g. Cook *et al.*, 2005; Pritchard & Vaughan, 2007; Pritchard *et al.*, 2009; Kunz *et al.*, 2012) and are subject to rapid climate warming from the atmosphere and ocean (Barrand *et al.*, 2013a). There is now extensive evidence that since the 1950s there have been significant changes in the climate on the AP such as an increase in air temperature (Vaughan *et al.*, 2003; Steig *et al.*, 2009; Mulvaney *et al.*, 2012), near-surface warming

in the seas to the west (Meredith & King, 2005), a corresponding reduction in sea-ice extent (Smith & Stammerjohn, 2001) and an increase in precipitation and snow accumulation (Turner *et al.*, 2005a; Thomas *et al.*, 2008). Ice mass change estimations suggest that glaciers in this region are particularly sensitive to these changes (Hock *et al.*, 2009), and an accelerated mass loss has occurred during recent years (Chen *et al.*, 2009; Ivins *et al.*, 2011). It is evident that the APIS is currently losing mass, but the state of the cryosphere must be understood in the context of longer-term trends.

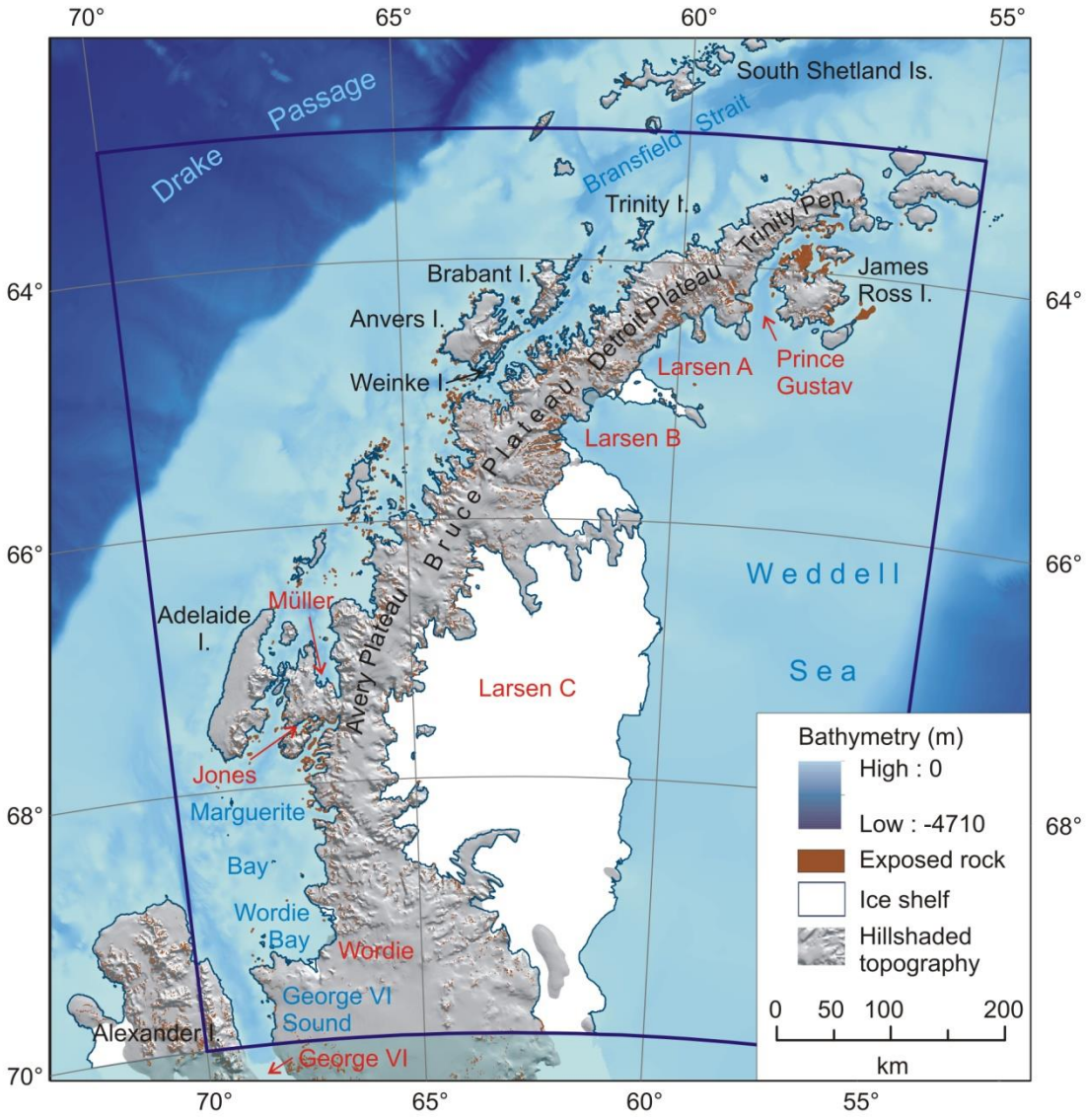

Figure 2.1: Antarctic Peninsula location map with key place names.
The graticule labels are degrees South; names in red are ice shelves (both existing and disintegrated) and the ice extent is during 2000-02; the bathymetry grid is from the International Bathymetric Chart of the Southern Ocean (IBCSO) and the topography is from BEDMAPv2.

2.2.1 History of the AP Cryosphere

2.2.1.1 The Last Glacial Maximum

Research into the state of the cryosphere in the AP since the Last Glacial Maximum (LGM) has been made possible using a variety of records including ice cores, marine and lake sediment cores and glacial geomorphological features measured both onshore and offshore. These records are a valuable resource for understanding palaeoenvironmental changes, but there remains a scarcity of measurements for some regions and there lacks a comprehensive temporal coverage since the LGM. Current knowledge on the climate and state of the ice sheet throughout the past 20,000 years has been achieved by scientists piecing together all palaeoenvironmental records that currently exist. A summary is given in this section.

It is widely understood that the APIS extended as far as the edge of the continental shelf during the LGM (~20-18 ka), although the exact position of the grounded ice and the timing of the onset of retreat is still uncertain in many locations (e.g. Johnson *et al.*, 2011; Livingstone *et al.*, 2012). Ice sheet retreat around the AP occurred progressively from the outer, middle and inner continental shelf areas throughout the period ~18-9 ka, roughly consistent with eustatic sea-level rise caused by Northern Hemisphere deglaciation (Heroy & Anderson, 2007). Retreat on the outer shelf occurred progressively from north (~18 ka) to south (~14 ka), and whilst estimates from sediment cores may vary by up to ± 1100 years, two steps in glacier retreat have been noted at approximately 14 and 11 ka (Heroy & Anderson, 2007).

Despite the non-uniform coverage of records surrounding the AP, some regional comparisons in the timing of retreats can be made. On the eastern side, geomorphological features such as streamlined subglacial bedforms suggest that the margin of the APIS grounded within 10 km of the shelf edge in the Weddell Sea at the LGM (Evans *et al.*, 2005). A small number of radiocarbon dates available in the Weddell Sea show that the eastern edge of the APIS had begun to retreat by 18.5 ka (Heroy & Anderson, 2005), with a maximum age of retreat onset of 20.4 ka inferred from sediment cores (Smith *et al.*, 2010). Marine evidence also shows deglaciation on the middle to inner continental

shelf between 16.7 and 11.5 ka (Pudsey *et al.*, 2006), and the transition from grounded-ice to ice shelf conditions in the Prince Gustav Channel (between NE Antarctic Peninsula mainland and James Ross Island (JRI)) was completed before ~11 ka (Evans *et al.*, 2005).

Marine data along the western margin of the APIS is more plentiful and radiocarbon dates indicate that retreat on the outer shelf occurred progressively from north to south, beginning in the northern AP by ~18 ka and continuing southwards by ~12 ka on the outer shelf off Marguerite Bay (Heroy & Anderson, 2007). Well-preserved landforms and the absence of retreat moraines indicate the ice shelves thinned and retreated rapidly in this region, becoming ice-free by ~9 ka. This is consistent with onshore data, which indicate that the George VI Ice Shelf began to collapse around 9.6 ka (Bentley *et al.*, 2005; Smith *et al.*, 2007). Heroy and Anderson (2007) noted that the north-south trend is less evident in the mid and inner shelf regions and in addition, there are no trends in the timing of retreats between the east and west AP prior to the Holocene, nor at different water depths.

The palaeo-ice streams that extended onto the outer continental shelf during the LGM have left many bathymetric troughs, with ten clearly defined troughs extending westwards from the AP and three towards the east (Livingstone *et al.*, 2012).

2.2.1.2 The Cryosphere since the early Holocene

From the early Holocene (~11.7 ka) to the present, cryospheric responses to palaeoenvironmental change have varied regionally, with differences in timing and duration of deglaciation particularly distinct between the eastern and western sides of the AP. Following the early Holocene climate optimum, from ~11 ka until ~9.2 ka (Masson *et al.*, 2000), complex patterns developed, such as ice shelf collapse on the west, when those on the east were stable (Hodgson *et al.*, 2006). Following the collapse of George VI Ice Shelf, it reformed from ~8 ka (Bentley *et al.*, 2005; Smith *et al.*, 2007), whilst on the eastern side there is evidence that the Larsen B ice shelf was stable throughout the Holocene (Domack *et al.*, 2005). Indeed, an ice core record collected in 2008 from JRI shows that the early Holocene warm period was followed by relatively stable

temperatures throughout the entire period from 9.2 to 2.5 ka and that these were similar to modern-day temperatures (Mulvaney *et al.*, 2012). The regional differences in ice sheet behaviour suggests there was an intensification of the contrast in climate between the two sides of the AP in the early Holocene, with a steepening of the thermal gradients to the north and west (Hodgson *et al.*, 2006). The earlier retreat of the ice sheet in the NW region may have made the glacial system more susceptible to the advection of warmer ocean currents, whereas the thicker ice shelves on the east remained buffered against these warm periods (Turner *et al.*, 2009).

Dating from moraines on JRI shows that several glacial advances occurred during the early- to mid- Holocene, with the oldest reported advance occurring between 7.3 and 7.0 ka, and the youngest, 4.1 ka (Strelin *et al.*, 2006). There is minimal evidence in the terrestrial record in the AP, however, because most currently ice-free areas were probably still ice-covered throughout this time (Ingolfsson *et al.*, 2003). Coastal areas in Marguerite Bay and parts of the South Shetland Islands were ice-free immediately after the early Holocene climate optimum. In general, on the west side of the AP, significant thinning and ice margin retreat continued until at least ~7-8 ka (Bentley *et al.*, 2006). The transition from glacial to interglacial conditions was broadly completed by ~6 ka (Ingolfsson *et al.*, 2003), although there is some evidence for a re-advance on Brabant Island after ~5.3 ka and northern JRI around ~4.6 ka, which coincided with cold marine waters and extensive sea-ice cover detected in some coastal areas (Turner *et al.*, 2009).

A significant period of warmth occurred in the mid-Holocene, with best dated records placing this between ~4.5-2.8 ka (Bentley *et al.*, 2009). This ‘Mid-Holocene Hypsithermal’ has been associated with the collapse of the Prince Gustav Ice Shelf in the NE AP between ~5 - 2 ka (Pudsey & Evans, 2001), and fluctuations of the Larsen A Ice Shelf between ~4 - 1.4 ka (Brachfeld *et al.*, 2003), while the Larsen B Ice Shelf remained stable. Not all ice cores show this warming period however (e.g. the JRI ice core) (Mulvaney *et al.*, 2012), and similarly, the signal is not apparent in all marine records (e.g. close to Anvers Island) (Domack *et al.*, 2003). This indicates that there may have been a continuous presence of warm Upper Circumpolar Deep Current water on the continental shelf for a period of over 5000 years with no obvious cooling prior to this period (Bentley *et al.*, 2009). Whilst there is widespread agreement that there was a mid-

Holocene warm period, the exact timing varies, either due to spatial differences in the timing, or due to an insufficient number of records available (Bentley *et al.*, 2009).

Following the end of the Mid-Holocene Hypsithermal, the AP was subject to colder climate conditions (the Neoglacial period). Many glacier advances have been recorded but few have been dated with certainty. Records show that the Prince Gustav Ice Shelf began to reform after 1.9 ka (Pudsey & Evans, 2001), as was the case with the Larsen A Ice Shelf which reformed approximately 1.4 ka (Brachfeld *et al.*, 2003). Pronounced cooling between 2.5 – 0.6 ka was recorded in the JRI ice core isotope record, coinciding with the development of ice shelves in this region (Mulvaney *et al.*, 2012). Here the temperatures steadily dropped until ~0.6 ka, when they reached a low of approximately 1 °C below present-day temperatures, or as much as 1.8 ± 0.3 °C cooler than present on a decadal timescale (Mulvaney *et al.*, 2012).

After the Neoglacial period, there is some evidence of a period of warming on the AP during what is termed the Medieval Warm Period, ~ 1.2 – 0.6 ka, but so far the proxy records are limited to marine records off the west coast (Bentley *et al.*, 2009). This warming is not apparent in the JRI isotope record (Mulvaney *et al.*, 2012). Similarly, proxy records for evidence of the Little Ice Age (dated in the Palmer Deep marine record as approximately 700 – 150 yr BP) are minimal, but marine records on the inner shelf off Anvers Island do show evidence of persistent sea-ice and cold water conditions, consistent with glacier advances in the region (Bentley *et al.*, 2009). The Müller Ice Shelf is thought to have advanced during a time that roughly corresponds with the Northern Hemisphere Little Ice Age (Domack *et al.*, 1995), but the timings of many terrestrial records of glacier advances are not well constrained (Bentley *et al.*, 2009). The JRI isotope record temperature excursions show that this region did not experience a Medieval Warm Period or Little Ice Age sequence comparable to the Northern Hemisphere, but rather sustained warming has been ongoing for several centuries (Mulvaney *et al.*, 2012).

The most recent climatic epoch on the AP is termed a period of Recent Rapid Regional (RRR) warming. There are pronounced regional differences in rates of warming, especially between the west (more warming) and east (less warming) (Bentley *et al.*,

2009). Proxy records, such as lake and marine sediment cores, indicate that increased sediment accumulation has occurred throughout this period, although Domack *et al.* (2003) suggest that the abundance of melt-water sediment and warm-water species of diatoms present in the mid-Holocene are not yet seen in recent samples, implying that conditions are not currently as warm as those that occurred ~4 ka. The JRI ice core record does show a high rate of warming of 1.56 °C over the past 100 years, which is unusually high, although not unprecedented (for example, during the transition to the early-Holocene optimum, ~13-12 ka) (Figure 4 in Mulvaney *et al.*, 2012).

Over the past 50 years, however, temperature in the NE AP has risen at a rate equivalent to 2.6 ± 1.2 °C per century (Mulvaney *et al.*, 2012). Meteorological station records have confirmed the rising temperatures measured in proxy records, showing that since the 1950s the AP has warmed on average at 3.7 ± 1.6 °C per century (Vaughan *et al.*, 2003). This period of RRR warming has been substantially more rapid than both the global mean and the rest of Antarctica, and climate proxies show that this rate is unprecedented over the last two millennia (Vaughan *et al.*, 2003). This is unlikely to be a natural mode of variability and several model studies now agree that anthropogenic change is primarily responsible for the climatic shift (Arblaster *et al.*, 2011). As has been stated by Mulvaney *et al.* (2012), if warming continues in this region, temperatures will soon exceed the stable conditions that persisted in the east AP for most of the Holocene.

It is important to understand the recent climate in the context of past climatic changes, and to recognise that the climate system is currently undergoing change that is faster than during previous warm periods. The association of air temperatures and ice shelf stability in the past demonstrates that as warming continues, ice shelf vulnerability will progress further southwards to affect ice shelves that have been stable throughout the Holocene (Mulvaney *et al.*, 2012). The collapse of the Larsen B in 2002 for example has been unprecedented (Domack *et al.*, 2005). A more detailed description of the current state of the cryosphere will be discussed in the following section.

2.2.2 Mass balance of the APIS

The Antarctic Peninsula Ice Sheet consists of complex glacier dynamics, including locally high imbalances in ice mass caused by the loss of ice shelves. Although it is known that the Antarctic Peninsula drains a large volume of ice, the question of how much of the increased outflow is balanced by increased accumulation is still an active research topic. Until very recently, the contribution of the APIS was often overlooked in global projections of sea-level rise (Meehl *et al.*, 2007). It is perhaps best to summarise research on the mass balance of the APIS as a whole, before discussing progress on understanding the glaciers and ice shelves that make up the glacier system.

2.2.2.1 Mass estimates

Mass balance estimates for the Antarctic Ice Sheet (AIS) and corresponding sea-level equivalent (SLE) calculations, have improved substantially in recent years using a variety of techniques and include mass change over different time periods, at various levels of spatial detail. Satellite geodesy has been the primary source of advance in this field. Since 1998 there have been 14 AIS mass balance studies in total , and in a recent project all estimates of ice sheet mass balance from both Polar regions were compared and combined, resulting in reconciled estimates of mass balance (Appendix 2.1) (Shepherd *et al.*, 2012). Each study included the APIS, although the region was not always defined as a separate ice mass.

Data sources used to produce ice sheet mass estimates of the AIS have included satellite altimetry, interferometry and gravimetry data sets: definitions and examples of these measurements are presented in Appendix 2.2. The reconciled mass balance estimate based on all data and methods for the APIS between 1992 and 2011, is –20 ± 14 gigatonnes year^{-1} (Shepherd *et al.*, 2012). It should be noted that the APIS in the mass balance estimate is defined as the region from 63° S to approximately 74° S, which is considerably greater in area than the region defined as the AP in this study. It is evident in the study by Shepherd *et al.* (2012) that although the APIS was close to balance during the 1990s, there has been significant mass loss since then. For the period 1992-2000, the APIS reconciled mass balance estimate was -8 ± 17 Gt a^{-1} whereas in the most recent

epoch 2000-2011 it was -29 ± 12 Gt a^{-1}. Mass loss was as high as -36 ± 10 Gt a^{-1} between 2005-2010. The study shows that the APIS now accounts for around 25% of all mass losses from Antarctic regions that are in a state of negative mass balance, despite occupying just 4% of the continental area (Shepherd *et al.*, 2012). The authors note that the spatial sampling of mass fluctuations at the APIS is at present inadequate and that improvements in spatial and temporal density of satellite observations of this region are needed.

2.2.2.2 Sea-level rise

In addition to the overall APIS mass balance estimates, a number of independent estimations of the AP contribution to sea-level rise have been made by measuring changes in various components of the ice sheet. In a mass-balance study based on a grid-based modelling approach, for the period 1961-2004 it was calculated that the mountain glaciers and ice caps (MG&IC) of Antarctica contributed 0.22 ± 0.16 mm a^{-1} sea-level equivalent (SLE) (28% of the global SLE from MG&IC), which originated almost entirely from the AP and surroundings (Hock *et al.*, 2009). One estimate of mass change due primarily to temperature-dependent increases in snowfall on the AP produces a contribution to sea-level of approximately -0.006 mm a^{-1} over the period 1972-98 (Morris & Mulvaney, 2004). A further study has shown that circa 2005, the AP was contributing to global sea-level rise through enhanced melt and glacier acceleration at a rate of 0.16 ± 0.06 mm a^{-1} (Pritchard & Vaughan, 2007). This can be compared to an estimated total AP ice volume (95,200 km^3) equivalent to 242 mm of sea-level (Pritchard & Vaughan, 2007). An assessment of changes in melting conditions on the AP based on long-term meteorological records, using established criteria to calculate snow-melt and run-off, has indicated that the AP contribution to global sea-level rise from run-off was 0.008-0.055 m a^{-1} between 1950 and 2000 (Vaughan, 2006).

2.2.2.3 Surface mass balance

Further studies have mapped the surface mass balance of the APIS (Turner *et al.*, 2002; Lenaerts *et al.*, 2012) and modelled future SMB and contributions to s.l. rise (Barrand *et al.*, 2013a; Ligtenberg *et al.*, 2013). SMB components include: precipitation; surface

sublimation; drifting snow transport, erosion and sublimation; meltwater formation, refreezing, retention and runoff (Shepherd *et al.*, 2012). Prior to the regular use of climate models, measurements from ice cores and snow pits collected over the last 50 years were used to examine how net surface mass balance varies across the Antarctic Peninsula and were compiled as the first detailed mass balance map (Turner *et al.*, 2002). The paper by Turner *et al.* (2002) describes that at sea level on the western side of the Antarctic Peninsula, all the snowfall melts during the summer, so that the annual mass balance is zero or negative. But inland the orography rises very rapidly, so that over a relatively short distance the summer mean temperatures fall below zero and the mass balance becomes roughly equal to the precipitation (Turner *et al.*, 2002). The largest SMB values are found down the spine of the northern part of the Antarctic Peninsula, where values in excess of 2.5 m a^{-1} (water equivalent) were found (Turner *et al.*, 2002). Areas where there is a high density of *in situ* data available, including George VI Sound and the high south central plateau part of the peninsula, show a high spatial variability of net SMB, suggesting that local orographic features play a major part in dictating the mass balance (Turner *et al.*, 2002).

Since then, a new high-resolution (27 km) surface mass balance map of Antarctica has been produced using Regional Atmospheric Climate Modelling (RACMO), for the period 1979-2010 (Lenaerts *et al.*, 2012). The SMB map confirms high accumulation zones in the western Antarctic Peninsula (>1500 mm a^{-1}) and the modelled SMB is in good agreement with in situ SMB measurements (Lenaerts *et al.*, 2012). No overall trend was found in SMB from 1979-2010, although some regional trends were detected. The western Antarctic Peninsula showed a positive, though insignificant trend of between 2 to 10 mm a^{-2} (Lenaerts *et al.*, 2012). Predictive models show that the future SMB change of the whole Antarctic Ice Sheet is dominated by the increase in snowfall and contributes negatively to global SLR (Ligtenberg *et al.*, 2013). Volume change estimates of the APIS resulting from surface mass balance anomalies calculated by the latest regional model RACMO2, predicted net negative sea-level contributions between –0.5 and –12 mm sea-level equivalent (SLE) by 2200 (Barrand *et al.*, 2013a).

2.2.3 Ice Shelves and Glaciers on the AP

Understanding the mass balance of the complete APIS system is important for estimating the long-term contribution of the ice sheet to sea-level change, but interpreting the behaviour of the numerous small glaciological features making up the system is critical for recognising responses to local and regional environmental changes. The glaciological complexity of the APIS has meant that although the recent changes in glacier extent, velocity and thickness are widely recognised, there is still little quantification of change in the mass balance of individual glaciers or the processes controlling changes in their extent. The grounded ice sheet is an alpine system consisting of more than 1100 individual glacier systems (Rau *et al.*, 2006) and there are seven ice shelves north of 70° S of sizes ranging from 25 km^2 to over 50,000 km^2 (Cook & Vaughan, 2010). Glacier types range from outlet glaciers draining the high and narrow mountain plateau, mountain glaciers constrained within individual basins, ice piedmonts along the fringe of the mainland or large islands, isolated ice caps and small ice-covered islands. The majority of glaciers flowing to the west are marine-terminating (both grounded and floating) and many of those flowing eastwards are ice shelf tributary glaciers.

Instrumental measurements of glaciers and ice shelves on the AP began after the early explorers reached Antarctica in the late 19th century. The first observations of the continuous Prince Gustav-Larsen ice front were made by James Clark Ross in 1843 , recorded as sketches from on-board the ship (Ross, 1847). Since then, records such as maps, ground surveys, aerial photographs and satellite images have provided direct evidence of the state of the cryosphere throughout the past century and have been invaluable for measuring changes in the glacier and ice shelf fronts.

2.2.3.1 Ice shelves

An overview of research on ice shelf changes north of 74° S is given in Cook & Vaughan (2010) along with a time-series of area change measurements for the past five decades for each of the ice shelves (Table 2.1). Results show that on the AP, the total area of ice shelf lost (from the earliest available records until 2009) was 28,117 km^2. This is a total of 18% of the original area of floating ice (where the ‘original area’ is based on the

earliest available areas for each ice shelf). Despite the episodic nature of the retreat of individual ice shelves, on the decadal timescale there has been a steady decline in total area of the Antarctic Peninsula ice shelves that began in the 1970s and continued to the present (Cook & Vaughan, 2010). The largest change in ice lost from all ice shelves combined, occurred between the 1970s and 1980s (from 1,621 km^2 ice gain in the previous decade, to 9,823 km^2 ice loss), with a slight decline in ice loss since the 1980s from 7,640 km^2 to 5,461 km^2 lost between 2000 and 2008/9.

Table 2.1: Decadal area changes of ice shelves on the AP.
(From Cook & Vaughan, 2010). Areas are in km^2.

Ice shelf	1950s	1960s	1970s	1980s	1990s	2000s	2008/9	Total change (km^2)	% remaining
Müller	78	69	60	64	45	44	40	-38	51
Jones	29	31	36	26	21	10	0	-29	0
Wordie	1420	1917	1538	827	906	312	139	-1281	10
Wilkins	16577			15986	14694	13663	11144	-5434	67
George VI	25984	25806	25249	24707	24260		24045	-1939	93
Bach	4798	4721	4825	4685	4582	4562	4487	-311	94
Stange			8286	8148	8030	7949	8022	-264	97
Prince Gustav	1632	1299	1328	1019	665	276	11	-1621	1
Larsen A	4021	3736	3873	3394	926	638	397	-3624	10
Larsen B		11573	11958	12190	8299	4429	2407	-9166	21
Larsen C		56131	58036	50241	51246	51593	50837	-5295	91
Larsen D		21716		22372	22345	21851	22602	886	104
Total Area	152246	151862	153483	143661	136020	129589	124128		
Total Change		-384	1621	-9823	-7640	-6432	-5461	-28117	82

Cook & Vaughan (2010) reported that over the past half-century, three of the twelve ice shelves north of 74° S (locations in Figure 2.2) have shown significant retreat, where less than 70% of the original area remains (Larsen B, Müller and Wilkins), and four have shown total disintegration, where 10% or less of the original area remains (Jones, Wordie, Prince Gustav, Larsen A). Five of the ice shelves (George VI, Bach, Stange, Larsen C and Larsen D) have more than 90% of their original area remaining and are showing no steady retreat. Larsen D is the only ice shelf to have shown overall advance,

albeit small, over this time period. The largest ice shelf, Larsen C, is still the largest contributor to the overall remaining ice-shelf area, and is currently at approximately 90% of its original area and shows no significant areal change.

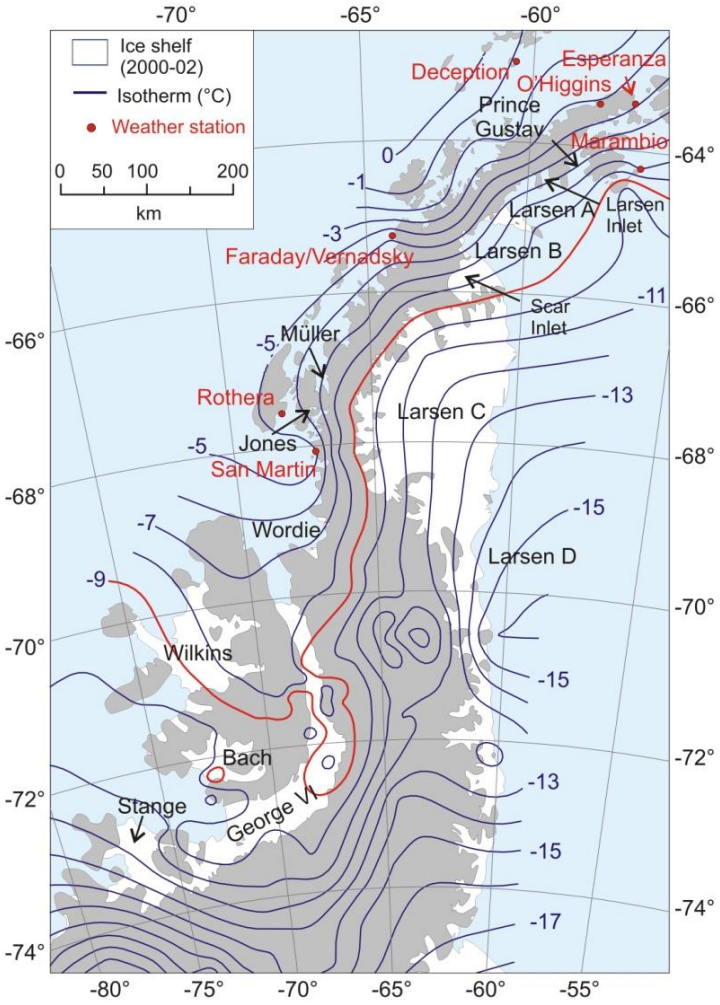

Figure 2.2: The thermal limit of viability of ice shelves.
The hypothesis was proposed by Morris & Vaughan (2003). Isotherms were produced from a database of mean annual surface temperatures, which show a strong climatic gradient from north to south and from east to west. The limit of viability for ice shelves is well approximated by the -9°C isotherm (in 2000), shown here in red. Ice shelf names are in black; weather station names are in red.

Despite the overall trend of retreat of ice shelves around the AP, individual ice shelves have shown considerable differences in the timing and course of their retreat. These variations result from the particular characteristics of both the local forcing experienced by individual ice shelves and their internal dynamics and specifics of their mass balance.

For example, Wordie Ice Shelf, the northernmost large (>1,000 km^2) shelf on the western AP, disintegrated in a series of fragmentations through the 1970s and 1980s, and was almost completely absent by the early 1990s. The Wordie break-up was followed in 1995 and 2002 by dramatic retreats of the two northernmost sections of the Larsen Ice Shelf (Larsen A and Larsen B) and the last remnant of the Prince Gustav Ice Shelf. A similar 'disintegration' event was observed in 1998 on the Wilkins Ice Shelf just south of 70° S (Scambos *et al.*, 2000), but much of the calved ice remained until 2008 when significant calving removed about 1,400 km^2 of ice. The ice bridge connecting the Wilkins Ice Shelf to Charcot Island disintegrated in early April 2009. In all these cases, persistent seasonal retreats by calving (Skvarca, 1993; Vaughan, 1993; Cooper, 1997) culminated in catastrophic disintegrations, especially for the Larsen A (Rott *et al.*, 1996; Scambos *et al.*, 2000) and Larsen B (Scambos *et al.*, 2003).

Specific mechanisms for ice shelf break-up have been much debated. The retreat of ice shelves around the AP have shown many reasons for them to become unstable, but the processes involved in the demise of the Larsen A and Larsen B ice shelves in particular are well-documented (see Cook & Vaughan, 2010). Satellite images revealed that prior to its disintegration in February 2002, the Larsen B ice shelf was subject to more extensive ponding of meltwater than in previous years (Scambos *et al.*, 2004; van den Broeke, 2005). As this water drained into pre-existing crevasses and filled them, the water pressure may have been sufficient to propagate the cracks through the entire thickness of the ice shelf (Weertman, 1973; Scambos *et al.*, 2003; van den Broeke, 2005; van der Veen, 2007). Banwell *et al.* (2013) found that there was synchronised drainage of all supraglacial lakes on the Larsen B ice shelf prior to collapse. Such self-stimulating behaviour can account for the sudden, widespread appearance of a fracture system capable of driving explosive break up. Satellite radar interferometry has been used with ice flow models to show that the ice shelf sped up considerably in the period before its final collapse because of weakening within its margins, perhaps as a consequence of this mechanism (Vieli *et al.*, 2007). Other ice shelves have had very different break-up mechanisms, for example surface melt had no influence on disintegration of Wilkins Ice Shelf, but rather buoyancy forces caused rift formation prior to break-up (Braun *et al.*, 2009).

The primary drivers of ice shelf break-up are subjects of much research. The retreat of ice shelves on the Antarctic Peninsula over the past century has been widely attributed to atmospheric warming (e.g. Mercer, 1978; Doake & Vaughan, 1991; Vaughan & Doake, 1996; Rott *et al.*, 1998; Skvarca *et al.*, 1999; Morris & Vaughan, 2003). One well-recognised theory is that the thermal limit of viability for ice shelves on the AP is north of the –9°C isotherm (Vaughan & Doake, 1996; Morris & Vaughan, 2003) and the ice shelf area-change results largely corroborate this theory as all five unchanging ice shelves lie south of the –9°C isotherm (in 2000) (Figure 2.2). The ice shelves that have retreated have generally followed a pattern that suggests a southerly migration of a climatic limit consistent with the observed warming trend of 3.5 ± 1.0°C /century (Morris & Vaughan, 2003). The Wilkins Ice Shelf is the latest and southernmost ice shelf to begin collapse, suggesting that the thermal boundary has continued to move southwards and may soon threaten the currently stable ice shelves on the southwest AP (Cook & Vaughan, 2010). Others have suggested different atmospheric factors can cause ice shelf break-up, such as an adjustment to negative surface mass balance (Rott *et al.*, 1998), or reduced fracture toughness due to a thickening temperate ice layer (Vaughan & Doake, 1996).

The role of atmospheric change as the primary driver of ice-shelf retreat is not, however, a view that is universally accepted, and recent research has suggested that ocean-driven ice-shelf thinning through basal melting could pre-condition ice shelves to retreat (Shepherd *et al.*, 2003; Holland *et al.*, 2010; Bindschadler *et al.*, 2011b; Rignot *et al.*, 2013). Rignot & Jacobs (2002) found that close to the grounding lines of large floating glaciers, the basal melting rate is positively correlated with thermal forcing, increasing by 1 meter per year for each 0.1 °C rise in ocean temperature. Where deep water has direct access to grounding lines, glaciers and ice shelves are vulnerable to ongoing increases in ocean temperature. Indeed, recent modelling has suggested that the basal melt of ice shelves would increase quadratically in response to ocean warming (Holland *et al.*, 2008). In the AP region ice shelves in the west are influenced by warm intrusions of Upper Circumpolar Deep Water currents and those in the east by Modified Weddell Deep Waters. Evidence shows that recent changes in Southern Ocean circulation have taken place such as warming water on the Bellingshausen Sea continental shelf, a

reduction of sea ice on the western side of the AP and a warming trend in intermediate and deep waters in the Weddell Sea (see Section 2.3.2). Each of these factors has an effect on basal melt and calving rates of ice shelves.

Important ocean-ice shelf interactions also include the formation of basal marine-ice (Holland *et al.*, 2009; Jansen *et al.*, 2010; Kulessa *et al.*, 2014) and tidal influence on melt (King *et al.*, 2011a; King *et al.*, 2011b; Mueller *et al.*, 2012). It has been hypothesized that marine ice formed by oceanic freezing currently stabilizes the Larsen C Ice Shelf (Kulessa *et al.*, 2014), and conversely the marine flow bands that developed beneath the Larsen B ice shelf could explain its instability (Holland *et al.*, 2009). Associated ocean modelling indicates that the incursion of warmer Modified Weddell Deep Waters into ice shelf cavities could prevent basal freezing and its stabilizing influence (Holland *et al.*, 2009). Tides can also directly or indirectly affect the mass balance and flow of floating ice, and possibly also play a role in iceberg formation. They influence ice shelf basal melt rate by contributing to ocean mixing and mean circulation as well as heat and salt exchanges with the ice shelf (Mueller *et al.*, 2012). In the ice sheet grounding zone, tides modify back stresses of inflowing glaciers, producing tidal variation in ice flow well upstream of the grounding line (King *et al.*, 2011a). This demonstrates that the ice shelf system is highly sensitive to relatively modest changes in forcing at its boundaries.

Research on ice shelf elevation change on the AP over the past 30 years using satellite radar altimeter missions showed that all ice shelves showed a net lowering between 1978 and 2003, with changes diverse between regions (Fricker & Padman, 2012). Fastest surface lowering occurred close to the fronts of George VI, Wilkins and Stange ice shelves, which may imply increasing basal melt caused by warming upper-ocean temperatures near the ice fronts. Regional differences suggest that surface lowering on Larsen C Ice Shelf are driven primarily by firn compaction while the western AP ice shelves are responding to changes in both surface mass balance and basal melt rates. Fricker & Padman (2012) theorise that synchronicity of change in elevation over time across the AP is driven by variations and trends in surface mass balance and firn compaction, while the more complex response of different ice shelf regions could be due to asynchronous ocean forcing.

In a recent paper by Rignot *et al.* (2013), the rates of melting and mass balance of all ice shelves around Antarctica were estimated for 2007-08, using surface accumulation, flow velocity and thinning measurements. It was found that basal melt outweighed calving flux rates, making ice shelf basal melting the largest ablation process in Antarctica. Half of the melt was found to come from 10 small warm-cavity ice shelves in the Southeast Pacific sector occupying only 8% of the area, which includes those on the south-west AP (George VI, Wilkins, Bach and Stange ice shelves). These are predicted and observed to be sensitive to ocean warming and circulation strength (Rignot *et al.*, 2013). Their results confirm the acknowledged theory that ice shelf melting is particularly high close to grounding lines (and also at the fronts of large ice shelves), with melting decreasing away from grounding lines and becoming negative (due to the accretion of marine ice). Their results indicate that basal melting accounts for a larger fraction of Antarctic ice-shelf attrition than previously estimated (Rignot *et al.*, 2013).

There is clearly a need for further long-term monitoring of changes in ice shelf fronts, velocity and thickness, along with more detailed information on ice shelf shape, seafloor topography, and atmospheric and oceanic forcing variability to understand the temporal variability and evolution of AP ice shelves. Existing knowledge on the processes driving ice shelf retreat around the AP is key to understanding the response of marine glaciers in the region.

2.2.3.2 Glaciers

The dramatic changes in ice shelves have attracted much interest, and have been the predominant focus for glaciological research in this region. There are a few glaciers that have been studied in detail, but the majority of smaller glaciers have been remarkably under-researched. Progress in AP glacier research is discussed here in terms of glacier frontal change, flow velocity and mass balance, all of which are vital for understanding the mass balance of the ice sheet as a whole.

A number of studies have been carried out to determine glacier retreat for a few specific regions on the AP, such as James Ross Island (Skvarca *et al.*, 1995); Marguerite Bay (Fox & Cooper, 1998; Smith *et al.*, 1998), and the South Shetland Islands (Park *et al.*,

1998; Calvet *et al.*, 1999; Simoes *et al.*, 1999; Braun & Gossmann, 2002; Arigony-Neto *et al.*, 2004). A wider study by Rau *et al.* (2004) showed how glaciers from six distinct regions across the AP changed in area from the period 1986-1990 to 2001-02. Their results showed a general trend of glacier recession on the AP, confirming the reported glacier area losses in each region from previous studies. Regional differences were apparent, such as larger area loss from regions in the northeast (E. Trinity Pen, James Ross Island) and southwest (Graham Coast, Loubet Coast, Marguerite Bay), and more stable glacier front behaviour in the northwest (W. Trinity Pen, Danco Coast) (Rau *et al.*, 2004). It was suggested that the differential behaviour of these glaciers could be explained by higher accumulation in the northwest offsetting the effect of rising air temperatures, and factors such as differences in local climatic regimes, internal thermal structures, flow dynamics and individual catchment characteristics (Rau *et al.*, 2004). Frontal geometry and terminus characteristics were also observed to influence the rates of retreat, whereby the highest retreat rates in all investigated regions are from glaciers with floating tongues (Rau *et al.*, 2004). Large regions of the AP were missing from this study, however, and with only two dates being considered the conclusions are inevitably limited. More recently a detailed study of glaciers on Trinity Peninsula and James Ross Island was carried out by Davies *et al.* (2012), in which all glacier attributes were recorded and assessed alongside frontal positions in 1988, 2001 and 2009. Similarly, it is with reservation that conclusions can be drawn about temporal patterns of advance and retreat when only two epochs are considered, but the authors noted a non-uniform response to atmospheric warming across the region.

The first comprehensive study of glacier change on the AP using all available frontal-position records was carried out by Cook *et al.* (2005). The changing position of the ice margin along the AP was mapped as part of the USGS *Coastal-change and Glaciological Maps of Antarctica* programme (Williams Jr & Ferrigno, 1998). As part of this programme, a complete time-series of ice-front changes was produced from all available sources (including maps, aerial photographs and satellite imagery) dating from 1940 to 2002. The results were published as three hardcopy maps, each with a detailed report (Ferrigno *et al.*, 2006; Ferrigno *et al.*, 2008, 2009) and digital data (Scientific Committee on Antarctic Research, 2005) and a summary of changes in 244 of the glaciers was

published in Cook *et al.* (2005). Analysis of the frontal-change data revealed that out of 244 marine glaciers that drain the ice sheet and associated islands, 212 (87%) had retreated since their earliest known position (which, on average, was 1953) (Figure 2.3). The other 32 glaciers had advanced, but these advances were generally small in comparison with the scale of retreats observed. The study suggested that the glaciers that advanced were not clustered in any pattern, but were scattered along the coast.

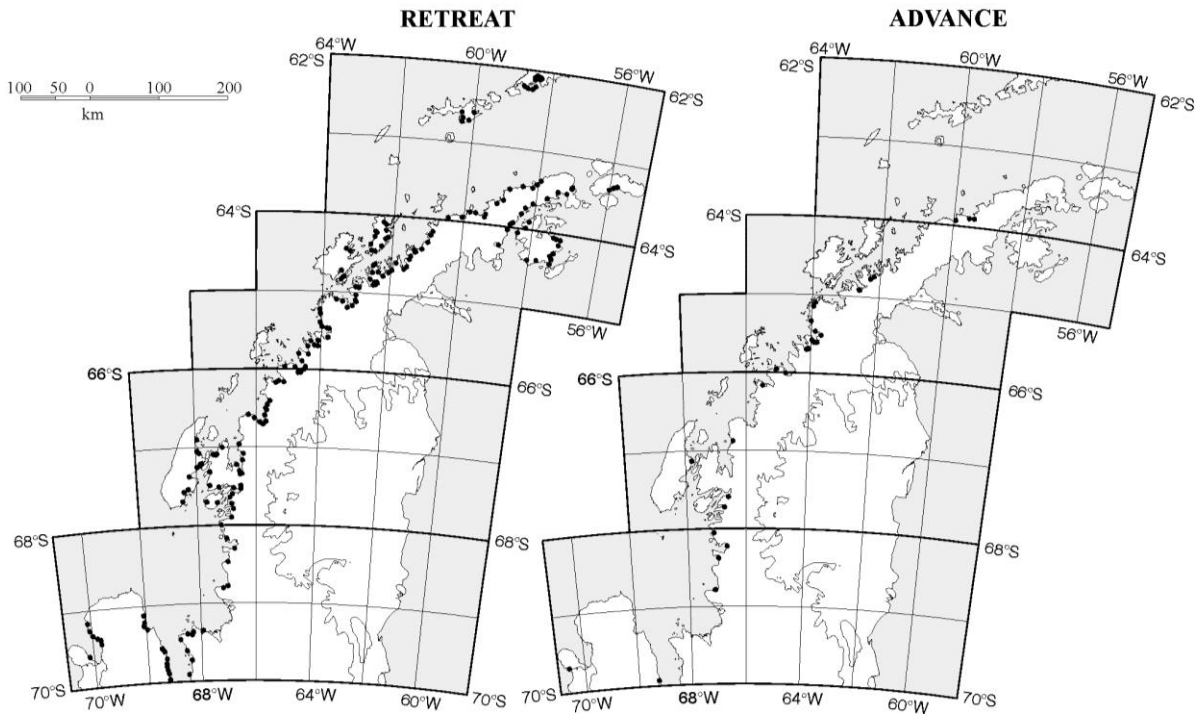

Figure 2.3: Spatial distribution of overall glacier length changes on the AP.
From Cook *et al.* (2005), showing spatial distribution of overall change in glacier length from earliest-latest records for 244 glaciers.

The number of records per glacier varied considerably, but even so, examination of the timing of changes along the peninsula indicated that from 1945 until 1954 there were more glaciers advancing (62%) than retreating (38%). After that time, the number retreating increased, with 75% in retreat in the period 2000-2004. The results indicated a transition between mean advance and mean retreat (Figure 2.4); a southerly migration of that transition at a time of ice shelf retreat and progressive atmospheric warming (Figure 2.5) and, most recently, a clear regime of retreat across the Antarctic Peninsula (Cook *et*

al., 2005). The study gave a summary of 244 glaciers and yet the dataset contained a wealth of information about ice front positions of other glaciers not analysed at the time.

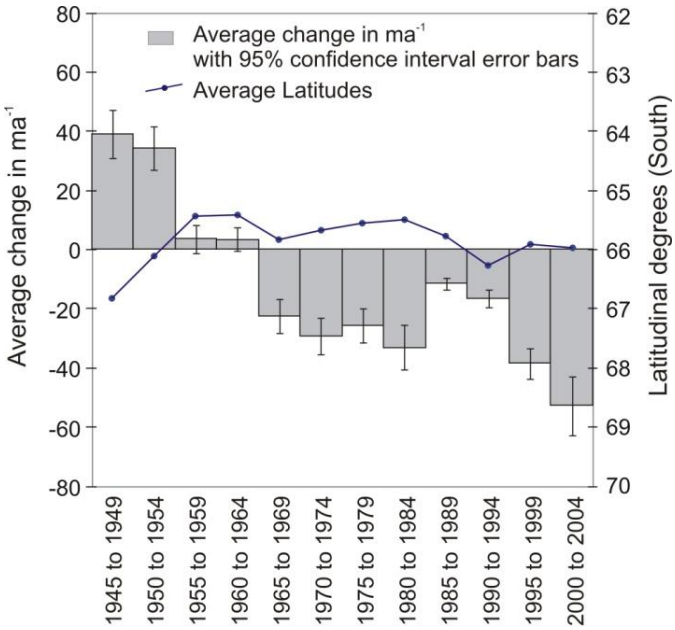

Figure 2.4: Glacier length change rates on the AP.
From Cook *et al.* (2005), showing temporal trends for 244 glaciers (average change rates).

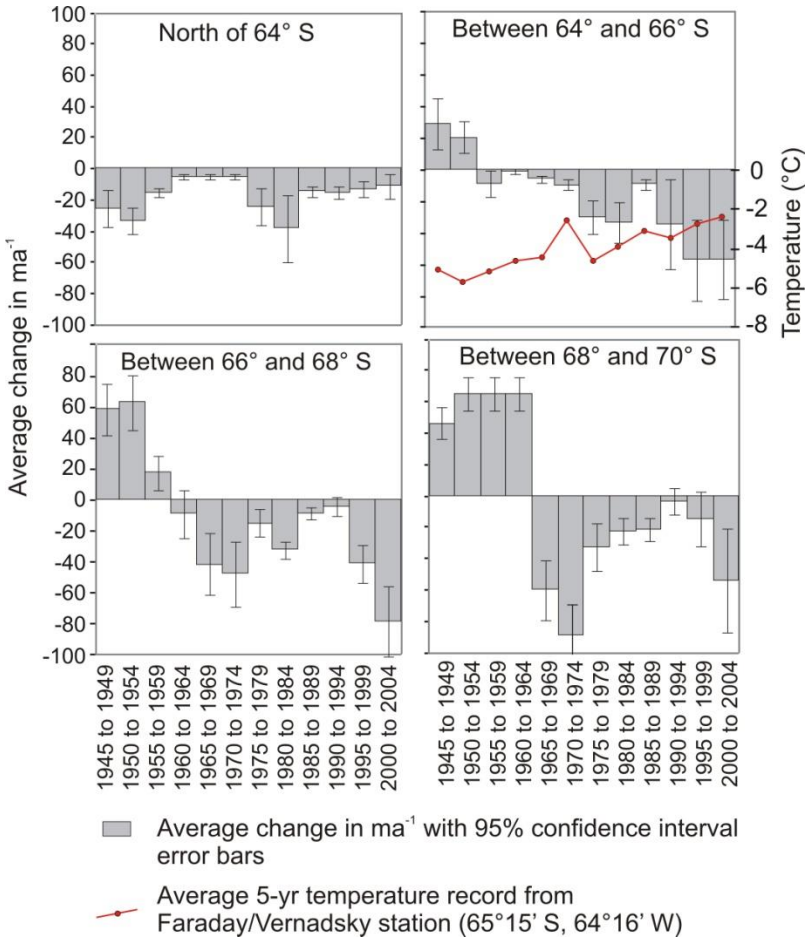

Figure 2.5: AP glacier length changes rates by latitudinal regions.
From Cook *et al.* (2005), showing latitudinal differences in glacier front change rates.

A subsequent study of flow rates of tidewater glaciers revealed a widespread acceleration of ice flow across the AP (Pritchard & Vaughan, 2007). This trend was attributed not to meltwater-enhanced lubrication or increased snowfall but to a dynamic response to frontal retreat and thinning. Measurements were taken from over 300 glaciers on the west coast through nine summers from 1992 to 2005. They showed that overall flow rate increased by 10% and that this trend is greater than the seasonal variability in flow rate. A comparison of measurements between the years 1993 and 2003 only (with profiles tailored to optimize coverage in just these years) revealed a slightly greater overall acceleration of 12.4 ± 0.9%.

Remotely sensed and modelled glacier speed and elevation measurements have revealed that ice shelves play an important role in controlling the dynamics and response time of the inland ice sheet. Ice shelves act as buttresses to grounded ice (Dupont & Alley, 2005)

and it is now widely recognised that when the floating ice is lost the tributary glaciers that feed them accelerate, thin and retreat rapidly, often for a sustained period of time. Acceleration of tributary glaciers following ice-shelf collapse has been shown for glaciers feeding the Prince Gustav Ice Shelf and the northern Larsen Ice Shelf (Rott *et al.*, 2002; De Angelis & Skvarca, 2003; Rignot *et al.*, 2004; Scambos *et al.*, 2004; Rott *et al.*, 2007; Hulbe *et al.*, 2008; Glasser *et al.*, 2011; Shuman *et al.*, 2011). For example, glaciers flowing into newly-collapsed sections of the Larsen Ice Shelf accelerated to speeds of 2 to 8 times the pre-disintegration flow rate (Rignot *et al.*, 2004; Scambos *et al.*, 2004). On the west coast, the glaciers flowing into the Wordie Ice Shelf also accelerated following ice shelf loss, and have been losing mass to the ocean ever since (Rignot *et al.*, 2005). One of these, Fleming Glacier, accelerated by about 50% during the period 1974-2003, and the region was losing mass at 18±5.4 Gt a^{-1}. A field campaign carried out in December 2008 using GPS measurements and an airborne laser survey confirmed that the glacier maintains these high flow rates and experiences a pronounced ice thinning (Wendt *et al.*, 2010). The combined estimate of mass loss (as of 2005) was 43±7 Gt a^{-1}, but a more recent assessment of the region suggests this rate has slowed to 28±45 Gt a^{-1} (Rignot *et al.*, 2008).

In addition to an increase in flow rates, glaciers undergo profound dynamic thinning following ice-shelf collapse. Much attention has been paid to the tributary glaciers of Larsen B in particular, where there has been ongoing glacier imbalance since the break-up event in 2002. Hulbe *et al.* (2008) undertook a detailed study of the glacial processes involved and demonstrated that the glaciers showed three different response patterns to break-up: prolonged frontal retreat accompanied by changes in ice speed and thickness (Crane and Jorum glaciers), frontal advance followed by retreat on accelerating and thinning glaciers (Green/Evans/Hektoria glaciers), and little or no change in front position and ice thickness (Pequod, Melville, Mapple glaciers). They conclude that the different patterns of behaviour demonstrate the importance of valley geometry, such as bed depth and ratio of valley width to ice thickness in mediating response to ice-shelf collapse (Hulbe *et al.*, 2008). It is not universally agreed whether dynamically-driven thinning causes enhanced calving and retreat or enhanced calving causes speedup, thinning, and retreat (Benn *et al.*, 2007). In the case of the Larsen B glaciers, however,

the range of responses to the same stress perturbation seems to favour the view that calving follows the lead of ice dynamics because under the same environmental conditions, calving was enhanced on some glaciers but not on others (Hulbe *et al.*, 2008).

Continued monitoring based on Moderate Resolution Imaging Spectroradiometer (MODIS) satellite imagery to track ice extent, and Advanced Spaceborne Thermal Emission and Reflection Radiometer (ASTER) and Satellite Pour l'Observation de la Terre Satellite (SPOT) digital elevation models (DEMs) plus Automatic Thematic Mapper (ATM) and ICESat laser altimetry to track elevation changes, has shown that the Larsen B tributary glaciers lost up to 160m in elevation during 2001–06, and thinning continued into 2009 (Shuman *et al.*, 2011). Elevation changes were small for the more southerly Flask and Leppard Glaciers, which are still constrained by a Larsen B ice shelf remnant. Rott *et al.* (2011) used TerraSAR-X radar imagery to measure ice calving fluxes in 2008-09, and compared these with velocity measurements from ERS SAR imagery in 1995 and 1999, when the same glaciers were in a balanced state. They found that in addition to significant thinning, ice flow acceleration gradually decreases in magnitude with distance upstream from the calving front. This suggests stress perturbation at the glacier front is the main factor for acceleration (Rott *et al.*, 2011). A further recent study has shown, through DEM differencing between 2002 and 2010/11, that mass loss of the Larsen B tributary glaciers continues unabated, with accelerating losses from Hektoria/Green glaciers (Berthier *et al.*, 2012). Continued thinning of glaciers in the Larsen A embayment to the north 14 years after ice shelf collapse suggests that mass losses of Larsen B tributary glaciers will continue for many years (Shuman *et al.*, 2011).

Differences in reconciled mass loss from Larsen tributary glaciers and mass loss estimated from GRACE measurements in the north AP suggest that substantial mass loss is also occurring from other glaciers in the region (Berthier *et al.*, 2012). This has been indicated in other studies, such as Röhss Glacier on JRI, previously a tributary of Prince Gustav Ice Shelf, which has continued to accelerate, thin and retreat since the ice shelf disappeared in 1995 (Glasser *et al.*, 2011), as have a number of smaller glaciers along north-east Trinity Peninsula (Scambos *et al.*, 2014). Indeed, Rignot *et al.* (2005) estimated that the recent annual mass loss from the glaciers of the northern Antarctic

Peninsula is sufficient to raise eustatic sea level by 0.1 mm a^{-1} (36 Gt a^{-1}), which is consistent with recent estimates of mass loss in the northern peninsula from changes in the gravitational field (Chen *et al.*, 2009).

Thinning rates of glaciers other than ice shelf tributary glaciers have been little studied. One recent study, however, used archival aerial photographs and photogrammetric methods to measure volume change of 12 glaciers distributed along the western AP over the past ~40 years (Kunz *et al.*, 2012). All observed glaciers show near-frontal surface lowering with an annual mean lowering rate of 0.28 ± 0.03 m a^{-1} at the lower portion of the glaciers, and an increased lowering of up to 0.6 m a^{-1} can be observed since the 1990s. In all 12 cases, surface lowering reduces to zero within 5 km of the glacier front at around 400 m altitude (Kunz *et al.*, 2012). In addition to these localized studies, an overview of thinning rates across the entire APIS has been given by Pritchard *et al.* (2009), who used ICESat laser altimetry to measure elevation differences around the grounding line of Antarctica for the period 2003-07. They found that slow-flowing ice caps and divides along the western AP coast are thickening at up to 1 m a^{-1}. This signal extends at high altitude to the AP's northern tip, contrasting strongly with the profound dynamic thinning of collapsed-ice-shelf tributary glaciers, which are thinning at some of the highest rates recorded in Antarctica (up to tens of metres a year) (Pritchard *et al.*, 2009). Glacier tributaries feeding the intact but thinning ice shelves of Larsen C and remnants of Larsen B, plus George VI Ice Shelf and the little-studied Larsen D also thinned at rates up to several metres per year. This behaviour confirms that glaciers are very sensitive to ice shelf thinning as well as collapse, and that shelf collapse leads not just to short-term and localized adjustment but to sustained, widespread and substantial loss of grounded ice from tributary glaciers. They conclude that although losses are currently partly offset by strong gains on the spine and western flank of the AP, numerous glaciers feeding intact ice shelves are also dynamically thinning (Pritchard *et al.*, 2009).

There is now ample evidence that although ice shelf disintegration does not contribute to sea-level rise in itself, with the loss of floating ice, the rate at which grounded ice discharges into the ocean is increased and thus the contribution to global sea level is amplified. In accordance with predictions, two studies showed that the major 2002

Larsen B ice shelf collapse was preceded by record high air temperatures, reduced sea-ice cover, and ultimately variations in the Southern Hemisphere Annular Mode atmospheric pressure system that are attributed to anthropogenic climate forcing (van den Broeke, 2005; Marshall *et al.*, 2006). Observed progressive north–south ice-edge retreats and glacier velocity increases, suggest that continued warming trends threaten remaining Antarctic Peninsula ice-shelf and glacier systems (e.g. Cook *et al.*, 2005; Pritchard & Vaughan, 2007). As discussed by Hughes (1975) and Mercer (1978) and more recently by Hulbe *et al.* (2008), understanding this effect and the response of individual drainage basins is critical to predicting ice-sheet mass-balance and sea-level changes under projected future warming conditions.

2.3 Recent changes in the climate and ocean around the AP

There is clearly a complex coupling between the atmosphere (temperature, radiation, precipitation and wind pressure), ocean (circulation, temperature and waves), and sea ice (concentration and thickness), each of which plays a crucial part in specific processes associated with mass balance of the APIS. Understanding the climatic and oceanographic setting and associated patterns of change are fundamental to determining how the glaciers and ice shelves may respond to future change. An overview of the climate and oceanography of the AP is covered in the following sections.

2.3.1 Climate

The climate of the AP is atypical of the rest of Antarctica for several reasons: it is long and narrow and therefore experiences a strong maritime influence; it has a rugged alpine topography and summer air temperatures that exceed 0 °C at sea level; it extends further north than any other region of the continent and so is subject to mid-latitudinal atmospheric influences (such as the warm moist air masses that occur along the west coast); and the spine of the AP, an unbroken mountain chain 1400-2000 m above sea level, forms a distinct climatic barrier, resulting in very distinct climate regimes on the east and west sides. The west and central regions have a maritime climate and are

exposed to the southern westerly winds, whereas the east side experiences a substantially colder and drier climate because of the northwards extension of cold continental air masses from the Antarctic interior (Reynolds, 1981). Conditions on the Antarctic Peninsula are strongly influenced by the atmospheric circulation to the west over the Amundsen and Bellingshausen Seas (ABS). A climatological centre of low pressure over the ABS drives a prevailing northwesterly flow onto the west coast of the Antarctic Peninsula, keeping it relatively mild (Vaughan *et al.*, 2003). These differences mean that the west coast of the Antarctic Peninsula is generally ~7 °C warmer than at similar latitudes and elevations on the east coast (Reynolds, 1981; Morris & Vaughan, 1994).

2.3.1.1 Air Temperature

A further difference between the AP and the rest of the continent is the rate at which its climate has changed over the past century. There is no evidence that overall atmospheric warming in continental Antarctica is significantly different from the global mean warming (0.6 ± 0.2 °C Century^{-1}) during the 20th century, whereas mean warming at the Antarctic Peninsula stations is substantially greater at 3.7 ± 1.6 °C Century^{-1}, with regional temperatures unprecedented over the last 2000 yr (Vaughan *et al.*, 2003). Temperature trends from the three stations with continuous records since 1979 all have trends an order of magnitude greater than the global mean, significant at the 10% level (Vaughan *et al.*, 2003). Stations with shorter records or summer-only records also show warming, although with low significance.

Warming has been particularly strong at Faraday/Vernadsky Station (Figure 2.2 for location) where mean annual temperature rose by +5.7 ± 2 °C Century^{-1}, significant at the 1% level. At this station, the changes in mean annual temperatures were dominated by winter warming, which increased by +11 ± 9 °C Century^{-1}, and although summer warming was significant at the 1% level, it was considerably less (+2.4 ± 1.7 °C Century^{-1}) (Vaughan *et al.*, 2003). This seasonal difference was also the case for other stations on the west coast, including Rothera station, which has a larger annual warming trend than Faraday/Vernadsky although the shortness of the record means that the trend is not statistically significant. The opposite trend is seen on the eastern side of the AP, where the largest changes have been during the summer season (Mayewski *et al.*, 2009).

Indeed, in recent decades the summer warming at stations in the northeast AP has exceeded that in the west: between 1965 and 2004 the summer near-surface temperature increase at Esperanza (northeast AP) and Faraday was 2.09 °C and 0.84 °C, respectively (Marshall *et al.*, 2006).

Significant changes in the atmospheric circulation of the AP region are thought to be the main cause of these summer temperature changes (Marshall *et al.*, 2006). The principal mode of variability in the Southern Hemisphere circulation is the Southern Annular Mode (SAM), which began a positive phase shift in the 1960s (Marshall, 2003). This has resulted in reduced pressures in the Antarctic region, with an increase in strength of the polar vortex and the circumpolar trough. These trends are statistically significant annually, and particularly in the summer season (Marshall *et al.*, 2006). The cause of the positive trend in the SAM is thought to be due to three principle external forcings: an increase in greenhouse gases (GHGs); a depletion of ozone in the stratosphere; and natural variability (Arblaster *et al.*, 2011). Natural variability may have played a role in driving these trends, since the recent summer temperatures in the east AP were similarly high in the 1960s (Marshall *et al.*, 2006), but several model studies agree that anthropogenic change, through a combination of GHGs and ozone depletion, is primarily responsible for the climatic shift (Arblaster *et al.*, 2011). Recent climate models show that even if ozone recovers in the stratosphere, ever-increasing GHGs will continue to change the SAM, and the resulting radiative forcing will produce large warming over most of the Southern Hemisphere by the end of the twenty-first century (Arblaster *et al.*, 2011).

One consequence of the increasing strength of the circumpolar vortex, is that the westerlies that encircle Antarctica and intrude on the west AP have intensified, bringing warmer air along the coast (Marshall, 2002). It has been proposed that the stronger summer westerly winds also reduce the blocking effect of the northern AP mainland and lead to the more frequent passage of air eastwards over the orographic barrier (Marshall *et al.*, 2006). The resulting climatological temperature gradient and formation of winds on the lee side (föhn winds) result in a summer temperature sensitivity to the SAM that is three times greater on the eastern side than the west (Marshall *et al.*, 2006). The SAM trend was calculated for 1979-2000 and those years with a particularly high SAM index

were identified as 1981, 1982 and 2000, and those with a low SAM index as 1985 and 1992 (Marshall *et al.*, 2006). A positive influence on summer temperatures of "high SAM" years was identified at all stations with the exception of Faraday/Vernadsky, which is thought to be too far south to be influenced positively by a stronger SAM. A summary of the main mechanisms in temperature variability in Antarctica showed that global warming and the SAM are the primary mechanisms involved in decadal trends on the AP, but the primary influence on interannual variability is as yet uncertain (Richard *et al.*, 2013). Although SAM has a strong influence on summer temperatures in most regions of the AP, the relatively small winter trends in the SAM suggests that other processes are playing a more dominant role in determining the region's temperature in winter (Marshall *et al.*, 2006).

Another recognised circulation change that may contribute to the rapid warming on the AP is the Semi-Annual Oscillation (SAO), a twice-yearly contraction/expansion of the circum-Antarctic low-pressure trough (CPT) (Holland *et al.*, 2010). The CPT moves south and deepens biannually, particularly during the spring season. The centre of low pressure experiences a longitudinal shift, with the trough centred on the Bellingshausen Sea in summer and further west in winter, with a deepening southward migration in spring (Holland *et al.*, 2010). Van den Broeke (2000) agrees that cycles in the SAO (at periods of 12 and 35 years) may have influenced Antarctic Peninsula temperatures.

2.3.1.2 Surface melt

Summer temperatures on the AP are close to melting so even a small degree of warming may have significant impacts. As mentioned in Section 2.2.3.1, temperature reconstructions have shown the migration southwards of the annual -9 °C isotherm over the past 50 years, which has been interpreted as a possible thermal limit of viability for ice shelves (Morris & Vaughan, 2003). There are also reports that summer warming has reduced snow cover (e.g. Fox & Cooper, 1998). Identification of temporal patterns of melt duration and onset are important for glacier studies for several reasons: variations in summer melt drive substantial inter-annual variability in glacier mass balance; the presence of meltwater may further accelerate the contribution of AP glaciers to sea level

rise; and increasing surface melt may trigger dynamic ice loss through acceleration of flow via enhanced basal lubrication (Barrand *et al.*, 2013b).

Vaughan (2006) investigated the annual increase in above-freezing conditions and how the warming trend has affected surface ablation over the APIS. Positive Degree Day (PDD) sums are a more useful measure than air temperatures alone, since they are the sum of 1-hourly (or six-hourly) temperatures in excess of melting point on days that are above 0 °C (Vaughan, 2006). Annual PDD sums were calculated for each austral melt season between 1950 and 2000, and although each station showed strong interannual variability, the trend was significant (Vaughan, 2006). The number of PDDs at Faraday/Vernadsky increased by 74%, with similar annual averages observed at Rothera and Bellingshausen. Using a parameterization of PDDs as a function of mean annual temperature, it was possible to estimate surface ablation, which was found to have doubled between 1950 and 2000 (Vaughan, 2006). This study has since been updated with melt records from the past decade, which shows that PDD sums were found to have increased by 95% in total from 1948 – 2010 (Barrand *et al.*, 2013b). The trends represent a strong and statistically significant increase in the annual duration of melting conditions on the AP at four of the six stations on the AP. Bellingshausen and Rothera stations PDD sums were below the long-term mean during seven cooler than average years since 2004. The largest positive trends in PDD sums were at the two stations on the east coast (Esperanza and Marambio). Long time series trends were strongly correlated between stations on either side of AP, indicating that these trends are likely to exist throughout the northern AP (Barrand *et al.*, 2013b). In addition to station records, melt onset and duration patterns detected from the scatterometer onboard the QuikSCAT satellite were analysed for the period 1999-2009 (Barrand *et al.*, 2013b). Melt patterns were typically more variable over ice shelves than grounded ice, but no evident link was identified between early melt season onset and ice shelf retreat or breakup events. However, these events were found to coincide with longer melt season durations, consistent with the findings of previous research (Barrand *et al.*, 2013b).

2.3.1.3 Sea-ice

All the stations along the west coast of the AP have shown greatest warming during the winter. Winter is the time of year when air–sea-ice feedback mechanisms are most effective and when a small reduction in sea-ice can have a large impact on the air temperatures (Turner *et al.*, 2005a). However, the relationship between the temperatures at coastal stations and sea-ice off the coast is complex and varies around the continent, and it is only on the western side of the Antarctic Peninsula that there is a demonstrated correlation between winter temperatures (at Faraday/Vernadsky station) and the extent of sea-ice (in the Bellingshausen Sea to the west of the station) (King, 1994). Cold winters in this region are almost invariably associated with extensive winter sea-ice (King & Harangozo, 1998). There is evidence of greater sea-ice cover in the 1950s and 1960s which, it has been suggested, may have been linked to weaker/fewer storms to the west of the peninsula and greater atmospheric blocking (Turner & Overland, 2009). Weaker northerly winds would have allowed the sea-ice to advance further north during the winter, giving colder temperatures along the western side at this time. Since then, there has been a progressive reduction in sea-ice extent in the Bellingshausen Sea (Turner & Overland, 2009).

Reliable satellite-derived sea-ice extent and concentration data only became available in the late 1970s, but since that time the mean winter temperature at Faraday/Vernadsky has been increasing and the sea-ice concentrations to the west of the AP decreasing (Turner *et al.*, 2005a). Variations in sea-ice extent and duration are geographically complex, however, and since other regions around the continent have shown an increase in sea-ice since 1979, winter-season warming is unlikely to be a result of changes in sea-ice universally (Zwally *et al.*, 2002a). Vaughan *et al.* (2003) found that the zone of greatest negative trend in sea-ice duration (>5 days per year) coincides with the two stations showing the strongest warming trend (Faraday/Vernadsky and Rothera), and showed that in addition to an interannual correlation there is a decadal relationship between sea-ice duration and air temperature.

Whilst the changes in sea-ice may be attributed to the increasing winter temperatures, it could be that the connection is causal and is an expression of regional feedback, similar

to that of the snow albedo effect (Vaughan *et al.*, 2003). Sea-ice suppresses the transfer of heat from the ocean to the atmosphere during winter, and increases regional albedo; when absent, the opposite is true. Vaughan *et al.* (2003) suggest that this may be the case for the wAP, with an initial impetus from warming air temperatures.

A more recent study on sea-ice trends between 1985 and 2010 confirmed that the region with the largest negative trend in annual sea-ice concentration from around the continent is the Bellingshausen Sea (Bintanja *et al.*, 2013). The study showed that this coincides with a statistically significant increase in sea surface temperature (SST). Another study found a thickening of sea-ice in the ABS sector, but the sea-ice volume trend showed overall volume loss during the summer due to the decreases in sea-ice extent (Kurtz & Markus, 2012).

The Weddell Sea (WS) to the east of the AP has very distinct sea-ice patterns. Much of the sea is covered in sea-ice for most of the year, and some of the thickest sea-ice surrounding the continent resides in the western WS (Kurtz & Markus, 2012). Sea-ice thickness trends from 2003 to 2008 show that thinning was prominent in this region, both perennially and during the Spring. As with the ABS, volume change showed negative trends, due to both thinning and retreat at the sea-ice edge (Kurtz & Markus, 2012). Recently it was demonstrated that surface wind-driven trends in ice advection can be linked to regional sea-ice concentration trends (Holland & Kwok, 2012). In the WS, ice circulates around the WS embayment following the contours of atmospheric pressure, leading to maximum ice export in this region. A reduction in sea-ice concentration in the WS in particular seem to be caused by decreased northward advection, closely linked to reduced wind-stress (Holland & Kwok, 2012).

2.3.1.4 Precipitation

On the west coast, in addition to increasing winter temperatures, there is evidence of an increase in winter precipitation. There has been a statistically significant increase in the number of reports of winter precipitation at Faraday station since 1956 (Turner *et al.*, 1997). The annual total of precipitation days at the station has also been increasing, at +12.4 days decade^{-1}, with the greatest increase taking place during the summer and

autumn (Turner *et al.*, 2005b). The number of precipitation days at Faraday is dictated to a large extent by the air masses that arrive at the station: moist north-to-northwesterly air masses result in a large number of precipitation days. As the precipitation levels are affected by wind direction it can be a more direct measure of air mass origin than temperature or sea-ice (Turner *et al.*, 2005b). It is likely that increases in precipitation levels (and also the decreasing sea-ice concentrations) are related to the change in the number of cyclones approaching from the Bellingshausen Sea, which implies changes in atmospheric circulation (Turner *et al.*, 1995). The seasonal trend is thought to be related to the change in the nature of the SAM. Ice cores taken from James Ross Island and from the far south of the AP have shown significant variability in snow accumulation over the past century (Miles *et al.*, 2008), but ice core measurements from a site in the south-west AP (Gomez: 73.6° S, 70.4° W) revealed a doubling of snow accumulation since the 1850s, with acceleration occurring in recent decades (Thomas *et al.*, 2008). Analysis alongside the primary modes of atmospheric circulation variability showed there was a strong, temporally stable and positive correlation of snow accumulation with the SAM, which also may have an influence on decadal timescales (Thomas *et al.*, 2008).

Since the AP has complex topography, station records and ice core data may not be representative of the wider area, so Miles *et al.* (2008) undertook analysis of European Centre for Medium Range Forecasts Reanalysis (ERA40) data and presented regional trends in accumulation for the period 1979-2001. The results reveal that accumulation variability on the AP is primarily related to pressure in the circumpolar trough and secondly, to temperature variability. Accumulation increase is particularly strong in autumn months, which is the season when the SAM has become most positive in recent decades, suggesting stronger westerly winds have caused an increase in orographic precipitation along the west Antarctic Peninsula (Miles *et al.*, 2008). The ERA40 data was further analysed by Marshall (2009), to assess annual and semi-annual differences and it was found that the north-west AP had a stronger seasonal variability in precipitation due to its location within the CPT. There was a marked change in the magnitude of the annual cycle of precipitation between the 1980s and 1990s on the west coast, where a decrease in winter precipitation is associated with a weaker and smaller

Amundsen Sea Low, which in turn is influenced by the oceanographic-climatic cycle, the El Niño Southern Oscillation (ENSO) (Marshall, 2009).

As was discussed in Section 2.2.2.3 on 'Mass Balance of the APIS', glacier surface mass balance studies must not simply consider precipitation but also the effect of snow drift and sublimation. There is a highly nonlinear relationship between wind speed and blowing snow transport, making it particularly difficult to distinguish these components (King *et al.*, 2004). A regional atmospheric model has been used for the period 1987-1993 to study these elements and it was concluded that precipitation was greatest on the northwest slope of the AP and that surface sublimation and wind transport of snow over the grounding line toward the sea are 9% and 6 ± 1% of the precipitation, respectively (Van Lipzig *et al.*, 2004). Upward motion of air is present on the western side of the orographic barrier, resulting in high precipitation.

Evidence from station records, ice core measurements and ERA40 regional analysis has shown a strong positive relationship between variability in the SAM and both temperature and precipitation in the AP, particularly along the west coast. Increasing westerlies and decreasing pressures in the CPT have also caused a negative trend in sea-ice extent alongside a positive trend in accumulation. Atmospheric circulation is strongly coupled to changes in ocean circulation patterns, so these will be considered in the following section.

2.3.2 Ocean

The Antarctic Circumpolar Current (ACC) flows clockwise in a broad zone around Antarctica, carrying Circumpolar Deep Water (CDW), and is separated from the coast by the katabatic-driven west-flowing Antarctic Coastal Current (Figure 2.6). The north–south landmass of the AP acts as a barrier to this flow and so the ACC runs along the edge of the western AP (wAP) continental shelf before being deflected to the north through the Drake Passage. The ACC is thought to play a fundamental role in the climate of the west coast of the AP and is linked to changes in both atmospheric and oceanic conditions between the Pacific, Atlantic and Indian Oceans (Simmonds, 2003). The eastern side of the AP has a very different oceanic regime, dominated by the cold deep

waters stemming from the continental ice margins and the large Weddell Sea sub-polar gyre, and is protected against the effects of the ACC and ENSO by the barrier of the AP. The oceans on each side of the AP will be addressed separately due to their considerably different characteristics.

2.3.2.1 West Antarctic Peninsula

Some areas of the wAP experience intrusions of CDW, which is a relatively warm (> 1.5 °C), salty (~34.7 ‰), intermediate depth (200 m and below) water mass that is derived from modified North Atlantic Deep Water (Klinck *et al.*, 2004). These intrusions bring heat and salt onto the shelf. CDW is substantially warmer than typical Antarctic surface waters and where mixing occurs, intrusions of CDW along the western AP shelf are characterized by surface waters that are above freezing in winter. In places, the flow of the ACC drives the CDW onto the shelf, particularly along the troughs that formed the paths of palaeo-ice streams (Smith & Klinck, 2002; Martinson *et al.*, 2008).

Once on the shelf, the CDW is modified by interaction with the overlying water masses, and the associated vertical transfer of heat, salt, and nutrients is significant for the properties of the upper ocean of the wAP shelf (Martinson *et al.*, 2008). The water that overlies CDW at the wAP is Antarctic Surface Water, which comprises a mixed layer in winter but becomes stratified in summer because of heating and freshening from insolation and ice melt, respectively. It is believed that shallow regions near the coast may be especially important for vertical mixing between these water masses, driven by processes such as coastal upwelling and the influence of internal tides and rough bathymetry (Wallace *et al.*, 2008).

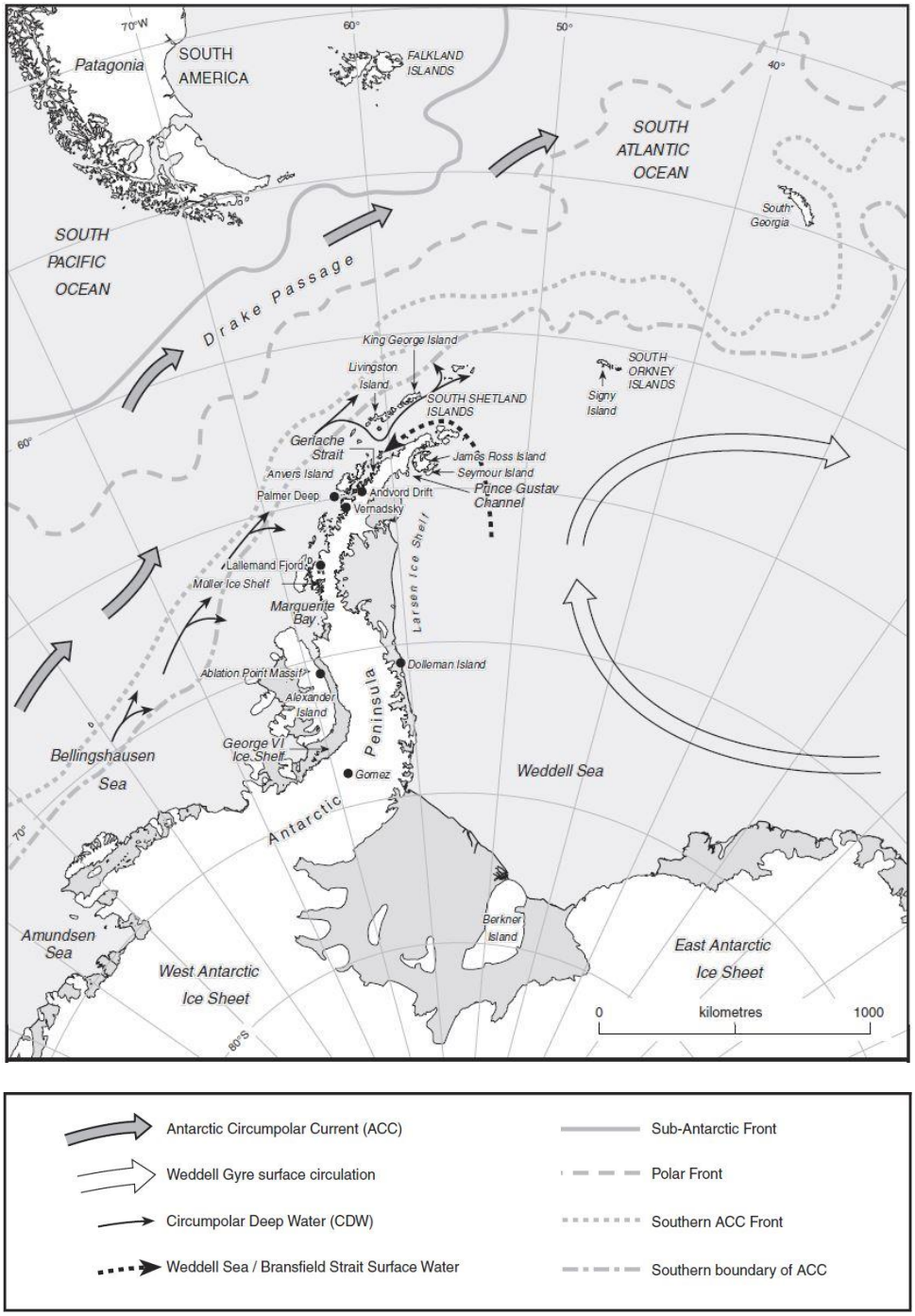

Figure 2.6: Ocean circulation patterns surrounding the AP.
From Bentley *et al.*, (2009)

A recent increase in CDW upwelling along the wAP is associated with winter SSTs greater than 0 °C, reduced sea-ice extent and duration, increased cyclogenesis, and ENSO variability (Martinson *et al.*, 2008; Stammerjohn *et al.*, 2008). A combination of decadal warming of the CDW (Gille, 2002; Böning *et al.*, 2008; Gille, 2008; Shevenell *et*

al., 2011) and an acceleration of its on-shelf flow, has been linked to stronger winds and the intensification of the SAM (Martinson *et al.*, 2008), demonstrating that changes in the CDW are coupled with changes in the wAP climate. The changes are consistent with a southward shift of the ACC (Gille, 2008). Some climate models suggest that the ACC shifts south in response to the southward shift of the westerly winds that are driven by enhanced greenhouse forcing and the positive trend in the SAM (Turner *et al.*, 2009).

The role of upper ocean processes in wAP climate change has also been investigated, and it has been shown that summer temperatures of the near-surface ocean rose here during the second half of the twentieth century by well over 1 °C, alongside a summer salinification of the upper ocean (Meredith & King, 2005). It was argued that these changes were induced by the trends in the atmospheric circulation, temperature and related changes in the sea ice, but also that they acted as positive feedbacks to enhance and sustain the atmospheric warming (Meredith *et al.*, 2010). It was noted that the role of the upper ocean (storing heat in the summer and releasing it back to the atmosphere in winter) will shift the seasonal phase of any long-term atmospheric trend, and hence could explain at least some of the marked seasonality in the wAP atmospheric warming (Meredith *et al.*, 2010).

Freshwater contributions to the wAP are also changing, such as an increase in glacial meltwater (both from extended annual melt duration and from glacier and ice shelf retreat), increased precipitation occurring as rainfall, and greater sea-ice melt (Meredith *et al.*, 2013). High levels of freshwater are found close to the coast, although there has been a temporal decline in the upper ocean further from the coast, likely caused by greater mixing of winter water layers. The southward flow of the AP Coastal Current (APCC) is thought to be at least partly driven by freshwater being released from land at the wAP and is therefore seasonal in nature. The strongest flow was seen to occur to the west of Adelaide and Anvers Islands, most likely due to the regular coastal topography, and the high concentrations of freshwater may be due to the proximity to higher levels of precipitation. In regions close to Charcot Island in the south of the AP high levels of freshwater are thought be due to accretion of glacial discharge brought with the APCC as it advects southwards (Meredith *et al.*, 2013). The authors state that reliable modelling of the physical circulation of the WAP requires accurate representations of precipitation and

glacial discharge, and with glacial discharge being the dominant freshwater source this will require close monitoring. Decadal trends in the wAP freshwater system concurrent with atmospheric warming mean that acceleration in flow of the APCC and increase in its seasonality are likely (Meredith *et al.*, 2013). These changes will have implications for the wAP climate and regional ecosystem.

2.3.2.2 Weddell Sea Sector

To the east of the Antarctic Peninsula, the ocean circulation patterns are very different, with waters significantly colder than those to the west of the AP. The shape of the large Weddell Sea embayment gives rise to a sub-polar gyre, which brings relatively warm, salty circumpolar water (Warm Deep Water) south from the ACC towards the Antarctic continent, and transports colder, fresher waters northward. The transformation of this source water mass is one of the major climatic processes in the Southern Hemisphere, affecting and involving the ocean, atmosphere and cryosphere (Turner *et al.*, 2009).

The water on the Antarctic continental shelves is typically fresh due to the addition of sea-ice melt, glacial ice melt from the Antarctic ice sheet and floating ice shelves, and from precipitation (Nicholls *et al.*, 2009). This freshening contributes to the formation of cold, dense WS Bottom Water, which can only escape the Weddell embayment by mixing with the saltier water above it, forming the WS Deep Water. The variability in the deep water masses seems to be relatively small in comparison to those of the surface water masses, but it is important because the large volume of the deep waters can store significant heat quantities or dissolved substances even if the changes in property is only minor (Turner *et al.*, 2009).

Robertson *et al.* (2002) noted a warming of 0.3 °C for the Warm Deep Water layer of the Weddell Gyre, which occurred over the period 1970s to 2000, and it was argued that this was due to anomalous intrusions of water from the ACC (Fahrbach *et al.*, 2004). A polynya (a persistent gap in the sea-ice) that formed in the 1970s caused a loss of heat from the ocean and a shift in ocean processes, which may have formed due to a change in the SAM (Gordon *et al.*, 2007). Although the SAM has been observed to modify the position of the southern front of the ACC and the sea-ice extent, its influence on the

Weddell Sea Gyre water mass properties and circulation are not well known and are subject to further research (Robertson *et al.*, 2002).

The scarcity of long-term observations, together with persistent sea-ice throughout the year in the Weddell Sea makes monitoring of deep ocean temperatures difficult, and although warming signals have been recognised in the WS Bottom Water and WS Deep Water, the causes (and effects) of these trends are still to be determined (Mayewski *et al.*, 2009). Patterns of sea-ice drift indicate that wind stress may be causing changes in the upper ocean (Holland & Kwok, 2012), and models suggest that modified WS Deep Water is affecting basal melt processes beneath ice shelves, causing both melting and re-freezing of marine ice (Holland *et al.*, 2009). The Warm Deep Water temperatures remain significantly colder than water to the west of the AP, and research has shown that the thinning of ice shelves on the margins of the Weddell Sea is attributed to atmospheric warming rather than oceanic basal melt (Pritchard *et al.*, 2012).

2.3.3 Ocean-Atmosphere Interactions

The AP is affected by a number of modes of climate and oceanic variability, including low-high latitude links (teleconnections), which operate on different timescales. One previously mentioned mode is the El Niño Southern Oscillation (ENSO), which is the furthest reaching climatic cycle on Earth on decadal and sub-decadal timescales (Mayewski *et al.*, 2009). An El Niño event is when warmer ocean surface temperatures occur along the west coasts of South America, at an interval of approximately every 2-7 years and lasting between 9 months to 2 years. The opposing circulation event is La Niña, which lasts 1-3 years, and for the remaining time the circulation conditions are neutral (Turner, 2004). It is related to the atmospheric component, the Southern Oscillation (SO), which, since the late 1970s has shifted towards a more negative phase, associated with more frequent and stronger oceanic El Niño events (Mayewski *et al.*, 2009).

The ENSO has a profound effect not only on the weather and oceanic conditions across the tropical Pacific, where it has its origins, but also in the South Pacific, with effects as far south as the AP and the surrounding seas. During an El Niño event the Amundsen-

Bellingshausen Sea (ABS) region shows anomalously high pressures whilst the Weddell Sea shows somewhat lower pressures (Turner, 2004). Meredith *et al.* (2004) report the impacts of the 1997-98 ENSO event on the Marguerite Bay area, on the mid-wAP, and found that the winter of 1998 was characterized by low sea-ice concentrations, high atmospheric temperatures and a high frequency of northerly winds. This, and additional studies (e.g. Harangozo, 2000; Lee *et al.*, 2010), suggest that following the peak of a warm ENSO event, the coastal AP shows a profound response to the strengthening Amundsen-Bellingshausen low pressure centre. Following the ENSO in 2009-10, the ABS region experienced record warming (Lee *et al.*, 2010). Shevenell *et al.* (2011) suggest that the wAP atmosphere and ocean show the strongest response to ENSO of any region outside the tropical Pacific. If ENSO increases in strength and frequency, as predicted for future climatic warming, there would be significant implications for Antarctic ice-sheet stability, ocean–atmosphere exchange of heat and CO_2, and sea-level rise (Shevenell *et al.*, 2011).

There are also interactions between the SAM and ENSO, which further complicate the linkages of the tropical and high-latitude climates. It has been demonstrated that the decadal variability of ENSO is governed by the phase of the SAM, such that when they are both in the same phase (i.e. El Niño occurring with negative phases of the SAM; La Niña occurring with positive SAM phases) the teleconnection is amplified, and when they are out of phase (i.e. El Niño occurring with positive phases of the SAM) the teleconnection is dramatically weakened (Mayewski *et al.*, 2009). Beginning in the 1990s, the SAM became more positive during summer/autumn, which has been implicated in asymmetrically strengthening the high latitude response to La Niña over El Niño events, and together help to explain the wind-driven sea ice decreases in the greater wAP region (Stammerjohn *et al.*, 2008).

A further coupled ocean-atmosphere interaction that must be mentioned is the Antarctic Circumpolar Wave, which circles the Southern Ocean in approximately 8 years and is thought to be associated with ENSO (White & Peterson, 1996). It moves eastwards with prevailing currents and consists of two ridges and two troughs, causing changes in sea level pressure, temperature and sea-ice extent. It is suggested that the Antarctic Circumpolar Wave could be a factor in the transmission of ENSO signals to high

southern latitudes, although it is not known to what extent the signal is stable in the long term since records are relatively short (Turner, 2004).

Finally, a new hypothesis to explain the ocean warming and sea-ice redistribution around the AP in winter has recently been proposed. Using both observational and reanalysis data, Li *et al.* (2014) suggest that the sea surface warming is related to the Atlantic Multidecadal Oscillation. A teleconnection between the north and tropical Atlantic and Antarctica has been identified that reduces the surface pressure in the Amundsen Sea on decadal timescales, and contributes to a dipole-like sea-ice redistribution between the Ross and Amundsen–Bellingshausen–Weddell seas, and to the Antarctic Peninsula warming. Although the Atlantic Multidecadal Oscillation is a well-recognised mode of global variability, its signal was not identified in Antarctic warming records until now. The authors state that although Pacific sea surface temperature variability—the ENSO in particular—dominates the inter-annual variability of Antarctic climate, the Atlantic appears to be a dominant driver of Antarctic climate on multi-decadal timescales (Li *et al.*, 2014).

2.4 Global glacier monitoring and applications to the AP

Before considering changes in glaciers on the Antarctic Peninsula, there is much to be gained from literature about glacier-changes elsewhere, to determine both the value of, and the methods used in this field of research. Quantifying glacier fluctuations world-wide are vital for two main reasons. Firstly, it is well recognised that glacier changes contribute to variations in sea level; indeed, glaciers have been one of the main contributors to sea-level change during the last century (Gregory *et al.*, 2013). Secondly, glaciers are key indicators of climate change (IPCC, 2007, 2013); they leave observable changes in the landscape and therefore past records of glacier change provide a long-term context for recent climatic changes (Leclercq *et al.*, 2014). It is clear that by observing and monitoring glacier changes, we can learn more about overall global trends, and about how glaciers respond to local and regional climate regimes.

The most commonly recorded properties for measuring glacier fluctuations are length, area and mass balance (Barry, 2006). Since the start of internationally coordinated glacier-change measurements in the late 19th century, the World Glacier Monitoring Service (WGMS) has accumulated 36,000 length change observations and 3,400 mass balance measurements for approximately 1,800 and 230 glaciers, respectively (Zemp *et al.*, 2009). The dataset is strongly biased towards the northern hemisphere and Europe, however, and only 30 glaciers have an uninterrupted series going back to 1976.

2.4.1 Mass balance monitoring

Glacier mass balance is the direct response to climatic conditions and therefore regular monitoring facilitates both climate modelling and determination of regional ice volume changes. Mass balance records include those determined by direct methods such as repeated measurements at stakes and snow pits or photogrammetric techniques, and indirect methods such as geodesy, relative to a fixed reference surface such as bedrock (Barry, 2006). Recently it has become easier to measure mass balance using satellite stereo-imagery, but in terms of long-term measurements there are still only a small proportion of glaciers world-wide that have records spanning the past few decades. In the Antarctic Peninsula, there are no *in situ* records of mass balance for individual glaciers in the region prior to the advent of surface elevation sensors such as ASTER, ICESat and SAR in the early 2000s. As a result, confidence in the AP component of glacier contributions to sea-level rise has been weak (e.g. Radic & Hock, 2010, 2011), and calculations of glacier mass change have either inferred AP mass balance from global averages (Leclercq *et al.*, 2011) or omitted Antarctic peripheral glaciers altogether (e.g. Gregory *et al.*, 2013).

One resource that can be used to measure change in mass balance in the AP is archival vertical aerial photography. This is restricted to glaciers that have complete coverage and since early aerial surveys did not photograph glaciers in a systematic fashion, only parts of the AP region can be analysed. In cases where photographs do exist, constraints associated with modelling surface elevation include: the image quality of the historic photographs; cloud-cover; photogrammetric problems associated with snow-cover; only

partial glacier coverage and limited repeat coverage. Until recently, one major issue was the lack of ground-control points for georeferencing the photographs. One pilot study using aerial photographs taken at five dates between 1947 and 2009, showed that historic photos could be linked to a newly acquired, highly accurate photogrammetric model adjusted through GPS positioning of the camera (Fox & Cziferszky, 2008). Since then this method has been used to calculate surface elevations for 12 glaciers on the AP, based on aerial photographs obtained between 1948 and 2005 (Kunz *et al.*, 2012). A programme to measure volume change of further glaciers with the same approach is currently underway. Aerial photographs are clearly a valuable resource for calculating mass balance change that should be exploited for future long-term monitoring of glaciers in the region.

The advent of ASTER spaceborne stereo imagery in 2001 has enabled more recent surface monitoring and, along with ICESat laser altimetry elevation differencing methods, mass change for glaciers in the northern AP have been recently quantified for the period 2001-2010 (Scambos *et al.*, 2014). Although these recent studies are advancing our knowledge of mass balance, long-term (in this context the post-instrumental period, or the past century) mass balance estimates are currently limited to a small percentage of the glaciers.

2.4.2 Glacier-length monitoring

Although glacier termini have a time delayed response to climate signals, glacier length records are nevertheless extremely valuable for understanding glacier behaviour. Changes in frontal positions are an easily measured signal of climate change, and counter to the paucity of mass balance data, glacier length is the property that has been the most abundantly recorded in the history of glacier monitoring (Leclercq *et al.*, 2014). For many glaciers around the world, length changes prior to the start of measurements can be derived from historical, geological and biological evidence. Where long-term mass balance records are not available, it is possible to extract details of climate change from length records using principles of glacier dynamics. For example, Hoelzle *et al.* (2003)

derived changes in glacier mass balance (δb) from length changes for 90 glaciers worldwide (and a separate set of 68 Swiss glaciers), via the relation:

$\delta b = b_T \, \delta L / L_o$

where L_o is the original length, δL is the change in length and b_T is the balance (ablation) at the terminus (Hoelzle *et al.*, 2003). Oerlemans (2005) also noted that long-term glacier records have often been overlooked, so a method was developed to construct a temperature history directly using length records for 169 glaciers world-wide, using a linear inverse model. More recently, length records were used to estimate the glacier contribution to sea-level rise since 1850, by calculating a globally representative length signal from 197 length records from all continents and calibrating this with mass-balance observations for the period 1961–2000 (Oerlemans *et al.*, 2007).

A dataset has now been compiled consisting of long-term glacier length changes of 471 glaciers world-wide, all of which have records that start before 1950 (Leclercq *et al.*, 2014). The goal was to reconstruct the glacier contribution to sea-level rise based on this updated, uniform dataset, using the methods applied by Oerlemans *et al.* (2007). It includes all perennial surface land ice masses, except for the ice sheets of Greenland and Antarctica (although glaciers not attached to the ice sheets are included). Since retreat of calving glaciers forms a substantial part of the glacier contribution to sea-level rise (Cogley, 2009), the length records of 85 tidewater glaciers and 19 glaciers calving in fresh water (mostly outlets of the Patagonian Icefields) are included. The glacier length changes were largely acquired from the WGMS records, and occur on all continents and virtually all latitude zones. There is an imbalance, however, because glaciers are strongly clustered in the major mountainous regions, and yet there are relatively few records from regions with large glacier coverage (e.g. Canadian Arctic, Alaska, islands of the Arctic Ocean, Antarctic periphery). The paper gives an up-to-date overview of regions that have plentiful records and those where there are significant gaps.

Despite the large variations in data quantity (both regionally and temporally), the available glacier length records show a coherent global glacier signal, of little length change in the 17th to mid-19th century, followed by a general retreat that continued throughout the 20th century (Leclercq *et al.*, 2014). Despite certain general global and

regional trends, the fluctuations of individual glaciers vary strongly, indicating the importance of understanding glacier characteristics in different climatic settings. The authors found that, in general, calving glaciers retreated more than land terminating glaciers (although the average relative change is similar for both glacier types) and that steep glaciers are less sensitive to climatic change than glaciers with a gentle slope.

The world-wide glacier fluctuation dataset includes a small sample of glacier length records for the Antarctic Peninsula, which originate from the work carried out by Cook *et al.* (2005), but this is one region that is severely underrepresented given the large area of glacier coverage. Indeed, in an overview of global and regional trends in glacier area by Barry (2006) the Antarctic Peninsula region was not included at all. Future updates and climate reconstructions based on global long-term glacier-length change would benefit from a significantly larger contribution from the Antarctic Peninsula. The archival resources exist for coastal positions since records began in the 1940s, and monitoring changes in glacier termini does not come with the same constraints as those for measuring mass change. These length records can be used to measure changes in area of individual glaciers, making it possible to calculate the combined area of ice loss/gain as well as absolute and relative change for individual glacier basins. A consistent dataset will also provide a basis for continued ice front monitoring in the future. It is clear that although long-term records of *mass balance* in the AP are sparse, the plentiful historical glacier *length* records can offer a crucial insight into past glacier change in the region.

2.5 Summary

Knowledge on the current state of the AP cryosphere has been presented, firstly in the context of its response to previous warm and cool periods. Research shows that from the farthest known limit of the ice sheet during the Last Glacial Maximum (approximately 18-20 ka), it subsequently retreated from close to the edge of the continental shelf, to the inner shelf, on both sides of the AP (Heroy & Anderson, 2007). From the early Holocene (~11.7 ka), cryospheric responses to climatic change varied regionally, differences being particularly pronounced between the east and west sides (e.g. Hodgson *et al.*, 2006). The overall trend throughout the Holocene has been one of retreat, with two periods of

relatively small re-advance. What is significant is that the climate system is currently undergoing change that is faster than during any previous warm period (Vaughan *et al.*, 2003). This period of RRR warming has caused locally high mass imbalances in the ice sheet, principally caused by the loss of large ice shelves. A recent reconciled mass balance estimate of the APIS revealed that this region now accounts for ~25% of all mass losses from Antarctic regions that are in a state of negative mass balance, despite occupying just 4% of the continental area (Shepherd *et al.*, 2012).

Interpreting the behaviour of the numerous small glaciological features making up the system is critical for recognising responses to local and regional environmental changes. The glaciological complexity of the APIS has meant that there is still little quantification of change in the mass balance of individual glaciers or the processes controlling these changes. The dramatic changes in ice shelves have attracted much interest, and have been the predominant focus for glaciological research in this region. The primary driver of ice shelf break-up has been widely understood to be atmospheric warming, although other research suggests ocean temperatures are the greatest cause through basal melting. Observations from existing AP glacier studies show a progressive north-south ice-edge retreat; increases in glacier velocity; and thinning, particularly of glaciers that once fed ice shelves. If the loss of floating ice continues, the rate at which grounded ice discharges into the ocean increases. Questions regarding the timing and course of retreat of individual glaciers are as important to address as they are for ice shelves.

The need for a better understanding becomes clear when changes in the principle control factors are considered. Air temperature trends from stations with continuous records since 1979 have trends an order of magnitude greater than the global mean. At one station on the West coast (Faraday/Vernadsky) temperature rose by +5.7 ± 2 °C Century^{-1}, with warming especially high in winter (Vaughan *et al.*, 2003). The warming on the East coast was greatest during summer months, highlighting the distinct climatic regimes on each side of the AP. Significant changes in atmospheric circulation are thought to be the main cause of the summer temperature changes, principally the SAM which began a positive phase shift in the 1960s (Marshall *et al.*, 2006). Several model studies agree that anthropogenic change, through a combination of GHGs and ozone depletion is primarily responsible for the climatic shift (Arblaster *et al.*, 2011). The APIS

is particularly sensitive to changes in air temperature as the summer temperatures are close to melting point. The increase of meltwater may further accelerate the contribution of AP glaciers to sea-level rise through increased run-off and acceleration of flow via enhanced basal lubrication.

The warmer winter temperatures along the western side of the AP are correlated with a reduction in sea-ice extent since the 1960s, alongside an increase in winter precipitation (Turner & Overland, 2009). A recent increase in CDW upwelling along the western AP is associated with the warm winter temperatures, increased cyclogenesis and intensification of the SAM, demonstrating the strong atmosphere-ocean circulation coupling in this region (Mayewski *et al.*, 2009). It has been suggested that the western AP region shows the strongest response to ENSO of any region outside the tropical Pacific. If ENSO increases in strength and frequency, as predicted for future climatic warming, there would be significant implications for Antarctic ice-sheet stability. There is ample evidence that both the ocean and atmosphere are undergoing changes that could affect glaciers on the AP well into the future.

Glacier mass balance prior to the past decade has been difficult to measure in Antarctica and little confidence has been placed in the AP component of long-term glacier contributions to sea-level rise. Glacier terminus positions are an easier feature to measure than mass balance, and archival resources exist for coastal positions since records began in the 1940s. These length records can be used to measure not only changes in area of individual glaciers, but also the combined area of ice loss/gain. Long-term records of mass balance in the AP may be sparse, but the plentiful historical glacier length records can offer a crucial insight into past glacier changes in the region. The importance of quantifying long-term glacier-change is clear both in the context of improving calculations of sea-level change and understanding how the glaciers are responding to regional environmental changes.

Chapter 3

A new Digital Elevation Model for Antarctic Peninsula glaciology

3.1 Introduction

The importance of measuring past glacier changes and monitoring glaciers in the future in the Antarctic Peninsula has been discussed in Chapter 2. Glaciological research in the region is hindered by the scale and inaccessibility of the terrain, and in addition it is difficult to distinguish separate flow units due to the complexity of the system. A key resource to overcome such issues is a Digital Elevation Model (DEM), which would enable the mapping of individual glacier basins and provide a dataset suitable for glacier morphology and change analyses. This chapter addresses the ways in which DEMs are being used by glaciologists to investigate features in regions that are difficult to access and how they enable analysis of spatial and temporal changes in glaciers on a regional scale. DEMs that are currently available for the AP and the need for a high-resolution, high-accuracy model are discussed. Since no existing DEM has been suitable, a novel method has been developed to make significant improvements to an erroneous DEM. The aim of this chapter is to explain the methods used to both produce the final high-quality DEM product and assess its accuracy. This is contained in one chapter as the DEM underpins the methods and results for the entire study. The finished DEM product is available to the public via the National Snow and Ice Data Center (NSIDC) website and the methods and accuracy assessment have been published in Cook *et al.* (2012). Some passages have been quoted verbatim from this paper.

3.2 Digital Elevation Models for glaciological applications

DEMs are increasingly being used by glaciologists for both regional and individual glacier studies. The number of applications has increased substantially in recent years following the introduction of stereo-image satellite sensors producing images with high resolution and accuracy, extensive coverage and low costs. DEMs have become invaluable for regions that are difficult to access. Many examples of world-wide glacier mapping projects performed using stereo image-derived DEMs are listed in a paper by Toutin (2008). Elevation models play an essential role in creating global glacier databases, for extraction of topographic data and glaciological parameters and for glacier monitoring. Studies that would normally require ground-control points no longer require ground-access due to the high geospatial accuracy of DEMs (e.g. Cziferszky *et al.*, 2010).

Elevation models are produced from data acquired from airborne campaigns such as aerial photography (followed by photogrammetric processing of stereo vertical photographs) or Light Detection and Ranging (LiDAR) based on a near-infrared laser scanner (processed using GPS and an inertial navigation system) (Hvidegaard *et al.*, 2012). These data can result in DEMs with sub-metre resolutions, depending on the flight altitude, and are used for local fine-scale feature identification studies. Satellite stereo image sensors are increasingly accurate and many freely-available satellite-derived DEMs are suitable for medium-scale (1:50,000 to 1:100,000) mapping (Toutin, 2008). DEMs with almost global coverage that are commonly used by research scientists include Shuttle Radar Topography Mission (SRTM) and Advanced Spaceborne Thermal Emission and Reflection Radiometer (ASTER) derived products, at 90-m and 30-m resolution, respectively. Other commercially available, regionally-specific satellite-derived DEMs are at higher resolutions (e.g. DEM mosaics produced from DigitalGlobe WorldView satellites).

One significant benefit of topographic models in glaciology is that they enable delineation of glacier drainage basins over large remote areas. Ice divides or watersheds can be identified by either manual or automated methods, as demonstrated for the Greenland Ice Sheet (Hardy *et al.*, 2000; Lewis & Smith, 2009); the Canadian Arctic (Burgess & Sharp, 2004; Svoboda & Paul, 2009) and Antarctica (Vaughan & Bamber, 1999; Bliss *et al.*, 2013). As discussed in Chapter 2, one of the most required datasets for an improved calculation of current and future global sea-level rise is a globally complete glacier inventory with topographic attributes (Frey & Paul, 2012). As basin outlines are required for glacier inventories, the DEM is a useful tool particularly where other glacier outline information does not exist (Bolch *et al.*, 2010). A DEM enables topographic inventory parameters such as the mean, minimum and maximum elevation values and the mean aspect (or glacier orientation) and slope to be calculated for individual glaciers using automated procedures (Kääb *et al.*, 2002b; Paul *et al.*, 2002; Paul *et al.*, 2009). In addition to their value for improving sea-level calculations, topographic parameters are useful for statistical modelling of glaciers (e.g. Paul & Svoboda, 2009; Frey & Paul, 2012). Mean slope can be used as a proxy for ice thickness (Haeberli & Hoelzle, 1995; Farinotti *et al.*, 2009; Paul, 2010) and hypsometry curves can be produced as an indirect measure of mass balance (e.g. Jiskoot *et al.*, 2009). One such study in the northern AP by Davies *et al.* (2012) used parameters derived from DEMs to compare glaciers in the James Ross Island and Trinity Peninsula region. Knowledge about glacier topographic characteristics can be fundamental to understanding glacier behaviour, and glacier changes in many regions world-wide have been analysed alongside characteristics extracted from DEMs. One example is from Bolch *et al.* (2010), who produced an inventory of glacier changes in western Canada (1985-2005), and analysed the area loss versus glacier size, aspect, slope and median elevation values.

A good elevation model is not only valuable for mapping purposes; it can be used to understand ice dynamics. Surface elevation at a suitably high resolution can be used to identify ice flow features such as crevasses, and subglacial features that may cause a change in slope at the glacier surface such as the grounding line or ice rises (e.g. Glasser *et al.*, 2011). In conjunction with visible-band or radar imagery, DEMs enable surface features to be identified and tracked over time. For example, the new TerraSAR-X twin

satellite TanDEM-X will soon deliver high-accuracy surface topography and roughness datasets in Antarctica (Gantert *et al.*, 2011). An initial study has been carried out successfully on an individual glacier in the northern AP using the first TanDEM-X datasets from 2010 (Eineder *et al.*, 2011).

It is becoming increasingly popular for glaciologists to assess glacier mass balance and volumetric change using time series of digital elevation data. Several studies in the AP have already used DEMs for measuring volume change of individual glaciers or local regions. For example, Fox & Cziferszky (2008) and Kuntz *et al.* (2012) used photogrammetrically derived DEMs to measure elevation from historical and recent vertical aerial photographs. Others have used DEMs derived from satellites such as ASTER and Satellite Pour l'Observation de la Terre (SPOT) to calculate elevation differences for AP glaciers at periods following ice shelf collapse (Glasser *et al.*, 2011; Rott *et al.*, 2011; Shuman *et al.*, 2011; Berthier *et al.*, 2012). A recent study has used ASTER and SPOT DEMs alongside ICESat elevation values to increase data availability for measuring mass change across the northern AP (Scambos *et al.*, 2014).

Advances in glaciology in the AP in recent years have been rapid and much of this is thanks to the increasing availability of DEMs. It is noticeable, however, that the attention has been focussed on localised regions and that glaciers across the region as a whole still lack research. Two significant products that are missing from this region are an inventory of all glaciers and a DEM for the whole AP at a sufficient level of detail to map their characteristics. With these elements it would become possible to advance glaciological knowledge in ways that can be seen in glacier studies world-wide. A DEM of the Antarctica Peninsula could be used to produce a glacier inventory with topographic parameters such as elevation statistics, slope, aspect and flow length, all of which are important in understanding ice dynamics, not only of individual flow units but of the complete glacier system.

3.3 High resolution gridded elevation datasets for the Antarctic Peninsula

In recent years, DEMs of Antarctica have been produced using a range of source data including radar missions, stereo satellite image processing techniques and laser altimetry. Continent-wide DEMs that are widely used and provide reliable surface elevation data for much of Antarctica include the ICESat/GLAS 500 m DEM (Dimarzio *et al.*, 2007) and the 1 km resolution DEM from Combined ERS-1 Radar and ICESat Laser Satellite Altimetry (Bamber *et al.*, 2009), but these are less reliable in the Antarctic Peninsula, with significant problems caused by the steeper topography and the coarser resolution. A DEM of ~100 m cell size, similar to the 90-m SRTM DEM available for areas elsewhere on Earth, would be more suitable for the varied terrain in this region. The SRTM dataset, however, does not cover high latitudes, with a southern limit of 56° South.

In order to find a DEM of the AP at the level of detail required for the rugged terrain, existing DEMs with a grid-spacing of 200 m or better were considered. Those with peninsula-wide coverage that are currently available to the international research community are the Radarsat Antarctic Mapping Project (RAMP) v2 model (Liu *et al.*, 2001) and the ASTER Global Digital Elevation Model (ASTERGDEM-ValidationTeam *et al.*, 2009). Regional DEMs include those produced from SPOT-5 High Resolution Sensor (HRS) stereoscopic data (Korona *et al.*, 2009) and from elevation data collected as part of Operation IceBridge using NASA/GSFC Land, Vegetation and Ice Sensor (LVIS) (http://lvis.gsfc.nasa.gov/index.html, 08/2012). As mentioned in Section 3.2, high resolution Tandem-X Interferometric Synthetic Aperture Radar DEMs are currently being generated (Gantert *et al.*, 2011) and Cryosat-2 Synthetic Aperture Interferometric Radar Altimeter (SIRAL) data (Cryosat: http://www.esa.int/SPECIALS/Cryosat/, 08/2012) will be used for creating surface elevation grids but, at the time of writing, these DEMs are not yet available for the Antarctic Peninsula. The Landsat Image Mosaic of Antarctica (LIMA), although not an elevation data source, has enabled identification of features at a spatial resolution of 15 m and it provides a base coastline from scenes that have a geospatial accuracy of ±54 m RMSE (Bindschadler *et al.*, 2008).

Of the regional DEMs, SPOT-5 stereoscopic survey of Polar Ice: Reference Images and Topographies (SPIRIT) is an International Polar Year (IPY) project in which a large archive of SPOT-5 HRS stereoscopic images and 40-m digital terrain models (DTMs) of Polar Regions were made available to the scientific community (Korona *et al.*, 2009). Certain regions were chosen and prioritised before acquisition and the SPIRIT DTM products were generated automatically from the optical stereo-images through a matching algorithm. The DTMs were validated by comparison with ICESat elevation profiles and for a highly-textured ablation region on the large outlet glacier in Greenland, Jakobshavn Isbrae, the SPIRIT elevations (for non-interpolated pixels) were within ± 6 m of ICESat elevations for 90% of the data, although the errors were greater on flat accumulation areas (Korona *et al.*, 2009). The DTM products are at a high resolution and have a horizontal precision of 30 m RMS but they only cover certain regions of the Antarctic Peninsula, primarily along the western coast and northern regions. Therefore, coverage is currently not sufficient to produce a DEM mosaic of the whole Antarctic Peninsula.

Of the two high-resolution products providing complete coverage, the Radarsat Antarctic Mapping Project (RAMP) v2 model (Liu *et al.*, 2001), available from the NSIDC (http://nsidc.org/data/nsidc-0082.html), is a DEM with widespread usage. It was originally created for use in processing images for the RAMP AMM-1 SAR Mosaic of Antarctica and since then has been widely used to detect glaciological properties of the ice sheet (Jezek, 1999). The DEM accuracy varies according to the terrain and accuracy of the wide range of data sources, and uncertainties that are introduced through data integration. For the Antarctic Peninsula the geolocation accuracy is thought to be generally better than the horizontal resolution (200 m in this region), and the vertical accuracy lies between 100-130 m (Liu *et al.*, 2001). Although RAMPv2 contains interpolated data, the source data in the AP is often of a sufficiently high resolution to make it a reliable surface topography dataset. It is widely used for scientific research and logistics operations throughout Antarctica. The vertical accuracy required, however, for glacier drainage basin delineation for mass balance analyses on the AP must ideally be greater than those specified in the RAMPv2 documentation.

ASTER Global Digital Elevation Model (GDEM) is the most recently released nearly global elevation dataset and is based upon a composition of automatically generated DEMs from ASTER stereo scenes acquired since 2000. It was produced by the Ministry of Economy, Trade and Industry (METI) of Japan and the United States National Aeronautics and Space Administration (NASA) and was first released to the public in June 2009 (ASTERGDEM-ValidationTeam *et al.*, 2009). ASTER consists of nadir and backward looking sensors, enabling a stereoscopic DEM to be generated based on photogrammetric principles. An automated approach was used to produce a stereo DEM between 83° North to 83° South, in 1-degree tiles, with a pixel size of 1-arc second. Validation tests were performed by both the U.S. and Japanese partners by calculating statistical accuracies based on reference DEMs and Ground Control Points for sample regions around the globe. Conclusions in the validation summary report (ASTERGDEM-ValidationTeam *et al.*, 2009) are that the overall vertical accuracy of the ASTER GDEM 1, on a global basis, is approximately 20 metres at 95 % confidence.

There is strong regional variation in the accuracy, however, with particularly large anomalies occurring in the Greenland and Antarctic ice sheet regions. These errors are introduced as a direct result of high reflectance and lack of features on the snow-covered plateaus. Although ASTER GDEM is considered unsuitable for much of the interior of Antarctica, the AP has significant areas of exposed rock, varying surface slope and texture that suggest it will be better suited to this region. ASTER GDEM cell size of 1-arc second equates to ~10 m east-west and ~30 m north-south in the AP and, if the errors on the plateau regions can be sufficiently reduced, it could provide an attractive solution to a finding a suitable topographic model for the Antarctic Peninsula. Indeed, an assessment for extraction of topographic parameters for a Swiss glacier inventory concluded that ASTER GDEM is suitable for this purpose (Frey & Paul, 2012). It is therefore worth considering how to maximize this dataset in the AP. Figure 3.1 shows a sample region that illustrates the ASTER GDEM compared against a visible-band image, the Landsat Image Mosaic of Antarctica (LIMA). The smoother, low-relief slopes visible on LIMA contain large spikes/pits on GDEM, whereas the higher-relief and greater texture coastal regions closely match the features visible on LIMA.

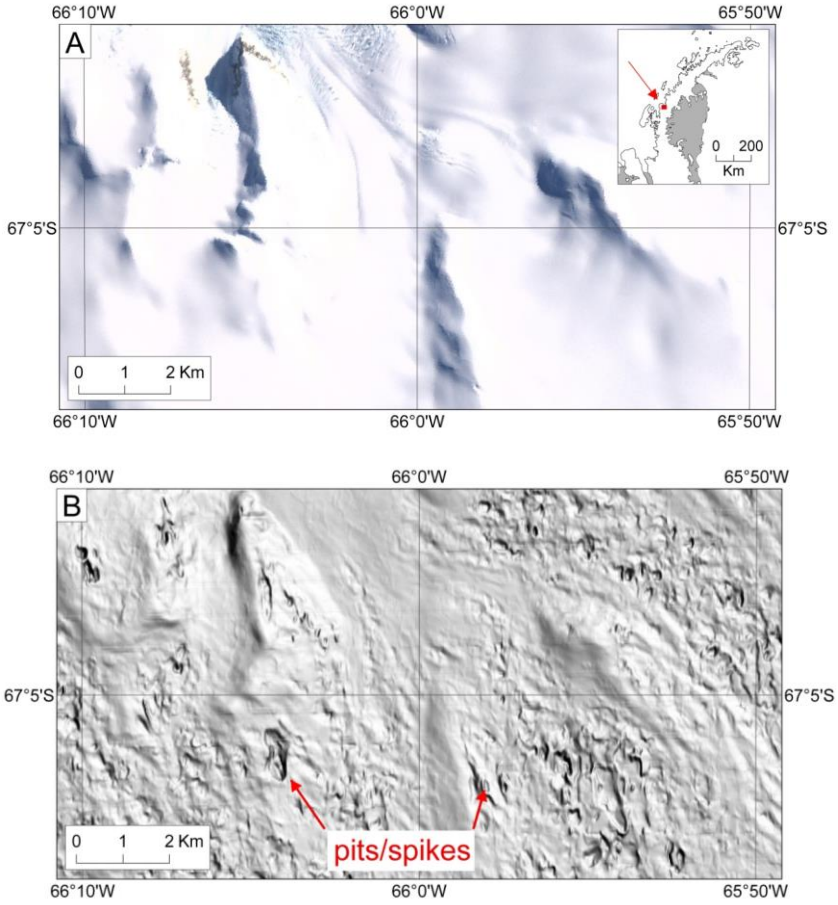

Figure 3.1: The surface texture of ASTER GDEM.
Sample area showing features visible on LIMA satellite image, displaying crevassed high-texture regions, rock outcrops and smooth surface low-relief slopes (**a**). The raw ASTER GDEM has been hillshaded to show the problems in the dataset such as pits/spikes, which primarily occur on the featureless surface slopes (**b**).

3.4 ASTER GDEM: limitations and potential for use in the AP

Although the majority of ASTER GDEM tiles have vertical accuracies within 20 m, "ASTER GDEM does contain residual anomalies and artifacts that most certainly degrade its overall accuracy" (ASTERGDEM-ValidationTeam *et al.*, 2009). No formal GDEM validation has been performed over Antarctica, but it is evident that there are significant errors within the tiles throughout this region. This is to be expected, as the snow-covered landscape results in low contrast and sparse repeat coverage, both of which contravene the essential criteria for stereo-image processing. Prior glacier surface

topography studies have encountered similar difficulties with photogrammetric methods in texture-less regions (Lodwick & Paine, 1985; Fox, 1995).

Recent independent assessments of ASTER GDEM in Arctic regions (Hvidegaard *et al.*, 2012; Rees, 2012) have shown that vertical accuracies vary according to terrain type but the number of independent ASTER DEMs contributing to the final elevation value for any given pixel (known as the stacking number) is a good indicator of accuracy. In areas where this number is greater than ~6, the GDEM root-mean-square-error (RMSE) is typically 5-10 m (Rees, 2012). At high elevations on the Greenland Ice Sheet, however, where GDEM tiles are dominated by cloud and striping artefacts, the majority of points have low stacking numbers. A study of GDEM accuracy in coastal regions of Greenland by Hvidegaard *et al.* (2012) showed that there was a bias of 10-20 m in the data and an RMSE elevation difference ranging from 15-65 m. Hvidegaard *et al.* (2012) attributed the large RMSE to low stacking numbers, reduced correlation between images due to snow cover, mis-registration between GDEM and the test dataset due to high sloping areas on the coast and seasonal changes in the ice sheet. ASTER GDEM 2 was released on 17th October 2011 and although it is a significantly improved version on a global scale (ASTERGDEM-ValidationTeam, 2011) a comparison of GDEM1 and GDEM2 in Greenland concluded that there was little difference in accuracy between the two versions in that region (MacFerrin *et al.*, In review). Since GDEM1 was the version available at the start of the present study, accuracy of GDEM2 in the AP has not been investigated.

Until now, GDEM has not been considered as a reference DEM for glaciological projects in Antarctica, although it has been used to derive elevations such as the Antarctic Surface Accumulation and Ice Discharge (ASAID) grounding line (Bindschadler *et al.*, 2011a). As the potential for ASTER DEMs to be used for glacier-change studies in the AP is becoming more recognised (Cziferszky *et al.*, 2010; Glasser *et al.*, 2011; Scambos *et al.*, 2011; Shuman *et al.*, 2011; Berthier *et al.*, 2012; Scambos *et al.*, 2014), it is important to consider how the GDEM artefacts can be reduced. For Greenland, recommendations for reducing errors include filtering regions where stacking numbers are low and cloud and striping artefacts are high, and either interpolating across remaining cells where the ice is relatively flat, or down sampling (MacFerrin *et al.*, In review). In some parts of the

Antarctic Peninsula, however, if the "noise" was filtered, there would be too few remaining points for interpolation to be viable, and valid elevations would be lost with down sampling.

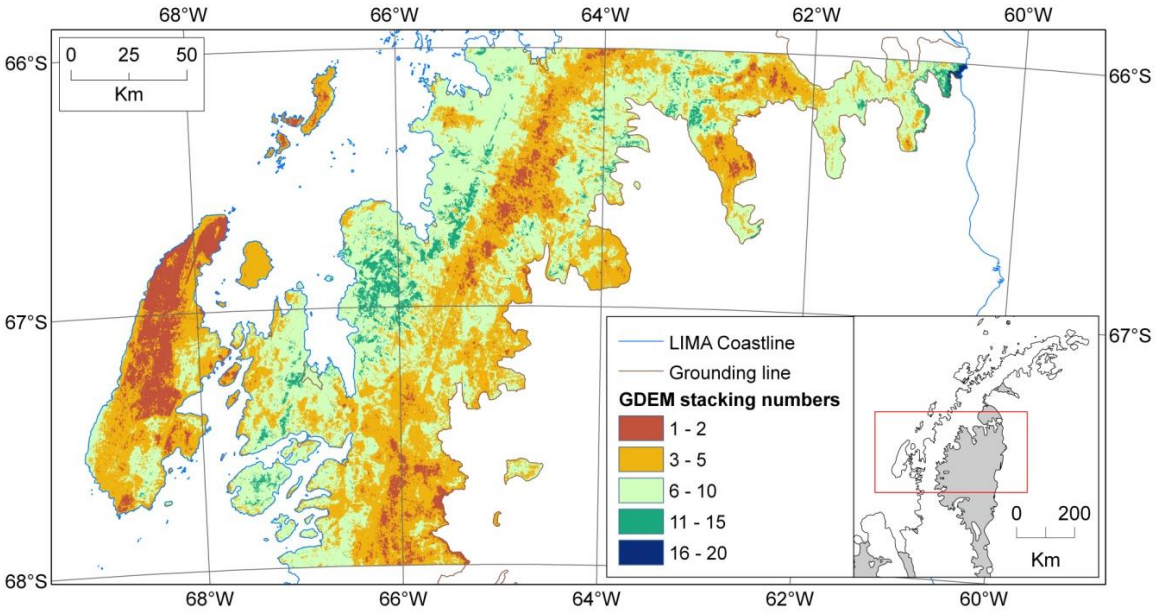

Figure 3.2: ASTER GDEM stacking numbers.
Number of stacked local DEMs (stacking number) used to calculate each GDEM elevation value, for tiles between 66° - 68° S. Stacking numbers of ~6 or higher are an indicator of higher DEM accuracy.

Figure 3.2 illustrates the stacking numbers of ASTER GDEM for a sample region of the AP between 66-68° S, in which extensive regions with stacking numbers less than six can be observed. One consideration is to insert other elevation datasets, such as NASA Ice, Cloud and land Elevation Satellite Geoscience Laser Altimeter System (ICESat GLAS) data. This is not a viable option, however, as the ICESat tracks are too widely spaced in this region to fill the extensive gaps.

The stacking number file that is provided with the elevation dataset also indicates regions that could be considered as accurate and should be compared with existing DEMs. When GDEM is contourised and placed over the LIMA, it fits closely to terrain features, particularly in coastal and feature-rich areas. Rock features, mountain slopes, crevasses and supraglacial water create texture for the image-matching algorithms, thereby increasing the stack numbers of valid ASTER scenes per pixel. In other areas, often

where the stacking numbers are low, the contours clearly do not fit terrain features and large pits and spikes appear. The contours are a way of visualising where the GDEM changes, often sharply, from good quality to poor. If the data are so noisy that it cannot be filtered or smoothed using recognised techniques such as a median filter method (as data quality is so variable across the modelled area) or methods described above, an alternative approach must be considered.

3.5 DEM correction methodology

3.5.1 An alternative approach to ASTER GDEM correction

A DEM generation approach already implemented in Antarctica used spatial interpolation algorithms within a Geographic Information System (GIS) environment to interpolate a surface between different vector data sources. The Radarsat Antarctic Mapping Project (RAMP) used a comprehensive collection of digital topographic source data, including cartographic data, remotely sensed data and survey data, which were then integrated and merged to produce the RAMP DEM (Liu *et al.*, 1999). One data type that was used was contours digitised from paper topographic map sheets, included in the Antarctic Digital Database (ADD) (BAS *et al.*, 1993). Contour-specific interpolation algorithms were tested by Liu *et al.* (1999), who found that the TOPOGRID-based method (Hutchinson, 1989; ESRI, 1991) was the most effective technique in terms of the consistency with the source contour data and preservation of the fine surface structures. With this method, linear interpolation is enforced along ridge and stream lines, which are automatically derived from points of maximum curvature on contour lines (Liu *et al.*, 1999). Although originally developed for use in ArcInfo, similar algorithms are now available in many GIS software packages.

A similar method was applied by Racoviteanu *et al.* (2007) to create a DEM from 1:50,000 topographic maps, for the Nevado Coropuna region of the Peruvian Andes. The maps were originally constructed from 1955 aerial photographs. Their method involved digitising on-screen the contour lines visible on the map and attributing the corresponding elevation values. Additional information such as lakes, rivers and spot

heights were also digitised. The authors examined common interpolation routines to create continuous data from the contours. These included: Inverse Distance Weighted (IDW), Splines (TOPOGRID) and Triangulated Irregular Networks (TINs). The following definitions are from Racoviteanu *et al.* (2007).

- The IDW method estimates the Z-value (elevation) of an unknown point based on a distance-weighted average of elevation points within a neighbourhood .
- Spline techniques use polynomial interpolation to fit a curve through all the data points. The TOPOGRID algorithm is a spline technique that fits a smoothing surface through the data points to minimize artefacts. TOPOGRID interpolates directly from the contour lines by determining areas of steepest slope and generating terrain morphology.
- Triangulated Irregular Network (TIN) data structures are terrain models represented by continuous triangular facets that store elevation at irregularly spaced nodes.

When each interpolation method was evaluated against SRTM and ASTER DEMs, it was found that the vertical accuracy of the DEM created with the TOPOGRID algorithm was 14.7 m, whereas the accuracy of the other interpolation methods ranged from ~21 to 24 m (Racoviteanu *et al.*, 2007). TOPOGRID was also found to create the smoothest surface and it was concluded that a DEM constructed in this way constitutes a valid elevation dataset for glaciology purposes.

The method developed in the present study is based on a similar principle, but instead of using map contours, contours generated from the ASTER GDEM are used. Erroneous contours can be easily identified and removed and a smooth and realistic new DEM can be produced from the remaining contours. If this is applied only to regions with spurious contours, the resulting DEMs can be merged with the unaltered high-quality GDEM regions. The method is made possible by the fact that the high-artefact regions are those where the real surface slope is less than ~20° (and therefore fewer contours are required to derive the new surface topography) and contours that are short in length can be removed from these regions since these represent spurious spikes and pits where the real-surface (as observed on LIMA) is smooth. The remaining contours occur where the DEM

has consistent elevation values between the anomalies and can be used to reconstruct the surface topography by interpolation.

3.5.2 ASTER GDEM improvement procedure

ASTER GDEM tiles were downloaded from http://www.ersdac.or.jp/GDEM/E/ and mosaicked according to each latitudinal degree across the Antarctic Peninsula. Each mosaic was projected onto a reference system suitable for minimising distortions in scale and for preserving angles locally. In this case, Lambert Conformal Conic (LCC) was used with standard parallels and other parameters according to latitude. The raw integer mosaic was converted to a 32-bit continuous floating point raster to minimise elevation errors at each stage of data processing. The subsequent methodology was then applied separately to each latitudinal degree raster between 63°–70° South. ArcGIS 10.1 was used for the whole procedure; all tools used are italicised.

a. Initial contourisation:

Using the *3D Analyst – Raster Surface - Contour* tool, contours were generated from the GDEM at 20 m intervals. A new polygon file was then created by digitising around regions of erroneous contours, using two steps. First, the stacking number file was used to generate the initial outline of poor quality regions by extracting only pixels with stacking numbers less than 6 (*Spatial Analyst – Extract by Attributes*) and converting these into a simplified polygon file (*Conversion Tools – Raster to Polygon*). The second step involved manual smoothing and corrections to the polygon outlines using visible band imagery (in this case, LIMA) to visually assess how well the contours match the terrain (Figure 3.3a). The spurious contours were usually easy to identify due to their spaghetti-like appearance. The resulting outline polygon file was then used to extract the noisy regions of the DEM (*Raster Processing – Clip*). The extracted poor-quality DEM was then down sampled to 200 m to simplify (*Raster Processing – Resample*) and, by using the *Spatial Analyst – Hydrology - Fill* and *Neighbourhood – Filter (low-pass)* tools, sinks in the DEM were filled and gross errors removed. New contours at 20 m intervals were then created for this filtered DEM.

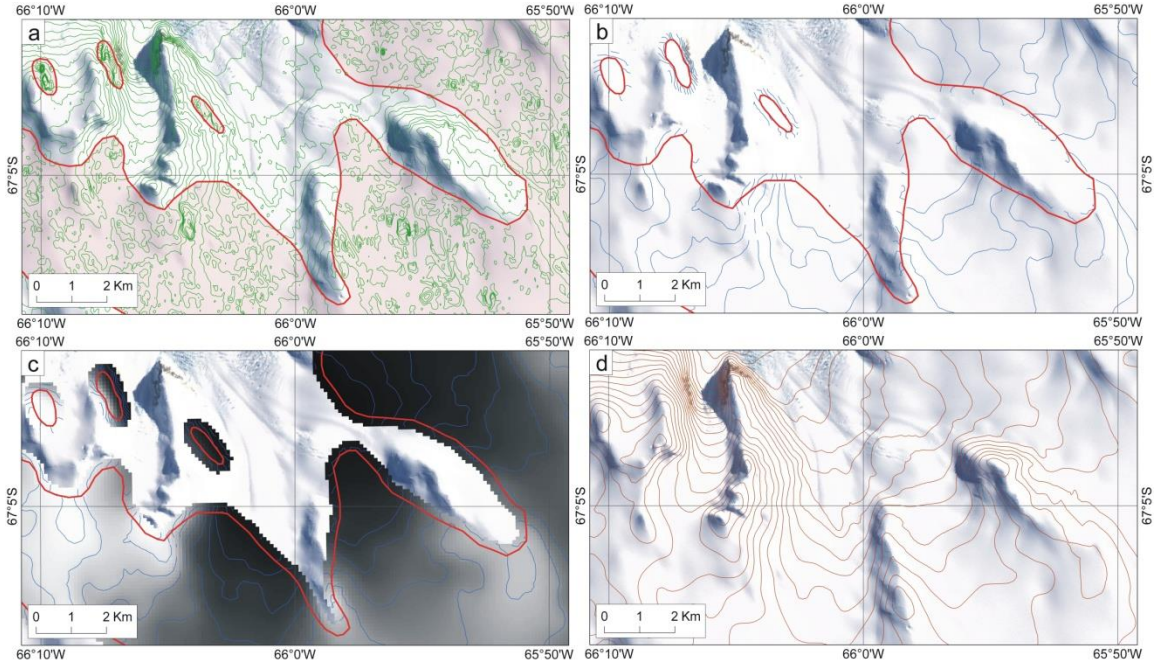

Figure 3.3: Sample map illustrating ASTER GDEM improvement procedure.
Sample area displaying 50 m contours generated from raw ASTER GDEM and error-region polygons (in pink) (**a**). This illustrates the first stage of the methodology: delineation of erroneous regions using contours draped over LIMA as a guide. The filtered and smoothed contours (**b**) were then used to produce a new DEM for edited regions (**c**), and merged with the surrounding original DEM. The end-product has been contoured to illustrate the improvement in the DEM from the original and also the consistency of the topography at error region boundaries (**d**).

b. Contour correction:

In order to correct the regions of erroneous contours two methods were applied. The first involved creating a slope model (*3D Analyst – Raster Surface – Slope*) and removing contours that fell within a slope angle of greater than 20° (this angle was chosen after testing various slope values). Since the erroneous regions occur on surfaces with low slope angles, any large anomalous peaks or depressions can be removed. The second step involved deleting contours less than 1 km in length (chosen as the best indication of a spurious contour at this DEM cell size, after testing a range of values). In order to minimise discontinuity between the corrected regions and the high-quality regions, a 200 m overlap or 'buffer' zone was created for all error-regions (*Proximity – Buffer*). The contours could then be manually checked

and any remaining spurious contours deleted or improved based on the terrain visible in the LIMA image (Figure 3.3b).

c. DEM generation:

It was then possible to generate a new DEM for the error-regions using the edited contour file. This was executed using the *Topo to Raster* interpolation tool available in ArcGIS (*3D Analyst – Raster Interpolation*), which is the equivalent of the TOPOGRID interpolation algorithm (in ArcInfo) used in previously mentioned studies. The interpolated DEM was given a 100 m output cell size (Figure 3.3c). In total, the edited region makes up 39% of the complete DEM coverage. The outer limit for the new DEM is the coastline that is visible on LIMA, plus a buffer of 500 m offshore. This means that all of GDEM is included, even where the horizontal positioning does not directly match LIMA. When GDEM1 was produced a coarse mask was applied, resulting in some coastal regions and almost all of the ice shelves being omitted from the finished product. The new DEM uses the Antarctic Surface Accumulation and Ice Discharge (ASAID) grounding line (Bindschadler *et al.*, 2011a) with a buffer of 500 m as a boundary where there is ice shelf.

d. DEM mosaicking:

The high-quality GDEM (i.e. the original GDEM with the erroneous regions removed) was resampled to 100 m, and filled to remove minor pits. A cell size of 100 m was determined to be optimal: if the grid size is smaller, artefacts remain on the high-quality regions, whereas sufficient topographic detail can be obtained at this spacing for the complexity of terrain in the Antarctic Peninsula. The DEM produced from corrected contours was mosaicked (*Raster Dataset – Mosaic to New Raster*) with the high-quality regions of GDEM, using a weight-based blend to ensure a topographically consistent DEM across the buffer zones (Figure 3.3d).

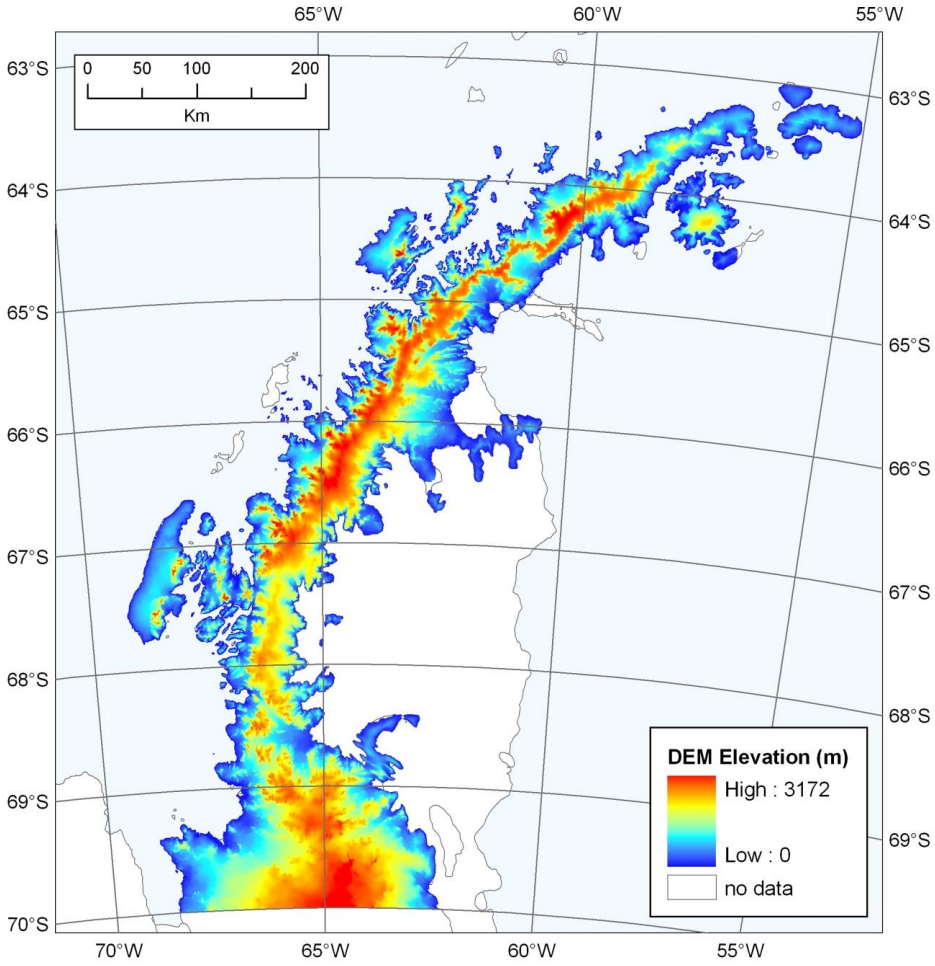

Figure 3.4: The new 100-m DEM of the Antarctic Peninsula.

Once these steps were completed for each individual latitudinal degree tile, a common reference system was selected before the tiles were integrated. For the Antarctic Peninsula, Polar Stereographic projection with a standard latitude of 71° South and a central meridian of 0° was chosen. As the ASTER GDEM is referenced to the WGS84 ellipsoid and adjusted to the EGM96 geoid model, the new DEM is also on this reference system and therefore gives height with respect to the geoid. The final step of the process involved mosaicking all tiles by blending, and a low-pass filter was applied to smooth the entire raster and reduce the significance of anomalous cells. Finally, any remaining artefacts along the coast were removed (e.g. clipped to the limit of GDEM or assigned as 'null' values), resulting in the finished DEM (Figure 3.4). Any remaining artefacts occurring in interior regions were identified and polygons were digitised around them, resulting in a supplementary 'remaining artefacts' file.

3.6 Error analysis

In order to validate the improved DEM, tests were undertaken to assess vertical and horizontal positional accuracy. In Antarctica, assessing the quality of the derived surface can be problematic, as high-accuracy ground-control points are limited and poorly distributed throughout the modelled area. A first assessment of ASTER GDEM tiles was undertaken by Reuter *et al.* (2009), in which ICESat elevations were used for absolute accuracy tests and SRTM was used for relative accuracy for 5 GDEM tiles from around the globe (Reuter *et al.*, 2009). A similar methodology was applied here. Vertical accuracy was addressed first, using ICESat as an absolute reference, followed by comparison of elevations of existing DEMs across the spatial extent of the new DEM. Vertical accuracy according to slope was also assessed to detect any slope-dependent bias, and accuracies of both edited and unaltered regions were calculated to determine any significant differences from the mean errors. Horizontal accuracy tests included calculating absolute geospatial accuracy using 10 peaks in one small sample region based on GPS points and a photogrammetric DEM. Peaks obtained from SPIRIT DEMs gave relative accuracies across a wider region to test for consistency across the model. Finally, horizontal differences from LIMA were calculated for when the DEM is used alongside LIMA. Table 3.1 is a reference for dataset acronyms.

Table 3.1: Summary of dataset acronyms

Acronym	Definition	Pixel size
ASTER GDEM	ASTER Global Digital Elevation Model	~20 m
New DEM	The new DEM of the Antarctic Peninsula derived from ASTER GDEM	100 m
RAMPv2	Radarsat Antarctic Mapping Project version 2	200 m
SPIRIT	SPOT-5 stereoscopic survey of Polar Ice: Reference Images and Topographies	40 m
SPIRITv1	SPIRIT DTM produced using parameters adapted for gentle topography	40 m
SPIRITv2	SPIRIT DTM produced using parameters adapted for rugged topography	40 m
SPIRITv1 masked	SPIRITv1 with interpolated pixels removed. Masked version = 83 % of SPIRITv1	40 m
SPIRITv2 masked	SPIRITv2 with interpolated pixels removed. Masked version = 70% of SPIRITv2	40 m
ICESat/GLAS	NASA Ice, Cloud and land Elevation Satellite/ Geoscience Laser Altimetry System	
LIMA	Landsat Image Mosaic of Antarctica	15 m

3.6.1 Vertical accuracy

3.6.1.1 Absolute vertical accuracy

The NASA Ice, Cloud and land Elevation Satellite (ICESat) mission from 2003 – 2009 consists of semi-continuous profiles of elevation points acquired using the onboard Geoscience Laser Altimeter System (GLAS) and provides consistent, near-repeat surface elevations (Zwally *et al.*, 2002b; Shuman *et al.*, 2006). ICSat has a footprint of ~70 m with an along-track spacing of 170 m and an across-track spacing of about 20 km at 70° South (Shuman *et al.*, 2006). The high precision and sub-decimetre accuracies of the along-track elevation values on low-slopes are ideal for measuring absolute-errors and determining the accuracy of other elevation products (e.g. Korona *et al.*, 2009; Nuth & Kääb, 2011). The GLAS accuracy in horizontal geolocation is ~15 m and for clear skies and low-slopes the surface elevation is accurate to ± 14 cm (Shuman *et al.*, 2006).

Release 28 GLAS/ICESat Global Elevation Data (GLA12), available from NSIDC (Zwally *et al.*, 2003), was considered most appropriate for accurate surface ground-truth data across the range of terrain in the AP (Figure 3.5). Height measurements from laser periods 3A and 3B from 2005-06 were chosen, which had been corrected for pointing errors and saturation by Pritchard *et al.* (2009). Measurement precision over the ice sheets for uncorrected data has been found to vary with surface slope from 0.14 to 0.59 m (Brenner *et al.*, 2007; Moholdt *et al.*, 2010). After correction for errors, however, the residual uncertainty for the Release 28 data for the laser periods 3A and 3B in this region were reduced to < 0.1 m (Pritchard *et al.*, 2009).

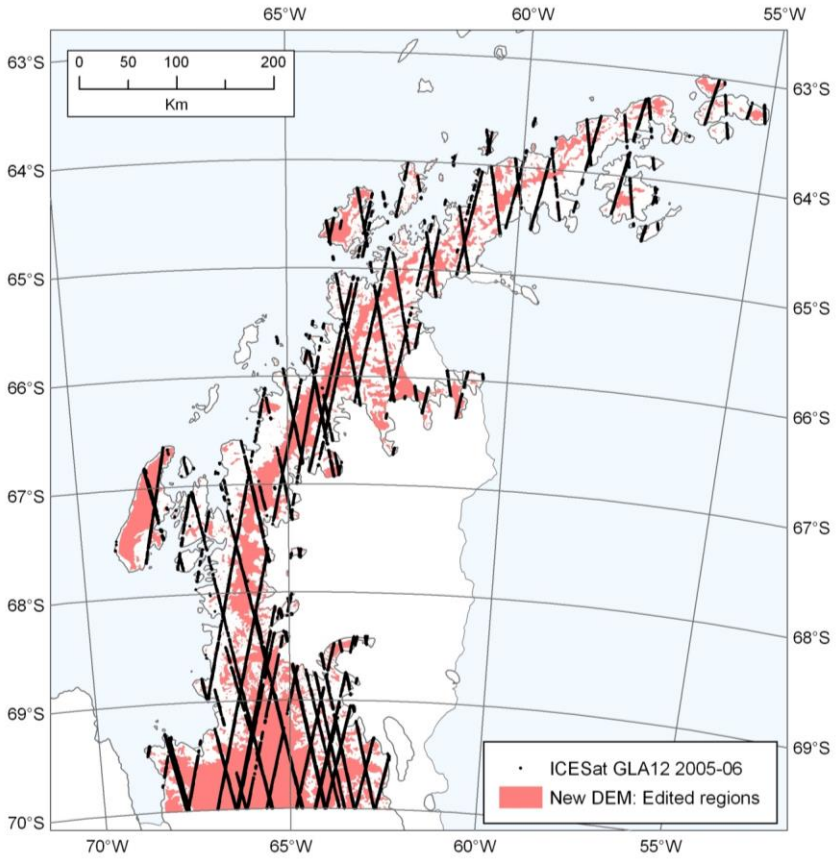

Figure 3.5: Edited region coverage.
The edited regions are shown in pink, along with the ICESat tracks used for assessing the vertical accuracy of the new DEM.

ICESat elevations from 2005-06 were chosen as this period corresponds approximately with the years that SPIRIT scenes were acquired. GDEM, however, is compiled from ASTER scenes from a range of dates between 2000 and 2009 that are unspecified in the

final product. Therefore, ice surface elevation change over time is a factor affecting relative elevation differences that must be recognised, even though it cannot be quantified. The surface elevation values of GDEM, the new DEM, SPIRIT DEMs (versions 1 and 2, both masked and unmasked) and the RAMPv2 DEM were calculated for each ICESat point. Each DEM is referenced to the WGS84 Ellipsoid and adjusted to the EGM96 Geoid. Although ICESat/GLAS uses a different ellipsoid (TOPEX/Poseidon), it results in elevation values only 70 cm higher than those obtained using the WGS84 Ellipsoid. The ICESat values have been corrected to the EGM96 Geoid.

Table 3.2: Mean elevation differences from ICESat across the new DEM.
N is the number of ICESat points. The mean difference from each ICESat point is measured at height with respect to the EGM96 Geoid and the root mean square error (RMSE) is shown in metres.

	New DEM	ASTER GDEM	RAMPv2	SPIRITv1	SPIRITv2	SPIRITv1 masked	SPIRITv2 masked
N	64593	64280	64747	16901	16915	13705	11127
Mean	-4	-13	-33	4	0	5	4
RMSE	± 25	± 97	± 201	± 60	± 69	± 50	± 40

All ICESat footprints that fall within the limit of the new DEM (Figure 3.5) were used to compare elevations and residual uncertainties, as summarised in (Table 3.2). The new DEM has a mean offset of -4 m, with an RMSE of ± 25 m, which is a significant improvement to the original GDEM error values (mean -13 m, RMSE ± 97 m). RAMPv2 has significantly larger error values (mean of -33 m, RMSE of ± 201 m). SPIRIT values are based on a mosaic of the SPIRIT tiles, where v1 is the version produced using parameters adapted for gentle topography, v2 for steeper topography and 'masked' is where interpolated pixels have been masked-out (using reliability masks provided with the SPIRIT products) (Korona *et al.*, 2009). It is important to calculate the accuracy of each SPIRIT product against ICESat before using them for further accuracy evaluations of the new DEM. Although the SPIRIT DEM mosaics have a relatively low mean offset from ICESat (ranging from 0 to 5 m), they have a relatively high RMSE (± 40 to 69 m). This is greater than RMSE values reported in other evaluations of SPIRIT DEMs (e.g.

Korona *et al.*, 2009; Moholdt *et al.*, 2010; Nuth & Kääb, 2011; Shuman *et al.*, 2011), but could be explained by the complex topography in this region and changes in glacier surface heights between the dates of the data sources.

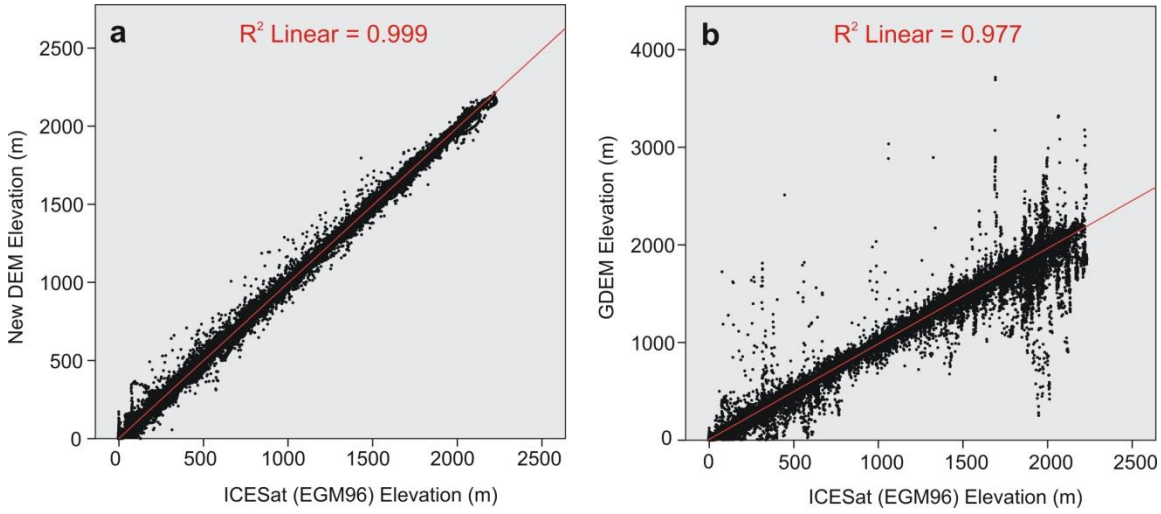

Figure 3.6: Scatterplots of ICESat and the DEM elevation values.
The relationship between ICESat footprint elevation values (in metres) and the New DEM (**a**) and the original ASTER GDEM before correction (**b**).

Figure 3.6 shows comparison plots of the new DEM and GDEM against ICESat elevations. In addition, a sample along-track profile illustrates the differences between the DEMs and ICESat according to elevation, slope and terrain (Figure 3.7) (further profiles can be seen in Appendix 3.1). The artefacts of the original GDEM are visible on the profile, particularly on the ice plateau regions, and it is clear that the new DEM closely matches the ICESat values in almost all sections of the profiles. From these absolute vertical error values it can be concluded that the new DEM is a significant improvement over existing surface topography models of the Antarctic Peninsula.

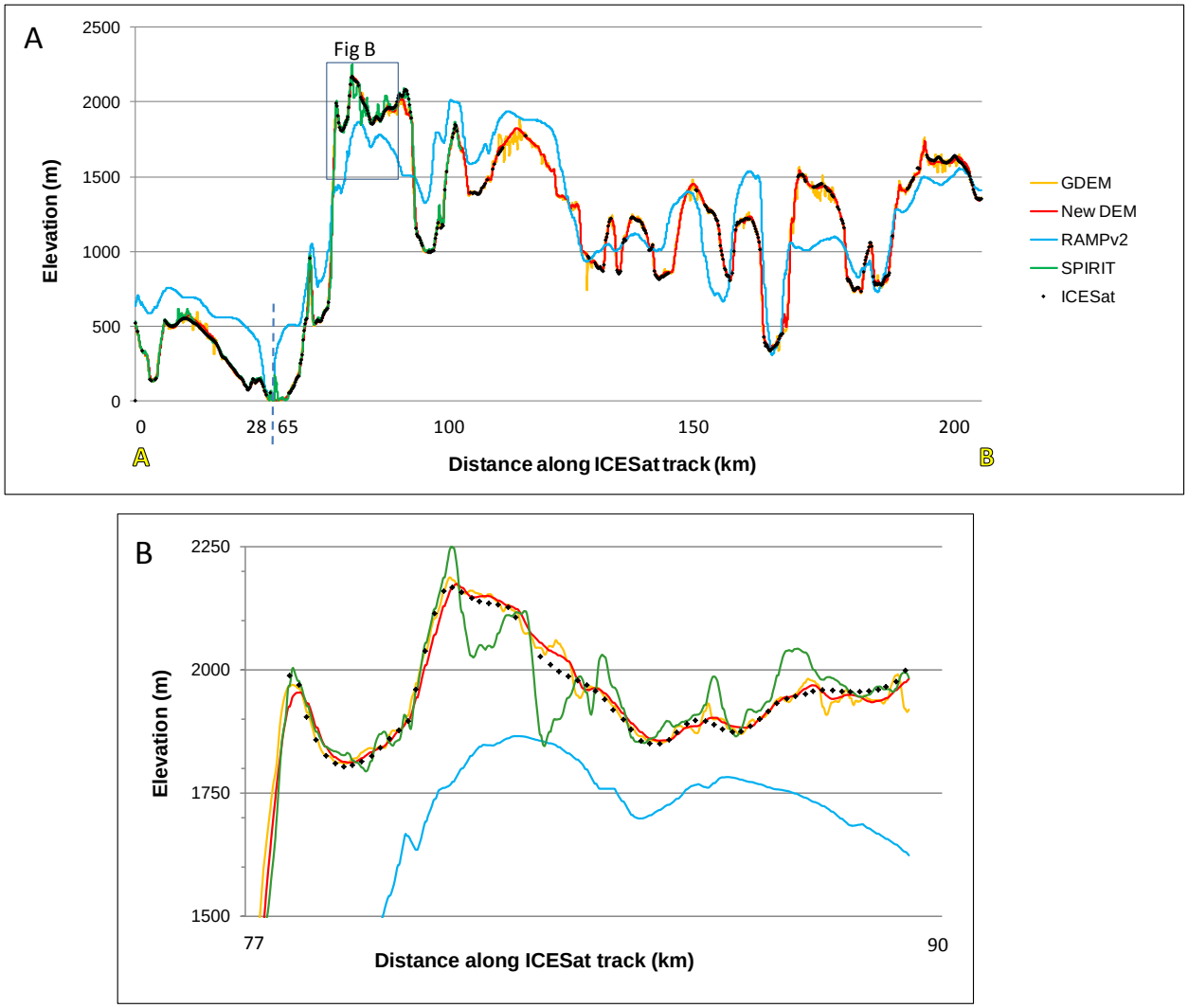

Figure 3.7: DEM profiles along an ICESat track.
The ICESat track (GLA06_0144) crosses a range of topography and illustrates relative differences between each DEM and ICESat elevations (a). Each DEM and the ICESat elevations are adjusted to the EGM96 Geoid. The SPIRIT DEM is based on version 2, unmasked. The inset (b) shows the differences in greater detail. The profiles for 4 other ICESat tracks and a map of the ICESat track locations can be found in Appendix 3.1. Definitions of acronyms of DEM datasets are in Table 3.1.

3.6.1.2 Vertical accuracy for corrected vs. uncorrected regions

Figure 3.5 shows the delineations of edited regions across the DEM. Comparisons can be made between GDEM and the new DEM for pre- and post-editing, both inside and outside these regions (Table 3.3). Error values for the new DEM within edited regions (mean -6 m, RMSE ± 24 m) are similar to the areas outside the edited-polygons (mean -1 m, RMSE ± 25 m). This is in sharp contrast to the raw GDEM which has much greater

error values (mean -23 m, RMSE ± 129 m) inside the erroneous regions before editing, illustrating the improvement by the removal of pits and spikes. This indicates that there is no systematic bias introduced as a result of the correction process.

Table 3.3: Comparisons between the new DEM and ASTER GDEM.
Both edited and non-edited regions (accuracies are relative to ICESat in metres). 'Non-edited' signifies regions where the original GDEM is considered to be of high-quality. N.B. the new DEM was down-sampled to 100 m and filtered in the 'non-edited' regions, which explains the higher RMSE.

	Edited regions		Non-edited regions	
	New DEM	ASTER GDEM	New DEM	ASTER GDEM
N	34858	34832	29735	29447
Mean	-6	-23	-1	-2
RMSE	± 24	± 129	± 25	± 19

3.6.1.3 Vertical accuracy according to slope

Vertical differences are highly slope-dependent. For example, a small horizontal offset between ICESat and the DEM can have a large effect on the vertical difference (i.e. on steep slopes there is much greater elevation change per horizontal distance), which could be misinterpreted as vertical error. In low-slope regions this will have less of an effect and so we can have far greater confidence that the error values are correct. The vertical error assessment was re-run according to a range of slope categories (Figure 3.8). The mean differences from ICESat follow a similar trend for all DEMs: a smaller mean error at low-slope angles, increasing with steepness of slope. The same is true for RMSE values, but the main difference is that GDEM has a very high RMSE at low-slope angle, steadily decreasing until it increases again at slopes > 30°. RAMPv2 has considerably higher mean and RMSE values than all other DEMs, and it is the only DEM to have a mean positive offset increasing with slope. The other DEMs begin to show a negative offset increasing with slope at > ~30°. If values at a slope angle > 30° are omitted from error-calculations, we can obtain a more reliable measurement of vertical accuracy unaffected by slope-dependent bias (Table 3.4). However, without horizontal co-

registration of the DEMs we cannot be sure whether the greater vertical offset as surface slope increases is actually increasing data error or greater vertical differences caused by mis-alignment.

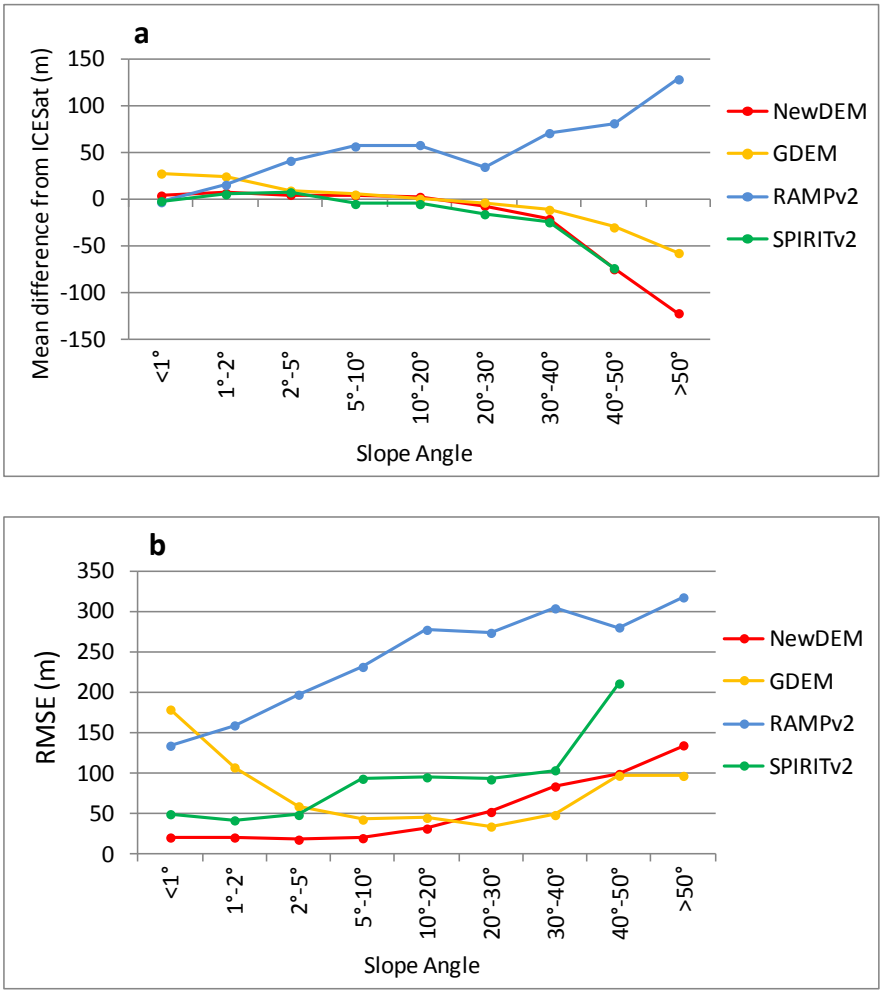

Figure 3.8: Graphs show DEM mean differences from ICESat.
The mean differences (a) and RMS errors (b) are categorized by slope angle.

Table 3.4: Mean elevation differences from ICESat in regions with real-surface slope < 30°. *N* is the number of ICESat points. Mean and RMSE are in metres and all datasets are with respect to the EGM96 Geoid.

	New DEM	ASTER GDEM	RAMPv2	SPIRITv1	SPIRITv2	SPIRITv1 masked	SPIRITv2 masked
N	63799	63486	63953	16561	16575	13392	10825
Mean	-4	-13	-32	3	-1	5	3
RMSE	± 22	± 97	± 199	± 57	± 66	± 47	± 33

3.6.2 Horizontal accuracy

If the DEM was shifted, rotated or re-scaled horizontally to fit ground-truth elevation data, it might give different vertical accuracy results. The problem with rectifying the DEM is that considerable distortion would occur in regions lacking ground-truth data and between gaps in the data. It is not possible to make a shift without first determining the scale and direction of horizontal offset across the complete DEM. A method outlined in Nuth & Kääb (2011) for co-registering DEMs centres on the fact that there is a characteristic relationship between elevation differences and the direction of the terrain (aspect), which is related to the x-y-shift between the two DEMs. The co-registration process involves computing slope, aspect and vertical differences and fitting a curve between two DEMs to allow a shift of one DEM to match the other (with further corrections for elevation-dependent bias and/or cross/along-track geometry as required). Non-stable terrain must be excluded from these calculations. Nuth & Kääb (2011) also suggest that this method can be applied using elevation data points, such as ICESat. Although this is a valuable way of co-registering datasets, there are two reasons that this cannot be applied to the new DEM:

a. The area of stable terrain across the Antarctic Peninsula DEM region is only 3.15% (as calculated using rock outcrop data available in the ADD).
b. The sample size will be reduced further by the scarcity of ICESat footprints that fall within these regions. The co-registration of the new DEM to these few points would not be valid.

If the new DEM cannot be co-registered to ground-truth elevation data, alternative tests must be carried out to assess horizontal accuracy. These tests can be based on the positions of mountain peaks since they are easily identifiable on each DEM. Although GPS points are limited, peaks detected on SPIRIT DEMs can be used to obtain a sufficient coverage across the whole Antarctic Peninsula.

3.6.2.1 Horizontal accuracy based on GPS points and a photogrammetric DEM

Ryder Bay on Adelaide Island (67.5° S, 68° W) (Figure 3.9) was chosen as a sample region from which to ground truth geodetic height and horizontal positions, as it has been GPS surveyed and a DEM at 2.5 m resolution produced from aerial photographs.

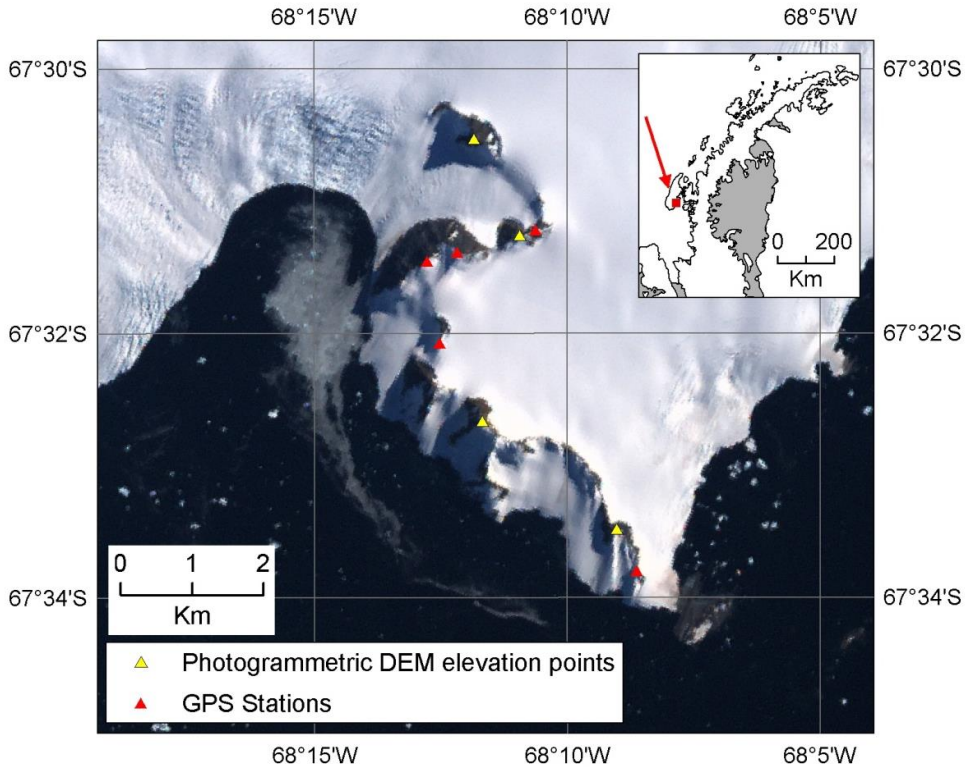

Figure 3.9: Horizontal offset sample region - Ryder Bay, Adelaide Island.
The location of GPS points and elevations derived from the high-accuracy photogrammetric DEM are displayed. (Location is shown on inset).

The GPS positions are better than 0.1 m in both horizontal and vertical accuracy and the photogrammetric DEM has a vertical accuracy of better than 0.5 m RMSE. The SPIRIT DEM does not cover this region, so only GDEM and the new DEM were compared to the

Ryder Bay DEM. Although the sample region is small and only 10 peaks are used, the positions can give absolute-error values (Table 3.5). The horizontal mean difference from the pixel centres for the raw GDEM is 40 m, and for the lower-resolution new DEM it is 64 m (i.e. below the 100 m pixel size). The mean vertical differences, however, are considerably greater than those calculated along the ICESat tracks. The mean peak difference for GDEM is 38 m lower, and for the new DEM is 77 m lower than the absolute value. Previous studies have shown that ASTER DEM accuracy is highly correlated to the steepness of the terrain, where gross errors are likely to occur at steep slopes and high peaks (Kääb *et al.*, 2002a; Toutin, 2008; Cziferszky *et al.*, 2010). Peak elevations on the new DEM have been further reduced during the resampling and filtering process.

Table 3.5: New DEM absolute errors in the Ryder Bay region.
The table shows the mean differences from the Ryder Bay DEM and GPS points for 10 peaks (metres).

	GDEM	New DEM
Horizontal	40	64
Vertical	-38	-77

3.6.2.2 Relative accuracy and consistency tests using SPIRIT DEMs

A wider assessment of geopositional accuracy can be carried out using SPIRIT DEMs, as they are well distributed across the new DEM. Although SPIRIT DEMs cannot be used for absolute error tests due to inaccuracies of their own (Korona *et al.*, 2009), they can be used as a suitable reference dataset for relative accuracy and consistency tests across the new DEM. Section 3.3, Table 3.2 and Figure 3.7 show the horizontal and vertical precision of SPIRIT DEMs. Based on the ICESat vertical accuracy test results, SPIRITv2 (masked) was chosen as the most suitable DEM for the horizontal comparisons.

Figure 3.10 shows the location of SPIRIT tiles and the sample regions chosen for relative error tests. Within each sample region, a number of peaks were identified on the SPIRIT DEMs, and the same peaks were then identified on the GDEM and the new DEM. The results are summarised in Table 3.6 and Table 3.7.

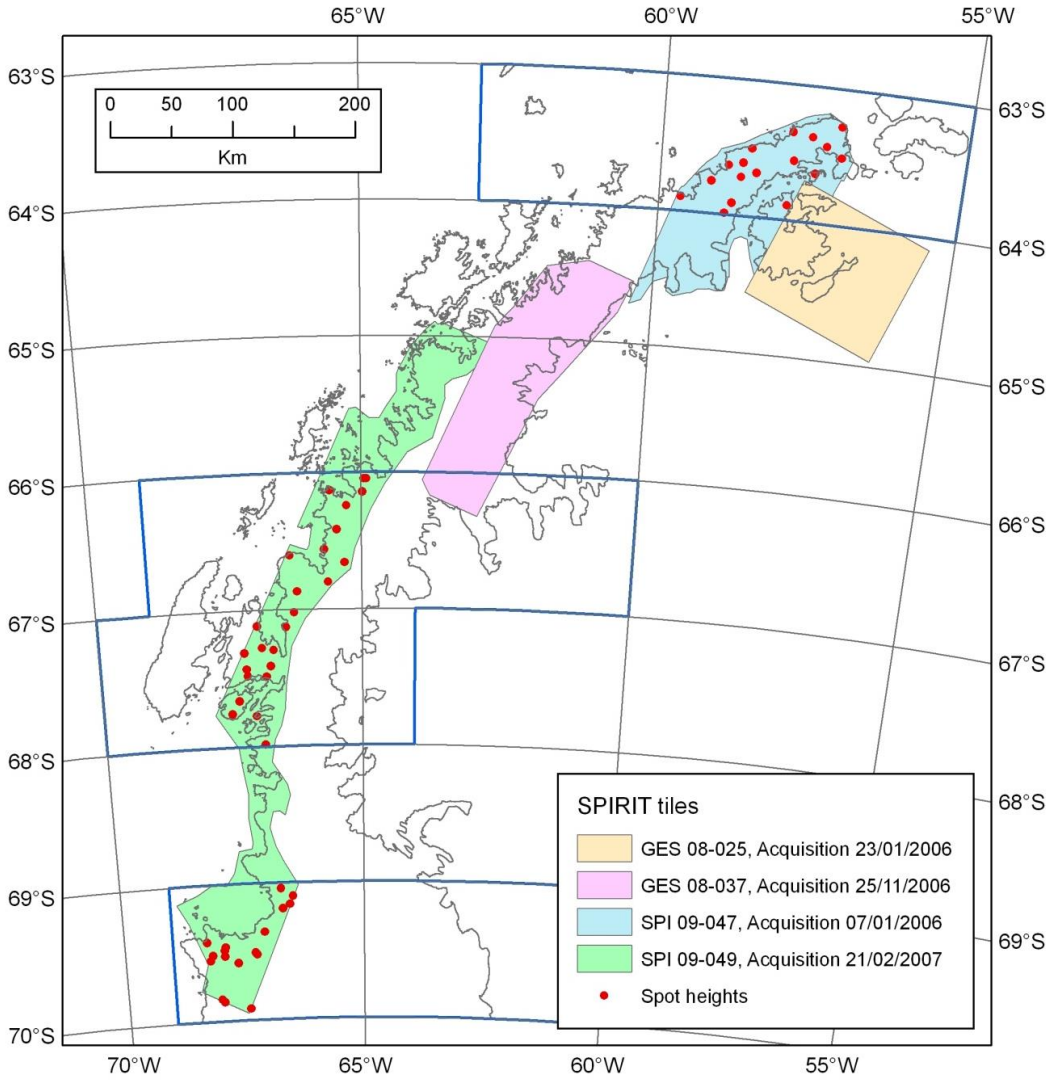

Figure 3.10: Map showing SPIRIT tiles used for relative accuracy tests.
It shows the tile limits and their acquisition dates, plus the location of spot heights chosen for consistency and relative error tests.

Firstly, using all 60 points from across the Antarctic Peninsula, differences between GDEM and the new DEM relative to the SPIRIT DEMs were measured. In each case the centre of the pixel was used as the geodetic position. The positions of the peaks on ASTER GDEM have a mean horizontal difference from their positions on the SPIRIT DEMs of 75 m (RMSE ±48 m) and the new DEM has a mean difference of 130 m (RMSE ±59 m). The peaks on ASTER GDEM have a mean vertical difference from the SPIRIT models of -8 m (RMSE ±24 m) and those on the new DEM a difference of -51 m (RMSE ±25 m). The reduction in height of peaks during the DEM editing process does not occur on lower relief slopes. The different resolution of the DEMs is one factor

influencing the height differences (Kervyn *et al.*, 2008). In order to assess the consistency throughout the new DEM, three regions can be compared (Table 3.7). The mean horizontal difference is less than 2 pixels for each region (between 106 – 161 m), and there is little variation in vertical errors, with mean heights ranging from 40 to 64 m below the SPIRIT DEM values.

Table 3.6: New DEM relative errors.
Values are a summary of the differences relative to SPIRIT DEMs for ~60 points distributed across the Antarctic Peninsula (in metres).

		GDEM	New DEM
Horizontal	Mean	75	130
	RMSE	± 48	± 59
Vertical	Mean	-8	-51
	RMSE	± 24	± 25

Table 3.7: New DEM consistency tests.
Based on points obtained from SPIRIT DEMs in north, mid- and south Antarctic Peninsula regions (See Figure 3.10). Values are mean differences in metres.

	GDEM	New DEM
63° - 64° S: 17 points		
Horizontal	55	131
Vertical	-6	-44
67° - 68° S: 25 points		
Horizontal	67	106
Vertical	-16	-64
69° - 70° S: 17 points		
Horizontal	106	161
Vertical	4	-40

3.6.2.3 Horizontal differences from the Landsat Image Mosaic of Antarctica

LIMA, at 15 m resolution, is often used as a base image for many glaciology studies so its geospatial accuracy relative to the DEMs must also be evaluated. The horizontal

positions of the peaks on the SPIRIT DEMs were compared with their positions on LIMA. In addition to the Ryder Bay points, 25 positions along the coast of Ryder Bay were measured from LIMA and compared to the coast digitised from the photogrammetric DEM. The raw GDEM was used against which to compare LIMA as it has a higher resolution than the new DEM whilst sharing the same geolocation. LIMA has offset values from each dataset ranging from 81 to 110 m, although it must be noted that the direction of offset is not consistent between datasets (Table 3.8).

Table 3.8: New DEM horizontal differences from LIMA (in metres).

	Ryder Bay (55 points)			SPIRIT (60 peaks)			GDEM (70 peaks)		
	x	y	distance	x	y	distance	x	y	distance
Mean	-81	-69	110	-25	4	94	18	-10	81
RMSE	± 39	± 39	± 41	± 70	± 84	± 62	± 59	± 77	± 56

3.6.3 Methodology errors

Some of the inaccuracies in the new DEM have been introduced through data processing methods. From the original GDEM tile, each process introduces the following horizontal differences:

- Reprojecting the original GDEM to LCC projection introduces a difference of ~15 m
- Resampling to 100 m reduces the horizontal precision by up to ~50 m
- Each tile was on an LCC projection with different parameters, so when re-projected onto Polar Stereographic before mosaicking, a further difference of up to ~50 m was introduced
- The filter process caused ‘expansion’ of up to 140 m at edges but did not change horizontal positioning within the DEM.

These processes can explain horizontal differences, but the principal vertical differences occur during the resampling and filtering processes. The average heights in regions of low-moderate relief were unaffected by smoothing, but the peaks and steep slopes were reduced in height. This can be explained by the relationship between elevation bias and

maximum curvature of the slope: where slopes have low curvature values, the DEMs are equally represented at low- and high-resolution, whereas slopes with high curvature values are less well represented on coarser DEMs (Kervyn *et al.*, 2008; Gardelle *et al.*, 2012).

The new DEM is an improvement over existing surface topography models of the Antarctic Peninsula, but it comes with a few caveats. It has been corrected for the purpose of measuring glacier basin outlines, geometry and topographic parameters, but it is not suitable for elevation change studies or accurate positional measurements of mountain peaks. This is largely because GDEM is from ASTER scenes spread between 2000-2009, meaning that seasonal and inter-annual differences in the ice surface are inherent in the data, and the RMSE value is too large to allow for precise surface measurements. Some anomalies along the coast have been removed, resulting in small gaps, and the DEM has a small number of remaining artefacts. It only covers regions included in ASTER GDEM, in which there are inherent gaps and some missing islands.

3.7 Summary

In this chapter, a methodology has been presented in which anomalies inherent within ASTER GDEM have been significantly reduced to produce a new DEM for the AP between 63° – 70° South. Although the technique is unconventional, it has enabled a new 100-m DEM to be produced that is a demonstrable improvement over existing surface topography models of this region. This new representation of the surface is at a resolution and accuracy on a par with DEMs used in medium-scale glaciological research elsewhere. It will facilitate production of a glacier inventory with topographical parameters such as elevations, slope, aspect and flow length for individual glacier basins. Since it was made publically available via the NSIDC datasets website it has already been used in a number of research projects (Barrand *et al.*, 2013a; Bliss *et al.*, 2013; Huss & Farinotti, 2014; Kulessa *et al.*, 2014; Scambos *et al.*, 2014) and has been included in the comprehensive BEDMAP2 dataset, a model of the bed and surface topography of the Antarctic continent (Fretwell *et al.*, 2013). The DEM has been validated by carrying out six accuracy tests, which highlight that whilst it has limitations,

it is the first DEM with the spatial coverage, resolution and accuracy suitable for glacier morphology studies in the region. Absolute vertical accuracies taken from ICESat tracks from across the varied terrain on the Antarctic Peninsula show that the new DEM has a mean vertical error of -4 m, with an RMSE of ±25 m. Absolute accuracies within the edited regions are similar (mean -6 m, RMSE ±24 m) so there is no apparent bias introduced through the editing process. Vertical values on peaks, however, were found to be significantly below real-values. This is as a result of the resampling and filtering processes, which are recognised to reduce elevation in regions with high-curvature of slope. Horizontal accuracies for the new DEM are below 2 pixels, as found in all error tests. The DEM is publically accessible via the NSIDC data portal: http://nsidc.org/data/nsidc-0516.html (doi:10.5060/D47P8W9D) and a low resolution (1 km) version is available from BEDMAP2.

Chapter 4

Glacier basins and area change: data acquisition and analysis methods

4.1 Introduction

A prerequisite for glacier-by-glacier mass balance studies is the definition of outlines for each individual ice mass. As explained in Chapter 3, one significant factor preventing the mapping of glacier boundaries in the Antarctic Peninsula is the lack of topographic data with sufficient resolution or accuracy to capture the steep-sided coastal regions and relatively small glaciers that are prevalent in this region. Now that a suitable DEM has been created, it is possible to distinguish boundaries between flow units and thus produce an inventory of glacier drainage basins with their topographic parameters. A glacier inventory provides a resource for further glacier research on mass balance and glacier behaviour in response to environmental change, and is a benchmark for continued monitoring of changes in glacier area. This chapter describes existing methods for producing glacier inventories and discusses the optimum method for creating one in this unique region. The processes involved in compiling the new glacier basin inventory, deriving individual glacier attributes and creating a comprehensive glacier-change database are outlined. This new dataset allows area measurements to be made, improving the possibilities for interpreting glacier changes in this region. The complex glaciology on the AP means that analysing area changes is not straightforward and an approach unique to this region is required to overcome issues not encountered elsewhere. These methods are explained here, alongside the limitations of the dataset and inherent uncertainties in calculating long-term glacier change in the AP. A summary of these methods is published in Cook *et al.* (2014 (In Press)).

4.2 Glacier outlines

4.2.1 Existing glacier inventory compilation methods

Glacier inventories have been recognised as a means for glacier distinction and parameterization since regional glacier mapping began in the late 19th century. The need for a world-wide inventory based on a consistent methodology was first recognised in the mid-1970s (Müller *et al.*, 1977), which led to the original World Glacier Inventory (WGI) being launched in the 1980s by the World Glacier Monitoring Service (WGMS, 1989). In 1989, the database consisted of point coordinates of ~25,000 glaciers with parameters such as location, area, length, elevation and classification, and increased to over 130,000 glaciers in 2012 (WGMS & NSIDC, 2012). An extension to the WGI is the Global Land Ice Measurements from Space (GLIMS) inventory, which includes delineations of glacier extent and rates of change in the form of glacier outlines mapped from satellite data and historical data such as maps and aerial photographs (GLIMS & NSIDC, 2005, updated 2012). In 2012, the database contained data for ~93,000 glaciers.

The majority of regional glacier inventories are now performed within the framework of the GLIMS initiative (e.g. Kargel *et al.*, 2005; Raup *et al.*, 2007). The GLIMS classification system includes parameters to characterize the morphological shape of glaciers, such as primary classification (e.g. mountain glacier, ice cap, ice stream), form (e.g. basin shape), frontal characteristics, longitudinal profile and activity of the terminus. These parameters are assigned on an individual basis, using sources such as satellite imagery and DEMs for feature interpretation. The variety of classes enables detailed descriptions of glaciers in all regions of the world, including the Antarctic Peninsula (Rau *et al.*, 2005). Most recently, the Randolph Glacier Inventory (RGI 3.0) has been produced, which combines outlines from GLIMS and other (often unpublished) sources by using the highest quality version for each region (Arendt *et al.*, 2012). While having the advantage of collating a larger number of glacier outlines, it is lacking in glacier attributes.

The outline inventories, GLIMS and RGI, include planimetric glacier outlines and/or polygonal glacier basin outlines. Glacier outlines are defined as the ice/rock interface,

whereas the glacier basin is the drainage zone encompassing the glacier and includes the steep-sided valley walls and rock outcrops (Kääb *et al.*, 2002b). Glacier basins are also used to separate contiguous ice masses into individual glaciers, typically along firn divides as estimated from DEM information (Kääb *et al.*, 2002b).

Glacier outlines have been produced for many glacier inventories in non-Polar Regions using semi-automated multispectral glacier mapping methods (e.g. Paul *et al.*, 2002; Paul & Andreassen, 2009; Svoboda & Paul, 2009; Bolch *et al.*, 2010). Semi-automated delineation of glacier outlines based on a shortwave infrared (SWIR) band in sensors such as Landsat Thematic Mapper (TM) or Multi-Spectral Scanner (MSS) is now a well-recognised approach (Svoboda & Paul, 2009). The method uses thresholded band ratios (red/SWIR or Near-IR/SWIR) from raw digital numbers to identify spectral differences of ice and rock. Since the principle is based on spectral contrast, the optimal satellite scene for glacier mapping is a) acquired at the end of the ablation season with as little seasonal snow as possible, b) free of clouds, c) includes a SWIR band for automated mapping and d) has a high solar position to avoid deep shadows. Manual correction is still necessary in the case of wrongly classified debris-covered glaciers, water bodies and attached snowfields, for both TM and MSS images. Recently, multi-spectral satellite sensors such as ASTER have been used alongside DEMs to automate glacier delineation and to derive topographic parameters for each glacier (e.g. minimum, maximum and mean elevation, length, slope, aspect) (Svoboda & Paul, 2009).

4.2.2 Glacier inventory challenges in the AP

In the Polar Regions, delineation of glacier outlines presents greater challenges. One main issue is that many glaciers originate from the ice sheet and therefore flow units are not independent. Glacier ice often becomes more distinct at lower altitudes, and mountain glaciers detached from the main ice sheet have distinguishable outlines, but other issues are also encountered. The ideal satellite image for the band ratio threshold method outlined above is difficult to find in the AP because: a) there is snow and firn cover year-round in many regions, b) the availability of suitable cloud-free scenes at the end of the ablation season is limited, c) the availability of multispectral images is

significantly reduced due to the frequent presence of cloud-cover and the lack of daylight throughout winter months, and d) the low solar angle for much of the year creates large shadows. Automated delineation of glacier outlines using established methods in the AP is therefore considerably more problematic.

Despite these obstacles, a number of regional inventories for glaciers on the AP have been produced using manual-interpretation methods. The first glacier inventory was produced in 1982 for 167 glaciers on James Ross Island and Vega Island based on topographic maps at 1:250,000, early satellite imagery and aerial photographs taken in 1979-80 (Rabassa *et al.*, 1982). Individual glacierized features were mapped and ice domes were identified on the large ice fields. Since then, a case study conforming to the GLIMS criteria produced a Geographic Information System (GIS) consisting of drainage basin limits, basin areas, altitudinal ranges, perimeters and mean lengths for glaciers on King George Island in the South Shetland Islands (Braun *et al.*, 2001). The parameters were derived using a combination of manual interpretation from ASTER and Landsat TM satellite images (Braun *et al.*, 2001) and delineation of drainage basins from SPOT images (Simoes *et al.*, 1999).

Glacier inventories for a further six distinct regions on the AP were produced by Rau *et al.* (2004), which made a significant contribution to the GLIMS project. The primary data sources were ASTER and Landsat-7 Enhanced Thematic Mapper (ETM+) imagery, alongside a digital Landsat TM mosaic as a common spatial reference (Rau *et al.*, 2004). The authors state that ground-based measurements and DEM datasets were used to derive information on the catchment and glacier boundaries, although the methodology is not described in the paper. A description of the GLIMS glacier inventory of the AP in 2006 states that the dataset comprised 1100 entries of all glacial systems and individual glaciers north of 70 S, including adjacent islands (Rau *et al.*, 2006). All features are publically accessible in point data format with attributes, but the only glaciers with outline polyons are a small number near Arrowsmith Peninsula (67.5° S, 67° W). Other glacier outlines available in GLIMS are in the James Ross Island and Trinity Peninsula region, provided by Davies *et al.* (2012). This dataset is a thorough inventory of glaciological structures in the region, digitised manually from 2001 and 2009 ASTER images and a SPIRIT DEM from 2006.

Finally, an inventory of glaciers on islands surrounding the AP has been published recently and made available in the RGI (Bliss *et al.*, 2013). Glacier basin outlines were derived from DEM data, visible-band satellite data, and rock outcrop data available in the Antarctic Digital Database (ADD). Although the inventory eliminates rock outcrops from the glacier basins and therefore represents ice-cover only, the rock-outcrop data available in the ADD is unreliable and in many cases shadow has been mis-interpreted as rock outcrop. It is not considered an accurate way to calculate the area of ice within a catchment. This dataset does not include the mainland, and the only parameters available in the RGI are the glacier ID and area.

It is evident that although glacier outlines exist for specific regions within the AP, a comprehensive inventory, using a consistent technique, is necessary to incorporate all glacier systems. The primary challenges are that the AP region is almost entirely covered in ice, making automated outline delineation difficult, and existing glacier definitions vary depending on the intended usage. It is clear that rather than mapping the glacier ice/rock interface, defining polygonal glacier basin limits is the best way to distinguish between glaciers in this region. The new DEM of the whole region allows delineation of the drainage zones encompassing individual glaciers and separation of contiguous ice masses along ice divides. Together with parameterisation based on the DEM, a glacier basin inventory can be produced for a region that has so far been difficult to map.

4.2.3 Glacier basin delineation methodology

4.2.3.1 Principles of basin delineation

Glacier basin delineation using a GIS approach has been carried out in a number of large glacierized regions of the world such as the Greenland Ice Sheet (Hardy *et al.*, 2000; Lewis & Smith, 2009), Devon Ice Cap (Burgess & Sharp, 2004; Burgess *et al.*, 2005) and Antarctica (Vaughan *et al.*, 1999; Bliss *et al.*, 2013). Automated methods have replaced manual delineation of drainage basins from ice-surface maps, which involved drawing flow lines perpendicular to smoothed elevation contours and manually drawing the boundaries of the catchment areas upstream from the edge to the highest point (e.g. Drewry, 1983; Giovinetto & Bentley, 1985; Björnsson, 1986). Similar principles can be

applied using a DEM alongside standard hydrological modelling tools available in a GIS. This automated approach was first used in Antarctica by Vaughan *et al.* (1999), who first artificially smoothed the surface of a DEM to make it hydrologically consistent, and then from this produced a grid with the direction of steepest descent (i.e. aspect) using the ArcInfo 7.0 GIS workstation. The grid of aspect data was converted to a vector description of the ice flow trajectories (i.e. the flow lines). The watershed (or basin outline) was defined as the upslope area contributing to flow across a defined section of coast and simply calculated from the flow trajectories (Vaughan & Bamber, 1999). The authors report that the overall drainage pattern was controlled by defining sections of the grounding line manually, which in this case were based on the coastline sectors given by Giovinetto & Bentley (1985). The automatic procedure used to delineate the 24 drainage basins was considered adequate, although there were two locations that needed manual amendment: where there were subglacial lakes and where elevation data were sparse.

Although GIS software has developed considerably in the past 15 years, the principles of basin delineation remain the same. Bliss *et al.* (2013) used a watershed algorithm available in ArcGIS to create basin divides in relation to manually defined points along the terminus of each glacier. These end points were chosen visually and the procedure used a combination of the Radarsat Antarctic Mapping Project (RAMP) and the new 100-m ASTER DEM for the islands surrounding the AP (Bliss *et al.*, 2013).

Delineating all drainage basins of the AP is therefore possible, using the same principles and a topographic model with a resolution sufficient for the scale of the features. The resolution (100 m) and elevation accuracy (mean 4 m ± 25 m RMSE) of the improved ASTER DEM is regarded as suitable for watershed delineation of both small steep-sided glaciers and those originating on the gentler relief of the plateau. Where glaciers are connected (e.g. an outlet draining an ice cap), the ice divide can be used as the basin limit. Since snow and exposed rock may be included within the boundaries, the output is glacier basin outlines rather than glacier outlines, but each contains only one glacier terminus.

The method developed for this project is similar to that employed by Bliss *et al.* (2013) although it was developed independently prior to the Bliss *et al.* paper being published. It

has been developed to meet the unique criteria of the complex AP glacier system and to overcome certain problems in this region. The procedure primarily uses hydrological tools available in ArcGIS 10.1 to semi-automate delineation of the glacier drainage basins. Normally such tools require a 'pour point' on the coast where the river exits the catchment and the algorithm calculates the distance upstream until it reaches the watershed. Instead of using a point outlet, a line denoting the entire glacier ice-front was used, forcing the algorithm to include the whole surrounding glacier catchment. The procedure for delineating the basins is described next.

4.2.3.2 Coastline digitisation

The first step was to digitize the AP coastline, which was done manually at an on-screen scale of approximately 1:25,000 from the Landsat Image Mosaic of Antarctica (LIMA). This mosaic consists of Landsat-7 scenes from dates between 2000-02 and was chosen as the base image for all data assimilation and analysis in this study, since it is geospatially more accurate (±54 m) and at a higher resolution (15 m) than other images of the whole AP (Bindschadler *et al.*, 2008). Importantly, it also means that all basins are based on a consistent time period. The positions of ice fronts are continuously changing, and grounding lines are also unstable and difficult to detect in this region, therefore the decision was made to use the coastline visible on LIMA for consistency. The coast was digitised around the whole AP, including all islands, with attributes 'glacier' or 'rock' assigned to denote the type of coast.

One exception to using the coastline for glacier delineation was the large region along the east coast of the AP south of 65.5° S, where the Larsen Ice Shelf abuts the mainland. In order to capture the individual drainage basins along this side of the mainland, the grounding line was used in place of the coastline. This was obtained from the Antarctic Surface Accumulation and Ice Discharge (ASAID) project data source (Bindschadler *et al.*, 2011a), which was acquired using a combination of ICESat/GLAS laser altimetry and manual digitisation from Landsat-7 imagery by a large number of international participants. Positional accuracies of the grounded ice boundary range from ± 52 m for open-ocean terminating segments, to ± 502 m for the outlet glaciers (Bindschadler *et al.*, 2011a). For the present project, the ASAID grounding line dataset was regarded as the

most consistent with the LIMA coastline, and has been digitised at a similar level of detail, from a similar time period and gives complete coverage around the AP. Alternative grounding line datasets (e.g. acquired from differential satellite radar interferometer or spectro-radiometer data) were considered but these have either incomplete data, inconsistent dates or are for large tributary glaciers only. It was necessary to edit the ASAID grounding line in some places, where the position clearly differed from grounding line features (such as crevasses and clear breaks in slope) visible on the LIMA and the ASTER 100-m DEM.

In addition, as the delineation algorithm works only within the boundary of the DEM, the lines have been clipped to the extent of the ASTER 100-m DEM, which is missing some small sections at the coast/grounding line (2% of the total area).

4.2.3.3 Coastline sector criteria

Drainage basin limits were determined by the width at the basin outlet, therefore the coastline was clipped at the mouth of each glacier, based on interpretation of features visible on LIMA, slope changes visible in the DEM and changes in ice velocity visible on an ice flow mosaic (produced by Rignot *et al.*, 2011a). Due to the complexity of the glacier system in this region, neighbouring glaciers are often difficult to distinguish and unique issues are encountered such as indistinct marine-terminating ice mass, semi-permanent sea-ice and ice-covered islands. Placement of glacier-front edges was therefore determined on a glacier-by-glacier basis, with an inherent degree of subjectivity. To make decisions as consistent as possible the following criteria were adhered to:

- A single glacier terminus determines the catchment, regardless of how many glaciers upstream coalesce to form the main branch. In most cases, the glacier terminus segment is obvious, particularly where it is constrained within an embayment. The coastline was clipped at each end of the line signifying the basin front, which may occur at the tip of rock promontories.
- Where glacier ice covers a long stretch of coast with no stable coastal features, divisions were placed where there are profound differences in flow rates.

- For large ice caps / ice fields, ice divides were created in place of drainage basins. For small ice caps or ice-covered islands where no ice divides are clearly visible, the ice-front was not divided.
- An 'ice wall' is a coastal region that is ice-covered but does not match a distinct glacier type: this feature is prevalent along the AP (Williams *et al.*, 1995). It does not extend into the sea, shows no signs of fluctuating in extent and it has no obvious flow features and no defined drainage basin. No ice front divisions were placed along an ice wall.

4.2.3.4 Watershed delineation

During the process of dividing the coastline, basic attributes were assigned to each section. These included an ID and the details of the source imagery from which the coastline was digitised. The LIMA in this region is compiled from Landsat ETM+ scenes from dates ranging from 29/01/2000 to 25/12/2002, and the relevant scene ID, date and year were assigned to each line segment. Any sections of coast that were not ice-covered were classified as 'rock' and all were allocated an identical ID number, unlike glaciers which each had a unique ID. The ArcGIS hydrological tools require the 'pour point' data in raster (i.e. grid) format. Therefore, following categorisation of each coastal segment, the line shapefile was converted to a raster file, based on the ID field.

Using the ArcGIS 10.1 *Spatial Analyst – Hydrology* tools, the ASTER 100-m DEM was filled to smooth the surface and create a depression-less DEM. Then, a raster representing the direction of flow from each cell to its steepest downslope neighbour was created from the surface DEM (*Flow direction*). The *Watershed* tool required both the flow-direction and pour-point raster files to determine the contributing area above the pour-point cells. Since the 'rock' segments all had a single ID number, this resulted in a raster grid with distinct watersheds for glaciers only. This file was then converted into a polygon shapefile. Correction of small artefacts in the watershed boundary polygons was necessary. For example, small 'box' artefacts (i.e. grid cells that appeared as individual polygons) were selected and eliminated. Remaining small polygons (< 0.5 km^2) were merged with neighbouring polygons with the largest shared border. Further manual edits were made based on visual interpretation from the DEM, LIMA and a flow accumulation

raster file derived from the DEM, to improve topographic fit and to smooth lines on large plateau regions.

In order to calculate basin areas with the best degree of accuracy, the drainage basin file was reprojected to Lambert Azimuthal Equal Area projection whose origin is at the South Pole and a central meridian at 65° West. A new attribute field was created and the area calculated using the geometry tool in ArcMap. Sections of rock coast, islands that are predominantly ice-free and basins smaller than 0.5 km^2 are not included in the final database. The result is a total of 1590 glacier outlines with area, date and source details (Figure 4.1), which are available for download from the ADD (http://add.scar.org/).

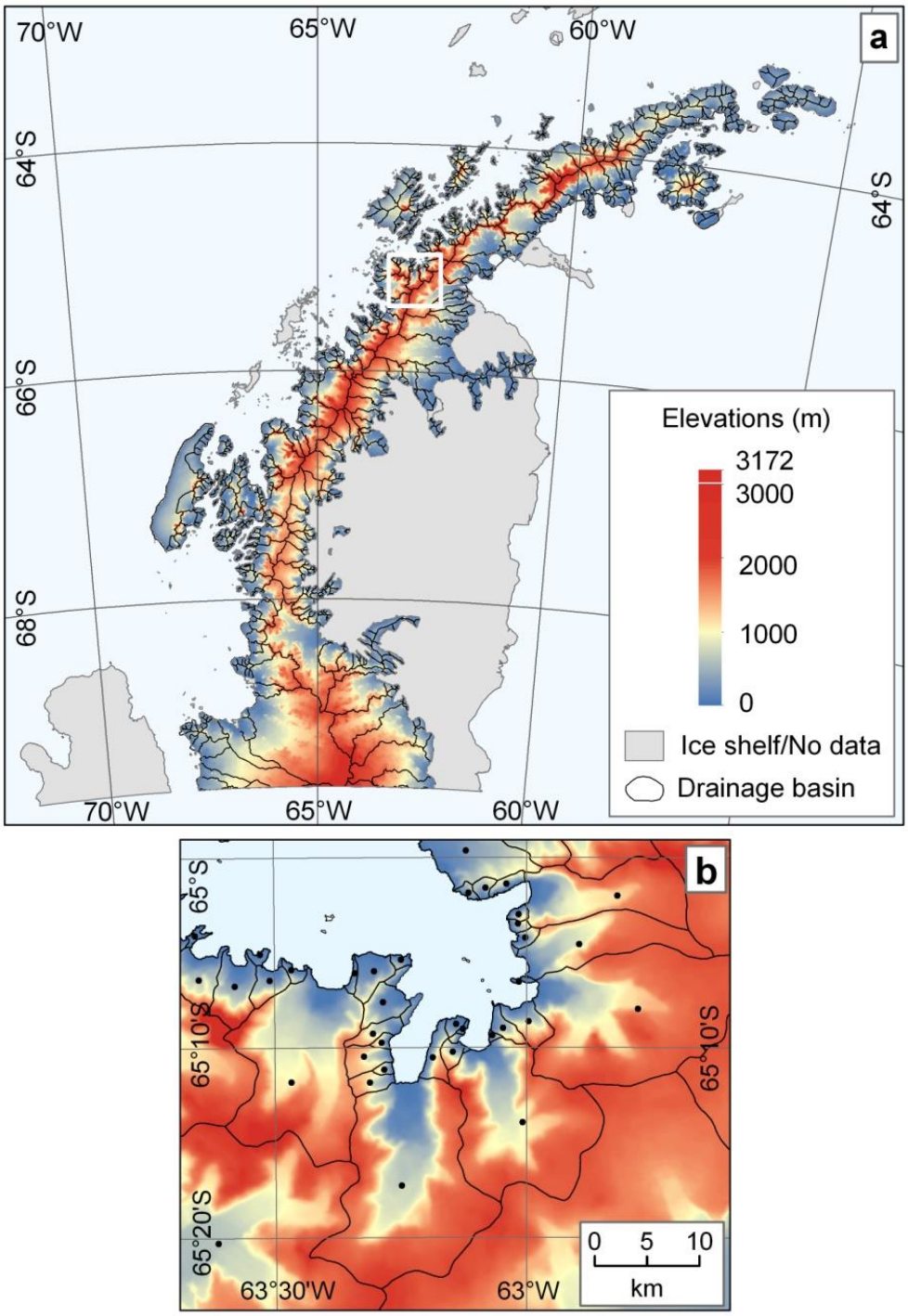

Figure 4.1: Glacier drainage basin outlines.
Panel **a** shows the spatial extent of the glacier outlines. The white box is the inset shown on panel **b**, which illustrates the level of detail of the dataset. The elevation model is the new 100-m Aster DEM.

4.3 Glacier attribution

4.3.1 Nominal glacier characteristics

Nominal glacier attributes have been assigned to each basin in accordance with the GLIMS inventory specifications (Rau *et al.*, 2005). Since the glaciers are not sub-divided into as many glacial units as are in the WGI, the attributes apply to the drainage basins and not the individual glacier entities within the basins. One attribute is the official glacier name according to the GLIMS database: where there are two or more glaciers within a basin, the name of the main branch glacier was assigned to the basin. A large proportion of glaciers on the AP are unnamed, but in some cases, where glaciers have no official name but have a name used in the Coastal-Change study (Cook *et al.*, 2005), these unofficial names were assigned. Further nominal descriptive characteristics include a Primary Classification (*Class*), basin shape (*Form*) and frontal-type (*Front*), as defined for the GLIMS inventory and an overall *Confidence Rating* has been added regarding decisions about these classifications. Nominal classifications are subjective in some cases, but feature definitions obtained from both the GLIMS manual and the Glossary of Glacier Mass Balance (Cogley *et al.*, 2011) were used as a guide. These characteristics are listed in Table 4.1, with definitions given in Appendix 4.1 and an example of primary classifications are illustrated in map form (Appendix 4.2).

Table 4.1: Nominal categories and classification types.
See Appendix 4.1 for descriptions of classifications. The 'Confidence' category relates to decisions on classifications for the three categories.

Class	Form	Front	Confidence
Uncertain/Misc	Uncertain/Misc	Uncertain/Misc	Confident about all
Ice-field	Compound basins	Calving	Confident about some
Ice-cap	Single compound basin	Calving/Piedmont	Unsure/guess as to all
Outlet glacier	Simple basin	Calving/Lobed	
Mountain glacier		Ice-shelf nourishing	
Small ice-covered		Floating	
		Land-terminating	

A point of note regarding the *Front* classification is that the grounding line is not clearly identifiable for many marine-terminating glaciers on the AP. The term 'floating' was therefore only assigned in cases where it was considered to be unambiguous. Where identification was unclear, either the term 'uncertain/misc' was assigned, or 'calving' if active flow features and/or icebergs were visible. These decisions were based on the positions of the ASAID grounding line, combined with interpretation from surface features visible on LIMA.

Where a glacier basin *Class, Form* and *Front* categories are all zero, this feature is what is termed an 'ice wall' and is prevalent along the AP coast. Due to the subjective nature of nominal categorisation, a degree of confidence in decisions made was assigned to each glacier. One *Confidence Rating* value was assigned to summarise the overall confidence in allocation of *Class, Form* and *Front* attributes.

Location descriptive attributes were added to all 1590 glacier basins such as Latitude, Longitude and Latitudinal Degree band, and whether it is situated on the mainland, or a large/medium/small island.

4.3.2 Geometric and topographic characteristics

The glaciers of primary focus in this study are marine-terminating, therefore additional characteristics have been determined for these glaciers. From the total dataset of 1590 glacier basins, those classified as land-terminating, small islands, ice walls, ice-shelf nourishing and ice masses smaller than 1 km^2 were removed, leaving a total of 925 marine-terminating glaciers. Certain geometric and topographic characteristics were derived for these glaciers, such as glacier basin length, outlet width, shape, elevation distribution, slope angle and aspect.

Due to the complex nature of many of the glaciers, defining a single measure of glacier basin length was not straightforward. For example, many catchments contain more than one glacier flowing towards a single terminus. The length of a straight centreline through the basin can therefore give a very different result from the lengths of the main branch or tributaries within the basin. Most glacier studies include a central flow line that is

manually digitised based on surface features, but it is subjective and for a sample size as large as this it is simply not practical. A test version of a GIS algorithm to automatically derive centrelines was applied to the AP glacier basins by C. Kienholz at the University of Alaska, who provided these data for further editing. The algorithm was based on a "least-cost route approach" between the glacier head and terminus, in which branch orders were allocated (Kienholz *et al.*, 2014). The initial centreline file contained a large number of anomalies due to the complex basin shapes and the fact that the outlines are basin limits and not glacier outlines. These data required considerable manual editing to remove extraneous lines and reshape lines to fit flow features, but the result was a line that best represents the central flow line of the main glacier branch for every glacier basin (Figure 4.2). The length of each centre line was calculated in metres and represents the three-dimensional distance along the glacier surface. This semi-automated method was considerably more efficient, and consistent, than the more commonly-used manual digitisation of flow lines.

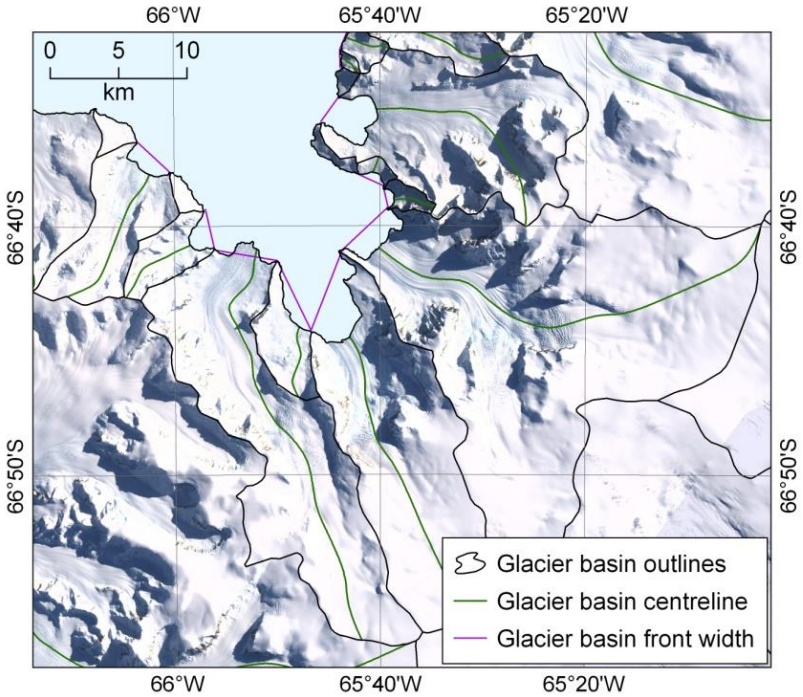

Figure 4.2: Sample regions illustrating glacier basin outlines, centrelines and outlet widths. The background image is LIMA.

The basin front width attribute was based on the straight line distance between the two end points defining the glacier basin front. This was calculated from the partitioned

coastline file, based on the x,y coordinates of the two end points per basin. Once these distances had been calculated the attribute was joined to the drainage basin file based on the ID values. The mean basin width was calculated by dividing the glacier basin area by its centreline length. Such geometric quantities can be used to characterize the basin shape; for example the degree of convergence. This is calculated by dividing the outlet width by the basin mean width, resulting in a dimensionless degree of convergence where $\alpha \leq 1$ (convergent) and $\alpha \geq 1$ (divergent).

Three-dimensional glacier geometry characteristics also included in the attributes are maximum, minimum and mean elevation (metres), slope (degrees) and aspect (degrees), which were calculated from DEM pixel values along the centreline. This was carried out using *3D Analyst – Functional Surface – Add Surface Information* tool. Although this gives biased results, since only values along the centre of the basin are considered, it is a more robust representation of the glacier surface than if values for the whole basin were used as it omits the ice-free steep-sided valley walls.

4.4 Glacier-change data

The glacier basin inventory can be used as the basis for further glacier studies and missing attributes, such as ice thickness and glacier behavioural characteristics, can be added as information is acquired in the future. One key aspect of ice dynamics is the level of activity at the glacier terminus, i.e. the scale and variability of change at the glacier front over time. As previously discussed, long-term mass change in this region is difficult to measure, but historical positions of ice fronts do exist for the AP. These ice fronts can be incorporated into the dataset to produce a comprehensive inventory of glacier changes since records began. Analysis of long-term glacier change has been undertaken for other regions and therefore methods and issues can be learned from existing studies.

4.4.1 Glacier-change studies

Many world-wide regional studies have used glacier length/area variations to extract a climate signal or understand glacier termini variations in relation to temperature change. Multi-temporal satellite imagery and older aerial photography have been used extensively to quantify glacier changes in non-Polar mountainous areas throughout the world. Several long-term glacier change studies based on large sample sizes have been undertaken in the Arctic (e.g. Moon & Joughin, 2008; Howat & Eddy, 2011; Leclercq *et al.*, 2012; Tennant *et al.*, 2012; McNabb & Hock, 2014). Glacier lengths, as opposed to areas, are the most common record of change, but area changes (especially when coupled with data on ice thickness) are considerably more useful for calculations of sea-level contributions. Area measurements can also be used in glacier scaling to estimate volume, using generalized relationships between glacier length, width and area (Bahr *et al.*, 1997). Furthermore, regional studies that aim to understand comparative glacier behaviour require glacier areas to measure change relative to glacier size.

Changes in glacier area and length are calculated based on either automated delineations from earlier satellite imagery or from manually digitized satellite imagery, aerial photographs or large-scale maps. In all glacier-change studies, inherent challenges include: assessing and quantifying the reliability of data sources, the accurate geometric correction of historical data, comparison of imagery at different scales or resolutions, cloud-cover or sea-ice affecting ice front identification, and subjectivity in relation to the manual digitisation of ice fronts. These challenges have been addressed on an individual basis. One common theme is to use an accurately geoferenced, high resolution satellite image as the base image on which all further images are placed. This is also used for correcting or validating data based on visible permanent features such as rock outcrops. Often, uncertainties associated with manual digitisation can only be estimated, although a few studies have carried out a rigorous assessment based on repeated digitisation of ice fronts or stationary features (e.g. Moon & Joughin, 2008; Carr *et al.*, 2013). This is practical for a small sample size of glaciers but unrealistic for large sample sizes where numerous ice front positions are digitised from different sources.

4.4.2 Glacier-change data in the AP

The material containing historical positions of glacier fronts on the AP was an untapped resource until 2002, when the data were digitised as part of a USGS *Coastal-Change and Glaciological Maps of Antarctica* programme. The aim of the ongoing programme is to map historical glacier changes around the entire continent (Williams *et al.*, 1995). So far, 10 of the 24 maps of the Antarctic coastline have been completed (http://pubs.usgs.gov/imap/2600/), 3 of which cover the Antarctic Peninsula. The majority of data for the AP obtained prior to the satellite era is held in the British Antarctic Survey's Archives, with additional material in the form of maps and written accounts held in the library at the Scott Polar Research Institute. Aerial photographs and maps acquired by Americans during explorations in the 1940s – 1960s are stored at the United States Geological Survey (USGS), situated in Reston, Virginia. Satellite imagery, including Corona, Landsat MSS, TM and ETM+, and Radarsat significantly increased the number of glacier-front positional records since the 1960s. These data were located and manually digitised, resulting in a comprehensive inventory of ice fronts on the AP using all available records up to 2002. The results were also published as maps and information booklets, and the data collection and analysis associated with the programme for this region was completed in 2009 (Ferrigno *et al.*, 2006; Ferrigno *et al.*, 2008, 2009). An overview of length-changes for 244 of the glaciers was published in Cook *et al.* (2005). In total, over 2000 aerial photographs and over 100 satellite images were used in compilation of the ice front inventory: all source material used in the project are listed in Appendix 4.3 and the methodology for digitising each data source is described in Appendix 4.4.

4.4.3 AP Coastal-Change dataset revision

The *Coastal-Change* inventory is a valuable resource and it became clear that it had the potential to facilitate a more detailed analysis of glacier change. For example, the initial study of glacier length changes could be improved by calculating changes in area, and a larger population of glaciers and a wide range of glacier types could be included. A number of alterations to the dataset had to be made to maximise its potential: it had to be

geo-registered to fit a more geospatially accurate base image; updated to include ice front positions post-2002; the ice-fronts had to be joined to specific glacier basins to create areas; and the glacier areas were separated into consistent temporal intervals. These updates were carried out using the following methodology.

4.4.3.1 Georegistering the coastal-change dataset

Coastlines in the original AP *Coastal-Change* dataset had been mapped onto the Institut für Angewandte Geodesie (IfAG) Landsat Thematic Mapper mosaic, which was georeferenced using 62 control points from the BAS geodetic control network of the area adjusted in 1985, using conventional block-adjustment techniques (Sievers *et al.*, 1989). At the time this was determined to be the most geodetically accurate image available of the AP, with a pixel size of 30 m and a horizontal accuracy of approximately ±150 m (Ferrigno *et al.*, 2006). The positional accuracy of all sources was assessed relative to the accuracy of the coastlines digitised from the IfAG mosaic.

A quantifiable error assessment could not be made for all individual source material due to the large number of data sources, each having different characteristics, spatial resolutions and geodetic accuracies. Source material was irregularly distributed both spatially and temporally, making it impossible to compare frontal positions at contemporaneous time periods across the whole AP. A method unique to the AP was developed, however, where reliability ratings were assigned to every data source. These provided a consistent measure of coastline accuracy that could be applied to the whole dataset. These reliability ratings ranged from 1 (within 60 m) to 5 (within 1 km). A detailed description of source material within each reliability class is provided in Appendix 4.5. It was decided that in order to maintain the highest degree of accuracy during analysis in the present study, only ice fronts with a reliability rating between 1 and 3 would be used. A discussion of uncertainties in the data appears in Section 4.6.1.

Subsequent to the completion of the *AP Coastal-Change* project, the Landsat Image Mosaic of Antarctica (LIMA) was released, with significantly greater geospatial accuracy. It superseded the IfAG mosaic to become the first true-colour, high-spatial-resolution image of Antarctica (Bindschadler *et al.*, 2008). It was constructed from

Landsat-7 ETM+ scenes that were individually orthorectified and adjusted, resulting in a high-quality nearly cloud-free image mosaic at 15 m resolution. The geospatial accuracy of the Landsat ETM+ scenes is ±54 m (Lee *et al.*, 2004) so the mosaic is an excellent benchmark data set for coastal-change measurements. After it was decided to use LIMA as the base image for this project, it was necessary to georegister all previously digitised coastlines to the LIMA mosaic. The IfAG mosaic did not have a consistent geospatial offset from LIMA across the AP, however, so in some regions IfAG was over 200 m offset and yet in other regions it overlay LIMA precisely. The standard georegistration process, based on placing control-points on identical features in each image and transforming one dataset to the other, introduced considerable errors and data warping. The only alternative was to split the coastal-change dataset on a glacier-by-glacier basis and georegister the coastlines to neighbouring stationary features (e.g. rock promontories) visible on LIMA using tie-points. All ice fronts per-glacier could be georegistered simultaneously as they remained relationally correct. Although rather time-consuming, it resulted in all the original data being adjusted to the new mosaic. Each coastline within the dataset retained its original degree of positional accuracy but now relative to LIMA rather than IfAG, so the absolute geo-location accuracy is improved.

4.4.3.2 Updating ice fronts post-2002

The benchmark ice front position for all glaciers is that digitised from LIMA, with the observational period between 2000 and 2002. The data were updated by manually digitizing more recent ice front positions to fill gaps since 2002 up to 2010. This was done primarily using Landsat-7 ETM+ satellite imagery, and where these were missing/cloud-covered, European Remote Sensing Satellite-2 (ERS-2) Synthetic Aperture Radar images were used. Landsat-7 imagery is freely available for download from the USGS Global Visualisation data portal and at 15 m resolution and high geospatial accuracy, this was the preferred choice. In 2003, the Landsat ETM+ sensor developed a problem and the scan line corrector was switched off, which means all imagery since then contains stripes with null values. Only ice fronts where the complete front was visible were digitised and any intersected by the stripes were ignored. As many glacier front positions as possible were digitised, and for some glaciers this resulted in bi-

annual or annual frontal positions. All ice fronts were assigned with associated attributes, including data source type, date, ID, year and reliability rating. A sample of glacier basins with their various frontal positions is shown in Figure 4.3.

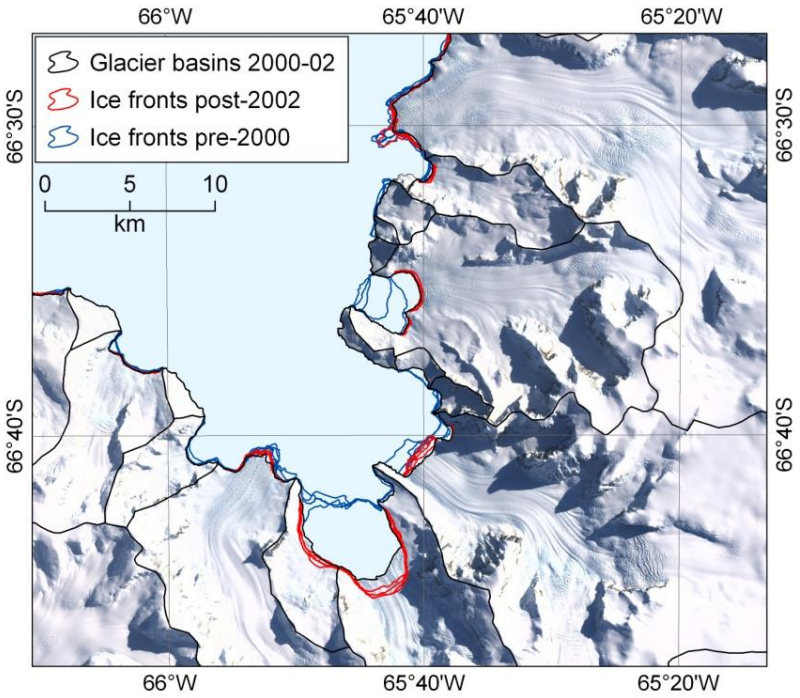

Figure 4.3: Sample region showing historical glacier front positions. The background image is LIMA.

4.4.3.3 Joining ice fronts to glacier basins

The original *Coastal-Change* dataset consisted of lines, some of which covered long stretches of coast and many of which were not associated with any specific glacier. The existence of the new drainage basin inventory meant it became possible to split these lines and join them to the relevant glacier basins using ArcGIS. This created a closed polygon for every data record, each with an ID, associated glacier attributes and ice front data record details. This method could not be automated and therefore it was a substantial task to join all ice fronts to basin outlines for every glacier. It involved not only splitting the coastlines and 'snapping' the glacier fronts to the basin edge, but in many cases the lines had to be tidied at the edges first (e.g. cut or extended). Each line was edited on an individual basis, with editing procedures slightly different for ice front positions either beyond or behind the LIMA coastline or incomplete ice fronts. The LIMA coastline was

used as a guide for the basin edge in all cases. This time-consuming task was partly undertaken by a work-experience assistant during the summer of 2012. These were then reprojected into Lambert Azimuthal Equal Area projection for calculation of the polygon areas.

4.4.3.4 Separation of dates into temporal intervals

The total number and temporal dispersion of glacier front records varies significantly between glaciers. As a consequence of dealing with such a large population, a method was developed to both simplify analysis and maintain the highest degree of consistency for temporal analysis. The first step involved assigning every ice front position to a 5-year interval; this approach was used for analysing the 244 glaciers in Cook *et al.* (2005). This way, ice fronts could be grouped and compared according to the time period in which they occurred. An 'area' attribute for every 5-year interval from 1945 to 2010 was calculated based on the coastline date. For example, if the coastline measurement was from 1947, its 'area' value was placed in the 1945-49 field; otherwise this field was left blank. The area of the glacier at each date was assigned to the associated time interval. After this, a Pivot table was created, to summarise area changes for individual glaciers, from all individual records.

It was necessary to make small edits to the dataset as a number of glaciers had more than one ice front record within a 5-year interval. In these cases only one line was retained during the data editing stage; this being the line with the highest reliability rating. Similarly, if there were less than 12 months between records spanning adjacent time intervals (e.g. a record in 01/10/1974 occurs in the interval '1970-74' and one from 15/01/1975 occurs in '1975-79'), the record with the lower reliability rating was removed. It should also be noted that although glacier fronts had been digitised at frequent intervals since 2000-02, only lines in (or around) 2005-06 and 2009-10 were selected for this project to ensure the interval spacing was as close to pentadal as possible.

Further temporal details were also calculated, namely the earliest and latest recorded years with corresponding areas, and from these values the overall change (in km^2) and

relative change (as % of glacier basin size in 2000-02) could be derived. The result is a new GIS database of 4343 marine-terminating glacier basin measurements presented as polygons, each with associated attributes. Table 4.2 shows the distribution of the number of ice front records per glacier basin.

Table 4.2: Ice front record counts per glacier basin

	Number of records per glacier										All records
	2	3	4	5	6	7	8	9	10	11	
Number of basins	56	122	214	157	105	108	62	21	12	3	860
Total records	112	366	856	785	630	756	496	189	120	33	4343
Mean first year	1984	1967	1959	1955	1955	1953	1949	1949	1948	1947	1958
Mean last year	2002	2002	2001	2002	2005	2007	2008	2009	2009	2009	2004

4.4.3.5 'Multiple' glacier basins and floating ice

A challenge when measuring changes in marine ice fronts is that they can change between floating and grounded, and also either merge with or separate from neighbouring ice fronts. These have been particularly pertinent issues in the AP, since the majority of the ice terminates at the ocean and, over the timescale being considered, many glacier basins that were once merged with other basins are now separate entities because they have receded past a point of convergence.

The matter of inclusion of floating ice must be considered first. This is primarily a study of changes in glacier drainage basins, rather than ice-shelves, yet an issue arises when these glacier basin fronts extend and coalesce with neighbouring glaciers downstream of the grounding line. An ice shelf is defined as "a floating ice sheet of considerable thickness attached to a coast and nourished by glacier(s)" (WGMS definition, in Rau *et al.*, 2005). It has been further explained for GLIMS classification as a "seaward extension of terrestrial glaciers beyond the grounding line" (Rau *et al.*, 2005). Although the understanding is that the development of an ice shelf starts with the confluence of several floating glaciers, it is unclear as to the minimum number of floating glaciers that

constitutes an ice shelf. Whilst large ice shelves are not considered in this project, an upper limit to the number of merged basins must be set.

All basin outlines are based on the ice front position as it appears on the LIMA (i.e. during 2000-02), regardless of the position of the grounding line. As has been explained previously (Section 4.3.1), the ASAID grounding line combined with interpretation from LIMA were used to determine whether or not the basin terminus was floating. In most cases where the terminus was deemed to be floating, there was only one glacier downstream of the grounding line, but in some cases the basin may have contained two or more glaciers that coalesced downstream of the grounding line. Since 2000-02, they may have receded and separated into basins with single glacier fronts (either floating or grounded) and therefore have been included in this study. There are only a few basins to which this applies (Prince Gustav Ice Shelf, Müller Ice Shelf, and Edgeworth, Jorum and Prospect glacier basins). The decision was made that if the basin terminus consisted of more than 5 floating glaciers in 2000-02 these would not be included. It was considered that these represent ice shelves of a size that is beyond the scope of this study and too complex to analyse in terms of change in individual glacier basins. The five basin limit means that measurements of glacier basins adjoining the Larsen A, B and Wordie ice shelves only begin after the major episodes of ice shelf collapse.

A related issue is for glacier basins that were once merged with their neighbours prior to 2000-02 but separated into individual basins by this time. After various attempts at measuring complex glacier changes, it became apparent that these basins should be treated separately as a distinct group, called ‘multiple-basins’. Complexities in multiple-basin analyses arise when the smaller basins within a larger surrounding basin separate at different time periods, and also if they re-merge following separation. This problem had no simple solution, but such glaciers could be grouped according to the maximum extent of the merged basins, to be considered as one individual basin. The limit for the number of basins within a multiple-basin was also set at five basins. If any more basins became merged, they were ignored until after separation into five basins or fewer (e.g. the glaciers flowing into the Wordie Ice Shelf were not considered until after its collapse).

Three new attribute categories were assigned to all glacier basins: MaxDB (to denote whether the basin was part of a wider basin at some point); MaxDB_ID (the ID of the maximum extent of multiple basins) and MDB_ID (the ID of individual basins within the multiple-basin). In total, 55 individual basins were merged into 21 multiple-basins. The multiple-basin group has required further processing due to their complex nature as they changed over time. For example: two individual basins in the 1940s merged to become one basin in 1974, before going back to individual basins. In some cases, parts of the multiple basins have different dates, and false area decreases occur when the basins separate (for example, one part of the newly-separated multiple-basin has a date measurement but the other does not have a measured position at all). Every case of multiple-basins was therefore treated individually in order to prepare the dataset for further analysis. In some particularly complex cases, certain ice front positions had to be omitted. The locations of all multiple-basins across the AP are illustrated in Figure 4.4, and Figure 4.5 illustrates examples of multiple-basins and the ways in which individual basins separate at different points in time.

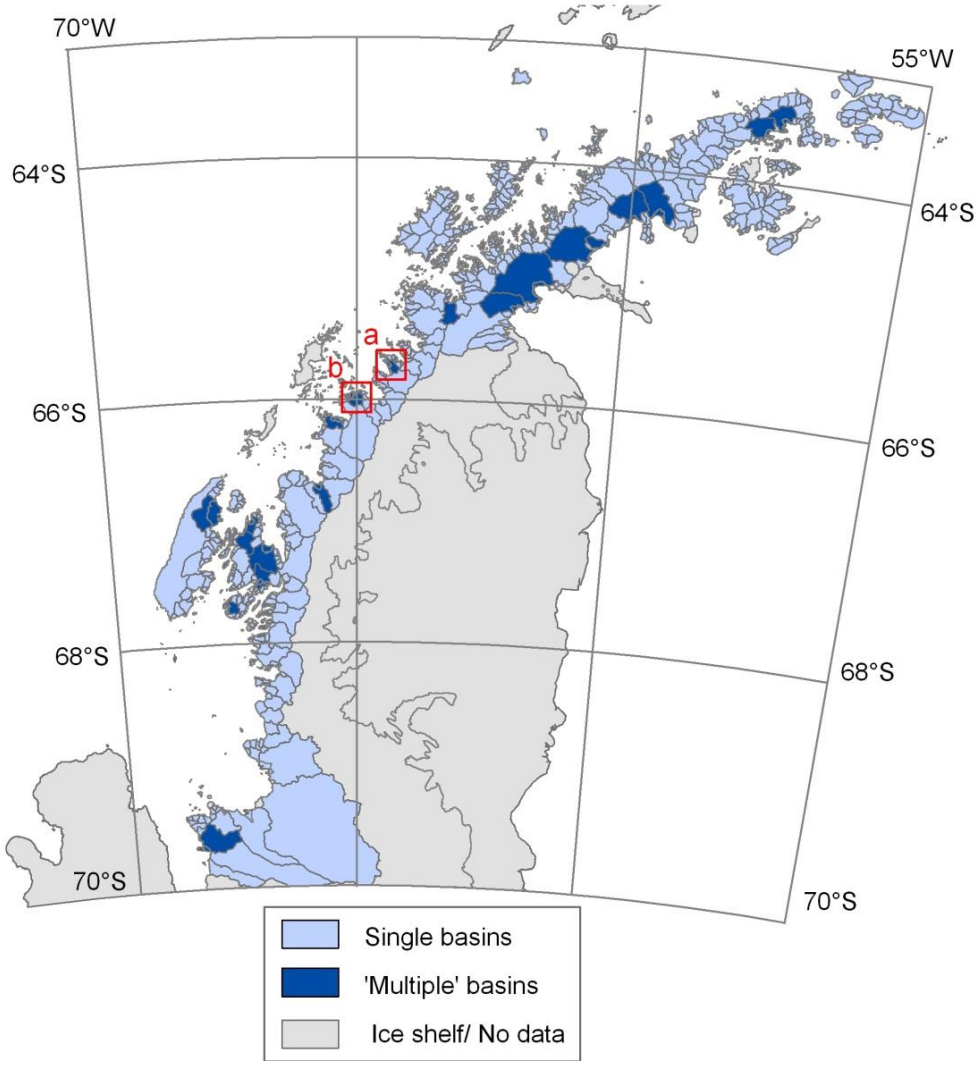

Figure 4.4: Location map showing all marine-terminating glacier basins.
Those that consist of 'multiple' glacier basins are highlighted in navy-blue. Boxes labelled **a**and **b** show locations of glaciers illustrated in Figure 4.5.

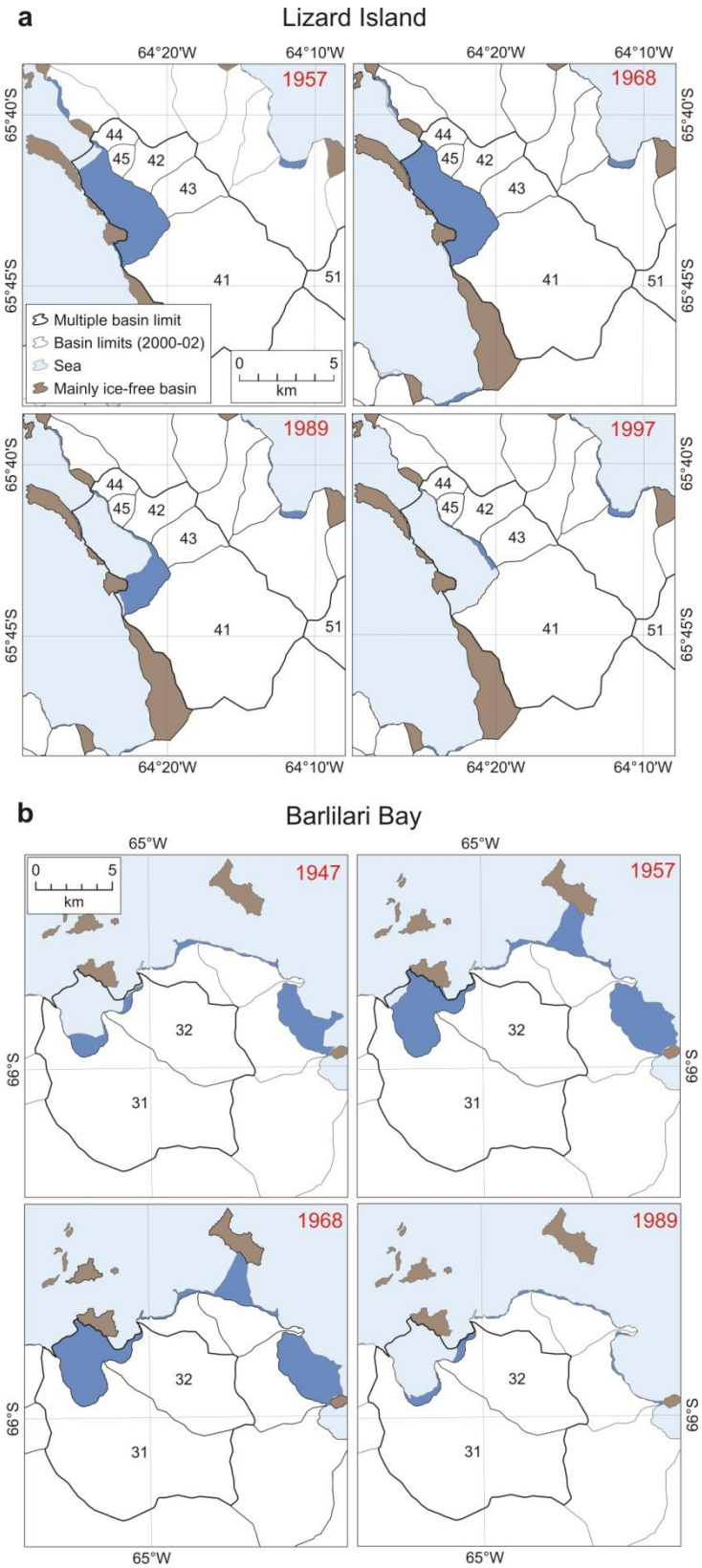

Figure 4.5: Examples of multiple glacier basins.

Figure 4.5: Lizard Island (**a**) and Barilari Bay (**b**) (locations shown in Fig 4.4) both have glacier basins that were once merged with neighbouring basins. The black line denotes the outer boundary of the 'multiple basin', which is treated as one basin during analysis. The Lizard Island multiple basin separates into five basins by 1997. Basin 41 was missing source data for 1997 (where the image only partially covered the ice front), illustrating the issues faced with inconsistent data. The Barilari Bay multiple basin consisted of two separate entities in 1947, which merged by 1957, before separating once more by 1989.

4.5 Glacier-change analysis methods

Analyses of glacier change over time prove to be complex due to the nature of the data available. Frontal positions are invariably measured at infrequent or irregular time intervals; glaciers within the same region may not have concurrent frontal position records, and records are often not consistent in accuracy. Over-interpretation must be avoided, especially where there are long gaps between records, or where there are too few records available. The temporal distribution of glacier frontal position measurements in the AP spans over 60 years, but as with similar studies, there is an uneven distribution of data (Figure 4.6). In order to identify spatial or temporal patterns that may be present in the frontal behaviour of the AP glaciers, suitable methods must be explored to maximise the information available.

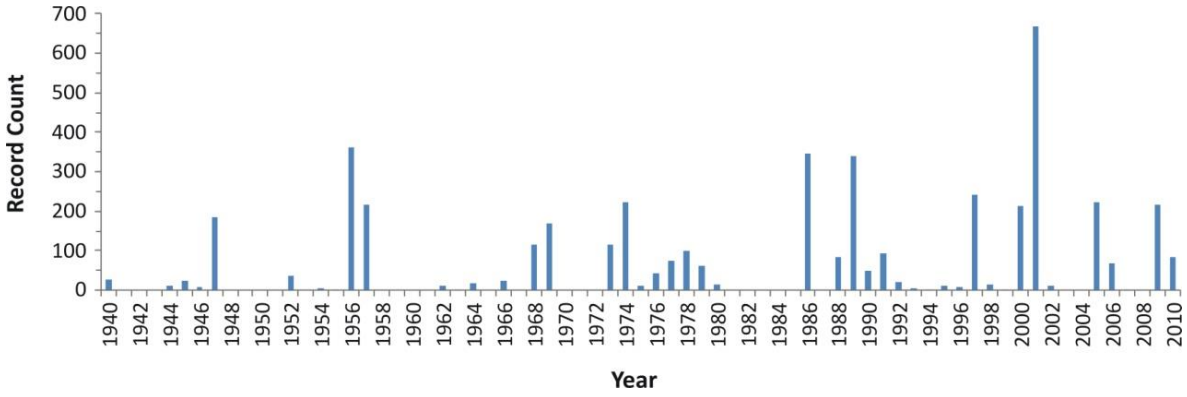

Figure 4.6: Source data temporal distribution.

A number of methods have been developed for assessing frontal change rates, which differ according to the time-scale, the number of glaciers being examined and the frequency of measurements for each individual glacier. Glacier studies involving data at consistent and high temporal resolutions are generally limited to change over the past

decade, due primarily to the improved availability and frequency of satellite imagery. One such study, by Box & Decker (2011) examined area changes for 39 marine-terminating glaciers in regions of Greenland at yearly intervals between 2000 and 2010. In this case, total annual area change could be calculated, which was only possible because all glaciers were measured at all intervals. Such studies clearly allow a high level of confidence about trends in glacier front changes, especially where measurements of the annual glacier cycle are included. For large regional studies using sparse data coverage the same level of confidence cannot be reached, but they do enable a greater understanding of patterns of frontal retreat over longer time-scales.

Most long-term glacier change studies have examined only a small number of glaciers: for example LeClerq *et al.* (2012) have analysed changes in length of 18 glaciers in West Greenland based on varying dates between 1811 and 2010. However, three studies of decadal change of a large number of glaciers in Greenland have been carried out: an assessment of changes in length of 210 marine-terminating glaciers spanning four decades (Howat & Eddy, 2011); an analysis of ice front changes of 203 outlet glaciers over three periods since 1992 (Moon & Joughin, 2008) and, thirdly, a calculation of change rates for 132 glaciers in Greenland since the 1930s (Bjørk *et al.*, 2012). Each existing study has used a different approach to calculate rates of change. The pros and cons of each of these methods were considered when designing an optimal methodology for the AP, and are discussed here.

4.5.1 Long-term glacier-change analysis methods in Greenland: case studies

4.5.1.1 Small sample, multiple observation periods

The study with the longest time-scale of glacier length changes was that recently carried out by LeClerq *et al.* (2012), in which changes in length of 18 glaciers in West Greenland were measured from varying dates from 1811-1900 until 2008-2011. The number of dates per glacier varied from 6 to 13 and the study maximised the historical records for these 18 glaciers, enabling quantification of retreat across a whole century. As with all decadal-scale glacier studies a number of issues were encountered, such as a different

number of records per glacier, inconsistent time intervals and missing data. In some cases there were gaps of up to 80 years between data points. In this case, LeClerq *et al.* (2012) chose to include all data points and interpolate between these points using Stineman interpolation (Stineman, 1980). The rate of length change in m a^{-1} was averaged over 10-year intervals between 1800 and 2010 for each glacier, and the average values for each glacier were displayed in graph form. Although this maximises existing data, this approach leads to smoothing across long intervals and may give misleading results, especially when being compared with a similar length of time that contains several positions. Furthermore, all 18 glaciers have two frontal records since 2000, whereas prior to 2000 there is little consistency in the frequency and timing of recorded positions, causing a bias in the results. The issue regarding the difference in accuracy between more historical records and recent records is mentioned in the paper although not quantified. The major difference between this and the Antarctic Peninsula glacier-change study is the size of the datasets: methods for analysing 18 glaciers are inevitably going to be different from analysing almost 900 glaciers, as are methods for displaying results (for example, graphs showing rates of change for all 18 glaciers are displayed adjacently). Other studies, such as the following three cases, provide examples of working with large sample sizes.

4.5.1.2 Large sample, minimal observation periods

Howat & Eddy (2011) consider a large number of glaciers in their study of glacier length changes around the coast of Greenland but there are several major differences from the AP study in the type of data being analysed. Firstly, although all 210 glaciers in the Howat & Eddy dataset have positions in 2000 and 2010, only half of these have coverage prior to 2000, and only 24 glaciers have measurements in all 5 survey periods. Howat & Eddy defined five survey periods based on availability of data and grouped these as follows: 1972, 1985, 1990-92, 2000 and 2010. Rates of change between survey periods 2000 and 2010 were calculated for all glaciers in m a^{-1} and results included average change rates and median rates (shown on box plots) and separated into four regions. For earlier rates of change, 105 glaciers had positions in the survey periods 1972, 1985, 2000 and 2010 but there was insufficient data for the period 1990-1992 so this period was

omitted from all further analyses. The results are shown to be rates of change between survey periods: 1972, 1985, 2000 and 2010, although within each individual survey period there are dates spanning up to 5 years (i.e. '1972' contains dates from 1972-76; '1985' includes dates ranging from 1984-87). There are only three time intervals, and the length of these varies between 10 and 15 years. The spread of dates within and between intervals therefore is certainly broad but it is an example of a method of grouping data with temporal inconsistencies into time intervals. It is also a demonstration of the complexity of measuring changes with inconsistent and/or sparse data.

4.5.1.3 Large sample, concurrent observation years

In another study, Moon & Joughin (2008) analysed 203 glaciers in Greenland between 4 survey years: 1992, 2000, 2006 and 2007. As opposed to the study by Howat & Eddy (2011), the defined survey periods contained only data from within those years (or the winter season associated with those years). The ice fronts were intersected with an open-ended box that was delineated based on the approximate sides of the glacier to an up-flow across-glacier reference line. The mean change in length (in m a^{-1}) was calculated as the area change divided by the mean width. This gave a better measure of ice front change than if a single along-flow reference line was used. Similar to the AP, imagery is not consistently available for all glaciers during all periods, which means that out of the 203 glaciers studied, only 122 tidewater glaciers have measurements in all three intervals. When split into 5 spatial regions this means that some regions only have a few measurements that cover all intervals. In contrast, in the AP the number of glaciers is almost 900 and the number of recorded positions per glacier ranges from 2 to 11 (Table 4.2). Due to the large population size of glaciers on the AP, there is a greater likelihood of glaciers with comparable data occurring within each region. Secondly, although the data were obtained for consistent time periods in the Moon & Joughin (2008) study, there are different lengths of time between these dates, i.e. 8 years, 6 years and then only 1 year (2006-2007). It is acknowledged in the paper that a time period of only one year may be influenced by the annual cycle and perhaps unreliable conclusions can be drawn by comparing with rate of change over longer time intervals. In the AP, the time difference between recorded frontal positions is greater than 2 years in all cases. Finally,

the 'box' method used by Moon & Joughin (2008) is suitable for measuring changes in length but for a dataset with areas measured at each interval, uneven changes along the ice front can be fully taken into account enabling not only length but also area loss or gain to be calculated more precisely.

4.5.1.4 Large sample, multiple observation periods

A third study that examined length changes for a large number of glaciers was that by Bjork *et al.* (2012). In this case, 132 glaciers in SE Greenland were studied, using data since the 1930s. Rates were calculated between seven observation periods: 1933, 1943, 1965, 1972, 1981, 2000 and 2010. Like the two studies already mentioned, this dataset consists of temporally inconsistent imagery, but it does have a greater number of observation periods. As was the case with Howat & Eddy (2011), the study periods are not always from one year only, e.g. '1933' consists of imagery ranging from 1931-1933, some glaciers are missing data from 1965 and some of those in the '1981' study period are from 1985. Similarly to the challenge faced by Moon & Joughin (2008), there are inconsistent gaps between observations, the difference being here that the gaps are significantly longer e.g. 10 years, followed by 22 years, then 7 years. The rate of change (in m a^{-1}) is calculated by taking an average across each interval, therefore those that are averaged over 22 years are being compared against those averaged across 7 years. Conclusions drawn from comparisons between glacier behaviour in different intervals must therefore be treated with caution. A method to ensure that time intervals are of a consistent duration would reduce the influence of smoothing over long time periods, and data with sparse coverage being compared with data of a higher temporal resolution.

4.5.2 AP glacier-change analysis: new methodologies

4.5.2.1 AP glacier-change analysis challenges

The case studies in Greenland (along with many other similar glacier studies world-wide) have shown that there is a need to further develop a technique that can combat problems such as inconsistency in data and differences in regional and temporal data coverage. The present study on Antarctic Peninsula glaciers is unique in that there are a significantly

greater number of glaciers being observed than in most other studies, a large amount of data are available over a longer time scale and the source material dates are inconsistent. The problems encountered in previous studies include: interpolative errors where there are large temporal gaps in data; over-interpretation from data with minimal observation records; preference to periods with more observation records leading to skewed results; inconsistency in duration of observation periods (e.g. data from 1972-76 summarised as 1972); comparison of change-rates between time-intervals of different duration; and errors associated with length as opposed to area calculations. The challenge for this study was therefore to avoid or reduce each of these issues to a minimum.

The dataset for analysing area changes of marine-terminating glaciers on the AP was prepared by first removing those with only one frontal-position record. From the dataset of 925 marine-terminating glaciers this left 892 glacier basins. Following this, multiple basins that were once one entity were entirely merged (as described in Section 4.4.3.5), resulting in a total of 860 glacier basins with 2 or more ice front position records. The spread of temporal data coverage is uneven across the Antarctic Peninsula, meaning that glaciers have a varying number of dates, some of which have large gaps between the intervals. The glaciers themselves are not evenly distributed spatially: for example, the majority of marine-terminating glaciers lie along the west coast whereas glaciers on the east coast glaciers south of 65.5° S flow into the Larsen C ice shelf. The glaciers are of varying sizes and shapes, meaning that comparative analyses are even more of a challenge. One consistency however is that all glaciers have a frontal record in the period 2000-04 and additionally, all recorded positions are of basin *Areas* meaning that changes in area can be calculated as opposed to changes in *Length*, which is a notable difference between this and most other studies.

The challenge faced in tackling the inconsistencies in such a large dataset can be illustrated with time series plots, using representative glaciers of a similar size and shape. Figure 4.7 illustrates the frontal positions over time for one glacier (ID 1628). Figure 4.7a shows the area of the glacier at each recorded date, and the point at which the record occurs within each five-year time interval. There are 8 frontal positions recorded for this glacier spanning between 01/12/1956 to 15/12/2010. Figure 4.7b shows 4 similar glaciers and the differences in the number of records and dates between these glaciers. Due to the

temporal irregularity of data, glacier changes cannot be compared by date, or even by first/last dates. However, two approaches for inter-comparisons can be made: calculation of change relative to one single time period and calculation of rates of change between time intervals.

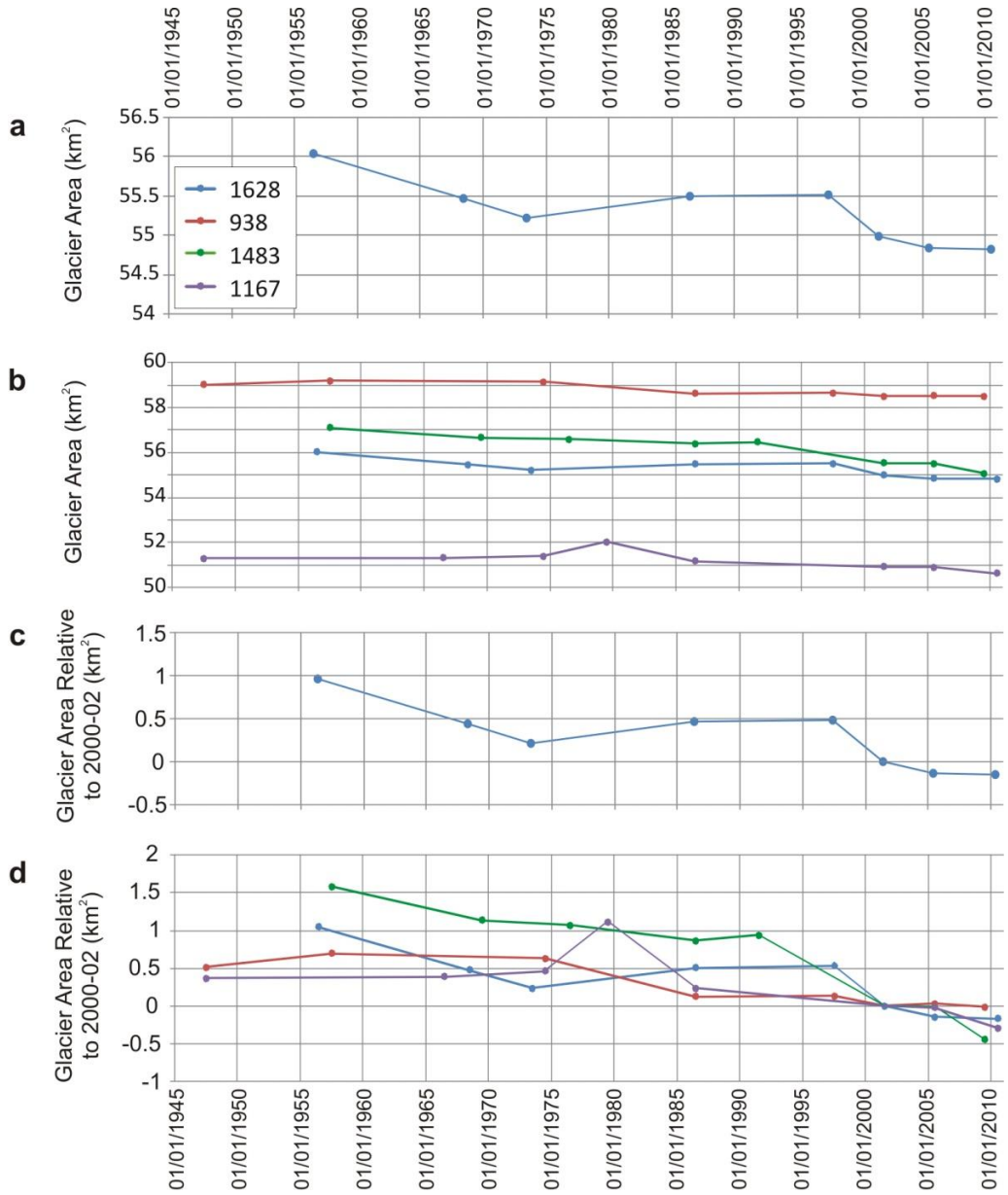

Figure 4.7: Time series plots for 4 sample glaciers.
Figure **a** is a simple plot showing area measurements for one glacier and where they occur along the timeline. The same glacier is shown in **b**, along with three others, illustrating the issue of comparing glaciers of different areas and with irregular durations between measurements. Figure **c** shows the glacier relative to its area in the period 2000-02, and **d** illustrates all 4 glaciers,

relative to their areas in 2000-02, enabling direct glacier area change comparisons. The measurements can be categorised into the five-year intervals as shown.

4.5.2.2 Absolute and relative area change calculations

The area of the glacier at each available date can be calculated relative to its area in 2000-04, since this is the period during which all glaciers have frontal records. Figure 4.7c shows these calculations for Glacier ID 1628, to illustrate that the trend is the same when measurements are made relative to 2000-04. Figure 4.7d illustrates that when the sample of 4 glaciers are calculated relative to 2000-04, they can be directly compared. Since measurements are made independently for each time period there is no problem associated with dates that are close to 2000-04 (whereas there would be an issue if measurements were being inferred from values between the points).

Furthermore, if the measurements are grouped into time intervals, data that fall within those intervals can be compared. In this study 5-yearly (pentadal) intervals were chosen, based on the temporal distribution of data available, and this was considered as the most suitable level of detail for assessing long-term change. There is insufficient data coverage for annual changes and yet in a majority of cases there are data available for intervals spanning less than 10-years. Intervals of 5-years mean that intra-annual variability in glaciers has less of an influence on overall trends when analyzing long term change. If the data are grouped into 10-year intervals, however, changes that occurred during that time could be lost in the averaging process. The method used to assign the records to corresponding time intervals is explained in Section 4.4.3.4. Measuring area differences from glacier sizes in 2000-04 enables statistical analysis of absolute changes in area (in km^2) between each interval and in addition, analysis of change relative to individual glacier sizes (in %). It is not possible to calculate total area change for glaciers peninsula-wide due to the data gaps. An interpolation between the 5-year intervals however would enable identification of temporal trends, which leads on to a second approach in quantifying changes.

4.5.2.3 Rates of change calculations

All studies in glacier frontal change have used a rate of change in order to have a consistent measure of change over time. These published studies have invariably presented changes in length and calculated in either metres or kilometres per year. The present study is different in that changes in area can be calculated rather than length, so the units $km^2\ a^{-1}$ are used.

A novel procedure has been developed for calculating change rates for the distinctive type of data in the AP, which minimises the problems encountered in other studies. The procedure for each glacier was as follows. Once each data record had been assigned to a 5-year interval, the number of months between each recorded position was calculated. The rate of change in $km^2\ a^{-1}$ could then be calculated between these two dates. The rate of change value was assigned to each 5-year interval that occurs between (and including) the dates of the two records. Data with gaps of >15 years were excluded from this process to remove the problem associated with averaging over long time intervals. A maximum of 15 years was chosen in order to include consecutive glacier positions that have a gap of only one or two 5-year intervals, but leave gaps where there are more than 2 intervals of missing data. For example, 01/01/1985 to 31/12/1999 is a time span of 15 years, so for a glacier with a position recorded sometime during the period 1985-89 and then again in 1995-99, the rate of change will be calculated across this period and the value assigned to all three time intervals (i.e. 1985-89, 1990-94, 1995-99).

Where two glacier change rates fell within one time interval, a weighted average of the two values was allocated to that interval. For example, if a glacier had positions recorded in 26/11/1992, 21/12/1997 and 21/02/2001, rates of change were calculated between these dates and the values assigned to intervals 1990-94, 1995-99 and 2000-04. For the interval 1995-99, a rate of change value from both before and after this date were relevant to this time interval, therefore a weighted average (based on the fraction of the 5-year interval covered by each date) of these two rates was assigned to this interval. An alternative way of making this calculation would have been to assign the 'rate of change' value only to one interval in order to avoid averaging. This alternative, however, would introduce a bias where a glacier date occurs at the start of one interval (e.g. 01/02/1995)

and the value calculated from the previous date is assigned to represent change during the interval 1995-99; or similarly, if a date is late in the interval (01/12/1999) it is inaccurate to suggest that the rate calculated from this to the following date is representative of the rate in 1995-99. By taking a weighted average, that bias is removed and is a more accurate representation of the rate of change that occurs within this interval. The principle of the method is demonstrated in Figure 4.8 for a single glacier.

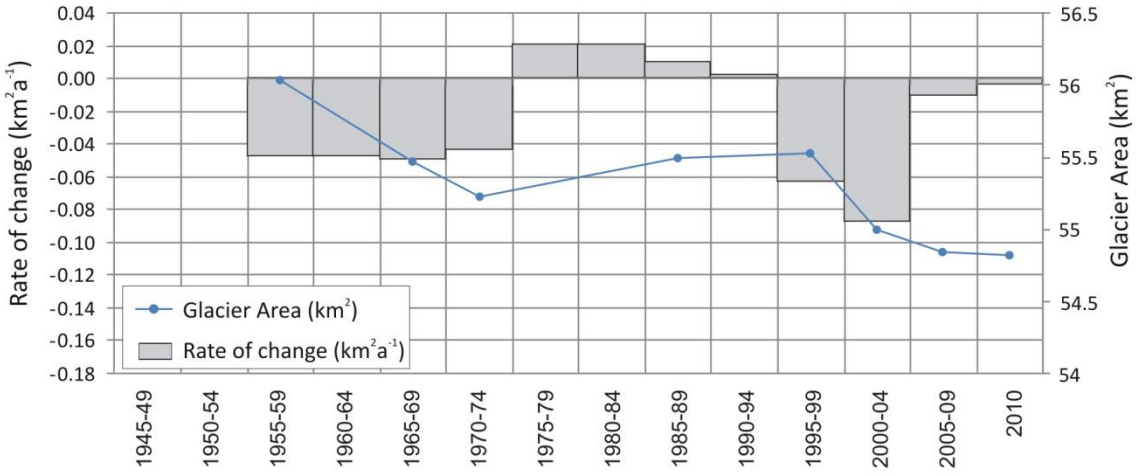

Figure 4.8: Change-rates single glacier plot.
The methodology used to calculate change-rates is demonstrated by this single glacier plot. The blue points are the area measurements that occur within the corresponding 5-year time intervals. The bars are the change rates calculated between each point in $km^2 a^{-1}$, with weighted mean values for intervals where two values occur.

4.5.2.4 Area-change over length-change calculations

In the *Coastal-Change* study by Cook *et al.* (2005) a similar principle was used to calculate rates of change in length of 244 glaciers, using sample lines intersecting the fronts of each glacier. The present study has improved the method in two significant ways. Firstly, a problem with the method in the *Coastal-Change* study was the inclusion of records that were less than 12 months apart. This not only confused seasonal change with longer term change, but the method for calculating long-term change introduced errors associated with fractions of a year. The basis of the methodology involved calculating the number of months between dates, dividing the amount of change by the number of months, followed by dividing this by 12 to give change in metres per year. Therefore, if the number of months is < 12, this will result in a fraction less than 1,

resulting in a potentially large value representing change over 5 years. This is exaggerated further when the dates occur across two different 5-year intervals and therefore imply that this large value applies to 10 years. The issue has been resolved in the present study because only one ice front position from within a 5-year time interval is used, even where there may be more than one position available. Where this does occur, the position with the higher reliability rating is chosen. This means that there are few problems with dates being too close to give valid results. There were only 22 cases with less than 2 years between the dates in adjacent time intervals, and edits were made to remove the resulting change-rate values. A minimum separation of 2 years was chosen to reduce the influence of the glacier annual change cycle.

A further difference between the two studies is that in the original study the length changes were calculated using points where sample lines intersected the coastlines, resulting in many more change-rate values per glacier. The original methodology involved calculating rate of change between ice front positions for all sample lines, then taking an average of these results. For each sample line, where two change-rate values applied to one 5-year interval an average of these two numbers was taken. For example, a glacier with positions in 1972, 1979 and 1983 resulted in 2 change-rate measurements, between 1972-79 and 1979-83. The 5-year interval '1975-79' included both change-rates, and the average was assigned to this interval. This method was applied to all sample lines, and then the average values were used. This means that averaging occurred not only for overlapping data within intervals, but also between sample lines, reducing the overall certainty in the result. This issue is significantly reduced by the new methodology. The use of sample lines is no longer required since areas can be calculated independently, removing the complication of obtaining averages from a large number of data points. The only averaging that occurs therefore is where two change-rate values apply to a single 5-year interval, in which case a weighted average of the two values is applied.

Many glacier-change studies use changes in the central flowline, or sample lines intersecting the front, to interpret changes in length. These can give biased results, however, depending on the quantity and placement of sample lines. A method that reduces this bias and now commonly used is the 'box' method, developed by Moon &

Joughin (2008), where a box is digitized across the ice front and the change in length is calculated by the width of the box divided by the area of ice within the box, for each period. This gives a more fully representative measure of change as it gives the average across the whole ice front. The method outlined in this study reduces the bias/averaging effects further by giving absolute change in area. The inherent uncertainties of the data and method are discussed next.

4.6 Further considerations

As is the case with all existing glacier-change studies, there are limitations to long-term change analysis from datasets with varying spatial and temporal coverage. Two primary issues to address are the accuracy of the data and methodology, and the scale of natural annual glacier cycles in the region. Quantification of errors at each stage of the glacier-change analysis is challenging but must be considered. Also, a glacier-front dataset should ideally use imagery acquired at the same time of year, preferably at the end of the melt season, but since this is not the case for all images in the AP it is important to ascertain whether intra-annual fluctuations could significantly affect conclusions about longer-term change. The lack of high temporal resolution imagery prior to the early 2000s prevents calculation of mean annual cycles on a decadal scale. Recent imagery is more plentiful and can be used to identify average seasonal glacier changes, although conclusions regarding trends in the annual cycle cannot be drawn and results that are based on individual years must be treated with caution. Errors inherent in the glacier-change measurements and the issue of intra-annual change are considered in this section.

4.6.1 Uncertainty estimates

The largest sources of uncertainty in measuring glacier change include the reliability of source material, measurement error and methods used to calculate change. Most published glacier-change studies recognise these issues, but have been unable to quantify the errors. Studies that have undertaken an error analysis include the previously mentioned study of 203 glaciers on Greenland (Moon & Joughin, 2008) and a study of 523 glaciers in the Canadian Rocky Mountains (Tennant *et al.*, 2012). Both studies had

consistent material for all glaciers, at 4 observation periods. Geolocation offsets and digitisation errors were rigorously calculated by repeat digitisation of features (Moon & Joughin, 2008) or approximated using a buffer equal to half the resolution of the data (Tennant *et al.*, 2012). The assessments in both cases were possible because all glaciers had the same source material at the same time periods. The majority of glacier-change studies however do not have these consistencies.

As discussed in Section 4.4.3.1, the wide range of data sources, with varying quality, spatial resolutions and geodetic accuracies, necessitated an accuracy assessment unique to the AP. The issue was first encountered during the *Coastal-Change* study (Ferrigno *et al.*, 2006) and a method was developed in which reliability ratings were assigned to every data source. This same approach was applied to all data sources in this study and the results show that the majority (68 %) of the records have a reliability rating of 1 (estimated to be accurate to within 60 m in length, equivalent to 0.0036 km^2), 25 % have a rating of 2 (within 150 m, or 0.0225 km^2) and 7 % have a rating of 3 (within 300 m, or 0.09 km^2). Glacier fronts with a rating of 3 are generally derived from vertical or oblique aerial photographs in which few reference features are visible, or from satellite images or large-scale maps which are poorly georeferenced but still show useful coastline data. There are specific periods in which records have lower ratings, such as the early 1950s, and this is taken into consideration when interpreting the results (Table 4.3). Although subjectivity is inevitable in assigning the ratings, they take into account manual digitization and interpretation errors, measured using stationary features as a guide, and are regarded as an upper error margin in all cases. A more detailed description of coastline accuracies can be found in Ferrigno *et al.* (2006) and the source material that falls within each category is listed in Appendix 4.5. Any ice fronts from the previous study with a reliability rating greater than 3 are not included in the present study as these introduce considerable biases, with accuracies of 600 m (0.36 km^2) or greater.

Unlike measurements of changes in glacier length, glacier area measurements take into account uneven changes along the ice front and offer a more precise assessment of change than can be obtained using along-flow sample-lines. They are also likely to reduce the influence of digitization errors since the entire front position is included in calculations rather than measurements from only the points at sample line intersections.

Differencing of polygon areas from one epoch to another can provide values of absolute area change, as well as change relative to the basin size. Although errors in the change-rate methodology are unquantifiable, the method has been developed to keep errors to a minimum and reduce problems encountered in similar studies.

A common source of methodology error is the interpolation of change-rates between gaps of varying durations: this issue has been reduced by ignoring any data with gaps of greater than 15 years. The duration of observational records is limited to 5-years and skewed results associated with uneven distribution of temporal data are reduced by limiting data to one record per 5-year interval. The 5-year time interval maintains a consistency for comparison of change rates between all glaciers. Lastly, area-change calculations remove bias associated with length-change sampling measurements. Although overall errors cannot be quantified, confidence in the quality of output has been achieved through rigorous analysis techniques and by maximising the data that is available, whilst removing spurious or less reliable data.

Table 4.3: Reliability ratings ice fronts within each 5-year interval.

5-year interval	Reliability rating	Count	5-year interval	Reliability rating	Count
1945-49	1	44	1975-79	1	53
	2	89		2	216
	3	71		3	18
1950-54	3	42	1980-84	1	14
1955-59	1	571	1985-89	1	617
	2	3		2	114
	3	3		3	14
1960-64	1	14	1990-94	1	147
	2	12		2	10
	3	8	1995-99	1	25
1965-69	1	71		2	164
	2	157		3	67
	3	74	2000-04	1	853
1970-74	1	20	2005-09	1	267
	2	301	2010	1	270
	3	13		2	1

4.6.2 Annual glacier cycles

A further consideration when assessing long-term trends is the scale of intra-annual variability in glacier front positions. Since not all ice fronts are recorded at the same time of year, it is important to establish whether the scale of long-term area change is not simply change that may occur naturally over the course of a single year. Glacier seasonal cycles in the Antarctic Peninsula are little understood so it is necessary to evaluate the expected changes. In most papers on long-term glacier change the issue of annual cycles has not been addressed. Two studies in Greenland (Howat *et al.*, 2008; Moon & Joughin, 2008), however, used summer and winter positions for a sample of glaciers to assess seasonal changes. In the Antarctic Peninsula, visible-band images cannot be used for winter months, therefore other sources such as radar imagery must be used for measuring positions in this season. Envisat Synthetic Aperture Radar Wide Swath Mode (SAR WSM) images, processed to approximately 90 m resolution by Polarview (http://www.polarview.aq/), were acquired year-round from 2009 to 2012. Similarly to the method used by Howat *et al.* (2008), scenes from winter (July-September) and summer (January-March) were compared for a large sample of glaciers across four well-distributed regions on the AP (Figure 4.9). The procedure was carried out for three years (2009, 2010 and 2011) to take into account unusual advance or retreat during any one year. Each year was analysed independently to remove the influence of inter-annual trends.

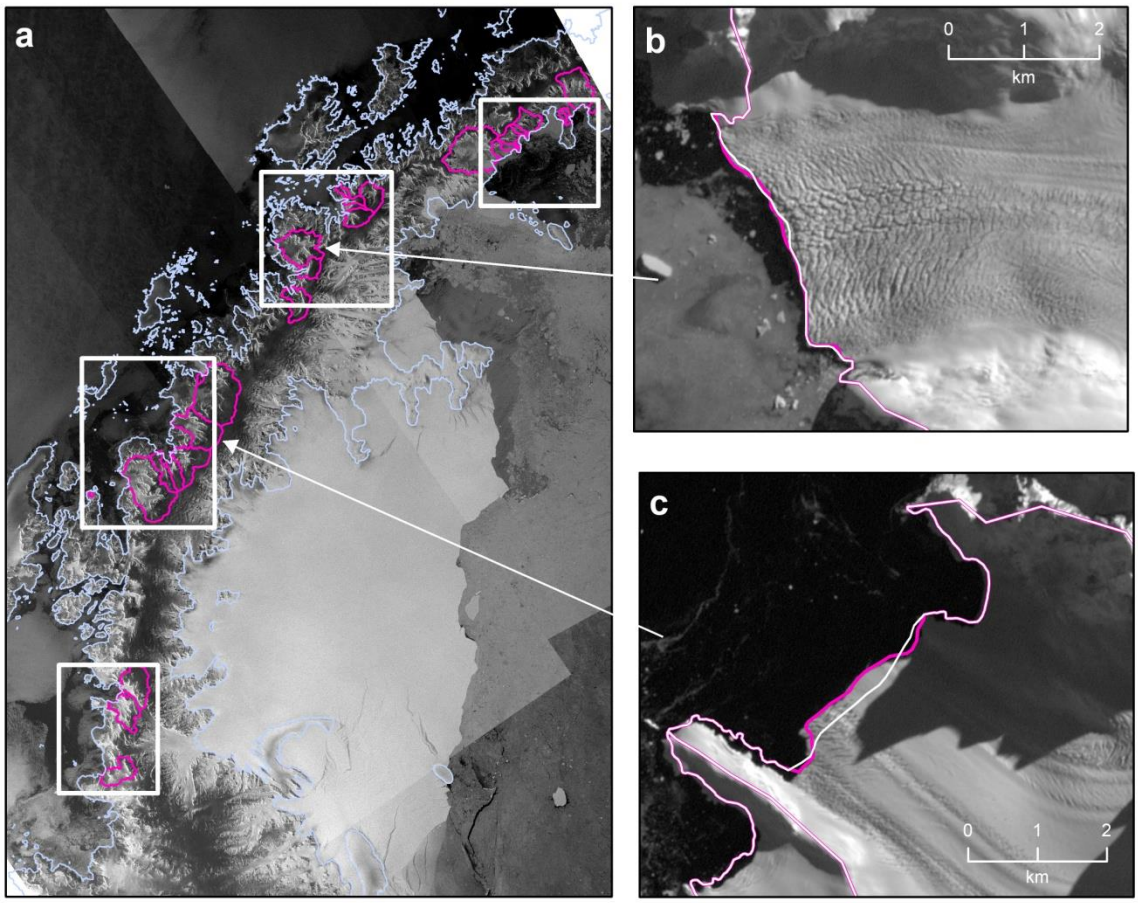

Figure 4.9: Intra-annual glacier front change.
Figure **a** shows the 4 regions in which 187 glaciers were assessed for intra-annual change for the years 2009, 2010 and 2011. The pink outlines are the 22 glaciers that changed by > 180 m in length during at least one of the three years. The background scenes are SAR WSM images from September 2011. Figures **b** and **c** illustrate fronts digitised for 2011 (pink = Landsat ETM+ 12/03/2011; white = SAR WSM 01/09/2011). The background scene is Landsat LE72191072011, Band 8.

Firstly, to assess the uncertainties associated with ice front digitization from SAR WSM scenes, a number of ice fronts from images acquired during a summer season were digitized and compared with ice fronts digitized from Landsat ETM+ scenes acquired on the same date, which are at 15 m resolution and have high geopositional accuracy. From these results, it can be concluded that the maximum uncertainty from the SAR WSM images is 2 pixels (i.e. 180 m, or 0.0324 km^2). Using the SAR WSM imagery, the summer-winter ice front positions were analysed for all 187 glaciers in the four sample regions. In total, only 22 out of the 187 glaciers changed by more than 0.0324 km^2 within

one or more of the three years (Table 4.4, Figure 4.10). Furthermore, the mean summer-winter difference for these 22 glaciers across all three years (0.014 km^2) is less than the margin of error. Intra-annual fluctuations are therefore not likely to be of a magnitude that could affect conclusions regarding changes on a pentadal scale. It should also be noted that the majority (87%) of all glacier fronts are recorded in late spring-early summer (Nov – Feb) from visible-band imagery, and those that are not are primarily from radar imagery and have a lower reliability rating. An in-depth analysis of seasonal change at a fine temporal resolution is not within the scope of the present study but is recommended for future research.

Table 4.4: Intra-annual area change summary
Summary table showing intra-annual area changes for the 22 glaciers (out of 187) that changed by > 180 m (0.0324 km^2) during at least one of the three years.

	2009	2010	2011	3-year Mean
Count (N) where Area change > 0.0324 km²	20	22	22	
% of total where Area change > 0.0324 km²	10.9	12.0	12.0	
Mean Area change (Km²) for N	0.1365	-0.0882	-0.0061	0.0141
Mean Area change (as % of glacier size) for N	0.0283	-0.0234	-0.0995	-0.0316

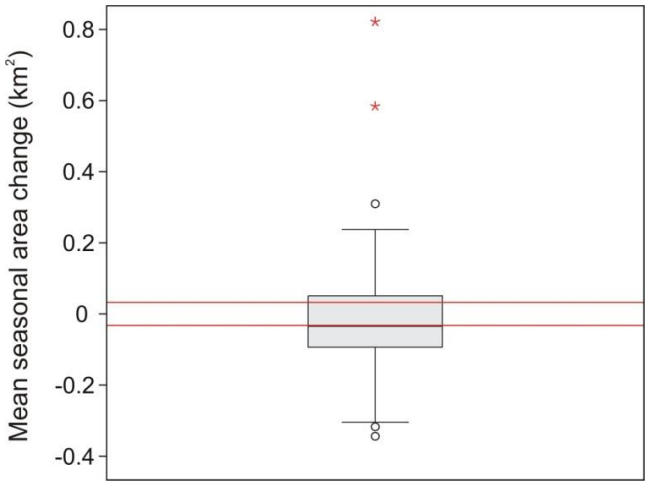

Figure 4.10: Boxplot showing distribution of mean seasonal area change
Seasonal means are across the years 2009, 2010 and 2011, for 22 glaciers that changed by > 0.0324 km^2 during one of those years. The red lines are at ± 0.0324 km^2. The circles are outliers and red stars are extreme outliers.

4.7 Summary

This chapter has described methods used to produce an inventory of glacier basins on the AP, together with attributes that distinguish their size, shape and surface topography. The inventory has been combined with the pre-existing dataset of coastal-changes to produce a new resource for measuring glacier change in the region. The area change inventory enables a rigorous analysis of all known ice front positions. Whilst the value of maximising the historical source material in this region is recognised, care has been taken to avoid over-interpreting change where there are long gaps between positional data. Methods unique to the region have been developed to contend with data issues such as uneven data distribution both spatially and over time. Although the data are too infrequent to enable analysis of short-term change, long term change calculations are possible, with up to 11 records per glacier since 1945.

Analysis of glacier-change in the AP is not straightforward and methods undertaken in other glacier-change studies were found to be largely inapplicable in this region. Each stage of analysis has involved an approach unique to this region. The well-georeferenced LIMA mosaic was chosen as the base image for the project, from which coastline features were manually digitised. The glacier basin outlines were created using a method based on hydrology principles, where individual glacier fronts denote the outlets for the basins. Nominal attributes for the glacier basins were individually assigned, using the DEM and LIMA for decisions on Class and Form, and a grounding line position as a guide for the Front attribute. In total, 1590 glacier basins with basic attributes were produced for the AP. Area-change analysis in the present study focuses on the marine-terminating glaciers, therefore additional attributes were assigned to these, including length along the central flowline, width at the basin outlet, mean basin width and shape, and three-dimensional attributes including elevation, slope and aspect values along the flowline.

Glacier-change analysis uses the pre-existing coastal-change dataset, updated with ice front positions to 2010. The data were georegistered to LIMA and matched to the corresponding glacier basin outlines. The unique issue of basins that merge and separate

from neighbouring basins was addressed by placing an upper limit of 5 merged basins at any one time, and analysing these complex 'multiple basins' on an individual basis.

The issue of temporal differences in data between glaciers is encountered in all long-term glacier studies. A new method developed for the AP data reduces inherent errors in interpreting change over long time-gaps or temporally clustered data, by assigning each record to a 5-year interval. Absolute changes in area are analysed in relation to the basin areas in the interval 2000-04, as all basins have a record during this interval. Rates of change are calculated between records, except where there is a gap of more than 15 years between records.

Limitations of the dataset and methodology are recognised, and this chapter has presented rigorous techniques in dealing with issues encountered in glacier-studies world-wide that are not straightforward to solve. Spurious and less reliable data have been removed and uncertainties in change-rate calculations are reduced to a minimum. Finally, the magnitude of annual glacier cycles has been assessed, which has shown that the seasonal differences in frontal positions are within the margin of error and not on a scale that would affect conclusions on long-term change.

The resulting dataset for further area-change analysis consists of 860 marine-terminating glaciers, each with a range of descriptive attributes and quantifications of area change (Appendix 4.6).

Chapter 5

Glacier area changes on the Antarctic Peninsula since the 1940s

5.1 Introduction

Preceding chapters have described how the dataset of the Antarctic Peninsula glaciers has been prepared. The new 100-m resolution DEM, along with outlines, attributes and change-measurements for all glacier drainage basins offer new resource material for detailed analysis on long-term changes in glacier area. The aim of this chapter is to give an account of glaciers on the AP and to quantify their changes in extent, so as to allow analysis of potential controls on these changes in subsequent chapters. This is carried out by first describing the glaciers in terms of their spatial distribution and characteristics, with observed correlations between attributes. As explained in Chapter 2, glaciers on the AP are little understood, hence establishing details about their glaciological features is fundamental for interpreting their behaviour. The changes in glacier area are then quantified, followed by analysis of spatial and temporal patterns in these changes. Further analysis indicates trends in the rates of change, and comparisons are made with trends in glacier lengths observed in the original *Coastal-Change and Glaciological Maps of Antarctica* study. Finally, comparisons of trends between glaciers with different characteristics are made. An overview of these glacier-change results have been published in Cook *et al.* (2014).

5.2 Glacier distribution and characteristics

5.2.1 All AP glacier basins

The total area of the AP in the period 2000-02 between 63° and 70° South is 98 293 km^2 (inclusive of exposed rock and small islands but excluding ice shelves). When small (<

0.5 km^2) islands and drainage basins that are predominantly ice-free are excluded, a total of 96,982 km^2 (98.7 %) in 1,590 glacier drainage basins remain. By further excluding an approximate area representing exposed rock (obtained from the ADD), the estimated ice-covered area for this region is 94,646 km^2 (96.3 %).

The complete dataset of 1,590 glacier basins has a strong asymmetry in glacier areas, whereby the majority are small glaciers, with a highly peaked distribution around the median value of 9 km^2 (Figure 5.1). Thus, comparative analysis between glacier basins in this region is strongly influenced by glacier basin area, and median values are the best measure of central tendency. When separated into basin size classes, and plotted alongside the sum of the total glacier area within each class, the opposing relationship between glacier size and summed areas is clear (Figure 5.2). Glacier basins smaller than 5 km^2 account for 36 % (n = 567) of the number of glacier basins but they represent only 1.5% (1,432 km^2) of the glacierized area in this region. Conversely, the 29 glacier basins larger than 500 km^2 are only 1.8 % of the population and yet represent a total of 42.5 % (41,246 km^2) of the overall area (see Table 5.1 for numerical values).

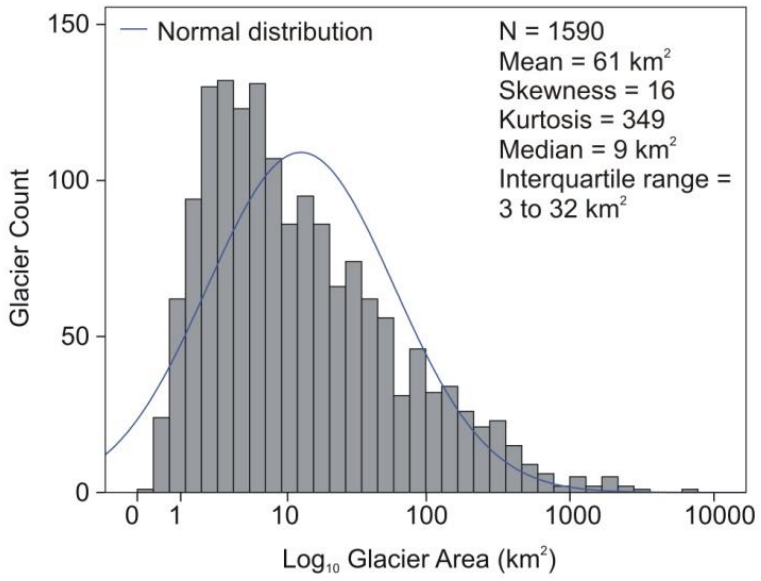

Figure 5.1: Histogram showing distribution of AP glacier basin sizes.
The plot shows how positively skewed the data are, even after a logarithmic transformation. The dataset distribution is highly peaked around the median value of 9 km^2, therefore this is the best measure of central tendency. 50% of the glaciers are between 3 – 32 km^2 in size.

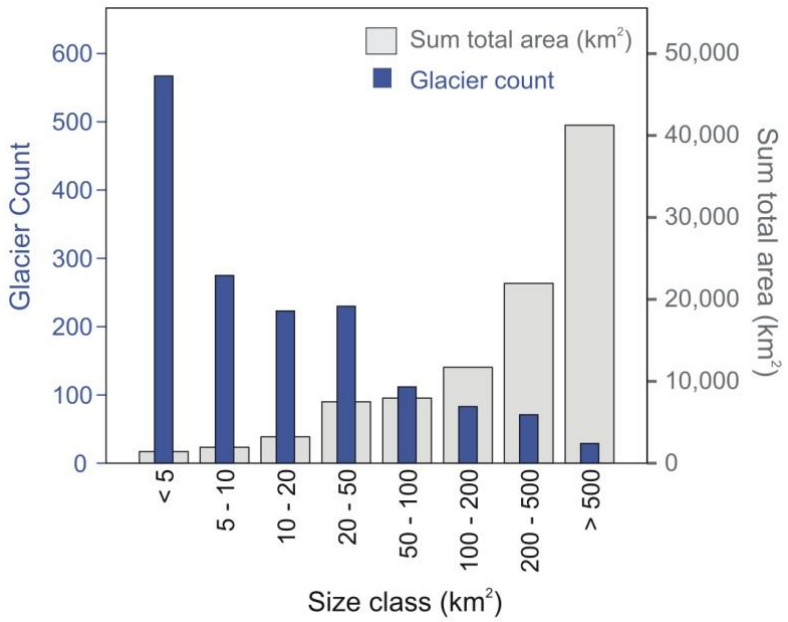

Figure 5.2: Number and area coverage of all glacier systems on the AP, by glacier size class.

Table 5.1: Number and percentages of glaciers in each size class, and sum total area.

Size class (km^2)	Count	% of total	Sum Area (km^2)	Sum Area (%)
< 5	567	35.7	1,432	1.5
5 - 10	275	17.3	1,955	2
10 - 20	223	14	3,228	3.3
20 - 50	230	14.5	7,509	7.7
50 - 100	112	7	7,953	8.2
100 - 200	83	5.2	11,710	12.1
200 - 500	71	4.5	21,949	22.6
> 500	29	1.8	41,246	42.5

Glacier basins in this region are little understood but it is now possible to summarize their characteristics. Glacier behaviour is highly dependent on the characteristics of the basin, including the primary glacier classification, form (i.e. basin complexity), frontal-type, area, length, outlet width, basin shape and mean slope, aspect and elevation. These variables are now available for all glacier basins and descriptive statistics can reveal relationships between glacier types throughout the region.

Glaciers can be summarized first according to their non-scalar variables: the primary classifications, form and frontal-types. The quantities of glaciers for each of these variables are listed as both the total count and by situation either on the mainland or on surrounding islands (Figure 5.3 and Table 5.2). The largest population of glaciers (35%) are the mountain glaciers, and although the overall count on islands is much lower, they are proportionally similar to those on the mainland. Glacier types that differ significantly between the mainland and islands are outlet glaciers (for which 85% occur on the mainland) and ice-fields (94% on the mainland). The sum of the areas of outlet glaciers far outweighs the total area for all other glacier types combined; they compose 71% of the sum total area of the whole AP. The 36 outlet glaciers that occur on islands drain from ice caps on James Ross Island, Adelaide Island and Anvers Island.

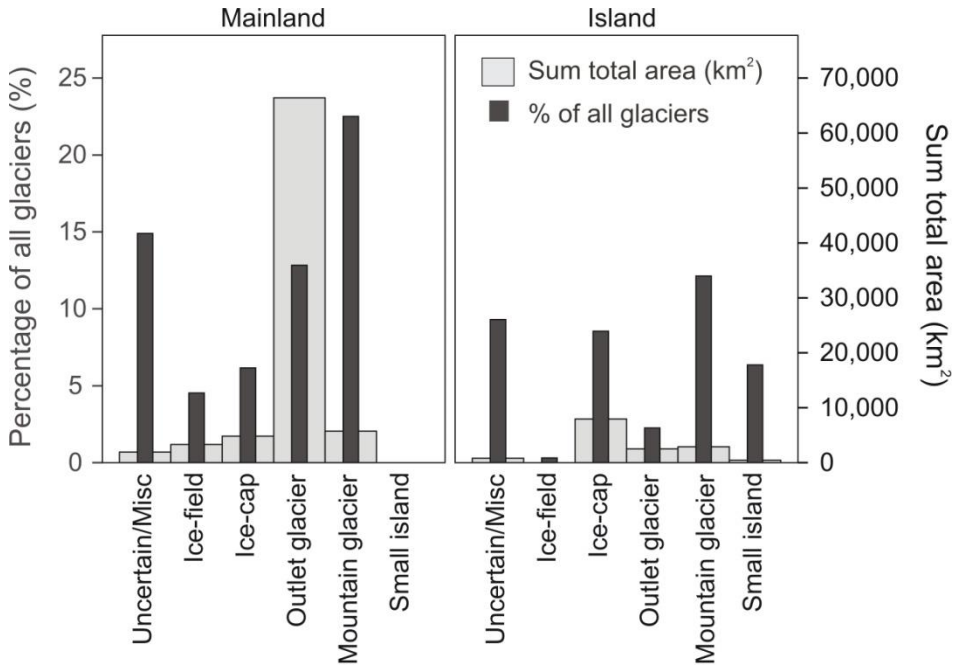

Figure 5.3: Graphs summarising total glacier count and area coverage per glacier type: The percentage of all glaciers, plus the sum total area for each Primary Classification are shown for both those on the mainland or on surrounding islands (see corresponding Table 5.2).

Table 5.2: Total glacier count and area coverage per glacier type
The number of glaciers within each classification, split by island/mainland and total, and the sum of the area covered by each glacier-type.

		Mainland	Island	Total Count	Total Count %	Sum Area (km^2)	Sum Area (%)
Class	Uncertain/Misc	237	148	385	24	2,740	3
	Ice-field	72	5	77	5	3,410	4
	Ice-cap	98	136	234	15	12,798	13
	Outlet glacier	204	36	240	15	68,944	71
	Mountain glacier	358	193	551	35	8,636	9
	Small island		101	103	6	455	0
Front	Uncertain/Misc	193	251	444	28	2,124	2
	Calving	379	293	672	42	27,900	29
	Calving/Piedmont	62	16	78	5	3,895	4
	Calving/Lobed	13	28	41	3	4,560	5
	Ice-shelf nourishing	250	14	264	17	33,739	35
	Floating	74	8	82	5	24,593	25
	Land-terminating	0	9	9	1	171	0
	Total	971	619	1590		96,982	

As regards frontal-type (Table 5.2), the highest percentage (42%) is the 'calving' type. As explained in Chapter 4 (Section 4.3.1), glaciers assigned the term 'calving' in this study are considered to be grounded: if calving glaciers have floating fronts they are in the 'floating' category. The allocation of the floating/calving attributes has been the most subjective and it is possible that those classed as calving glaciers are in fact floating, or vice versa. The decisions were based on grounding line positions from ASAID or interpreted from LIMA. Without the existence of more reliable grounding line positions, however, these allocations are the best estimate. A large proportion of glaciers (28%) were assigned 'uncertain/miscellaneous' where it was not possible to make a decision because the grounding line was entirely unclear. There were only 9 glaciers that could be described as 'land-terminating' during the period on which the front-type designation was based (2000-02), and all of these occur on James Ross Island.

Glacier characteristics, such as their primary classification and frontal-types, vary considerably according to the basin size (Figure 5.4). For example, regarding classifications, almost all glaciers in the largest size class are 'outlet' glaciers, and the proportion of outlet glaciers decreases with glacier size (Figure 5.4a). Conversely, the smaller glaciers are predominantly 'mountain glaciers' which decrease in percentage with increasing glacier size. The exception is the smallest category, which has a large number in the 'uncertain/misc' category, since the ice mass was more difficult to identify. 'Ice-caps' and 'ice-fields' are found in all size categories, except the largest, with largest percentages in the middle size classes. For glacier frontal-types, there is no such distinct relationship with size, although one observation is that floating glaciers make up an increasing proportion of glaciers as size increases (Figure 5.4b).

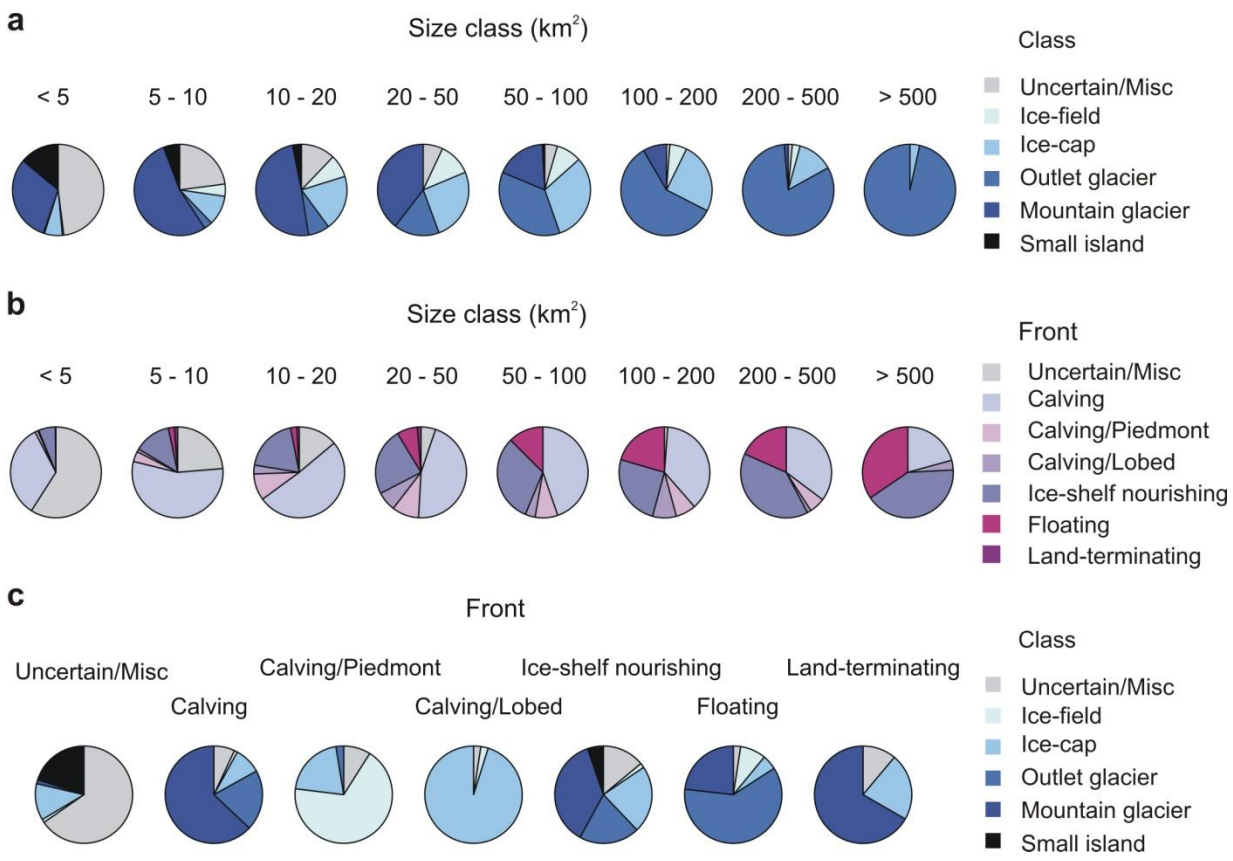

Figure 5.4: Size class, Primary Classifications and Front types of all 1590 glaciers. See Appendix 5.1 and 5.2 for glacier counts within each category.

Similarly, the percentage of ice-shelf nourishing glaciers increases with size class. 'Calving' glaciers are found in approximately similar proportions in all size classes, although rather lower for glaciers > 500 km^2, which are dominated by floating or ice-shelf nourishing glaciers (Appendix 5.1).

Inevitably, some primary classifications are coupled to the front-type variable (Figure 5.4c and Appendix 5.2). For example, calving/lobed fronts by definition occur where an ice-cap meets the ocean, and calving/piedmont fronts are generally the termini of ice-fields. With these exceptions, the majority (63%) of glaciers with calving (i.e. grounded) fronts are mountain glaciers, and 61% of glaciers with floating fronts are outlet glaciers. Ice-shelf nourishing glaciers have the widest range of classifications. When undertaking these observations the number of glaciers within each primary category must be considered; for example there are only nine land-terminating glaciers in total therefore the mountain glacier majority (67%) are actually only three glaciers. All other classifications have at least forty glacier basins (Table 5.2). Considering Class alongside Front categories, the largest percentage of all glaciers on the AP are mountain glaciers with calving fronts (n = 423, 26%) (Appendix 5.2). Regarding glacier basin complexities (i.e. Form), the majority of glaciers (n = 968; 61% of all glacier basins) are 'uncertain/misc' in the Form category, followed by 423 (27%) that are 'simple basins'. When Form is considered alongside Class, the largest number (n = 370; 23%) of glaciers on the AP are mountain glaciers with simple basins. Finally, when all three Class, Form and Front categories are considered simultaneously, the most common glaciers on the AP are mountain glaciers with simple basins and calving fronts (n = 301, 19%) (Appendix 5.2).

To best facilitate spatial analysis of glacier types, the AP was divided into eastern and western sides and into the seven one-degree latitudinal bands that cross the 1000 km-long peninsula (Figure 5.5). These region intervals were considered most suitable for the distribution of glaciers. The glaciers were assigned east or west depending on which side of the plateau the terminus falls. The latitudinal degree band allocation is determined by the location of the centre point of the glacier basin. The western region has a strong negative relationship between the size class and number of glaciers, and an opposing similarly strong positive relationship with the sum total area (Figure 5.6). The former

relationship is not as pronounced in the east, where there are fewer glaciers in the smaller size categories.

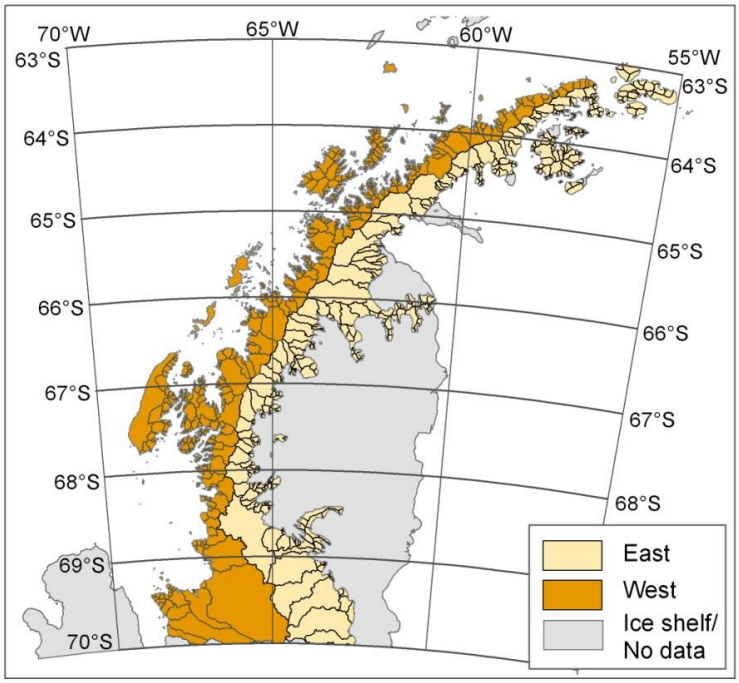

Figure 5.5: Reference map showing spatial boundaries
The one degree latitudinal bands and glacier basins according to east/west regions are highlighted for reference.

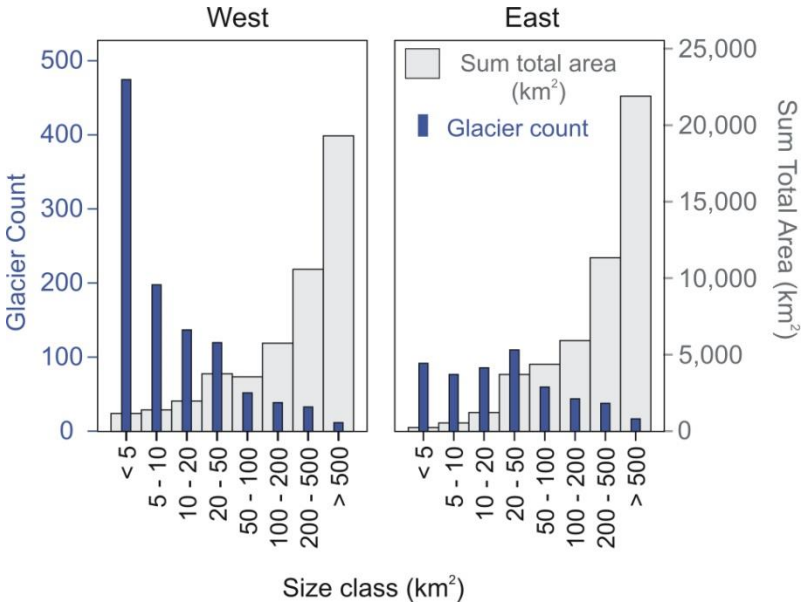

Figure 5.6: Number and area coverage of all glacier systems, binned by size class

The number of glaciers is spatially more evenly distributed along the eastern side than along the western side (Figure 5.7). From the total of 1,590 glaciers, by far the largest number (n = 427) occurs in the west between 64° S - 65° S and yet only 31 glaciers are found within the most southerly western band 69° S - 70° S (Table 5.3). The total glaciated area in this section is, however, by far the largest (21,000 km^2; 22% of the entire region) and it contains the largest glacier basin on the AP (containing Fleming, Seller and Airy Glaciers), at 7,021 km^2.

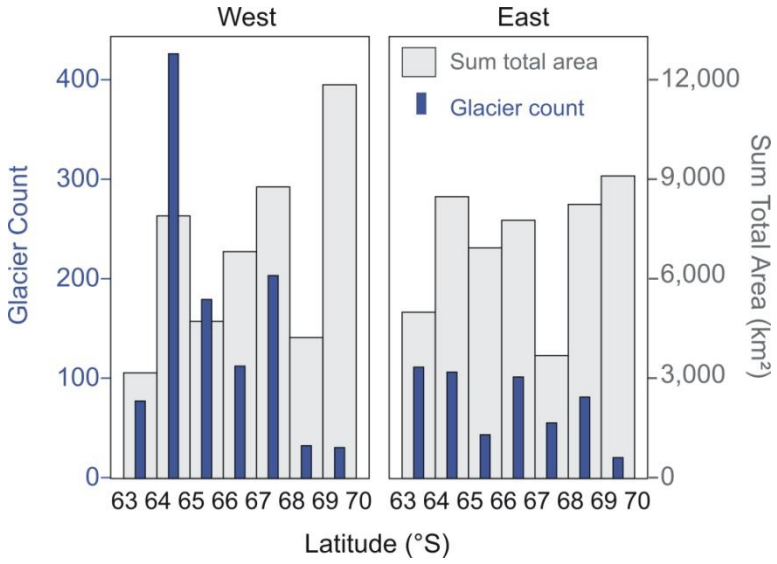

Figure 5.7: Number and area coverage of all glacier systems, split by east/west and degrees latitude.

Table 5.3: Glacier count and area by degrees latitude.
Number and percentage of glaciers and the sum of the glacierized area within each latitudinal degree band.

Degree Latitude (°S)	West	East	Total Count	Total Count %	Sum Area (km^2)	Sum Area (%)
63 - 64	78	112	190	12	8204	8
64 - 65	427	107	534	34	16423	17
65 - 66	180	44	224	14	11699	12
66 - 67	113	102	215	14	14630	15
67 - 68	204	56	260	16	12504	13
68 - 69	33	82	115	7	12522	13
69 - 70	31	21	52	3	21000	22
Total	1066	524	1590		96983	

5.2.2 Marine-terminating glacier basins

As explained in the Methods chapter (Section 4.5.2), additional details were attributed to marine-terminating glaciers for more detailed analysis. The dataset was prepared by first removing non-marine terminating glacier basins (namely land-terminating, ice-shelf nourishing, ice-walls and small islands), and remaining glaciers smaller than 1 km^2 (n = 5). From this total of 925 glacier basins, those with only one frontal position record were also excluded, resulting in a total of 892 marine-terminating glaciers suitable for area-change analysis. The relationship between glacier count and sum total areas with size class are similar to those observed for the population of all AP glacier basins, although there are a substantially lower percentage of small (less than 5 km^2) glaciers (22.6% as opposed to 35.7%) (Appendix 5.3).

Marine-terminating glacier counts within each Class, Front and Form category are listed in the Appendix (Appendix 5.4). A comparison of categories shows that the relative proportions of glaciers are similar to those observed in the entire glacier population. A summary of marine-terminating glaciers, based on their non-scalar classifications are as follows:

- The majority (n = 436; 49%) are ‘mountain glaciers’.
- The predominant Form types are ‘uncertain/misc’ (n = 387; 43%) and ‘simple basin’ (n = 353; 40%)
- The most common Front type is ‘calving’ (n = 650; 73%).

When all the three categories are considered together, the most common marine-terminating glaciers are mountain glaciers with calving fronts and simple basins (n = 294, 33%), followed by mountain glaciers with calving fronts and uncertain/misc basins (n = 77, 9%).

The dataset enables qualification of glacier types in many ways, including details based on surface elevation. Elevation and slope were measured from DEM pixel values along the centreline of each glacier basin to give values representative of the glacier surface. The overall distribution of maximum elevation values is reasonably normally-distributed, with a median value of 902 m, and an interquartile range of 580 – 1416 m. When divided

by individual glacier types, differences become apparent: mountain glacier elevations are skewed with fewer glaciers at high elevations, and ice-caps are centred at lower elevations (Figure 5.8a). Outlet glaciers on the other hand are negatively skewed, with the majority at high elevations. Overall slope values are positively skewed, with a median value of 18 percentage rise (%) and an interquartile range between 10 and 30 %. Differences between the glacier types are again apparent: outlet glaciers, ice-fields and ice-caps have low slopes, averaging about 10%; mountain glaciers however have a wider dispersion with a higher median value of 30% (Figure 5.8b).

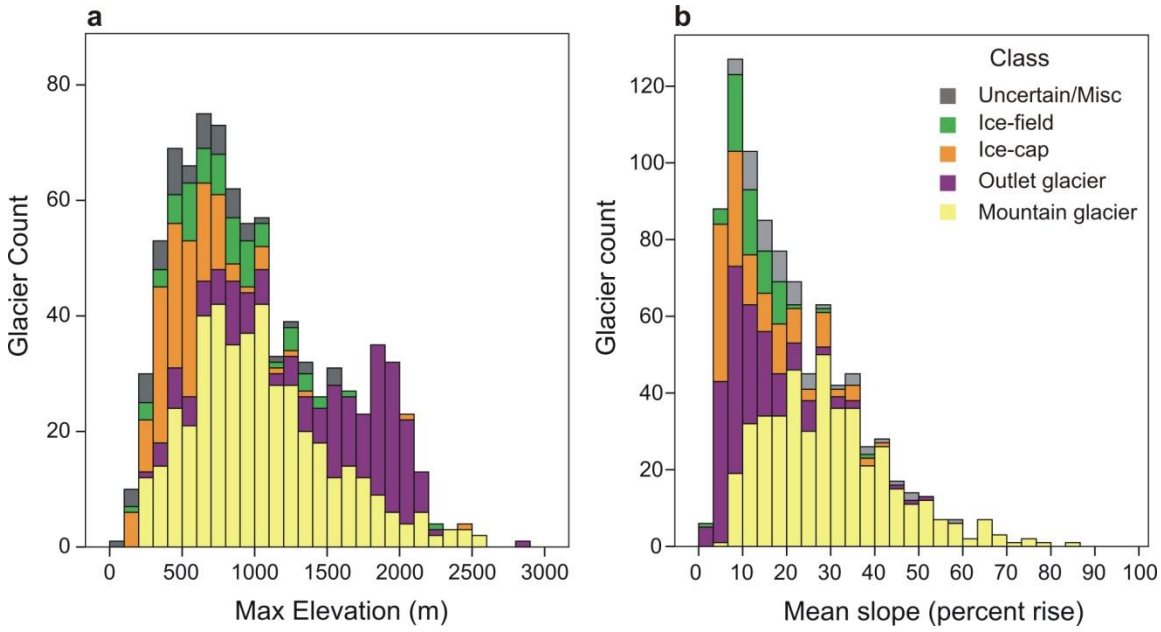

Figure 5.8: Glacier classes and elevation attributes
Stacked histograms illustrating the number of marine-terminating glaciers at each elevation (**a**) and mean slope (**b**), separated by primary classifications.

The glacier basin variables have highly skewed distributions making correlations difficult to identify using parametric statistical analyses. However, trends between some of the main characteristics can be observed visually when plotted on scatterplots on a logarithmic scale (Figure 5.9), and the corresponding values calculated as Spearman's rank correlation coefficients (r_s) show those that are statistically significant (Table 5.4). Many glacier characteristics are inter-related and therefore strong correlations are expected. The strongest correlations, with significance at the 0.01 level, are between basin area and both surface length ($r_s = 0.954$) and mean basin width ($r_s = 0.932$). Area and outlet width also have a significant positive correlation although not as strong (r_s =

0.650). Each of these variables have significant positive correlations with each other, with the weakest correlation between surface length and outlet width (r_s = 0.516). The degree of basin convergence is based on these variables and yet the correlations are weak (although still significant), with r_s values less than 0.5. The degree of convergence has a negative correlation with most geometric variables (for example, basins that are larger, longer and wider tend to be less convergent), except for the correlation with the outlet width which is positive, although weak (r_s = 0.348). In this case, basins that have large outlet widths tend to be divergent, and those with narrow outlets tend to be convergent.

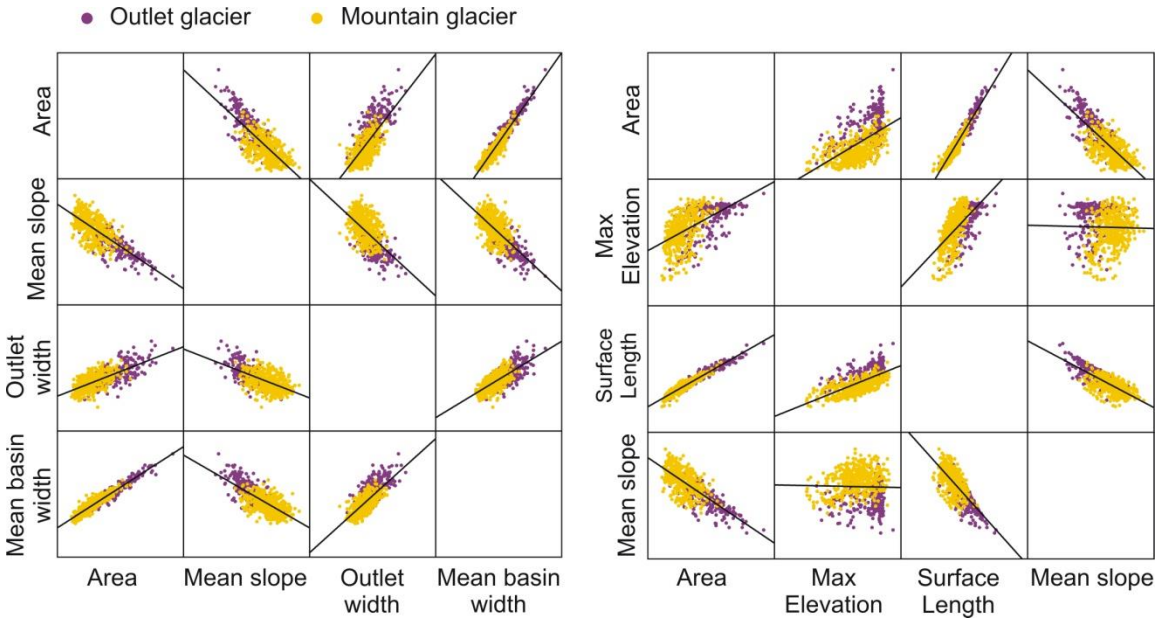

Figure 5.9: Scatter matrix for selected glacier attributes
The plots show data distribution and trend lines. Both axes are on a Log_{10} scale.

When elevation details are considered, statistically significant (< 0.01) negative correlations are seen between mean slope and basin area (r_s = -0.705) and surface length (r_s = -0.653): the smaller basins tend to have steeper surface slopes. Similar negative correlations occur between mean slope and outlet width (r_s = -0.605) and mean basin width (r_s = -0.658): narrow glaciers tend to have steeper surface slopes. There are positive correlations between maximum elevations and surface length (r_s = 0.601) and area, although this is weaker (r_s = 0.486): longer glacier basins tend to originate on the AP plateau which is at high elevation. Maximum elevation has a very weak correlation with surface slope. Variables that have little or no correlation to any other variables are mean basin aspect and flow direction.

Table 5.4: Correlations between glacier characteristics
Spearman's Rank Correlation Coefficients (r_s) and statistical significance for glacier characteristics. Those highlighted in red are significant at < 0.01 level, and those in red and underlined in bold are where the relationship is strong ($r_s > 0.5$ or $r_s < -0.5$).

		Surface Length	Max Elevation	Mean slope	Mean basin aspect	Mean flow direction	Outlet width	Mean basin width	Degree of conv.
Area	r_s	**0.954**	0.486	**-0.71**	0.06	0.042	**0.65**	**0.932**	-0.36
	Sig.	0	0	0	0.074	0.217	0	0	0
	N	881	881	881	887	877	875	881	875
Surface Length	r_s	1	**0.601**	**-0.65**	0.094	0.058	**0.516**	**0.788**	-0.359
	Sig.	.	0	0	0.005	0.085	0	0	0
	N	881	881	881	876	877	875	881	875
Max Elevation	r_s		1	0.158	0.097	0.019	0.025	0.33	-0.429
	Sig.		.	0	0.004	0.581	0.458	0	0
	N		881	881	876	877	875	881	875
Mean slope	r_s			1	-0.01	-0.044	**-0.605**	**-0.658**	0.067
	Sig.			.	0.763	0.195	0	0	0.046
	N			881	876	877	875	881	875
Mean basin aspect	r_s				1	-0.186	-0.047	0.021	-0.083
	Sig.				.	0	0.17	0.538	0.014
	N				887	876	870	876	870
Mean flow direction	r_s					1	-0.01	0.015	-0.036
	Sig.					.	0.757	0.666	0.287
	N					877	871	877	871
Outlet width	r_s						1	**0.718**	0.348
	Sig.						.	0	0
	N						875	875	875
Mean basin width	r_s							1	-0.347
	Sig.							.	0
	N							881	875

Outlet and mountain glaciers were selected as two distinct glacier types (Figure 5.9) and the differing characteristics are clear: outlet glaciers have larger areas, surface lengths and mean widths, and lower slopes than mountain glaciers. There is little distinction between outlet and mountain glacier correlations for maximum elevation and mean slope. If these variables are separated into size classes however (Figure 5.10), the differences

between glacier types are more apparent. Elevations and slopes of mountain glaciers are very dependent on glacier area; for example, small glaciers tend to have low mean elevations and high mean slope angles. Large outlet glaciers tend to have low mean slope angles irrespective of the mean elevation.

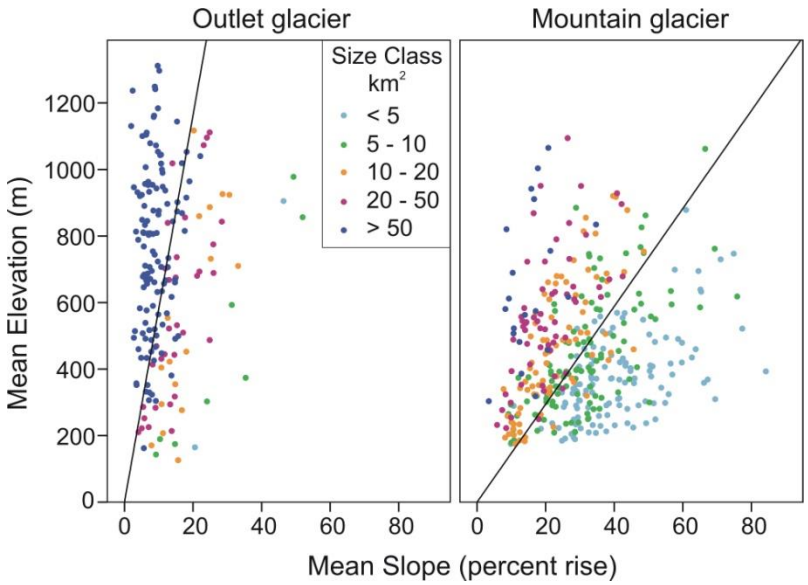

Figure 5.10: Scatterplots for outlet and mountain glaciers.
Elevations (y-axis) and slopes (x-axis) are grouped by glacier size class.

A further way of demonstrating the inter-dependence of variables is shown when mean surface length and mean slope are plotted by size class (Figure 5.11). The correlation between mean slope and surface length was identified as significant (<0.01) and negative and reasonably strong (r_s = -0.653) (Table 5.4). When the glaciers are separated by size class, however, and mean values for both slope and surface length are plotted, the distinct and opposing relationships between the two variables and basin size can be seen.

Glacier basin aspect has no strong correlation with other variables, but a polar diagram can show the percentage distribution of glacier aspects around the AP region (Figure 5.12). The predominant mean aspect orientations for all glacier basins on the AP are south westward- and westward-facing, and there are no glaciers within the northward or north eastward-facing sectors. These orientations are primarily due to the geographical shape of the AP however and aspect is not considered an important factor in the development of glaciers in this region.

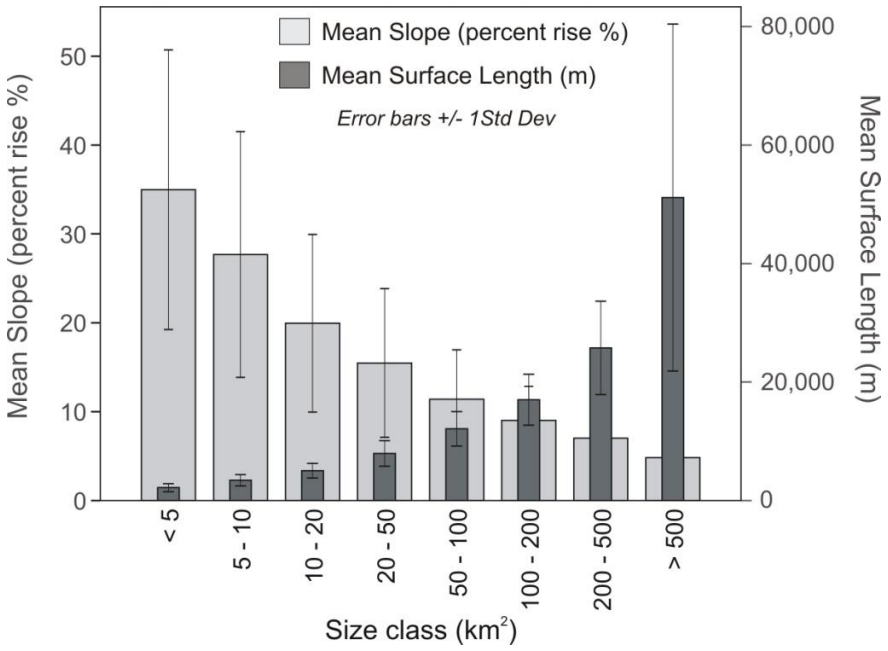

Figure 5.11: Inter-dependence of characteristics: glacier slopes, surface length and size.

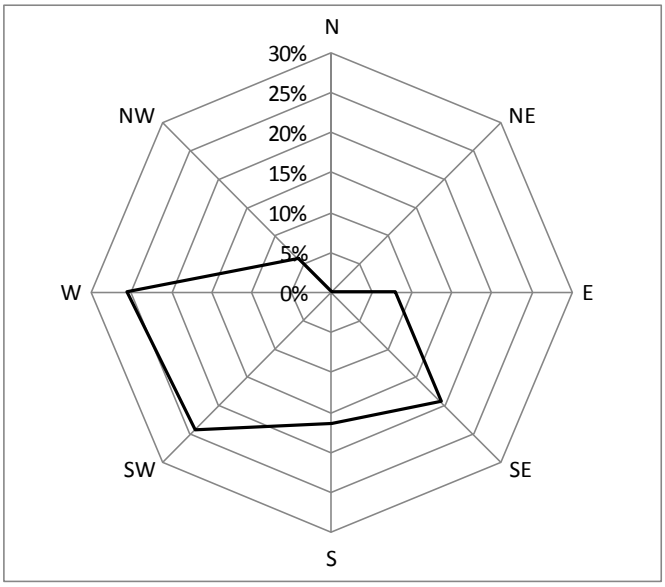

Figure 5.12: Aspect sectors
The percentage of all marine-terminating glaciers within each aspect sector (the aspect value for each glacier is the mean value for the whole basin).

These qualitative results demonstrate the strong inter-relationships of glacier characteristics and that basin area is a strongly determining factor for many other variables. Further statistical analysis is limited due to the skewed nature of each variable;

however these descriptions of glacier basin characteristics provide a basis for interpreting behaviour at the ice fronts.

5.3 Glacier changes

5.3.1 Overall change since earliest records

Area-change analysis of individual glaciers on the AP is made more challenging by basins becoming merged or separated over time. As described in Chapter 4 (Section 4.4.3.5), those that were once one entity have been grouped and are treated as single basins for glacier-change analysis, resulting in a total of 860 glacier basins.

This study shows that 778 (90.5%) of 860 marine-terminating glaciers on the AP have retreated since the earliest recorded ice-front position (average 1958) (Figure 5.13). This reinforces the result of the glacier length-change study which showed that 87% of 244 glaciers in the region retreated since records began (Cook *et al.* 2005).The overview map (Figure 5.13a) shows that those that have advanced are predominantly in the west/northwest region of the AP mainland. The presence of glaciers is not evenly distributed along the coast, but the graph (Figure 5.13b) shows that proportionally, those in the northwest have the highest percentage of glaciers that have advanced. This percentage decreases with latitude: there is an apparent slight increase in the southern-most band, but this is misleading because the sample size is small and actually only one glacier advanced. The scale of overall change must first be calculated to assess the significance of any spatial patterns.

In total, 30 (3.5%) glaciers lost > 10 km^2, 190 (22%) glaciers lost between 1–10 km^2 and the majority (n = 558, 65%) showed minimal retreat (< 1 km^2). Of the 82 (9.5%) that advanced, 80 of these changed by < 1 km^2 (Figure 5.14a). When area change is calculated relative to the basin size, the distribution is also negatively skewed but with a greater dispersion around the mean (Figure 5.14b). This can be explained by the diverse range of glacier sizes; for example there are many small glaciers that may show only a small absolute area change but a large relative change. This relationship can be seen in Figure 5.14c, where there is a positive correlation between absolute and relative change

for all size classes, but with a decreasing gradient with increasing glacier size. Thus, larger absolute change results in greater relative change for small glaciers, whereas there is a lesser increase in relative change for large glaciers. Linear relationships are strong, although weaker for the largest size class ($r^2 = 0.507$).

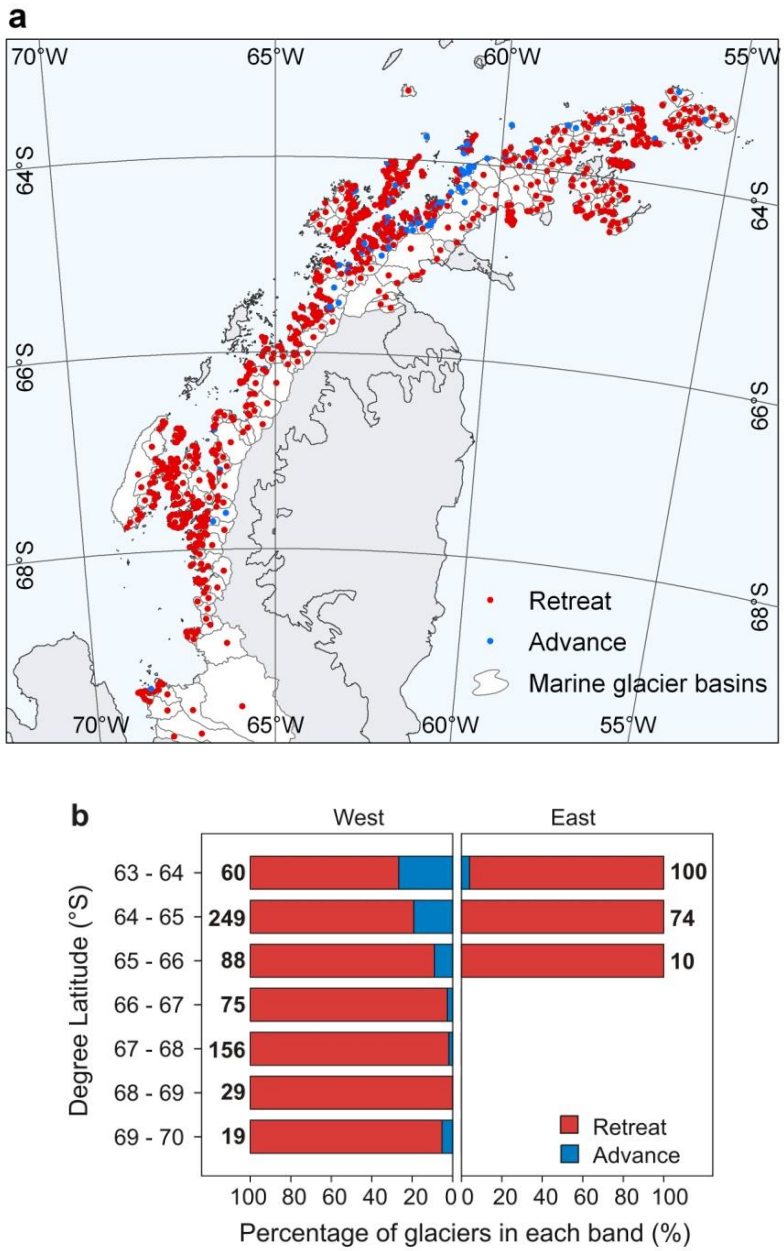

Figure 5.13: Summary map showing spatial distribution of overall advance/retreat. Simple overview map of overall advance/retreat for marine-terminating glaciers (**a**). The percentages of glaciers that have advanced/retreated within each latitudinal degree band and split by West/East AP are shown in (**b**): the total glacier count in each band is shown in bold at the end of each bar.

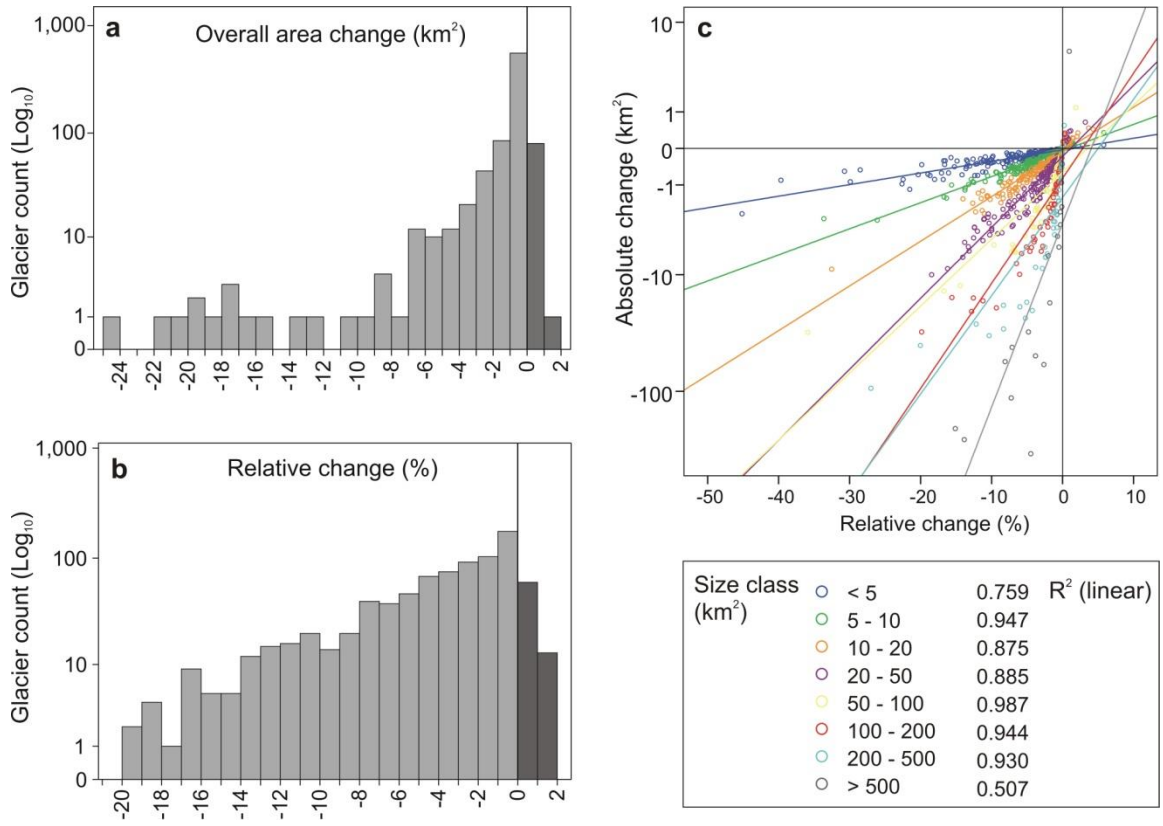

Figure 5.14: Histograms showing overall change per glacier
Change in km^2 (**a**) and as % of basin size (**b**), from earliest-latest records. Records are variable for each glacier but earliest positions are, on average, 1958 and latest positions are, on average, 2004 (N.B. weighted by basin area these are 1968 and 2007 respectively). Due to the large negative dispersion range, data from the extremes (<0.02 and >0.98) have been excluded from the histograms. Panel **c**. is a scatterplot showing the relationships between absolute and relative changes by glacier basin size classes. The y-axis is displayed on a Log_{10} scale; R^2 values are based on non-transformed values.

5.3.1.1 Overall absolute and relative change: correlations with glacier variables

The skewed nature of the area-change data means that non-parametric tests are most appropriate. Table 5.5 shows a statistically significant correlation between glacier basin area and absolute area loss (Spearman's rank $r_s = 0.51$). Although there is a weak correlation between glacier area and relative loss ($r_s = -0.26$), it is significant and negative, implying that smaller basins show larger relative ice loss. When other glacier attributes are correlated against absolute area changes, length and outlet width show significant positive correlations (i.e. the longer glaciers and those with wide fronts have

shown large area losses), and mean slope angles show a negative correlation (i.e. the lower the mean slope angle the larger the area loss).

Table 5.5: Correlations between overall change and selected glacier characteristics. Spearman's rank (r_s) correlations between glacier attribute and total change (both absolute change and change relative to basin size as %). Those highlighted in red are significant at < 0.01 level.

Area loss	Glacier area	Length	Mean Elevation	Mean slope	Outlet width	Degree of conv.
Absolute (km²)	.51	.42	-.03	-.47	.56	.02
Relative (%)	-.26	-.32	-.44	.05	.09	.31

When non-scalar variables, such as Class, Form and Front, are included in the analysis, there are no significant correlations with total loss. Within the Front category, however, 'floating' glaciers show a notably larger mean absolute change than other frontal types (Figure 5.15). However, there is no correlation between any frontal type and mean relative change. Many of the glacier variables are inter-related thus further interpretation would require using a multivariate statistical approach. Parametric statistical analysis is prevented, however, by the highly-skewed nature of the data, and furthermore, the overall change values cannot be easily transformed into normally distributed data due to the presence of both positive and negative data values. Multivariate analysis is arguably not profitable since no single variable is likely to have overriding influence on frontal behaviour.

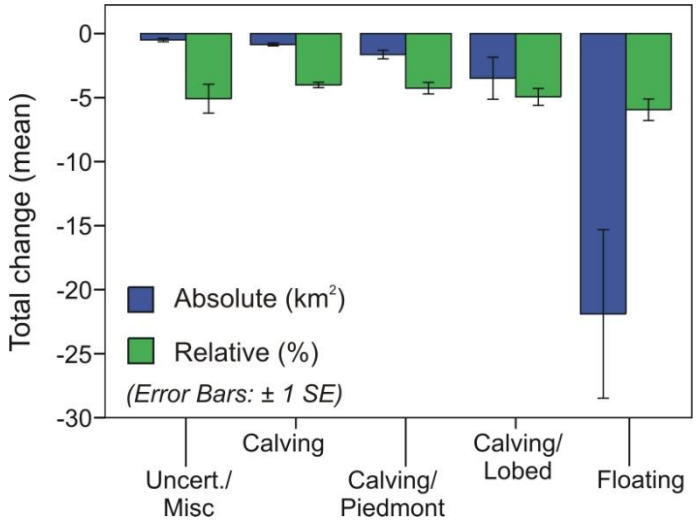

Figure 5.15: Overall mean change according to Front type.
The mean absolute loss (km^2) for floating glaciers is considerably greater than any other category.

5.3.1.2 Spatial distribution of overall change

The spatial distribution of absolute change in km^2 (Figure 5.16a) shows that the largest area loss has occurred to glaciers flowing into Wordie Bay, where Fleming Glacier (consisting of Fleming, Airy and Seller glaciers) lost 329 km^2 between 1997 and 2010, following collapse of the Wordie Ice Shelf. The two large neighbouring glaciers (Hariot and Prospect glaciers) lost 251 km^2 and 204 km^2, respectively. Large losses also occurred to glaciers such as Hektoria (113 km^2), Crane (50 km^2) and Jorum (43 km^2) which once flowed into the Larsen B Ice Shelf, and Pyke (56 km^2) and Edgeworth (32 km^2) glaciers which once fed the Larsen A Ice Shelf to the north. These results correspond with studies that have shown mass deficit due to tributary glacier acceleration and thinning post-ice shelf collapse (Scambos *et al.*, 2004; Rignot *et al.*, 2005; Wendt *et al.*, 2010; Glasser *et al.*, 2011; Rott *et al.*, 2011; Shuman *et al.*, 2011; Berthier *et al.*, 2012). The largest single area loss that was not due to sudden removal of an ice shelf buttress was from the large Fuchs Ice Piedmont on Adelaide Island (60 km^2).

Although quantifying absolute area of ice loss is important, calculating relative changes is also essential when comparing the behaviour of glaciers with such diverse sizes

(compare Figures 5.16a & b). Glaciers such as Fleming Glacier may have shown a large absolute change but this area is a relatively small percentage of its basin size. Similarly, Fuchs Ice Piedmont has a long ice front which has contributed to the large overall ice loss, but the basin size is also large, resulting in a smaller relative change. Trooz Glacier is one of only two glaciers that have advanced by > 1 km^2, and yet it changed by < 1% of its basin size.

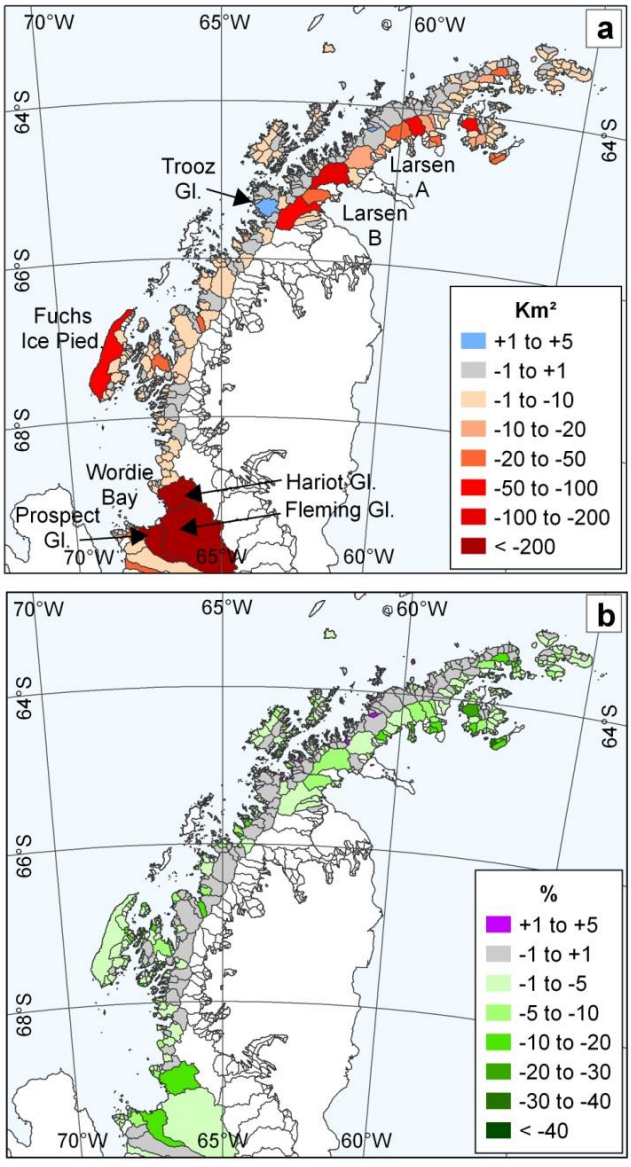

Figure 5.16: Spatial distributions of overall change in area from earliest to latest records. Total change is shown as km^2 **(a)** and as % of basin size (**b**). Earliest recorded positions are, on average, 1958; latest positions are, on average, 2004.

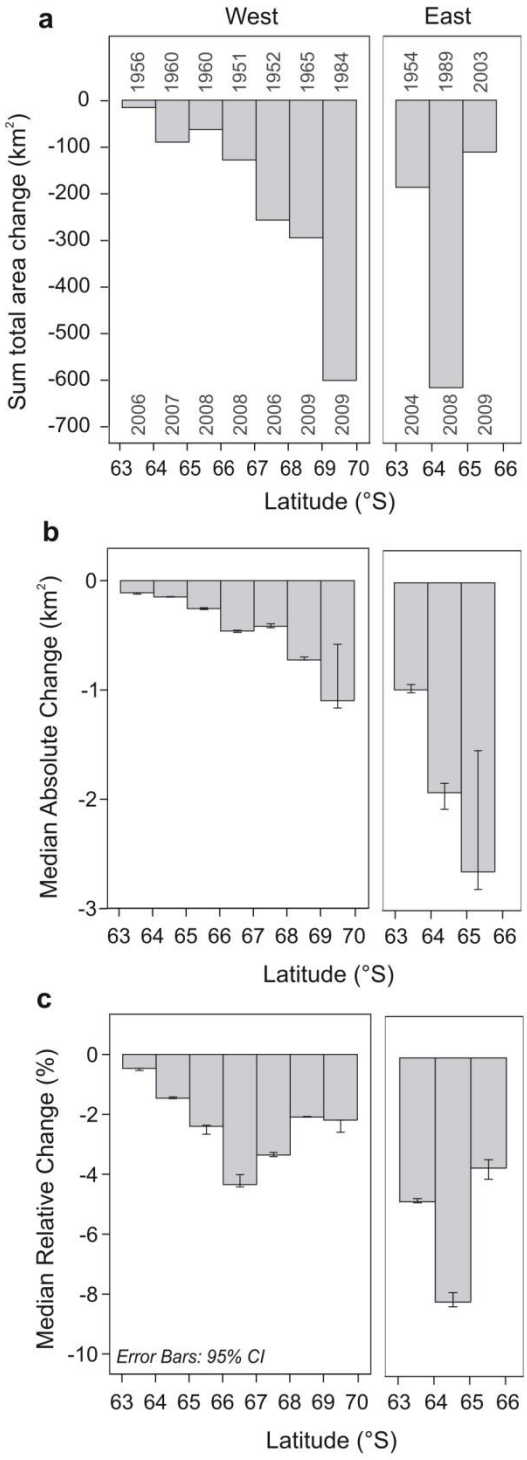

Figure 5.17: Overall area change by degrees latitude.
Sum total area change of all glaciers combined (**a**), median absolute change (**b**) and relative change (**c**) at each degree latitude. On panel **a**, the mean years (weighted by basin size) of the first and last recorded positions are shown along the upper and lower x-axis respectively. Panels **b** and **c** show median values to account for the wide range in basin sizes and are weighted according to the number of years between the first and last dates.

Regional total area changes show that on the west coast, there is a substantial gradient in increasing ice loss from north to south (Figure 5.17a). The east coast glaciers have a large overall loss between 64° S - 65° S (in the region of Larsen A and Prince Gustav ice shelves), although it must be noted that because the earliest and latest dates differ the overall area loss between 65° S - 66° S is only recorded since the Larsen B Ice Shelf collapsed in 2002. The mean first date (weighted by area) for the Larsen B tributary glaciers is 2003; positions were recorded for the Hektoria, Jorum and Crane glaciers in 2002, but records for the Mapple, Melville and Pequod glaciers were not available until 2005 when a further section of the ice shelf collapsed.

A north to south gradient in increasing absolute area loss per glacier (Figure 5.17b) also indicates that there is a strong regional difference in controls on mass loss. Relative changes (Figure 5.17c) in the west do not appear to increase south of 67° but this is probably due to the lack of small glaciers with associated large relative changes. The glaciers in the east show considerably larger mean relative changes at each of the three latitudes than those in the west, which could be explained by the medium-sized glaciers feeding the Larsen A and B ice shelves that retreated rapidly following the demise of the ice shelves. The east and west sides of the AP exhibit markedly different spatial patterns of ice loss, highly influenced by the location of former ice shelves.

5.3.2 Temporal patterns of change

5.3.2.1 Area differences relative to 2000-04

The overall ice loss from earliest to latest positions can tell us about the amount of change over the longest available time frame, but as previously shown, the earliest dates are not consistent. The scale of glacier changes can be calculated in more detail by classifying the data into temporal bins. As described in Chapter 4 (Section 4.5.2.2), every ice front position was assigned to a 5-year interval and all areas have been measured relative to the glacier area in the time interval 2000-04. This is the one time interval for which all glaciers have data: box plots of the area differences are shown in Figure 5.18. The data are highly skewed, and widely dispersed, within each interval. However, the

patterns observed in both the absolute difference in km^2 (Figure 5.18a) and the relative difference in % (Figure 5.18b) are broadly similar throughout the past 65 years.

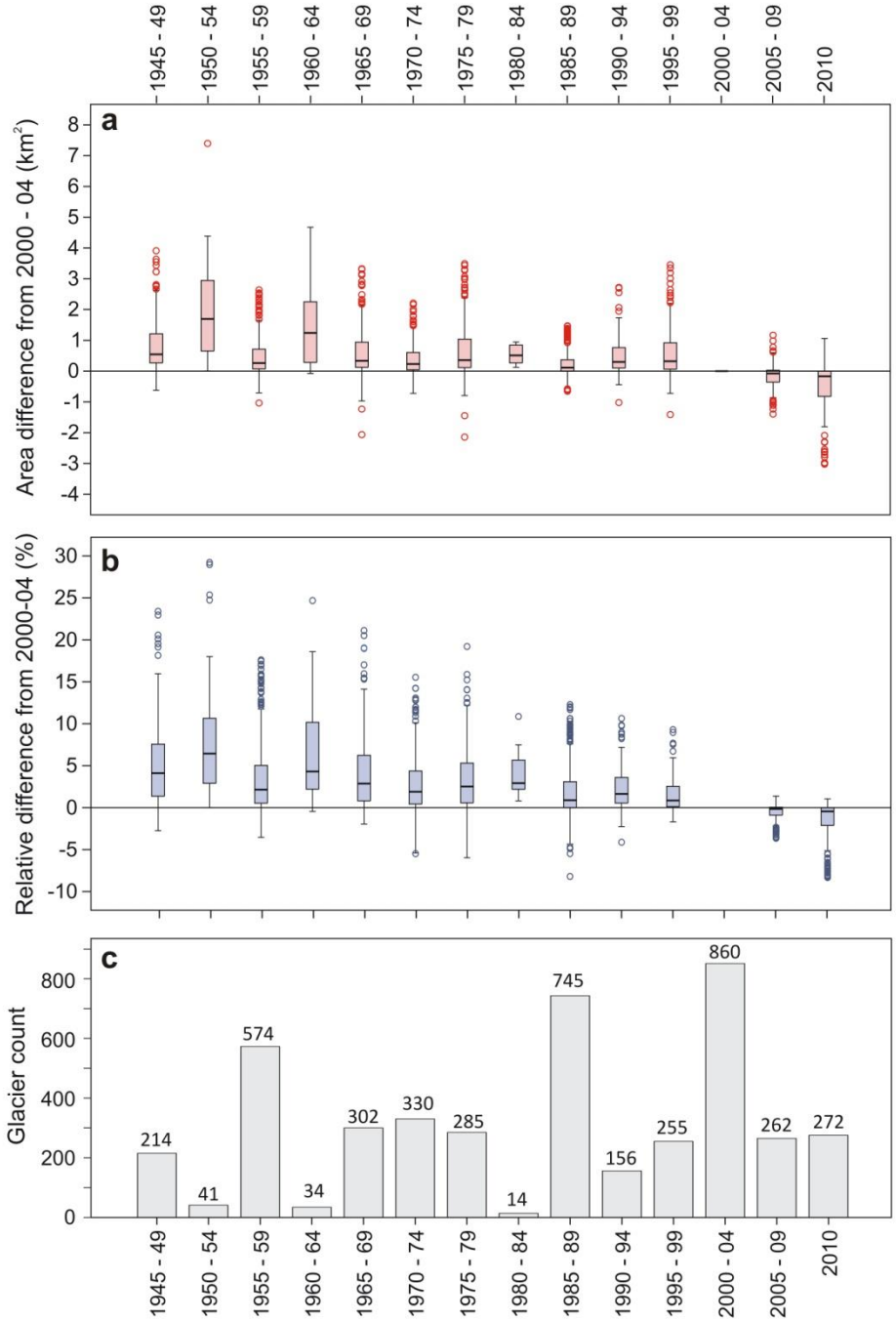

Figure 5.18: Box plots of glacier basin areas relative to the basin areas in 2000-04. Panel **a** is the absolute area difference and **b** is the relative difference as % of the basin size in 2000-04. The thick dark line in the box centre is the median value, the box represents 50% of the data, the whiskers are the limits of data not considered as outliers and the circles are outliers. Panel **c** shows the number of glaciers with ice front positions in each interval.

One variation between the two graphs is for the interval 1995-99, which has a slight overall increase in area values and a positive dispersion, whereas there is a small decrease in the median and minimal change in dispersion for relative difference values. One hypothesis to explain the apparent increase in area is that new glacier basins were introduced to the sample after ice shelf break-ups around this time: these glaciers may be considerably greater in area in 1995-99 than in 2000-04, and yet result in only small relative differences (e.g. large glaciers flowing into Wordie Bay).

The box plots present a summary of the data, but it is difficult to identify temporal trends, primarily due to the variance in sample sizes between each interval (Figure 5.18c). One way to contend with these varying sample sizes is to up-scale the data on a spatial basis, by calculating areas of glaciers with data and applying the area ratio to the rest of the sample (Figure 5.19a). This gives an estimation of total area during each time interval. These results are based on only glaciers with a first-date prior to 1995 (816 glaciers from 860) to remove the effect of the spurious increase in the overall area when glaciers were added post ice shelf collapse. Figure 5.19b shows how many glaciers have data within each interval: data in intervals with fewer than 5% of glaciers are removed since reliability from up-scaling would be significantly reduced. Furthermore, to reduce misinterpretation of temporal trends from such a large sample size, the results can be assessed against a sub-set of glaciers that have positional records at as many adjacent intervals as possible. The total number of glaciers that have 9 or more records since 1945 (n = 36) were selected and data in all intervals containing more than 20 records were up-scaled (Figure 20).

The overall trend in both Figures 5.19a and 5.20a is of broadly consistent retreat, although differences prior to 1980 mean it is difficult to draw conclusions about any early trends. The main observation from this period is that the area is greater in all pre-1980 intervals than in any interval since then. There appears to be a steady decrease in area from the late 1970s through to 2010 for both datasets, with the exception being a notable advance in the late 1990s in the complete dataset.

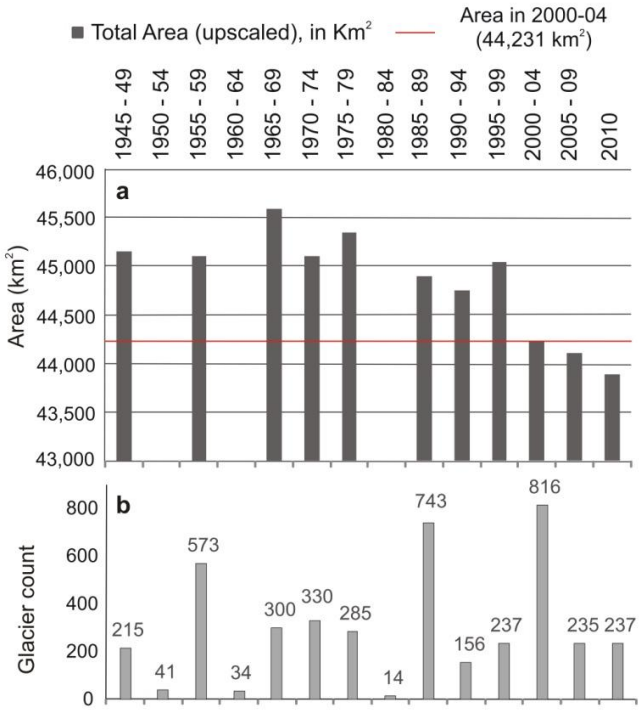

Figure 5.19: Up-scaled areas by 5-year time intervals since 1945.
Up-scaled areas for all 816 glaciers with first-dates prior to 1995 (**a**), and the number of glaciers with ice front positions in each interval (**b**).

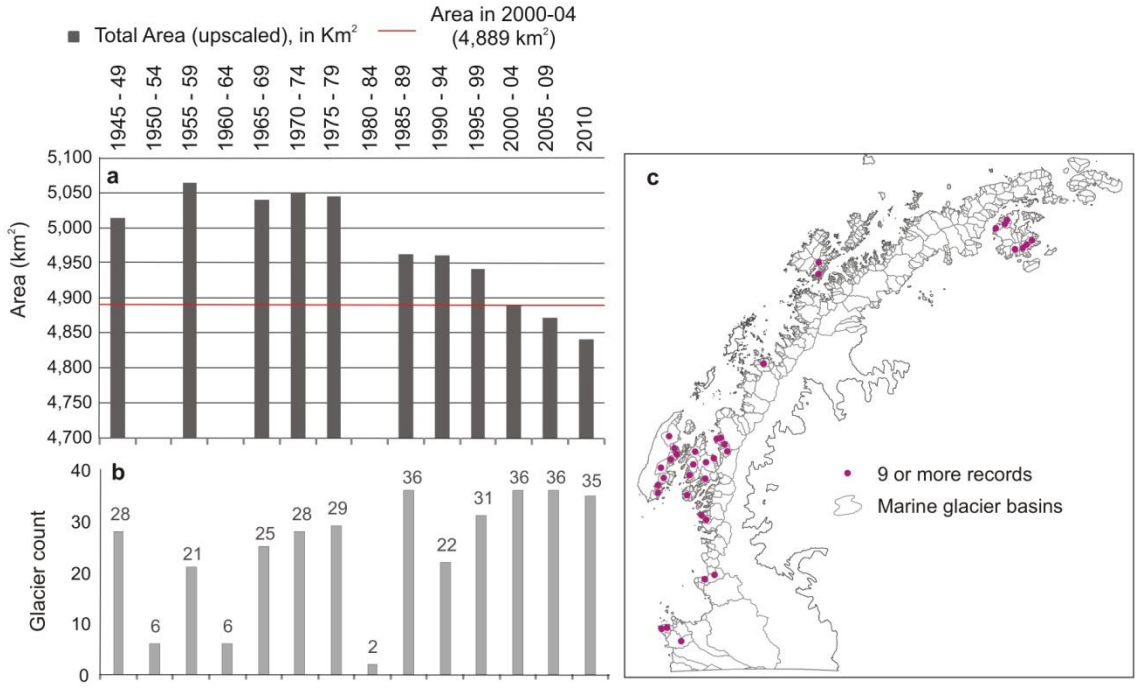

Figure 5.20: Up-scaled areas for glaciers with records in 9 or more intervals (36 glaciers).
Up-scaled areas (**a**) and the number of glaciers with ice front positions in each interval (**b**). The spatial distribution of the 36 glaciers is shown in **c**.

The difference between the two datasets for this interval could be due to one of two reasons: either the small sample of 36 glaciers does not capture all temporal signals since they are not evenly distributed throughout the AP (Figure 5.20c); or the up-scaling method for the complete dataset is less robust during the 1990s than intervals on either side, since fewer glaciers have data at this time. However, it can be argued that the 237 (30%) glaciers with data in 1995-99 are widely distributed throughout the AP and represent all glacier types, and therefore the area increase does represent a true signal at this time. There is no clear difference in rate of retreat between other adjacent intervals.

5.3.2.2 Rates of change

Glacier frontal change studies invariably use rates of change calculations in order to have a consistent measure of change over time. The procedure developed for calculating change rates for the distinctive type of data in the AP has been explained in Chapter 4 (Section 4.5.2.3). The rates of change (in km^2 a^{-1}) between recorded dates were calculated for each glacier. These values were assigned to the relevant 5-year interval as a measure of change occurring throughout the period. This maximises the available data and maintains a consistent measure of change between all intervals. It is therefore a more accurate representation of glacier change and the data provide greater flexibility than area-differencing data. Change-rates spanning more than 15 years are ignored in the analysis, thus minimising over-interpretation of the data. All change-rate data are summarized in graph form in Appendix 5.6.

Before further analysis, it is useful to consider the most suitable way to present glacier change-rates. The two graphs in Figure 5.21 present lines showing the median and mean values. The mean *absolute* rates of change (Figure 5.21a) are considerably larger than the median values due to the highly-skewed data. The large standard error bars are a further indication that the mean value is a misleading measure of average change-rates. The median values therefore give the best measure of central tendency for these data, and 95% confidence intervals give a measure of how well the sample median represents the population median. The mean and median *relative* rates of change (Figure 5.21b) are of a corresponding scale and follow a comparable temporal trend, although they become more disparate over time. The influence of basin size has been reduced resulting in more

normally distributed data. Mean values are considered a suitable measure of the average, with standard error bars to show how close the sample mean is to the population mean. In further analysis, either median absolute change (with 95% confidence intervals) or mean relative change (with standard errors) are used as a measure of the average, depending on the variables being examined.

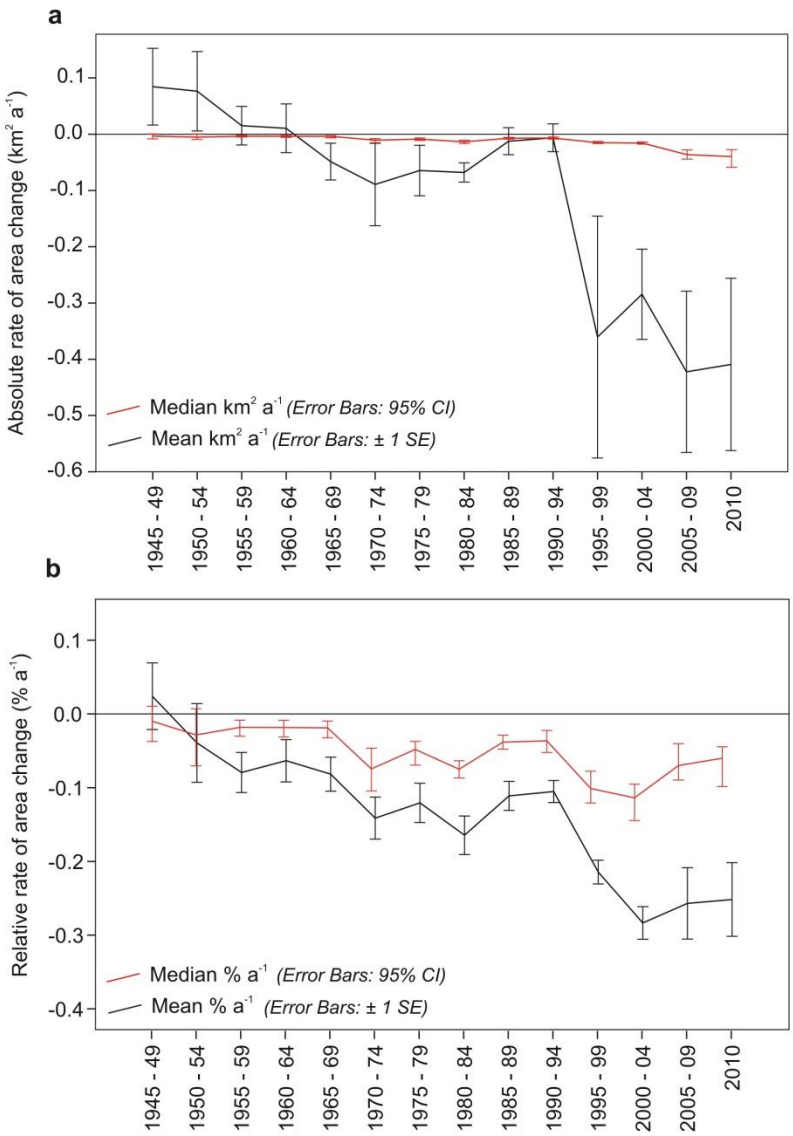

Figure 5.21: Rates of change for all glaciers across all intervals.
In panel **a**, median change-rate values in $km^2\ a^{-1}$ are shown in red, and mean $km^2\ a^{-1}$ values are in black. The widely differing mean and median values are due to the highly-skewed data. Median values give the best measure of central tendency. In panel **b**, the rates of change are as a percentage of the basin size (% a^{-1}), with mean and median values on a corresponding scale. Relative rates of change reduce the influence of basin size.

Interpretation of temporal changes of all glaciers must take into account the distribution of glaciers at each time interval. There are two primary data distribution criteria to achieve before temporal comparisons can be made: that data are not spatially clustered, and there are a sufficient number of glaciers in adjacent time intervals. The simplest way to show data distribution is in graph form showing the glacier count in each interval, split by one degree latitude bands in order to identify any spatial gaps (Figure 5.22 and Appendix Table 5.5).

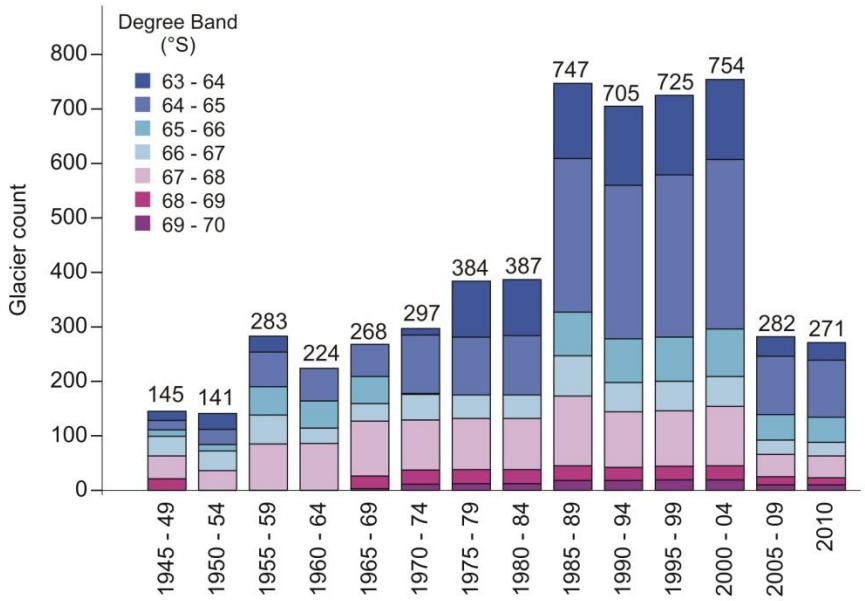

Figure 5.22: Latitudinal spread of data availability (stacked) per 5-year interval.
Average rates of change values are strongly influenced by the availability of data, and the spatial distribution of the glaciers. The valid numbers of glaciers in each interval are shown (total numbers at the top of each bar), separated by latitude. The glacier count in each degree band is listed in Appendix 5.5. There is a reasonable latitudinal distribution of glaciers in each interval, suggesting the average is not unduly influenced by an uneven spatial distribution of data.

All time intervals have a good latitudinal spread of data, except for an underrepresentation of southern regions between 1950 and 1969. Regarding data quantity, the smallest numbers of glacier change-rate data are in the earliest two intervals (minimum 16% of all glaciers) but otherwise all intervals contain over 25% of glaciers. The data distribution shows that the temporal trends observed in Figure 5.21 are therefore not biased and are a reliable representation of average peninsula-wide changes.

Absolute change (in $km^2 a^{-1}$) median and mean values show very different trends, owing to the skewed data distribution. When these are considered alongside relative retreat rates (in $\% a^{-1}$), a summary of the temporal trend in glacier change rates Figure 5.21a and b is as follows:

- There was a general trend of increasing retreat rates from the late 1940s until 1980-84.
- This was followed by a decrease in retreat rates until 1990-94.
- There was then acceleration in retreat rates from 1990-94 until 2000-04.
- There has been an apparent slow-down in relative retreat since 2000-04; however the large error bars suggest that this is not significant. These data have greater variability and could be heavily influenced by the behaviour of a small number of glaciers.

The short-term rates of change values may be small but over the long term there is a distinct trend in area-change rates. Trends observed in data with such wide dispersion, however, must be tested for statistical significance.

5.3.2.3 Significance of temporal trends

A key issue is whether any observed differences between two epochs are consistent with random variation or whether they represent genuine differences between epochs. To determine the statistical significance of differences between epochs, two different tests were considered. When data are normally distributed, a Student's t-test is conventionally used, which calculates the probability (p value) that differences in the mean values are due to natural variability in the data. Although the t-test is reasonably insensitive to violations of normality (especially with large sample sizes) a non-parametric alternative is the Wilcoxon signed-rank test, which does not assume data normality. As was previously discussed, the glacier relative change-rate data are moderately normally distributed and with a large sample size, therefore it was decided to use the t-test, following the conventions that p=0.05 indicates a 'significant' difference, p=0.01 indicates a 'highly significant' difference (99% confidence) and p=0.001 indicates a 'very highly significant' difference. These tests were also undertaken in a study of

glacier-change rates between epochs for a large sample of glaciers in East Antarctica (Miles *et al.*, 2013).

A paired-sample t-test (i.e. using only data from glaciers measured in both epochs) was carried out on the relative glacier change data (Table 5.6). Seven out of thirteen paired samples have significant differences (where $p < 0.05$) between their means and therefore these changes can be regarded as genuine: it must be noted however that the apparent decrease in retreat rates since 2000-04 is not significant. The absolute area change rate data are highly skewed therefore it was prudent to use the Wilcoxon signed-rank test. In this case, the same epochs were regarded as significantly different, the exception being between 1965-69 and 1970-74. Temporal differences that are not significant are the small fluctuations in retreat until 1980-84 and the apparent slow-down in relative retreat rates since the early 2000s. This means that the general trend, including the decrease in retreat rates in the late 1980s, is based on statistically significant data. It must be re-iterated that the trend described is the median and there is a wide dispersion of data in each interval.

Table 5.6: Paired sample Student's t-test for glacier relative rates of change (% a^{-1}).
Values highlighted in red are where differences between epochs are significant at < 0.05 level. These relate to the trend observed in Figure 5.21b.

Pair	n	Mean	Std. Dev	t	Sig. (2-tailed)
1945 - 49 & 1950 - 54	118	0.002	0.022	1.06	0.29
1950 - 54 & 1955 - 59	136	0.055	0.313	2.07	0.04
1955 - 59 & 1960 - 64	218	0.028	0.195	2.12	0.04
1960 - 64 & 1965 - 69	222	0.018	0.250	1.10	0.27
1965 - 69 & 1970 - 74	195	0.082	0.398	2.90	0.00
1970 - 74 & 1975 - 79	270	-0.028	0.412	-1.12	0.26
1975 - 79 & 1980 - 84	383	0.045	0.302	2.91	0.00
1980 - 84 & 1985 - 89	387	-0.042	0.150	-5.48	0.00
1985 - 89 & 1990 - 94	693	0.005	0.425	0.28	0.78
1990 - 94 & 1995 - 99	705	0.079	0.318	6.56	0.00
1995 - 99 & 2000 - 04	725	0.056	0.383	3.91	0.00
2000 - 04 & 2005 - 09	275	-0.038	0.409	-1.56	0.12
2005 - 09 & 2010	271	-0.010	0.163	-1.05	0.29

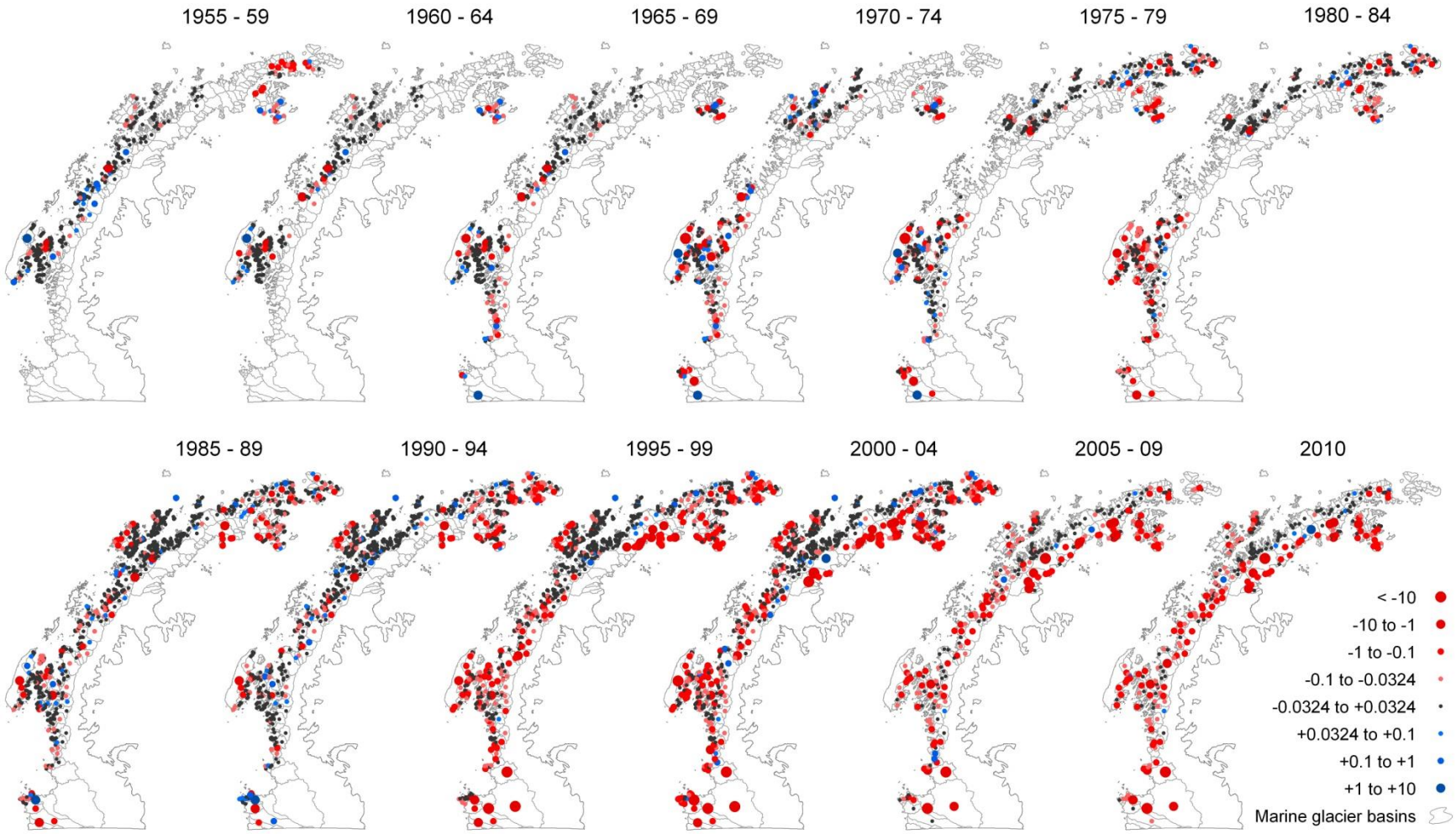

Figure 5.23: Maps plots showing the spatial distribution of area change rates (in km^2 a^{-1}) over 5-year intervals, since 1955.

5.3.3 Spatial patterns of change

Analysis of overall change since the first recorded positions showed spatial patterns such as a north to south gradient of increasing absolute change, and distinctive behaviour on the north and west sides of the AP (Figure 5.17). Identification of spatial and temporal patterns combined can be achieved initially by mapping the scale of changes observed at each 5-year time interval (Figure 5.23). This illustrates not only the spatial distribution of data available, but changing patterns that occur over time.

One challenge in analysing glacier change-rates is what defines a 'stable' glacier front in this region (i.e. not in active advance or retreat). Glaciers in the AP are little studied and since this is the first analysis of the scale of advance and retreat, the definition of frontal stability can only be estimated. In Chapter 4 (Section 4.6.2), the issue of annual glacier cycles was addressed and in this, the estimate of average intra-annual frontal change was considered to be less than 180 m in length, or 0.0324 km^2. Annual frontal changes may be smaller than this but the analysis was restricted by the 90-m pixel resolution of the images. A detailed analysis of glacier stability is outside the scope of this study, therefore the benchmark of 0.0324 km^2 is used as an estimate defining a 'stable' glacier.

Each point in Figure 5.23 represents a glacier with change-rate data available: those that are grey are considered stable; those that are red are retreating and blue are advancing, with the size of the point denoting the magnitude of the change-rate. The two earliest intervals, 1945-49 and 1950-54, are not shown as these have relatively low data coverage. Although data are sparser in the early time periods, there are no obvious patterns amongst data that do exist. Although there are regional gaps, the Adelaide Island region has data in all intervals, and by the late 1980s, there is peninsula-wide coverage of glacier change-rates. Observations include:

- Glaciers along the west/north-west mainland have been stable throughout all periods, whilst glaciers on the east side of the AP have been in long-term retreat (although there are data gaps in the 1960s and early 1970s).
- There is a diverse mixture of glacier behaviour along the west coast from the 1950s through to 1990-94.

- From the late 1990s onwards there is a distinct shift in spatial patterns of change-rates throughout the AP. Almost all glaciers surrounding the AP are in retreat at this time, except for those in the west/north-west mainland region which remain stable.
- This pattern remains consistent from the late 1990s right up until 2010.
- There appears to be a gradient in increasing retreat rates along the west coast from north to south.
- The largest retreat rates since the late 1990s are glaciers along the east coast (from the northern tip down to the edge of the Larsen ice shelf) and in the south-west: these are in regions where ice shelves have recently collapsed.

5.3.4 Correspondence with previous AP glacier-change study results

Temporal trends are difficult to validate when data-types are diverse and their accuracies complex and hard to quantify. One way to substantiate the observed trends is by comparing them to results from the previous study by Cook *et al.* (2005). As explained in Chapter 2 (Section 2.2.3.2), the study examined changes in length of 244 glaciers on the AP, from the 1940s to 2000. The sample size was smaller but with a comparable spatial distribution to the present study. The glaciers flowing into Wordie Bay and Larsen B were removed from the present dataset as these have a large influence on the results and they were not part of the previous study. Results from the present study have been plotted here in such a way as to replicate Figure 4 in Cook *et al.* (2005), i.e. separated into two degree latitudinal bands and as mean area change rates ($km^2 a^{-1}$) (Figure 5.24).

It can be seen that in a broad sense the mean area-changes of all glaciers (Figure 5.24a) follow similar temporal trends to those in the original length-change study (Figure 5.24c). This constitutes a transition from advance to retreat over time in all sectors apart from north of 64° S, which has been largely stable throughout; a southerly migration of this transition; greater rates of retreat with increasing latitude and a slow-down in retreat rates in the late 1980s/early 1990s. The last two time intervals (2005-09 and 2010) were not available in the previous study, but a slow-down in mean area retreat rates is apparent south of 68° S.

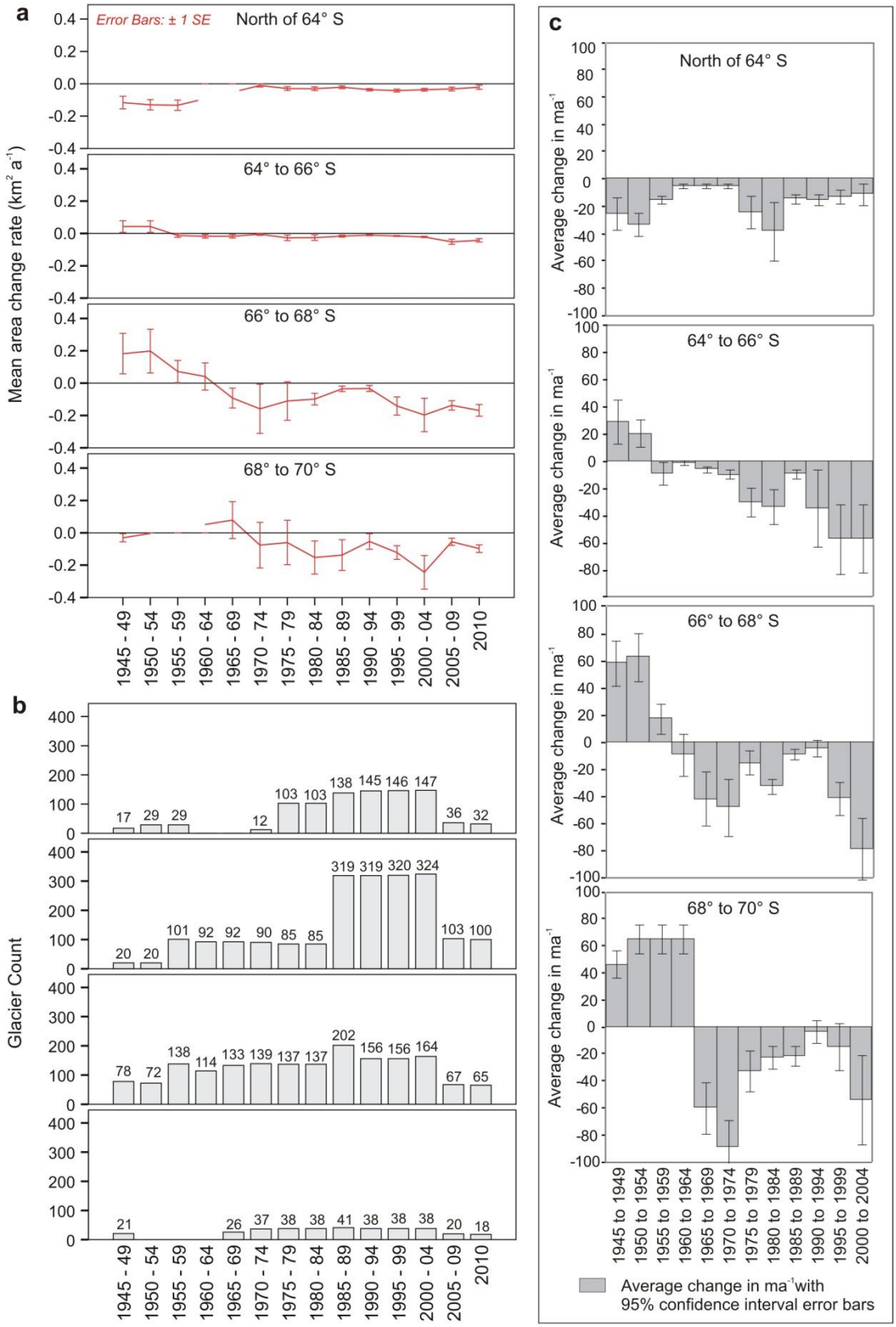

Figure 5.24: Glacier area changes compared to length changes from earlier coastal-change study by Cook *et al.* (2005).

Figure 5.24: The area-change rates (**a**) and the corresponding glacier counts (**b**) cover the same regions as the length-change results (**c**). The graphs in (**c**) are from Cook *et al.* (2005). The glaciers flowing into Wordie Bay and Larsen B have been removed from the current study in order to maintain consistency between the two studies. Glaciers on the South Shetland Islands and Alexander Island however are missing from the present study.

There are also a number of differences between the studies: for example, area-changes in 64-66° S are minimal compared to the length-changes; the advance rates in 68-70° S are considerably larger for length-changes than area-changes, as are the retreat rates from 1960 to 1975. As shown in Figure 5.24b, however, there are minimal data in the region 68-70° S in the early intervals and so these results are unreliable. One explanation for the other differences is that change-rates for the length-change study were calculated across gaps regardless of their duration, whereas the area-change results do not include gaps over 15 years. Furthermore, absolute area-changes are heavily influenced by the glacier basin size, resulting in wider data dispersion than for length-changes. Another factor is the large difference in sample sizes between the two studies: there are almost four times the numbers of glaciers in the area-change study than the length-change study. In spite of the diversity in data and methods, the general patterns across the AP are similar, suggesting that the observed regional temporal trends are genuine.

5.3.5 Spatial and temporal patterns: regional summary

The results from the previous *Coastal-Change* study have been improved in a number of ways: the area change calculations offer a more accurate assessment of ice loss, both in absolute and relative terms; the sample size has been significantly increased; the method to calculate rates of change has been considerably improved; and glaciers have details on their characteristics which allows behavioural comparisons. A way to improve on summarizing the results is to split the AP into east/west, since the two sides are distinct in their frontal change patterns, climate and ocean settings. In addition, area-changes are most accurately represented by relative change rates: absolute change rates do not accurately reflect regional behavioural response to environmental changes since they are strongly influenced by glacier size. A latitudinal spacing of two degrees is regarded as optimum for spatial and temporal analysis: at a finer latitudinal spacing the glacier count within some intervals are significantly reduced, especially in early time periods.

Therefore, regions defined by east/west and two degree latitudes are considered most suitable for further analysis when considering wide scale climate and ocean patterns.

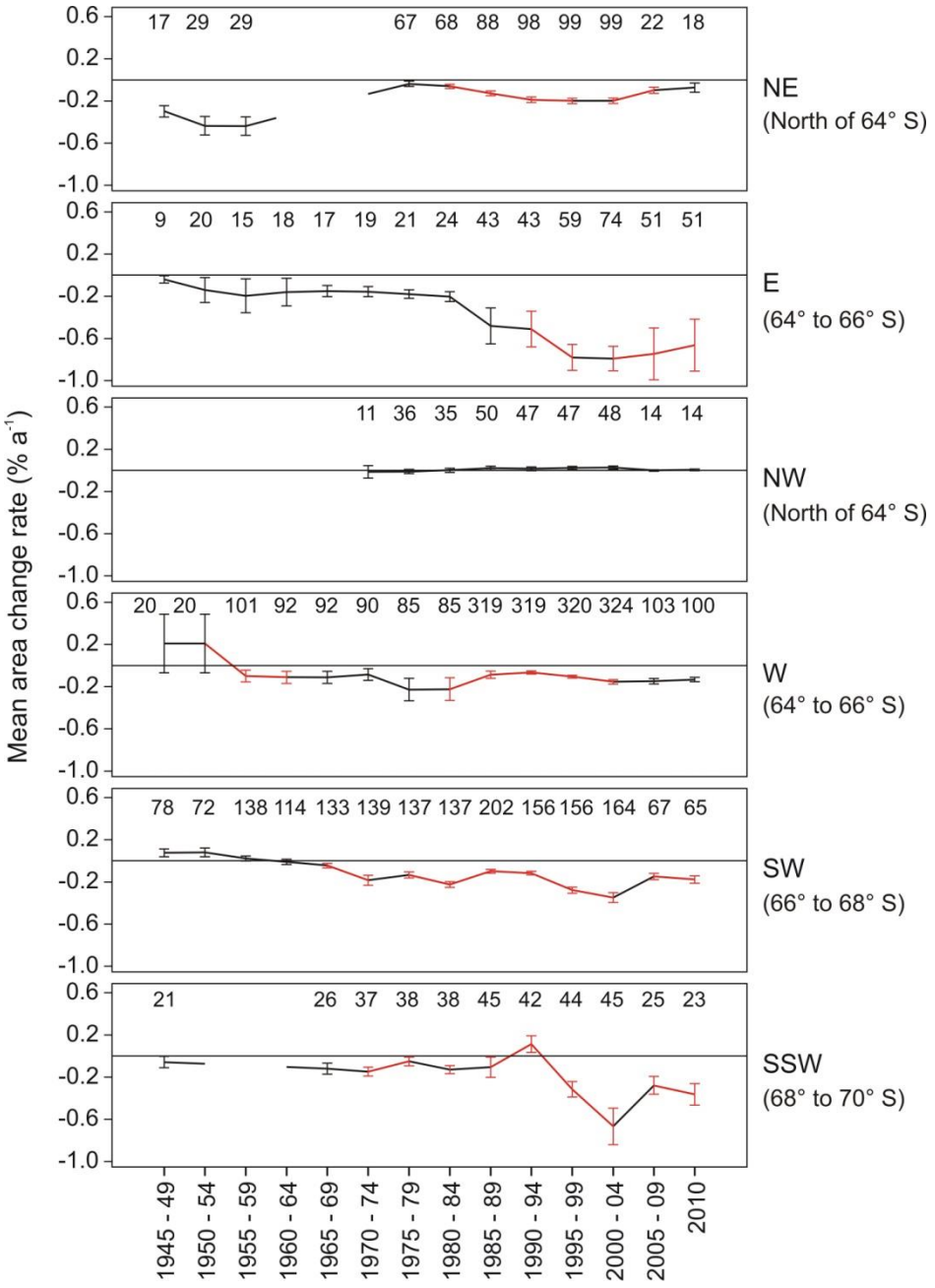

Figure 5.25: Area-change rates by region (% a^{-1}).
The regions are split into east and west, and by the 2 degree latitudinal bands (shown on the right hand side). The corresponding glacier counts are shown along the upper x-axis. Error bars are ± 1SE. Where lines are red, the trends are significant at < 0.05 level. The Wilcoxon significance test results relating to these trends are in Appendix 5.7.

Spatial and temporal patterns for the six regions (Figure 5.25) can be summarized as follows (mean values are listed in Appendix 5.7):

- The long-term area-change trends are distinct for the east and west of the AP.
- In the east, glaciers in the NE were undergoing large retreats in the 1940s: since the late 1970s they have still been in retreat, but at reduced rates.
- Glaciers in the E showed relatively small retreat rates from the 1940s to the early 1980s; after then retreat has accelerated and glaciers reached maximum retreat in the early 2000s (mean = -0.79 % a^{-1}).
- Glaciers in the west have shown progressively greater retreat rates from north to south, with a southerly migration in the transition from advance to retreat over time.
- In the NW, glaciers have been stable since the earliest records (1970-74). They have shown minimal changes rates throughout.
- In the W, the small numbers of glaciers with positions available in the early time periods were advancing at this time. Since the late 1950s glaciers have been retreating, but with relatively small rates.
- In the SW, small advances became retreats in the early 1960s and since then there has been a gradual acceleration in retreat. The retreat slowed down in the late 1980s/early 1990s. There has also been a reduction in retreat since 2000-04.
- In the SSW, small retreat rates changed to small advances in the early 1990s. Since then there was a rapid acceleration in retreat rates, which occurred following the break-up of Wordie Ice Shelf. Since 2000-04 there has been a slow-down in retreat rates.

The Wilcoxon signed-rank test was carried out to determine the statistical significance between epochs for each region, the results of which can be found in Appendix 5.7. Points of note are that there are no statistically significant differences in changes between any epochs in the north-west; the trends in the W and SW are significant between 1980-84 and 2000-04; in the SSW the trend is significant between 1985-89 and 2000-04; and the apparent reduction in retreat rates in 2005-09 in the SW and SSW are not statistically significant. Differences in the east are more varied but the reduction in retreat rates between 2000-04 and 2010 are considered to be statistically significant.

A more detailed interpretation of these trends is possible if individual glacier variables are taken into consideration.

5.4 Behavioural comparisons between glacier-types

The issue of inter-dependence of glacier characteristics has been previously discussed (Section 5.2.2). Comparative statistical analyses are challenging since the area-change dataset consists of multi-characteristic glaciers on a diverse spatial and temporal scale, and the data in many of the categories are highly skewed. In addition, there are certain glacier characteristics missing from the dataset that play a key role in glacier mass balance (e.g. ice thickness, equilibrium line altitude and bedrock topography). Despite these shortcomings, much information can be extracted from the dataset, first by identifying which glacier characteristics are correlated and then by assessing the timing and scale of area-changes for glaciers with different characteristics.

Basin area was found to be the attribute with the highest correlation with other glacier characteristics (Section 5.2.2 and Table 5.4). Correlations between glacier characteristics and overall change (in both absolute and relative terms) showed that glacier area, length and outlet width had significant positive correlations with absolute change, and mean slope had a negative correlation on a similar scale (Section 5.3.1.1 and Table 5.5). Mean elevation was the variable with the strongest correlation with relative change.

Section 5.3.2 identified peninsula-wide temporal trends in area-change (Figure 5.21). The overall trend may not apply to all glacier types, however, and individual variables may have a dominant influence on the trend. To assess whether different glacier-types display inconsistencies in timing and scale of area-change, the graphs in Figure 5.26 show area change rates for glaciers with particular contrasting characteristics. The characteristics selected are those that are considered to play a role in the changes that occur at the glacier front. Median absolute area change rates ($km^2\ a^{-1}$) are displayed rather than relative change, since the characteristics are being compared irrespective of basin size.

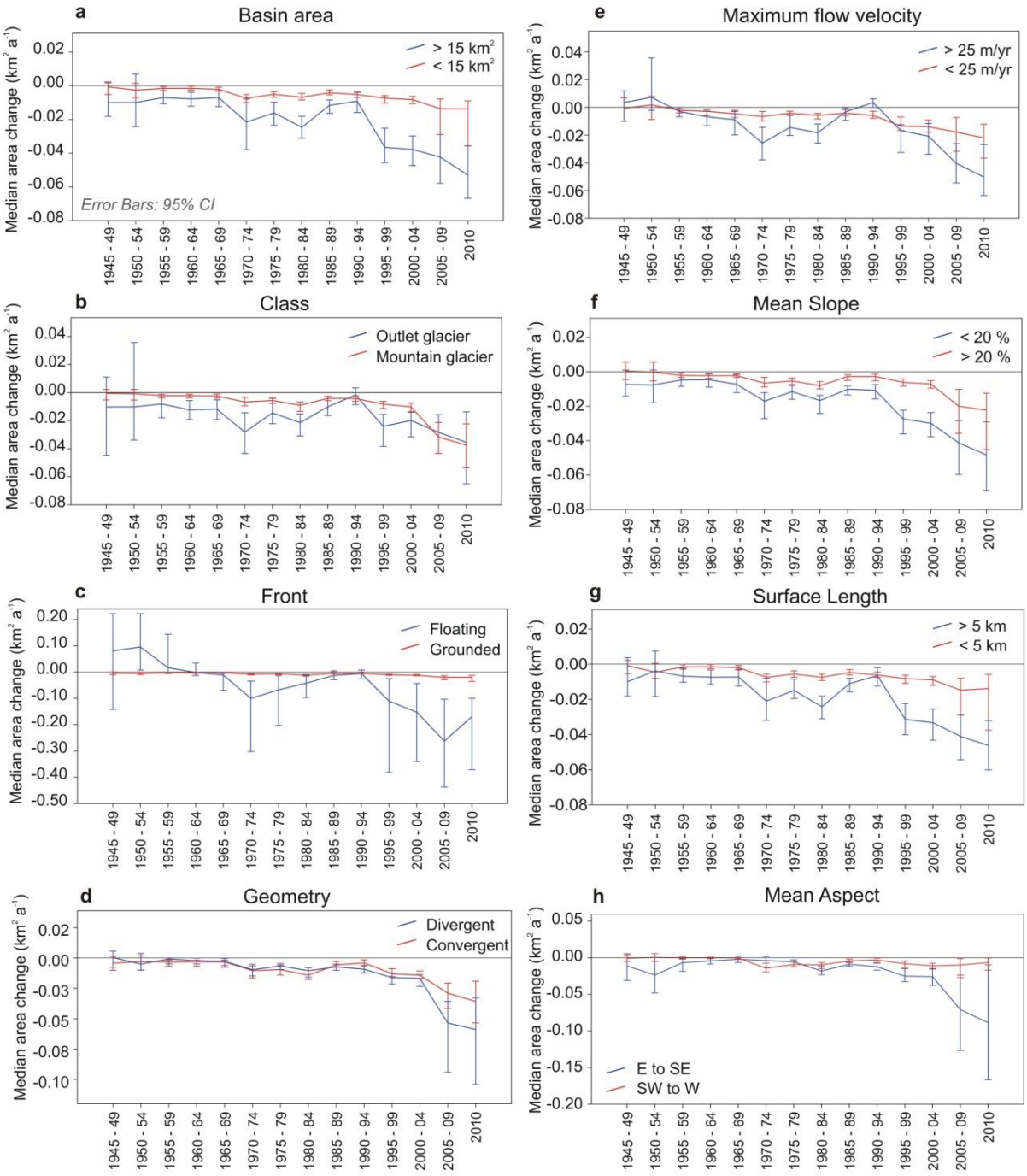

Figure 5.26: Rates of change (km^2 a^{-1}) for glaciers with contrasting characteristics.
The valid numbers of glaciers that contribute to the average values are listed in Appendix 5.8.

The area-change behaviour of glaciers with contrasting types can be summarised as follows (with reference to Figure 5.26):

(a) Basin Area - The contrasting frontal behaviour of small/large glaciers is clear: glaciers < 15 km^2 have shown small change-rates with a uniform slight increase in retreat; glaciers > 15 km^2 however have shown greater variation and a large increase in retreat rates, punctuated by a decrease in retreat in 1985-89 and 1990-94.

(b) Class - Glaciers in the outlet and mountain glacier categories show differences in their area-change rates but on a relatively small scale: mountain glaciers show small change rates and have small error bars whereas outlet glaciers show greater retreat and more variability. The two glacier types are in synchronous retreat post 2000-04.

(c) Front - The glacier characteristic with the largest contrast in behaviour is frontal-type: the y-axis is on a considerably larger scale than the other graphs, due to the large change-rates and variations in floating glaciers. These glaciers also have a slow-down in retreat rates between 1985 and 1994. Grounded glaciers are much more stable throughout the study period.

(d) Geometry – Converging (i.e. narrow mouths relative to mean widths) and diverging (wide mouths relative to mean widths) can be a proxy for ice dynamics. If a glacier converges, it is likely to be more constrained and therefore changes in mass balance may result in length fluctuations and non-uniform retreat. Conversely, diverging glaciers are less constrained and likely to show a more regular retreat. The behaviour of convergent and divergent glaciers did not match this hypothesis however: the rates of area change of both types are synchronous throughout, until 2005-09, at which point divergent glaciers begin to retreat more than convergent glaciers. The synchronicity could be because divergent glaciers may change little in length but this equates to a relatively large change in area, whereas convergent glaciers may change substantially in length, but relatively little in area, hence the areas equal out. Further research on glacier length changes could explain these ice dynamics.

(e) Maximum flow velocity - Glaciers with low flow-rates have a more uniform trend with smaller changes than faster glaciers. The decrease in retreat rates between 1985 and 1994 is noticeable for fast flowing glaciers.

(f) Mean Slope - Glaciers with lower mean slopes have shown larger area-changes than steeper glaciers, particularly since the early 1990s.

(g) Surface length - Similarly, longer glaciers have retreated at higher rates than shorter ones and with greater variation. The decrease in retreat rates between 1985 and 1994 is clear for long glaciers but there is no change at this time for short glaciers.

(h) Mean Aspect - There is no obvious difference between the two basin aspect sectors, until 2000-04 when those in the E to SE show rapid retreat (although with large error margins). This is most likely due to the loss of the Larsen A and B, when the tributary glaciers (all of which have E to SE facing basins) rapidly retreated.

As already stated, inferences from these graphs are inherently limited due to the inter-relationships between variables, and in addition the median change-rate values are small. However, what is clear in almost all graphs is that the temporal trend observed for all glaciers combined (Figure 5.21) can be identified, implying that there is no individual variable that has a dominant influence on the trend. In particular, the decrease in retreat rates between the early 1980s and early 1990s is clearly visible. For each characteristic, except for glacier geometry and aspect, one of the two glacier-types reveals this trend more than the other, e.g. large glaciers, outlet glaciers, floating, fast-flowing and long glaciers closely follow the overall trend, whereas their opposing glacier types do not. Since these characteristics are inter-related, glaciers that have all such characteristics may have the greatest influence on the overall trend. There were 10 or fewer glaciers with these characteristics prior to 1985-89, which show a transition from advance to retreat over this time. From 1985-89 onwards there were 21 glaciers with data and the majority of these showed small advances in 1990-94 and a steady increase in retreat rates since then. The advance rates occurring in 1990-94 could explain the apparent increase in ice coverage in 1995-99 which was calculated by up-scaling area differences from 2000-04

(Section 5.4 and Figure 5.19). These large glacier basins would have greater influence on the total area when the values were up-scaled.

The change rates of large, fast-flowing, long outlet glaciers with floating fronts follow the trend observed for all glaciers but there are too few to have a dominant influence in producing this trend. Average area change rates on the AP since the 1940s have been small, primarily due to the strong skew towards small glaciers, but nevertheless there is a distinct trend present.

5.5 Summary

This chapter has given a qualitative account of the distribution and characteristics of glaciers on the AP, and a quantitative analysis of glacier area changes, in which spatial and temporal patterns of retreat were identified.

A summary of the characteristics of all 1,590 glacier basins revealed an opposing relationship between glacier area and their sum total areas: there are a large number of small glaciers (with a small total area) and a small number of large glaciers (with a large total area). Based on their classifications, basin complexities and frontal characteristics, the largest population of glaciers on the AP were found to be mountain glaciers with simple basins and calving fronts (n = 301, 19%). The spatial distribution of glaciers shows that by far the largest number of glaciers (n = 427) occur in the west between 64° S - 65° S, whereas only 31 glaciers are found within the most southerly western band 69° S - 70° S, although this region has the largest glacierized area (22% of the entire region).

The marine-terminating glaciers were described in more detail, including their surface elevation characteristics. Mean slope and elevation of mountain glaciers are very dependent on glacier area; for example, small glaciers tend to have low mean elevations and high mean slope angles. Large outlet glaciers tend to have low mean slope angles irrespective of the mean elevation. The qualitative results demonstrate the strong inter-relationships of glacier characteristics and that basin area is a strongly determining factor for many other variables.

The analysis of overall glacier changes showed that 90.5 % of the 860 marine-terminating glaciers have reduced in area since the earliest records. There is a clear difference in glacier behaviour between the east and west sides of the peninsula, with those in the north-east showing greater overall relative change than those at the same latitude on the west side. There is a north-south gradient of increasing area loss along the west coast and greatest ice loss is strongly associated with the location of recently-collapsed ice shelves. Largest areas have been lost from large glaciers flowing into Wordie Bay in the south-west, and those flowing into the Larsen A and B embayments. These results correspond with other studies that showed mass loss due to glacier acceleration and surface lowering following ice-shelf collapse.

There is an inherent difficulty in summarizing the area-changes over time: there is a different subset of glaciers in each interval and there are such a wide range of glacier sizes and characteristics that central tendency values may not give a robust measure of change between time intervals. Different approaches were taken to determine any trends that may exist.

Firstly, by up-scaling area changes (as differences from basin areas in 2000-04) it was shown that there was a largely uniform retreat from the late 1970s to 2010, punctuated by a period of advance in the late 1990s. The differences prior to the 1980s meant it was difficult to draw conclusions about early trends. The up-scaling method gives an approximation of total area in each interval, but is less reliable for intervals with a low percentage of glaciers and is strongly influenced by basin sizes within each subset.

The quantification of glacier change rates enabled a more rigorous analysis of temporal trends, based on a consistent measure of change over time. The median (and inter-quartile) values up until the late 1990s are small, indicating that the majority of glaciers have remained relatively stable throughout this time. Despite the small median values, the similar trend is observed in glaciers with many different characteristics: largely uniform retreat since the 1940s until the early 1980s, after which there was a statistically significant decrease in retreat rates until the early 1990s. Since then there has been a significant increase in retreat rates. Glaciers defined as “large, long, fast-flowing outlet

glaciers with floating fronts" showed small advances between 1985 and 1994, which could explain the up-scaled area increase in 1995-99.

Finally, spatial analyses of temporal trends showed that there has been a southerly migration of the transition from advancing or stable rates to increasing rates of retreat. There was a mixed pattern of change rates along the west coast from the 1940s, but a significant change began in the late 1990s, when the majority of glaciers throughout the AP were retreating. Glaciers in the north-west/west region, however, have remained stable throughout the entire study period. This spatial pattern has stayed similar ever since. External forcings must be investigated to understand this regional shift in glacier behaviour.

Chapter 6

External controls on glacier change on the Antarctic Peninsula

6.1 Introduction

6.1.1 Regional patterns of glacier change

The previous chapter has demonstrated that there are distinct regional patterns in glacier front changes on the Antarctic Peninsula (Section 5.3). The primary differences occur between the east and west AP, and there is a notable region along the north-west coast, between ~65° S and the northern tip, where glaciers have remained stable while those on the rest of the AP have undergone overall retreat. No obvious spatial pattern in frontal changes existed prior to the 1980s, but between 1985 and 1994, there was a statistically significant reduction in retreat rates, noticeable in glaciers at all latitudes and across many glacier-types. There was a significant shift in frontal change from 1995-99 onwards, when almost all glaciers surrounding the AP (except those in the north-west) began to retreat. Finally, a trend in increasing rates of retreat from north to south was observed, with a southerly migration of these increases over time. Glacier change rates were generally small (<1 km^2 a^{-1}), suggesting that the impacts of regional controls have not been dramatic, and yet the long-term trends contain statistically significant patterns.

Glaciers displaying trends over a wide area are clearly subject to external control factors that outweigh the influence of local controls on glacier front behaviour. As discussed in Chapter 2 (Section 2.3), regional controls on glacier front behaviour originate from the atmosphere and the ocean. Interpretation of each of the trends must therefore involve analysis of spatial and temporal patterns in these external controls. A regional analysis of the principal drivers of glacier-front change is undertaken in this chapter, with the aim of

identifying possible correlations with glacier-front behaviour which will be undertaken in the subsequent chapter.

6.1.2 Regional drivers of change

The primary driver of glacier and ice shelf change on the AP has been much debated in recent years. Ice shelf break-up has been widely attributed to atmospheric warming, with retreat following a pattern that suggests a southerly migration of a climatic limit (e.g. Morris & Vaughan, 2003). Atmospheric change however is not universally regarded as the primary driver of ice shelf retreat, as ocean-driven ice-shelf thinning through basal melting is thought to pre-condition the ice shelves to retreat (e.g. Rignot *et al.*, 2013). It is unlikely that either atmospheric or oceanic temperatures singly determine ice front change, as both systems are closely coupled (see Section 2.3.3). If they are first considered independently, however, patterns may determine the degree of synchronicity of the ocean-atmosphere systems and highlight any disparities on a regional scale.

6.2 Atmospheric patterns

A change in atmospheric temperature is popularly considered to be the primary driver of glacier and ice shelf retreat in the region (as discussed in Section 2.2.3). Indeed, changes in glacier terminus positions in East Antarctica were recently found to be consistent with a response to air temperature and sea-ice trends (Miles *et al.*, 2013). The dominant mode of atmospheric variability (the Southern Annual Mode) was found to be a significant driver of these glacier front changes along the Pacific coast. The extent to which this plays a role in glacier front positions in the AP is yet to be determined.

In understanding atmospheric patterns, the primary components of air temperature and precipitation should be considered. There are a number of different source materials for recent air temperatures on the AP. Meteorological station records provide temperature measurements over the past half-century, although they are sparsely distributed across the AP and some only have a few years of records (Barrand *et al.*, 2013b). It is therefore useful to also consider surface-melt data, acquired from scatterometer satellite data since

2000, to corroborate the mean regional temperature distribution and provide more spatial detail (Barrand *et al.*, 2013b). Thirdly, surface temperatures have been obtained from radiometer satellite data between 1979 and 2008 and, although at a coarser resolution, they provide a useful temporal record (Comiso, 2000). Finally, surface mass balance (SMB) data from 1979 to 2010 can be used to assess changes in accumulation across the region (Lenaerts *et al.*, 2012). The coverage for some of the source data is not sufficient for local comparisons; the analysis of atmospheric and oceanic patterns is therefore on a more general scale, with regional delineations at two degree latitudes and divided into east/west along the drainage divide (Figure 6.1).

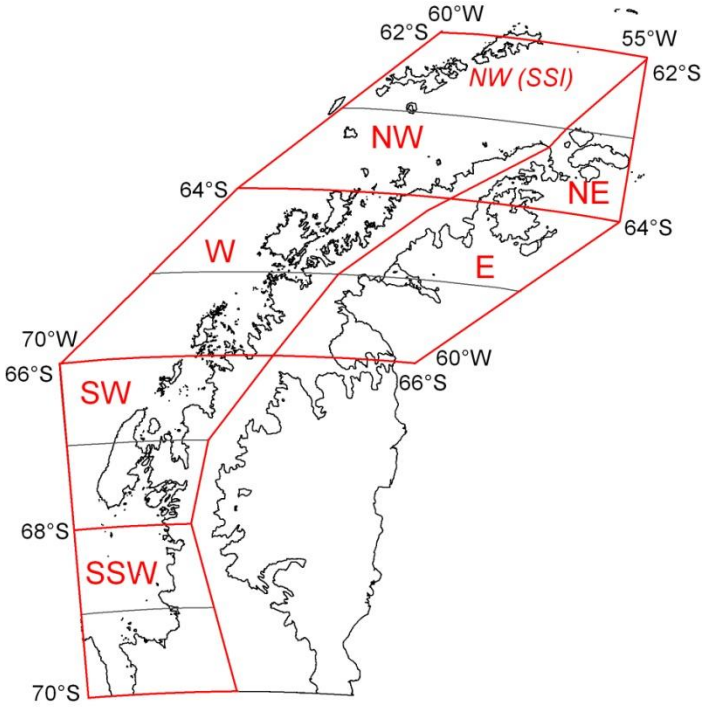

Figure 6.1: Region definitions.
The interior division is along the ice divide on the AP plateau. The area marked 'NW (SSI)' is the South Shetland Islands; meteorological records from this area are included in climate record analysis for the NW region.

6.2.1 Station and AWS temperature records

Summer temperatures on the AP are close to melting and so even small increases in temperature may have significant impacts (Vaughan 2006). Summer melt is known to alter the mass balance of the ice sheet, such as triggering flow acceleration (Barrand *et*

al., 2013b) and the retreat of ice shelves (e.g. Morris & Vaughan, 2003). Almost all small glaciers and ice caps on the AP experience melt every year and consequently, melt duration is a more suitable index for measuring changes than melt extent. Although there are no temperature records prior to the start of the study period (and therefore it is uncertain when changes began), there are meteorological records from as early as 1947 showing increases in melt duration throughout the AP.

A comprehensive dataset of all known air temperature records from both manned stations and Automatic Weather Stations (AWS) was compiled by Barrand *et al.* (2013b), who then used these records to calculate annual positive degree day (PDD) sums for each station. This follows the approach used by Vaughan (2006), in which the PDD sum for each austral melt season is the sum of the temperatures on days that the temperature is above 0 °C. The PDD sums ($ø_n$) for each station are used here to produce time series plots for each region, with linear fit lines where records are > 30 years in length (Figure 6.2). The AWS measurements that are for shorter time spans can provide a valuable addition to the time series plots for the periods that they are available. Since there are only two stations in the NW region on the mainland and both have very few records, the stations on the South Shetland Islands (SSI) have also been included. Although these stations are separated by the Bransfield Strait, they are within the same latitudinal band as defined by the NW region and are the closest stations to the north-west mainland. There are four stations on the AP mainland where the records are > 30 years in length and, of these, three show strongly positive and statistically significant increases in $ø_n$. In addition, two stations on the SSI have records > 30 years in length, one of which shows a significant positive trend in $ø_n$.

The stations with the strongest increases in $ø_n$ are on the eastern side of the AP: Esperanza, in the NE region, which has increased at 3.4 ± 1.24 K d per year since 1960, and Marambio in the E region, where the $ø_n$ has increased at 2.51 ± 1.25 K d per year since 1971 (Table 6.1). At Faraday/Vernadsky in the W region the trend has been less strong but also significant, at 1.38 ± 0.58 K d per year since 1947. The trend at Rothera in the SW region has been lower at 0.95 ± 1.34 K d per year since 1976, and is not statistically significant. It can also be observed that the trend line maximum and

minimum values are considerably higher at Esperanza than at any other station on the mainland, thereby showing the climate has been the warmest since the earliest records.

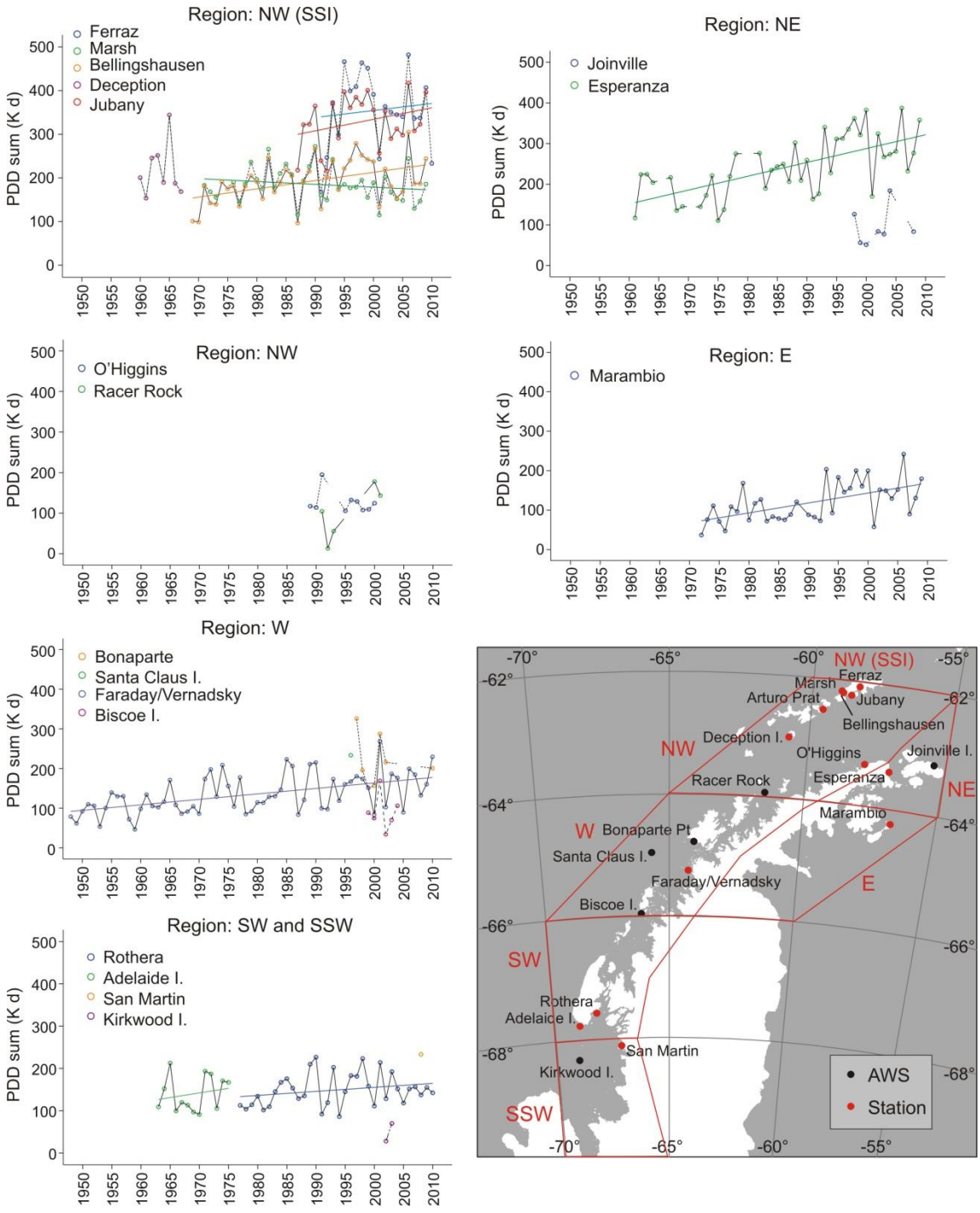

Figure 6.2: Station temperature records time series graphs
Positive Degree Day (PDD) Sums calculated for each station presented as time series graphs and with linear trend lines. Each graph represents one of the six regions and includes data from all stations within the region. Locations of manned stations and automatic weather stations (AWS)

on the AP are shown on the map. The South Shetland Islands (SSI) are included as additional station records near the NW region. The data records were compiled by Barrand *et al.* (2013b) and provided by the authors for the present study.

Table 6.1: Summary of temperature records obtained from Automatic Weather Stations and manned stations.
Stations labelled NW_SSI are located on the South Shetland Islands. The data records were compiled by Barrand *et al.* (2013b) and provided by the authors for the present study. The results are expressed as Positive Degree Days ($ø_n$) and linear trends (along with significance level, Sig.) and have been calculated only for long-term records, defined as >30 years in length. Uncertainties in the trends are quoted at the 95% confidence level.

Station	Region	Lat	Long	Earliest record	Latest record	n (years)	Mean $ø_n$	$ø_n$ trend (K d a^{-1})	Sig.	Linear Min $ø_n$	Linear Max $ø_n$
Joinville I.	NE	-63.18	-55.4	1997	2008	7	95				
Esperanza	NE	-63.4	-56.98	1960	2009	42	243	3.40 ± 1.24	0.00	155	322
Marambio	E	-64.23	-56.72	1971	2009	37	120	2.51 ± 1.25	0.00	73	166
Larsen Ice Shelf	SE	-67.02	-61.52	1986	2010	8	60				
O'Higgins	NW	-63.32	-56.68	1988	2000	9	126				
Racer Rock	NW	-64.07	-61.61	1990	2001	5	99				
Ferraz	NW_SSI	-62.08	-58.38	1986	2010	20	355			340	370
Marsh	NW_SSI	-62.18	-58.98	1970	2009	37	185	-0.65 ± 1.15	0.26	173	198
Bellingshausen	NW_SSI	-62.2	-58.93	1968	2009	41	192	1.90 ± 1.16	0.00	154	230
Arturo Prat	NW_SSI	-62.5	-58.68	1983	2003	16	226				
Deception I.	NW_SSI	-63	-60.7	1959	1967	8	218				
Jubany	NW_SSI	-62.23	-58.63	1985	2009	23	329			300	361
Bonaparte Point	W	-64.78	-64.07	1992	2010	7	219				
Santa Claus I.	W	-64.96	-65.67	1995	2000	1	234				
Faraday/Vernad	W	-65.25	-64.27	1947	2010	63	135	1.38 ± 0.58	0.00	92	177
Biscoe I.	W	-66	-66.13	1998	2004	6	91				
Rothera	SW	-67.57	-68.52	1976	2010	34	149	0.95 ± 1.34	0.16	133	165
Adelaide I.	SW	-67.8	-68.9	1962	1975	13	140			127	153
Dismal I.	SSW	-68.09	-68.83	2001	2003	2	110				
San Martin	SSW	-68.12	-67.13	2007	2008	1	233				
Kirkwood I.	SSW	-68.34	-69.01	2001	2003	2	49				

The increase in duration of melting conditions at Faraday/Vernadsky has been sufficient to raise the PDD sum in 2010 (177 K d per year) to above that at Rothera (165 K d per year). The PDD sums for stations in the South Shetland Islands have been greater throughout the duration of the records than most stations on the AP, with the exception

of Marsh, which has shown lower mean values and a weak, insignificant negative trend since 1970.

The climate systems observed in each region are distinct, and the SSI and the NE region of the AP have considerably warmer climates than all other regions. The W region (represented by the station records at Faraday/Vernadsky) is warming at a more rapid rate than at Rothera in the SW region, but there are too few records available in the NW to draw conclusions about changes in melt duration in this region. If glacier frontal change is closely related to trends in long-term air temperatures, glaciers in the NE region would have retreated since 1960 at a faster rate than in any other region, as both the mean PDD sum and the rate of increase are the highest. The glacier retreat rates in the NE have indeed been in retreat since the earliest records, but glaciers in the cooler neighbouring E region, have shown a considerably larger magnitude of retreat.

By the same reasoning for the west coast, glaciers in the W region should be retreating at a faster rate than those to the south, where the PDD mean and rate of increase is lower. What is observed however is that retreat rates are in fact greater in the two more southerly regions (i.e. SW and SSW), than those in the W and NW regions. It is not possible to draw firm conclusions from only a few stations with air temperature records, especially since the NW region is distinctly lacking in station records, so other data should be used to assess the hypothesis.

6.2.2 Spatial patterns of melt 2000-09

Melt extent and duration, detected from satellite data such as scatterometer data onboard the QuikSCAT (QSCAT) satellite, can be used for interpreting spatial differences in air temperature in recent years. Changes in melt onset and duration are crucial indicators of atmospheric change and although surface snowmelt is not directly proportional to air temperature, there are significant correlations in Antarctica between melting anomalies and anomalies in the Southern Annular Mode (SAM) and the Southern Oscillation Index from 1979 – 2009 (Tedesco & Monaghan, 2009). Barrand *et al.* (2013b) found that summer melt on the AP is linked to regional-scale atmospheric variability, by correlating melt season onset and extent using the November near-surface air temperatures, with the

Oct-Jan averaged index of SAM. The QSCAT data used by Barrand *et al.* (2013b) is at a high resolution (2.225 km) for the past 10 years, and gives a synoptic view of summer climate variability far from climate stations and AWS sites. The principles and methods of scatterometer data analysis are described in detail in Barrand *et al.* (2013b) but in summary, there is a significant reduction in microwave backscatter caused by the presence of liquid water in near-surface snow and firn layers. The SeaWinds scatterometer onboard QSCAT observed the polar regions several times a day between June 1999 and November 2009, from which daily melt trends were derived. Melt was defined on a pixel-by-pixel basis, based on the absolute difference in backscatter magnitude between 'wet' snowpack conditions and a 'dry' reference state during austral winter (Barrand *et al.*, 2013b). Linear regression between melt days identified from QSCAT pixels and positive air temperature days from all station records on the AP confirms the relationship. Since summer melt occurs in almost all regions on the AP, the melt duration is regarded as a crucial index and has a strong correlation with annual PDD melting totals. The very high spatial resolution (2.225 km) of QSCAT data is a valuable resource for analysing both regional and local climate variability.

A broad overview of Mean Melt Duration (MMD) between 2000 and 2009 is that the north-west coast shows a higher number of melt days than the south-west coast (Figure 6.3). The melt duration is minimal on the high plateau, with a rapid increase in number of melt days towards the coast. The north-eastern side of the AP shows a medium to high MMD, but the longest melt durations occur along the west coast mainland north of 64.5° S, on Anvers Island (64.5 °S), and the west coast between 65° S and 66.5° S. However, this summary is not a true indication of mean melt duration close to glacier fronts. The 860 marine-terminating glaciers on the AP are of such a wide range in size that the decision was made to calculate the MMD within 5 km (upstream) of the glacier front. Melt patterns between the lower and upper reaches of large glacier basins can significantly differ, but the melt values at lower elevations and close to the front will be those that have most control on ice front behaviour. The 5 km buffer also ensures a consistent measurement for glaciers of all sizes. By attributing the MMD values to individual glaciers, spatial patterns in relation to glacier-front changes can be more accurately determined.

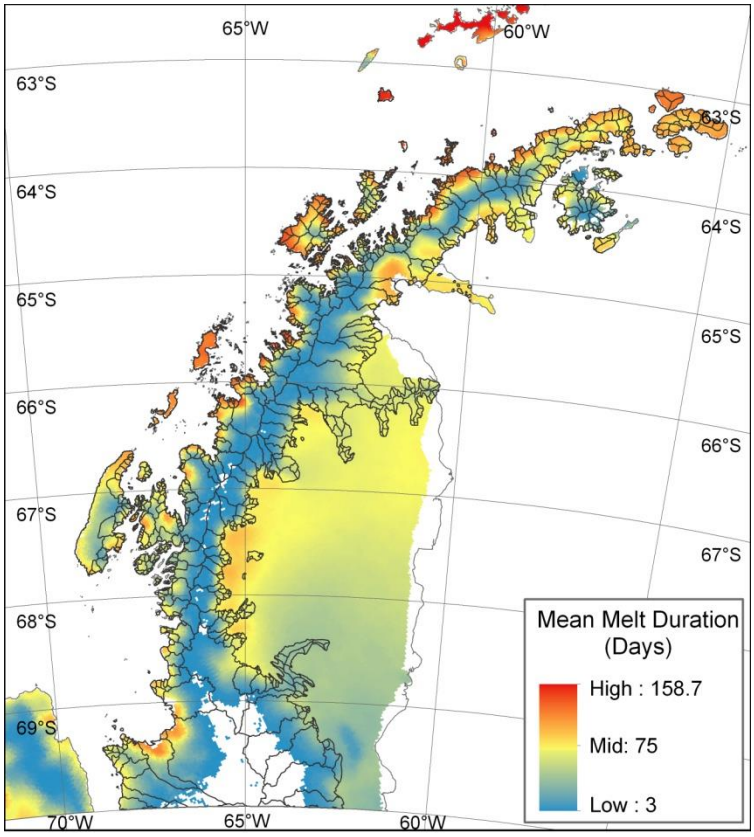

Figure 6.3: Annual Mean Melt Duration (in days) between 2000 and 2009.
Plotted from data published in Barrand *et al.* (2013b) and provided by the authors for the present study.

A scatter diagram of MMD for all glaciers by degrees latitude and east/west illustrates a wide dispersion in melt durations (Figure 6.4), but there are two distinct north-south patterns: a high-low gradient between glacier MMDs from the northern tip to ~65° S in both the east and west, and a second high-low gradient from 66 to 68° S in the west. The mean regional values are summarised in Figure 6.5 which indicates an overall reduction in MMD on glaciers towards the south with a small increase south of 68° S. The PDD measurements have a linear relationship with glacier surface melt patterns (Barrand *et al.*, 2013b), therefore the regional summary for recent melt duration close to glacier fronts can be regarded as reliable. However, this spatial distribution is only applicable to the years 2000-09, which limits analysis associated with long-term glacier-front trends.

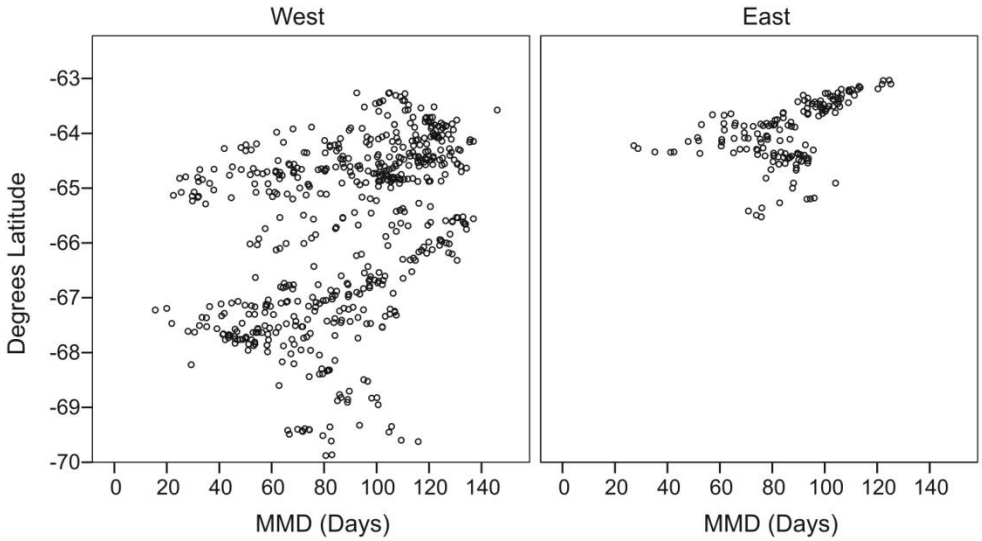

Figure 6.4: Mean Melt Duration (MMD) close to glacier fronts, by degree latitude.
Each point is the mean MMD value per glacier (within 5 km of its front) during the interval 2000-09. The values were calculated from the MMD gridded data published in Barrand *et al.* (2013b).

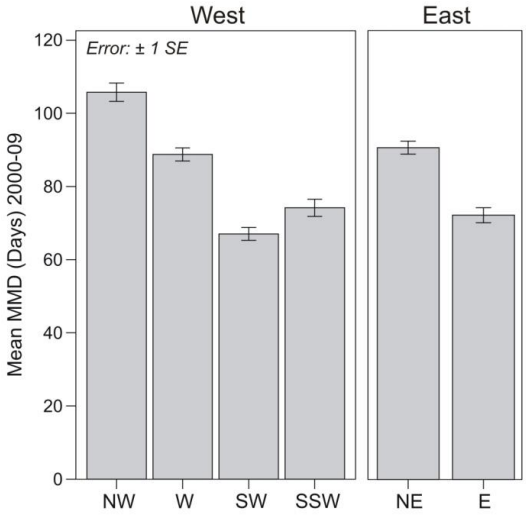

Figure 6.5: Mean Melt Duration (MMD) between 2000 and 2009, by region.
Mean values within 5 km upstream of the glacier fronts, by region (region definitions in Figure 6.1). The values were calculated from the MMD gridded data published in Barrand *et al.* (2013b).

6.2.3 Surface temperatures from AVHRR imagery, 1980-2008

6.2.3.1 Surface temperature data

Air temperature station records are sparsely distributed and melt duration data do not exist prior to 2000, but surface temperatures interpreted from infrared satellite imagery are a further resource for identifying spatial and temporal climate patterns on the AP. Mean surface temperatures show both local and regional differences in climate and therefore can be used to identify the strength of the relationship between temperature and glacier front change across the whole region. Comiso (2000) processed infrared data from the Advanced Very High Resolution Radiometer (AVHRR) for the period 1982-1998, and combined these with data from the Temperature Humidity Infrared Radiometer (THIR) for the period 1979-1985, resulting in surface temperature maps of Antarctica at annual and monthly intervals. The accuracy of surface temperatures derived from infrared imagery with temperature data from 21 stations across Antarctica were evaluated and a strong correlation was found between the two ($r^2 = 0.98$, St Dev 3 °C) (Comiso, 2000). In terms of trend analysis, he found that a 20-year record length is about the minimum length required for a trend analysis study, and reported that inter-annual fluctuations of the temperatures on the ice sheet are large (-0.177 to 0.094 °C a^{-1}). The THIR data was processed at a grid cell size of 25 km, while the AVHRR data have a grid cell size of 6.25 km. The two datasets when combined have resulted in grids at 12.5 km cell size.

Since the study was completed in 2000, J. Comiso (NASA) has updated the dataset to 2008. These data were further processed by P. Holland (British Antarctic Survey) to produce a grid of the mean surface temperature for the entire period for which there is data (1980-2008). Mean temperatures were calculated per season, defined as January-March (JFM), April-June (AMJ), July-September (JAS) and October-December (OND), across this time period. For the purpose of analysing the temperature trends in relation to the long-term glacier changes, pentadal mean grids were created for both mean and seasonal temperatures, at the same intervals as used for the glacier front analysis, beginning in 1980. These data were provided with permission from J. Comiso and P. Holland for the present study.

6.2.3.2 Surface temperature spatial patterns

The grids are at a resolution of 12.5 km, which are considerably coarser than the 2.225 km Mean Melt Duration grid. Even so, they are valuable resources with temperature data back to 1980, from which much spatial and temporal information can be extracted. The overview map (Figure 6.6) of mean annual surface temperature between 1980 and 2008 shows a distinct spatial pattern: the warmest areas are north of 64° S (plus James Ross Island at ~64.5° S in the east), and close to the mainland coast and neighbouring islands to ~65° S in the west. The eastern side of the AP south of ~64.5° S is considerably cooler than the western side and the air temperatures decrease towards the southern interior region. Seasonal mean temperatures (Figure 6.7) are greatest in the northern tip of the AP and along the north-west coast to Anvers Island. The contrast between the north-west and the rest of the AP is more pronounced during the winter months.

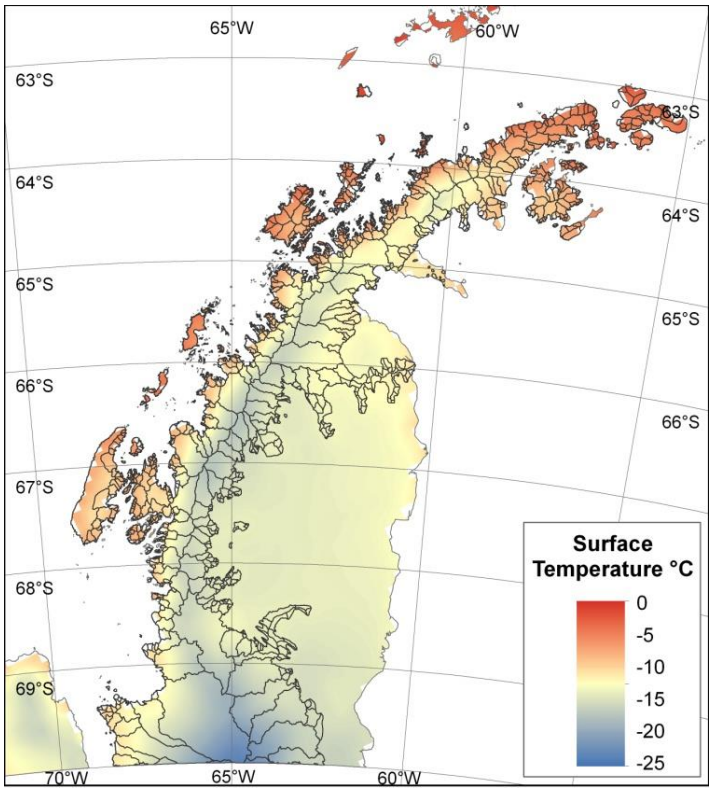

Figure 6.6: Mean Annual Surface Temperatures 1980-2008.
Plotted from data provided by J. Comiso (NASA). The data was processed from infrared imagery from the Advanced Very High Resolution Radiometer (AVHRR) and Temperature Humidity Infrared Radiometer (THIR). The first edition of the data (1980-1998) was published in Comiso (2000).

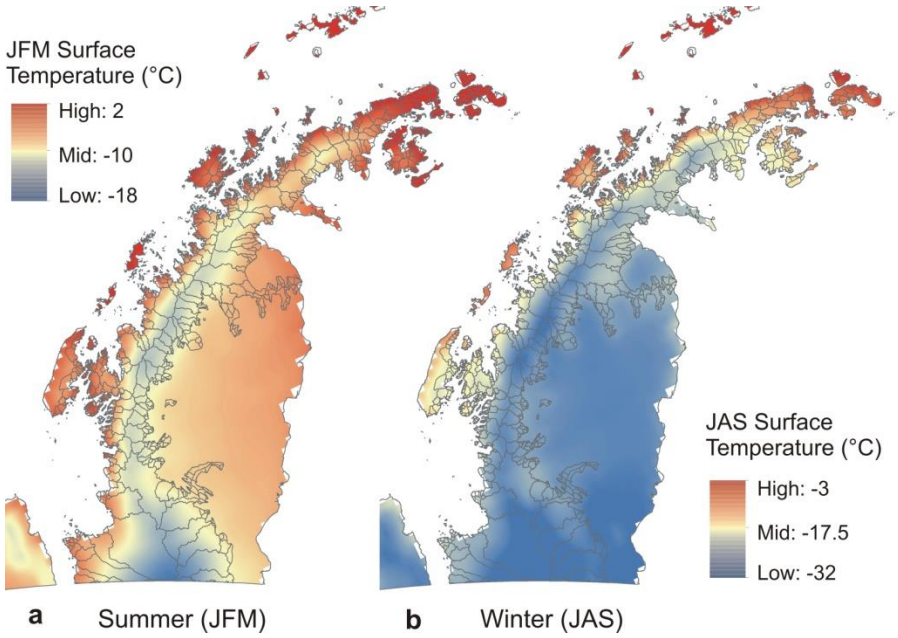

Figure 6.7: Seasonal average surface temperatures 1980-2008 (°C).
Austral summer months (**a**) are defined here as January-March (JFM) and winter (**b**) July-September (JAS). The mean values were calculated from data provided by J. Comiso (NASA).

As discussed in the previous section, surface temperatures across a large glacier basin strongly differ between its interior and close to its front. Using the same approach as for the mean melt duration dataset, the mean surface temperatures that lie within 5 km of each glacier front were attributed to the marine-terminating glaciers. Due to the relatively low resolution of the grids, a single grid cell occasionally contained the centre point of more than one glacier; in such cases the same grid value was attributed to both glaciers. Where larger glaciers included both whole and partial cells, the partial cell values were also included in the mean values. This was done by upsampling the grid to a higher resolution (2.5 km), converting the values to point data and spatially joining the values of these points to the glaciers, based on the mean values of all points within 5 km of the glacier front.

Mean annual surface temperatures close to the glacier fronts have a latitudinal gradient on both the east and west sides of the AP (Figure 6.8), i.e. temperatures become cooler towards the south. This correlation is particularly strong on the eastern side, both annually and during the summer and winter. On the west coast, the correlation is stronger and more significant during the winter than in the summer. When the mean annual temperature between 2000 and 2008 is considered alongside the MMD data (2000-09),

there is a reasonable trend ($r^2 = 0.413$) along the west coast, but no trend ($r^2 = 0.115$) on the east coast.

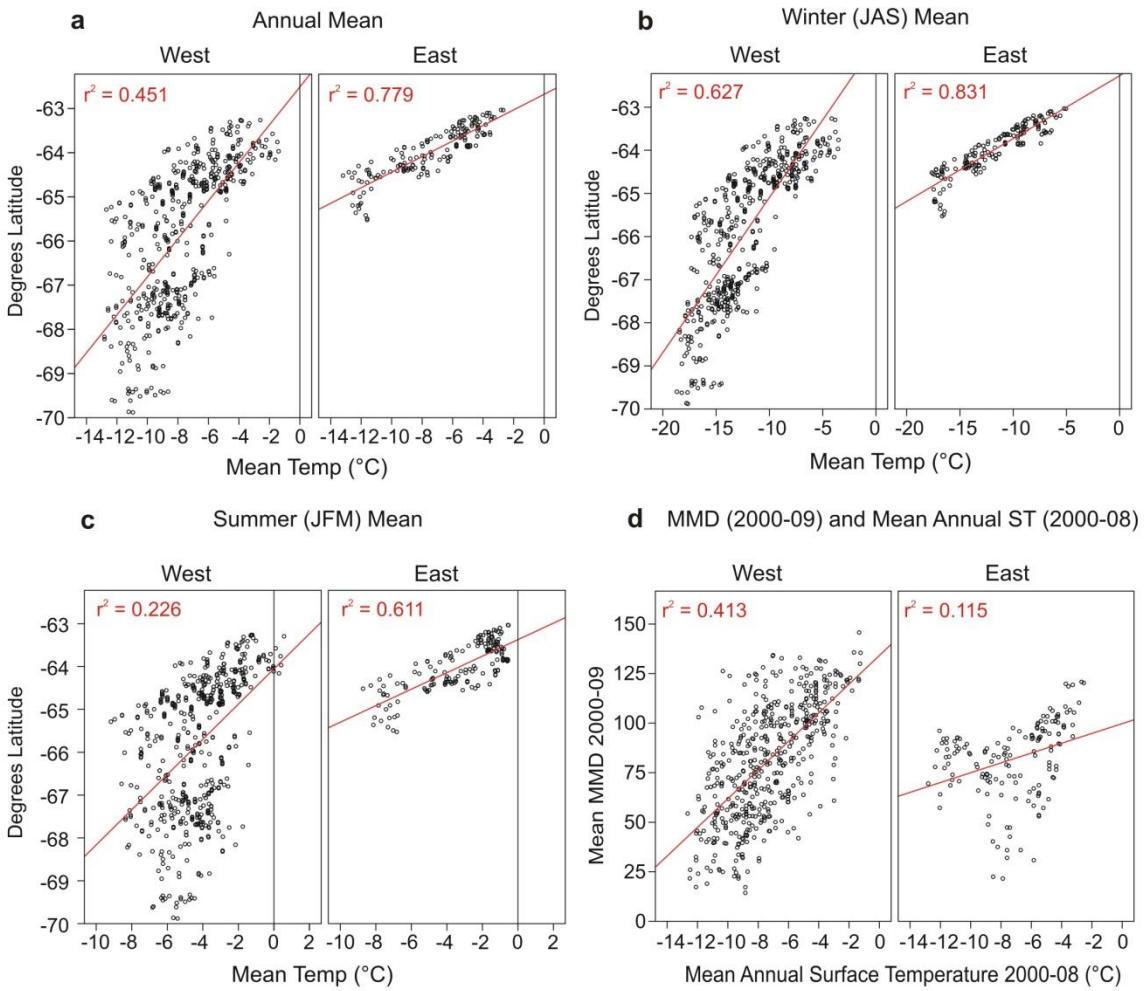

Figure 6.8: Surface temperatures by degrees latitude, for annual (**a**), winter (**b**) and summer (**c**) means between 1980 and 2008.
The mean values were calculated from processed infrared satellite imagery provided by J. Comiso (NASA). Each point represents a glacier, and the value is the mean surface temperature within 5 km of the glacier front. Panel **d** shows the correlation between Mean Annual Surface Temperature in 2000-08 and Mean Melt Duration (MMD) 2000-09.

The relatively weak correlations with MMD values highlight the limitations of the mean surface temperature data, since they do not provide information on how much surface melt takes place. The original data for surface temperatures are available as monthly mean values, whereas mean melt duration data in 2000-09 is measured in days. Nevertheless, the mean surface temperatures show distinct regional patterns of air temperature and the variances will have had an impact on rates of glacier surface melt

and calving. Regional mean surface temperatures within 5 km of glacier fronts (Figure 6.9) show the trend from north to south in decreasing temperatures in both annual and seasonal mean temperatures.

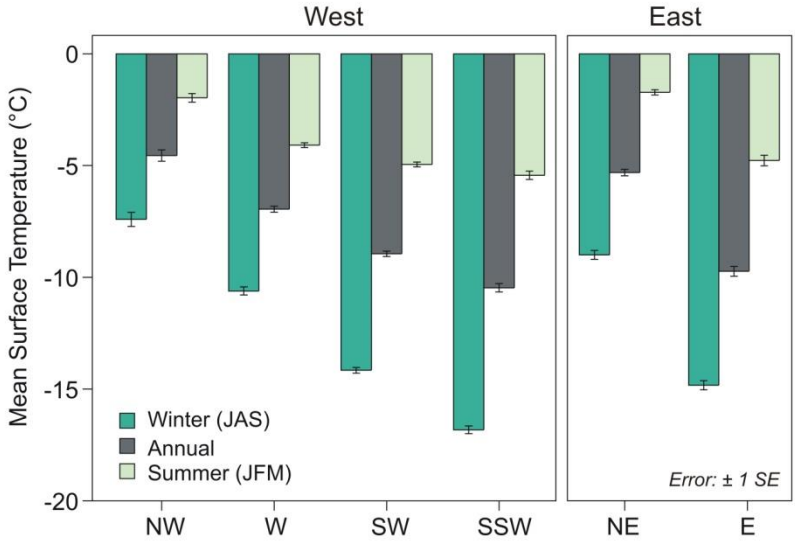

Figure 6.9: Mean Surface Temperatures (1980-2008) within 5 km of glacier fronts, by region. Region definitions are in Figure 6.1. The mean values were calculated from processed infrared satellite imagery provided by J. Comiso (NASA).

6.2.3.3 Surface temperature temporal patterns

The mean annual surface temperatures over 5-yearly intervals have been calculated and illustrated as anomalies from the mean annual values (1980-2008) (Figure 6.10). There are a number of temporal trends observed:

- From the earliest to the latest records, peninsula-wide warming has occurred
- Prior to 1995-99 temperatures were generally cooler than the mean, with coolest temperatures occurring along the west coast in 1980-84
- A large contrast in surface temperatures from cooler to warmer than average occurred between 1990-94 and 1995-99.
- 1995-99 was a particularly warm period throughout the AP, with perhaps the greatest difference from the mean along the north-west coast
- In 2000-04 temperatures cooled slightly, although still above the mean, before a further increase in 2005-08.

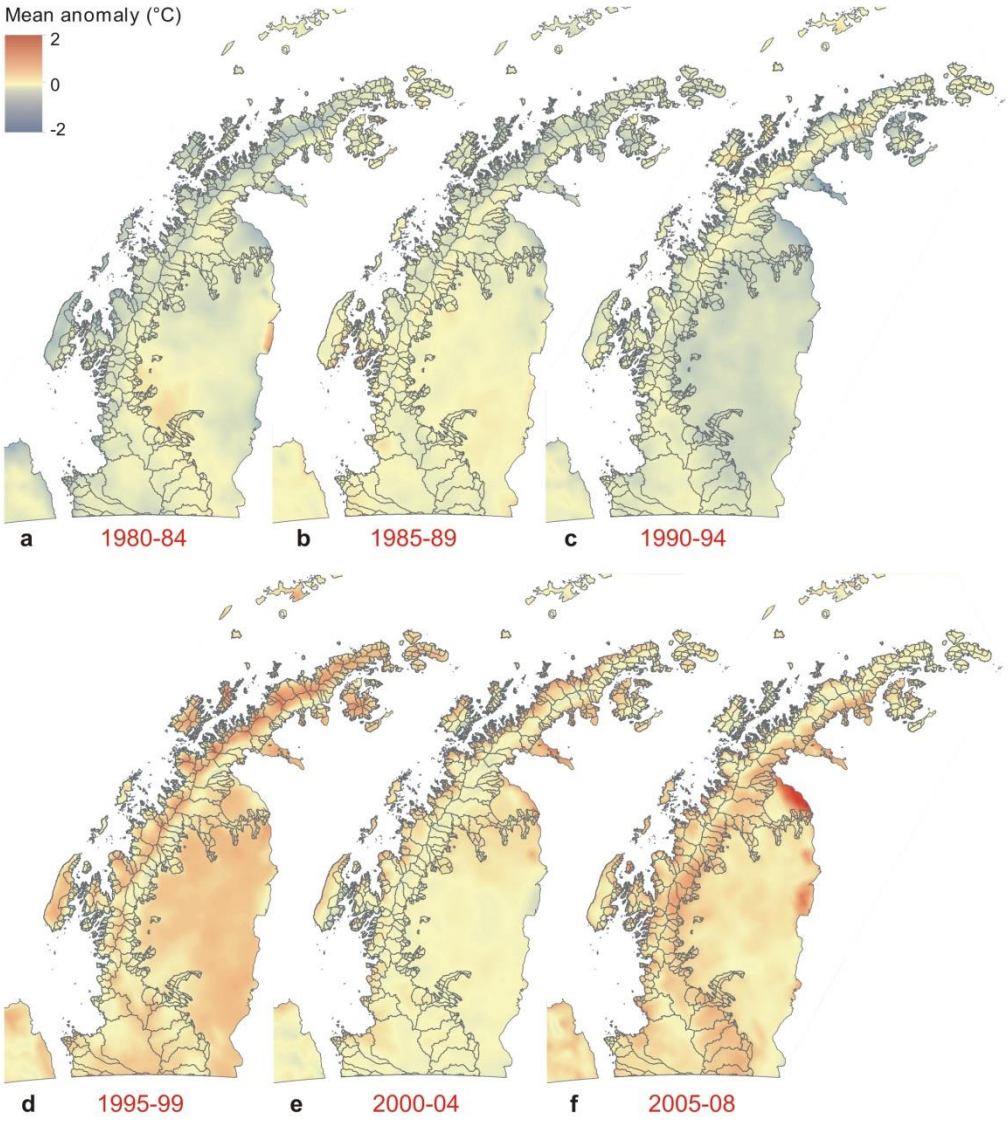

Figure 6.10: Surface temperature anomalies, 1980-2008.
Anomalies are from the mean annual surface temperature (1980-2008), in pentadal intervals. The plots were produced from processed infrared satellite imagery provided by J. Comiso (NASA).

Although these plots illustrate changes in the AP as a whole, the surface temperatures close to glacier fronts may not reveal the same trend. The mean surface temperatures within 5 km of every glacier front are calculated since 1980 and are summarised as regional mean values over time (Figure 6.11). The difference in temperatures between north and south is clear, although the E region is distinctly cooler than W at the same latitude. Most regions follow a synchronous temporal trend: a slight overall decrease in

air temperature from 1980-84 to 1990-94, followed by a marked increase in all mean annual temperatures between 1990-94 and 2005-08 (although regions in the NW, NE and E level out by 2000-04). Regarding summer air temperatures, the NW and NE follow the same trend (a gradual increase and a dip in 2000-04), whereas other regions show overall increase but greater variability.

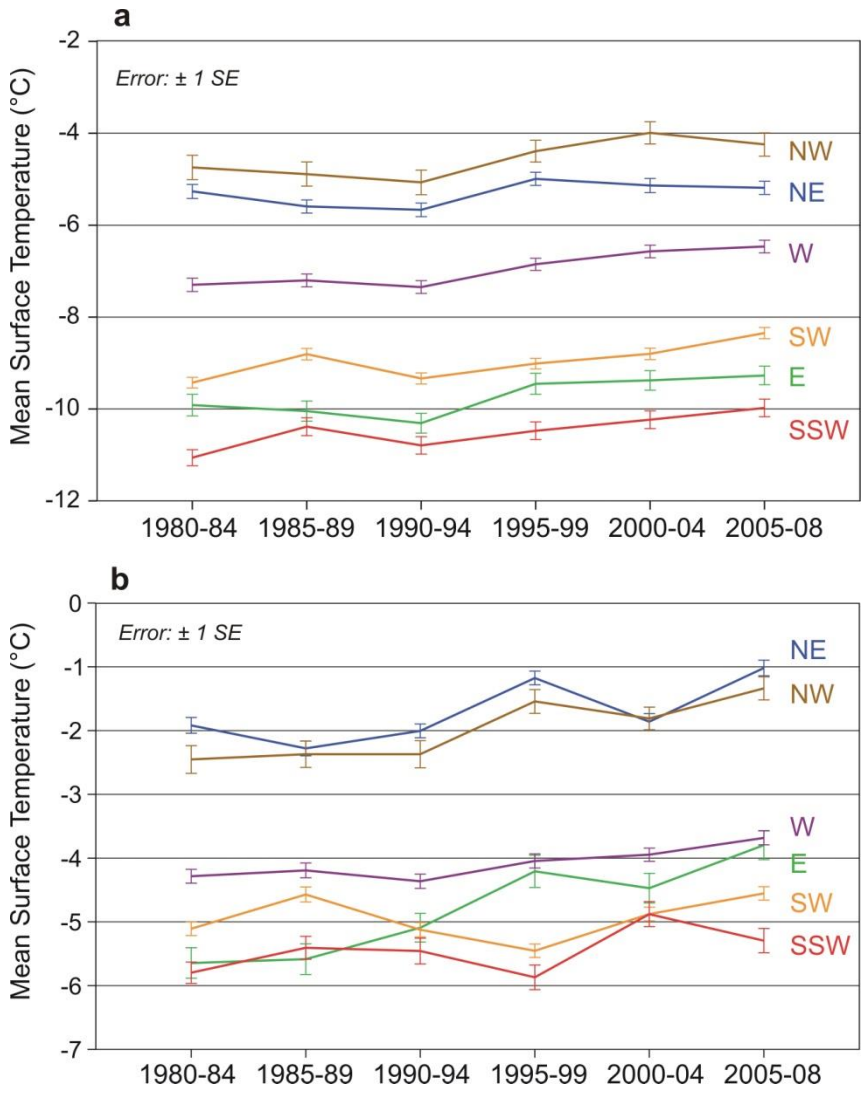

Figure 6.11: Mean surface temperatures (ST) by Region, in pentadal intervals.
Mean values are within 5 km of glacier fronts. Panel **a** is mean annual ST, and panel **b** is mean summer (JFM) ST.

6.2.4 Surface Mass Balance from modelled data, 1979 – 2010

A new surface mass balance (SMB) map of Antarctica was released in 2012, based on output from a regional atmospheric climate model (Lenaerts *et al.*, 2012). This model was run using reanalysis data from the European Centre for Medium-Range Weather Forecasts (ECMWF) ERA-Interim data, between 1979 and 2010. The calculated SMB (mm w.e. y^{-1}) includes precipitation, surface sublimation, meltwater runoff and processes of drifting snow. This recent regional atmospheric climate model (RACMO2.1/ANT) is regarded as the most capable of simulating the near-surface temperature and wind climate of Antarctica (Lenaerts *et al.*, 2012). The model, at 27 km resolution, confirms high accumulation zones in the west AP and is in good agreement with *in-situ* SMB measurements.

The resolution of the model means it is unsuitable for assigning grid values to individual glacier basins, but regionally, it provides a further valuable dataset for assessing atmospheric patterns across the AP. Wide-scale temporal differences can be analysed for any significant trends over time. As outlined in Chapter 2 (Section 2.3.1.4), it is well understood that the western side of the AP has significantly more accumulation than the east, with values in excess of 5000 mm y^{-1} in places (van den Broeke *et al.*, 2006). This is primarily because the orography forces westerly air masses to rise, leading to adiabatic cooling and precipitation over the up-wind slope (Miles *et al.*, 2008). In addition, the AP acts as a barrier, separating maritime air in the west from colder, continental air masses in the east. There is evidence, based on ice core measurements in the far south AP, that there has been a doubling of snow accumulation since the 1850s, with acceleration occurring in recent decades (Thomas *et al.*, 2008).

The RACMO2.1 SMB data, in monthly intervals between 1979 and 2010, was provided for the present study by J. Lenaerts (Utrecht University). From these, the SMB (mm w.e.) for each year, and the mean annual SMB based on all years were produced. Data from the period 1980-2009 were used for this study in keeping with the minimum-maximum years in the pentadal analyses. Regardless of the coarse grid resolution, the distinct differences in mean annual SMB between the east and west sides can be seen (Figure 6.12). There is no strong latitudinal trend, however, with high SMB values irregularly

distributed between 64° and ~67° S. North of 64° S and on the west coast south of 67° S the SMB is lower, but the lowest SMB is found along the eastern AP.

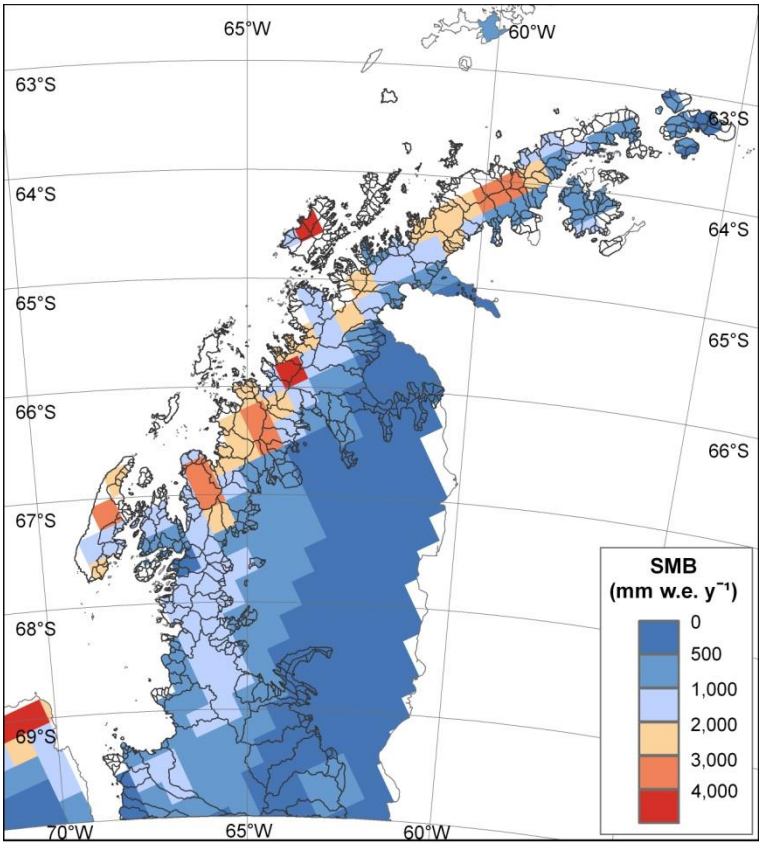

Figure 6.12: Mean annual surface mass balance (SMB) between 1980 and 2009. Mean values are in mm w.e. y^{-1}, as simulated by RACMO2.1 (Lenaerts *et al.*, 2012). The modelled data were provided for this study by J. Lenaerts (Utrecht University).

The mean SMB map of the Antarctic Ice Sheet in Lenaerts *et al.* (2012) showed that the highest accumulation zones in Antarctica are along the western AP, with high accumulation also occurring along much of the coastal region of West Antarctica. In their study, no significant trend was found in the SMB, but a number of regional trends were observed, including a positive but insignificant trend on the western side of the AP. When the mean annual SMB data were analysed for the present study, the variation in the SMB from 1980-2009 was found to be considerable. The data were averaged into pentadal intervals and anomalies from the mean illustrate this variability (Figure 6.13). The differences from the earliest to latest data measurements suggest a small increase in accumulation in the north-west and a decrease for most of the rest of the AP. This is a misleading conclusion however due to the variation in SMB that takes place over time.

On a peninsula-wide scale, the periods 1985-89 and 1995-99 had considerably greater accumulation than in 1980-84, 1990-94 and 2005-09. There are no distinct regional differences in SMB over time.

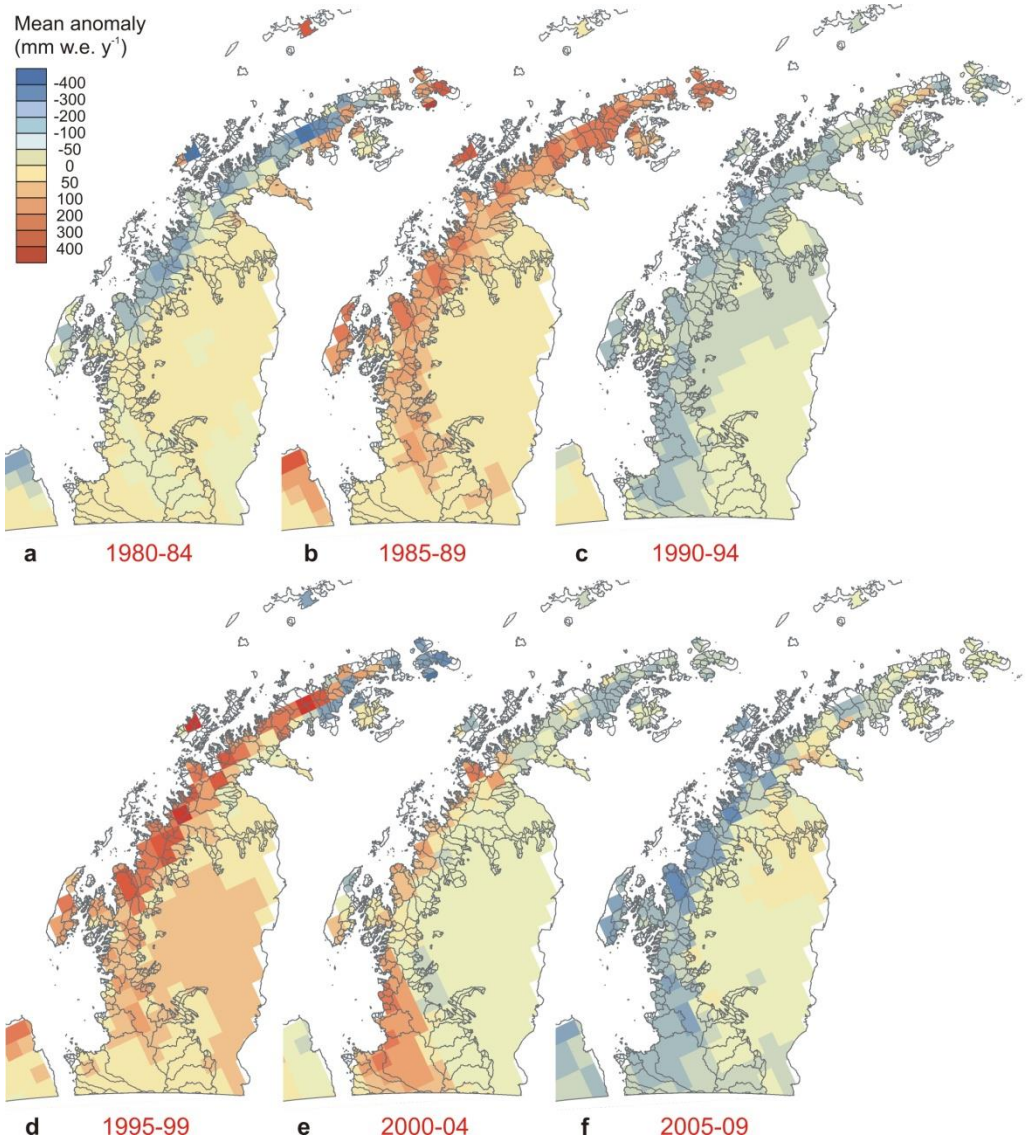

Figure 6.13: Mean pentadal surface mass balance anomalies from the mean (1980-2009). Values are in mm w.e. y^{-1}. The plots were produced from RACMO2.1 modelled data (Lenaerts *et al.*, 2012).

6.2.5 Surface temperature and mass balance patterns

Mean annual surface temperatures between 1980 and 2009 are greatest between 63° S and 64.5° S, continuing along the north-west coast to ~65° S (Figure 6.6). Temperatures are correlated with latitude: there is a distinct decrease in surface temperatures from north to south, on both sides of the AP. Mean surface mass balance over the same period shows a distinct difference between east and west, with significantly higher SMB in the west (Figure 6.12). There is no north-south gradient, but on the western side the SMB is lower south of ~67.5° S than to the north. In general, there is a positive correlation between mean SMB and air temperatures, apart from the region north of 64° S (both in the east and west), which has high surface temperatures and low SMB.

When peninsula-wide temporal SMB anomalies (Figure 6.13) are compared alongside surface temperature anomalies (Figure 6.10), there is no universal correlation between the two factors between all pentadal intervals. However, observations include the following:

- During the intervals 1980-84, 1990-94 and 1995-99, there was a positive correlation between SMB and surface temperature anomalies: SMB and temperature were both low in 1980-84 and 1990-94, whereas both factors were high during 1995-99. The SMB increase across most of the AP in 1995-99 suggests that this must have been a time of particularly high precipitation, counteracting the high surface melt. With the same reasoning 1980-84 and 1990-94 must have been particularly dry periods.

- Surface temperature and SMB during intervals 1985-89 and 2005-09 have an inverse correlation. High SMB and low surface temperatures in 1985-89 suggest that surface lowering through melt was less than than surface gain through precipitation. Low SMB and high surface temperatures in 2005-09 suggest greater melt than precipitation.

- There are no distinct regional correlations between SMB anomalies from the mean and surface temperature anomalies from the mean.

6.3 Ocean temperature patterns

Ocean-driven ice-shelf thinning through basal melting is now a well-recognised mechanism in driving ice shelf retreat (discussed in Chapter 2, Section 2.2.3). Recent results by Rignot *et al.* (2013) strengthened the theory that ice shelf melting is particularly high close to grounding lines. One example is unstable retreat now underway in West Antarctica, where a model indicates that Thwaites Glacier may be in the early stages of collapse (Joughin *et al.*, 2014). In total, six glaciers in the West Antarctic region are now known to be undergoing sustained retreat (Rignot *et al.*, 2014) and it is recognised that warming oceans have been a key trigger in these events.

In the AP region, glaciers and ice shelves in the west are influenced by warm intrusions of Upper Circumpolar Deep Water currents and those in the east by Modified Weddell Deep Waters. Ice shelves in the region are highly sensitive to relatively modest forcing at their boundaries, with mass balance affected by basal melt, formation of basal marine-ice and tidal influence on melt (Holland *et al.*, 2009; King *et al.*, 2011a; Mueller *et al.*, 2012). Fast surface lowering has occurred close to the fronts of George VI, Wilkins and Stange ice shelves (situated on the west coast, 70° - 74° S), and it was proposed that this was likely caused by warming upper-ocean temperatures near the ice fronts (Fricker & Padman, 2012).

The sensitivity of glaciers to ocean warming in Antarctica has only been studied in relation to large glaciers with floating tongues, or ice shelves. The impact of warming oceans on small glaciers around the Antarctic periphery is less well understood. With 860 glaciers surrounding the AP, all of which terminate at the ocean edge, it is of key importance to assess the impact of the ocean temperatures on these ice fronts. There is now a wealth of information on ocean temperatures held in the World Oceanographic Database (WOD), made available by the NOAA National Oceanographic Data Center (NODC). These data have yet to be analysed in relation to coastal change surrounding the AP. Here, the spatial and temporal trends in ocean temperatures are quantified, with a view to assessing alongside glacier-changes in the following chapter.

6.3.1 Ocean temperature data

Until the advent of satellite imagery in the 1970s/80s, ocean temperature data were sparse across large areas of the Southern Ocean and some challenges to obtain subsurface temperature data, particularly below winter sea-ice, still remain. Despite these challenges, there is evidence of large scale changes in the Southern Ocean including a strong warming of the waters in the Antarctic Circumpolar Current; a warming of the Antarctic Bottom Water exported to the South Atlantic and a rapid ocean warming of the upper layers of the ocean adjacent to the western AP (Meredith & King, 2005).

Ocean measurements collated by the NODC are taken from a variety of samplers, sensors and platforms, such as drifting buoys, subsurface floats, current profilers, echo sounders and animal-borne instruments. Over the last decade, several hundred seals have been equipped with conductivity-temperature-depth sensors in the Southern Ocean, filling a substantial observational gap in regions that are difficult to access by ship (Roquet *et al.*, 2013). The majority of loggers were deployed on Elephant seals and, on average, profiles are 500 m deep, although some seals occasionally reach 2000 m or more (Roquet *et al.*, 2013). A calibrated collection of seal-derived hydrographic data makes up a significant proportion of measurements in the latest version of the WOD.

For the present study, ocean temperature data were downloaded from the WOD by P. Holland (British Antarctic Survey), who provided temperature measurements at various depths for the region surrounding the AP. For wide-scale regional analysis these data were then constrained to within 100 km of the AP coast and split into two-degree latitudinal bands and east/west, in keeping with delineations used in the climate data analysis. The offshore distance of 100 km was chosen as this is approximately the edge of the continental shelf, whilst maintaining consistency relative to the coastline. The extensive nature of the ocean temperature database meant that it was necessary to constrain measurements to particular depths. Therefore, measurements were extracted at depths considered to represent the range of bathymetry across the region. Measuring the potential influence of ocean temperatures on glacier frontal behaviour first involves assessing the bathymetry close to the glacier fronts. Clearly, if the ocean is consistently shallow close to the ice fronts the deeper ocean temperatures will have little impact. The

mean depths near the glacier fronts give an idea of the depths at which the ocean temperature measurements should be considered.

6.3.2 Bathymetry data

6.3.2.1 Wide-scale regional bathymetry

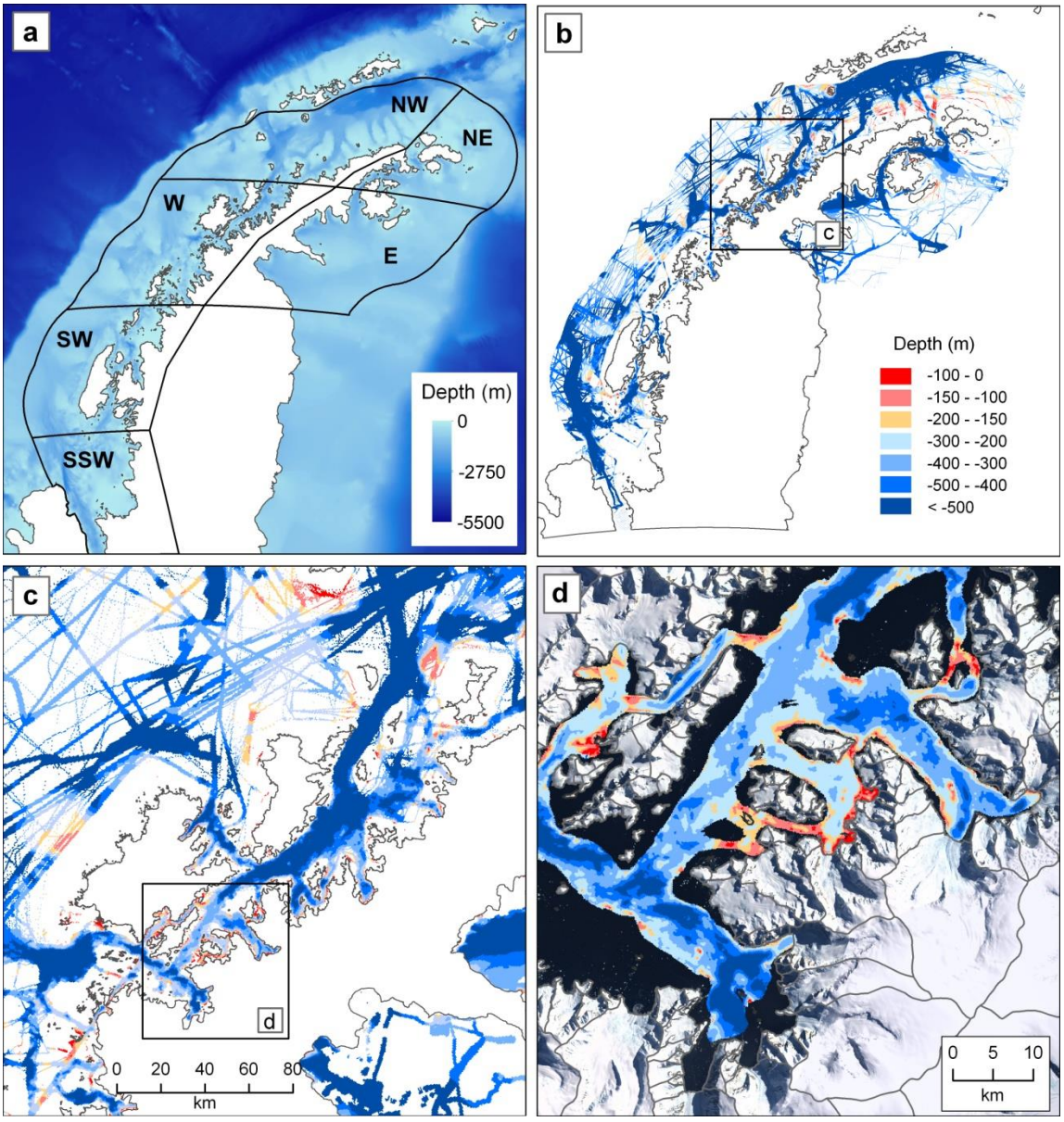

Figure 6.14: IBCSO bathymetry data.
The interpolated grid is at 500 m, shown here alongside regional outlines (**a**). Non-interpolated data were clipped to the regional outlines and depths were binned (**b**). Waters reach a depth of more than 500 m along much of the AP coastline, although there is a region of shallower water

off the north-west coast. Some deep troughs occur close to the shore, such as between islands and the mainland (**c**), and where ship tracks reach close to glacier fronts, many reach depths of up to 500 m or more (**d**). The depth scale in (**b**) also applies to (**c**) and (**d**).

The most up-to-date bathymetry data are from the International Bathymetric Chart of the Southern Ocean (IBCSO) data source, released in 2013 (Arndt *et al.*, 2013). This map was compiled from a combination of Multibeam and Singlebeam Radar tracks obtained from a number of research vessels, plus other data sources including Nautical Charts, Steering-points and BEDMAP2. The remaining areas have interpolated data. The data in grid format has a resolution of 500 m (Figure 6.14a).

The bathymetry surrounding the AP shows the edge of the continental shelf to the west to be approximately 100 km offshore. On the shelf, the sea bed is strewn with troughs deeper than 500 m, most of which are perpendicular to the coast. The largest trough is in Bransfield Strait to the east of the South Shetland Islands, which is up to 70 km wide and up to 500 km long. There are two deep narrow troughs visible to the north and east of Anvers and Brabant Islands, and one to the south-east of Adelaide Island. The region in the far north-west of the AP has shallow water from the coast up to ~50 km offshore, on what looks to be a shelf: many of the tracks show the water to be shallower than 100 m. There are several deeper troughs however that intersect this shelf enabling deep water from the Bransfield Strait deep trough to be channelled towards the coast.

6.3.2.2 Bathymetry close to the coastline

The IBCSO grid contains a reasonable coverage of measurements but there are also large regions that have been interpolated. For example, some regions near the coast consist of interpolated data that span areas up to 50 km wide. The interpolation was made between the ship track data and the bedrock elevations obtained from BEDMAP2, which has forced the interpolated grid to be shallow towards the coast in many regions. The interpolated data are therefore unsuitable for assessing the depths close to the glacier fronts. For greatest reliability, these data were omitted from further analysis and only ship track data have been used in this study (Figure 6.14b).

Although ships tend not to go close to the fronts of glaciers, there are many tracks that do lead into the bays and fjords along the west coast: most of these bays contain bathymetry

deeper than 500 m (Figure 6.14c). Whilst troughs may channel offshore water towards the coast, bathymetric ridges or features between near- and far-offshore may act as a barrier, preventing deep offshore water from reaching the bays. There are very few ridge-like features or shallow water further offshore that can be identified from the track-data but regions of note are shallow areas in Marguerite Bay and a small shallow region south of Trinity Island, which may obstruct deep ocean water from reaching the glacier fronts (see Figure 2.1 for place names). In addition, some narrow straits have shallower water, such as the narrow channel between Weinke Island and the mainland which has average water depths of ~300m (Figure 6.14d).

Wide regional ocean temperature patterns must be assessed against patterns observed closer to the coast. If deep off-shore ocean temperatures are to affect the ice fronts, the depths at the coast must be sufficiently deep. Bathymetric measurements close to the coast may be limited, but by creating buffers at various distances from each glacier front, the mean ocean depths can be calculated for the vicinity of glaciers where depth data do exist. The hypothesis is that if the percentage of glaciers with deep bathymetry within a wide offshore buffer (where data are prolific) is similar to the percentage for those with data closer to their fronts (where data are more limited), then it could be considered feasible that the deep water reaches the glacier fronts. The distances of 5, 2 and 1 km were regarded as suitable buffers, taking into account the cell size of the IBCSO grid (500 m), the size of bays and the glacier front widths (Figure 6.14d). Any closer than 1 km and the bathymetric data sample size would be too small. The spatial distribution of glaciers with depth measurements within these distances is shown in Figure 6.15: 74% of all 860 glaciers have at least one bathymetry measurement within 5 km, 45% within 2 km and 30% within 1 km (Table 6.2). The minimum depths decrease closer to the coast, reaching 270 m within 1 km of the glacier fronts. Perhaps more reliable are those that have at least two depth measurements, in which case the minimum depths are, on average, 321 m within the 1 km buffer. Glaciers with bathymetric measurements within 1 km have a similar spatial distribution (albeit more sparse) to those within 5 km: the deepest ocean measurements close to glacier fronts are found close to Anvers Island and on the mainland close to Adelaide Island (Figure 6.15; Figure 2.1 for place names).

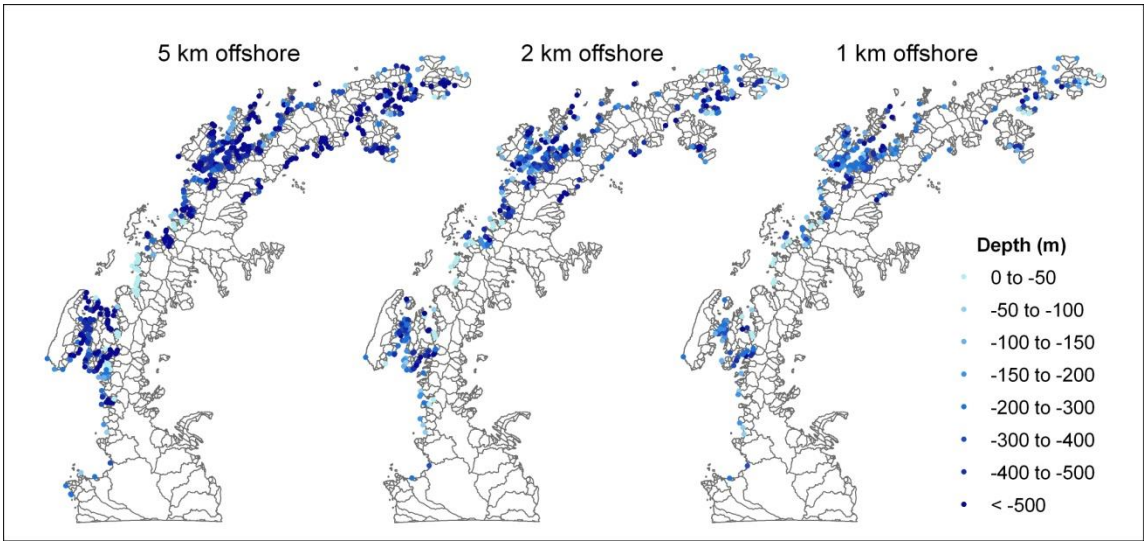

Figure 6.15: Glaciers with depth measurements available within 5 km, 2 km and 1 km . There are 656 glaciers with bathymetry measurements within 5 km, 400 within 2 km and 265 within 1 km.

Table 6.2: Glaciers with depth measurements available within 5 km, 2 km and 1 km. Glacier counts (N) are listed for those with at least one bathymetric measurement (**a**) and only those with more than 2 bathymetric measurements (**b**). Although there are fewer glaciers with >2 bathymetric measurements, the values are likely to be more reliable than results that include glaciers with only 1 or 2 measurements.

a	5 km	2 km	1 km
Glaciers (N) with bathymetry data	656	400	265
% of all glaciers	74	45	30
Minimum depth (mean, m)	-471	-337	-270
b			
Glaciers (N) with > 2 bathymetry data points	592	326	186
% of all glaciers	66	37	21
% of glaciers with data	90	82	70
Minimum depth (mean, m)	-511	-386	-321

The majority of glaciers have at least one depth measurement below 200 m within 1 km of its front (Table 6.3). Where there are two or more depth measurements, the percentage of glaciers with bathymetry deeper than 200 m is similarly high within 5 km (92%) as within 1 km (81%), giving confidence that even though bathymetry data are missing,

ocean depths are typically deeper than 200 m within 1 km. Furthermore, 49% of glaciers with measurements within 1 km have depths below 300 m, and 26% have depths below 400 m. These percentages indicate a strong likelihood that deeper ocean waters reach the glacier fronts and therefore water temperatures at depths as low as 500 m can be considered.

Table 6.3: Glacier counts and percentages with bathymetric data at a range of depths. Counts are given for all glaciers with bathymetric measurements (**a**) and only those with >2 bathymetric measurements (**b**). Percentages are relative to the glacier count with bathymetric data within each particular distance. The majority of glaciers have minimum depths deeper than 200 m in all categories.

	Distance from glacier front					
a	Count			Percent (%)		
Depths under	5 km	2 km	1 km	5 km	2 km	1 km
50 m	610	364	241	93	91	91
100 m	593	342	224	90	86	85
150 m	564	315	205	86	79	77
200 m	549	288	170	84	72	64
300 m	501	218	103	76	55	39
400 m	416	155	55	63	39	21
500 m	296	77	21	45	19	8
b	Count			Percent (%)		
Depths under	5 km	2 km	1 km	5 km	2 km	1 km
50 m	579	322	184	98	99	99
100 m	570	309	179	96	95	96
150 m	551	293	172	93	90	92
200 m	542	270	150	92	83	81
300 m	497	211	91	84	65	49
400 m	413	153	49	70	47	26
500 m	296	77	20	50	24	11

6.3.2.3 Ice thickness at the ocean edge

In addition to bathymetry close to the glacier fronts, it is important to establish whether the ice itself reaches these depths for ice-ocean interactions to take place. The large quantity and varying types and sizes of glaciers around the AP mean that variations in ice thickness at the glacier termini are likely to be substantial. For example, glaciers flowing into an embayment 500 m deep may be grounded in water at this depth (and hence the

ice front is exposed to water up to 500 m deep), floating (and therefore at a thickness of less than 500 m below sea-level) or grounded on bedrock close to sea-level. In the latter case, the ocean water may have little or no role in driving ice melt at the glacier front. Ice thickness data at glacier fronts on the AP are distinctly lacking, however, and there is still a gap in knowledge regarding grounding line positions for the complete coastline (Section 5.2.1).

Huss & Farrinotti (2014) have published a new 100-m resolution bedrock map of the AP, using ice thickness calculations based on surface topography and simple ice dynamic modelling. Thickness measurements, where available (acquired by NASA's Operation IceBridge), and gridded ice flow speeds were used to constrain the model. The dataset indicates deeply incised troughs and reveals that 34% of the ice volume is grounded below sea level (Huss & Farinotti, 2014). This calculation is based on ice thickness inland from the ice edge however and floating ice is not considered in their study. The dataset therefore does not allow an assessment of ice thickness at the ocean-ice interface. Alternative ice thickness measurements at ice fronts include radar-sounding measurements acquired for specific glaciers by Operation IceBridge, and ICESat surface elevation data which enable ice thickness calculations where they cross floating glacier tongues. These are regarded as valuable data for local glacier thickness calculations but currently not practical for use on a wide scale.

The aim of ocean temperature analysis in the present study is to assess the hypothesis that ocean temperature is a key driver of glacier front change in the AP. Until ice front thickness data becomes available for the complete coastline it must be assumed that the ocean temperatures at depths close to the ice fronts reach the interface. The subjective nature of the grounded or floating classification method means that there is inherent uncertainty involved but, as stressed in Section 5.2.1, this is a field for further research. An alternative stance is that if ocean temperatures play a significant role in glacier front change on a regional scale, the ocean-temperature/glacier-retreat patterns that emerge will indicate whether or not the warm ocean waters are reaching the ice fronts.

6.3.2.4 Pressure melting point at ice fronts

The temperature at which the ocean causes melt at the front of calving glaciers is determined by the pressure melting point (T_m) of ice at each depth, calculated as follows:

(1) $P = \rho_i gh$

(2) $T_m = y * P$

where P is ice pressure (in Pascal), ρ_i is ice density (917 kg m^{-3}), g is gravitational acceleration (9.81 m s^{-2}), h is ice thickness (in metres), and y is temperature change with pressure (-7.4^{-8} K Pa^{-1}).

The temperature at which ice melts decreases as ice is placed under increasing pressure, meaning that ice at 500 m thick would reach melting point at -0.33 °C. At an ocean depth of 500 m, and if the glacier front is floating, the ice thickness is 562 m due to buoyancy. In this study, calculations of temperature equilibrium at each depth are made based on ice thickness at flotation. As this is a regional overview and ice thickness details are not known at individual glacier fronts, the assumption of buoyancy of all glacier fronts enables an estimate of whether the ocean temperature causes melt at the glacier fronts. A further consideration of the impact of ocean temperatures on glacier ice is the melt rate, or thermal driving, controlled by ocean salinity and water pressure at the interface, and ice flow velocity (Holland *et al.*, 2008). Thermal driving is not considered in this study as this is a topic for research at a more local scale. Calculating the temperature at which melt occurs, however, shows whether or not the ocean temperatures are sufficient to cause melt.

6.3.3 Wide-scale regional ocean temperatures

6.3.3.1 Spatial ocean temperature patterns

The raw temperature data used in this study are displayed in plots at the specific depths the measurements were taken (Figure 6.16). These are a combination of all temperature measurements recorded between 1945 and 2009.

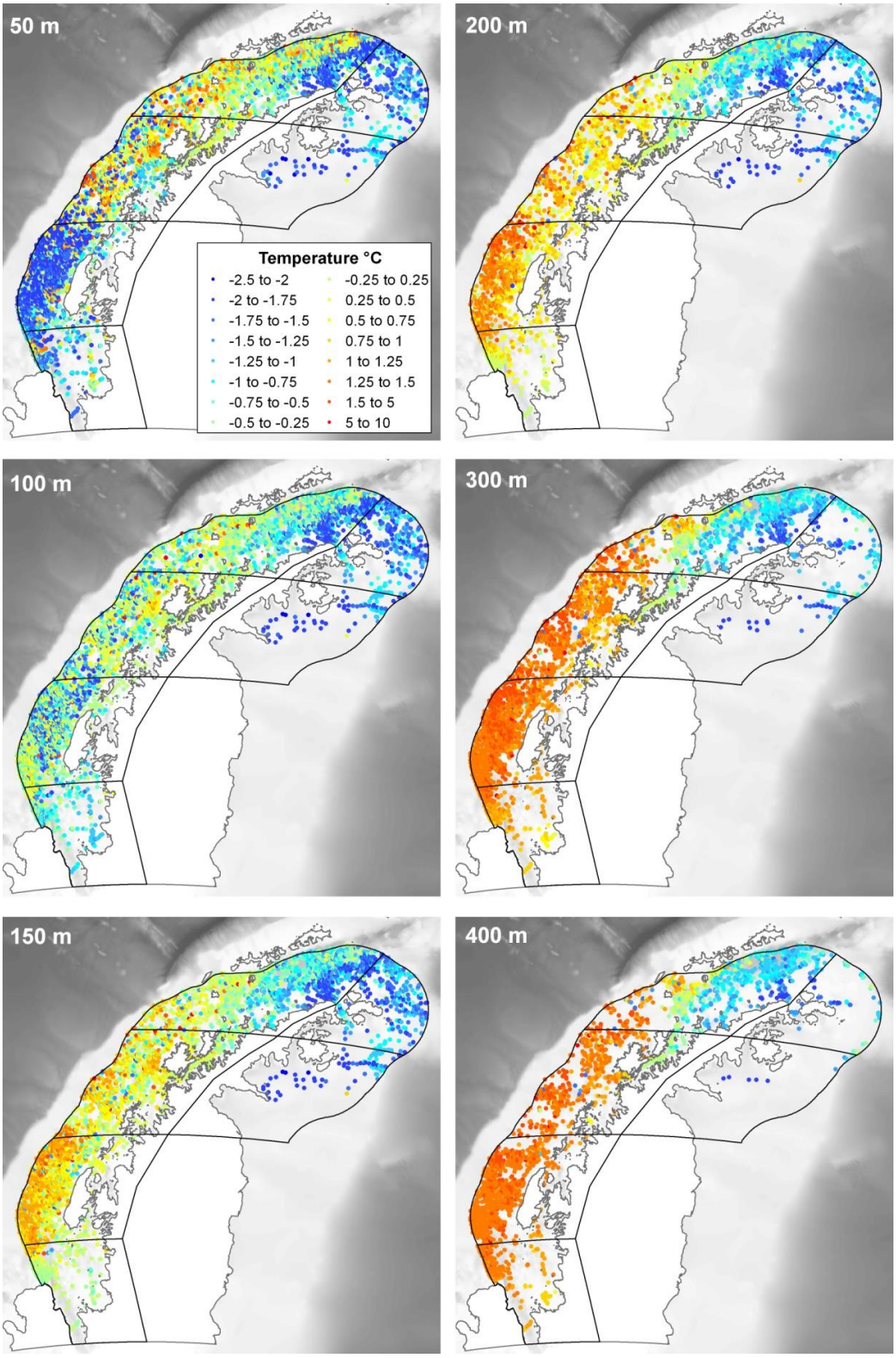

Figure 6.16: Ocean temperatures at specific depths.
These plots show all point measurements at each depth, downloaded from the World Oceanographic Database and provided for this study by P. Holland (British Antarctic Survey).

A clear spatial pattern is observed (Figure 6.16):

- At the shallowest depth (50 m) the temperatures are generally mixed north of ~66° S, with the coldest water occurring south of 66° S and off the north/north-west coast and to the east of the AP
- The same pattern is largely maintained at 100 m, although the ocean temperature south of 66° S is warmer than it is at 50 m.
- At a depth of 150 m, there is a shift towards considerably warmer waters along the entire west coast south of 64° S, with the warmest region occurring south of 66° S. Cold water remains in the north-west and east of the AP.
- This gradient along the west coast between the north and south becomes further enhanced at depths of 200 m and deeper, with maximum ocean temperatures occurring south of ~66° S.
- Regions that remain cold at all depths are the north-west (from Anvers Island at 64.5° S) and the ocean surrounding the north and east coasts.

The data distribution varies considerably throughout the region, and interpolation between measurements would introduce substantial variability errors. A grid based on the mean of values within a regular cell size, however, reduces the influence of data clusters and results in equal spacing where values are dense. A cell size of 5 km was chosen as most suitable for the data availability. The mean temperature values used in regional comparisons are based on the cell values.

The most distinct regional difference in ocean temperatures is between the east and west of the AP. To the east, the mean ocean temperatures at each depth are below the pressure melting point (T_m) at all depths, with little difference in temperature between depths. In contrast, temperatures to the west are warmer than -0.5 °C at all depths, steadily becoming warmer with increasing depth, to +0.72 °C at 300 m depth (Figure 6.17, Table 6.4). At depths shallower than 150 m the ocean temperatures would have no effect on melt as the temperatures are below the T_m, whereas at 150 m deep the temperature rises above the T_m, therefore eliciting ice melt at the ocean-ice interface.

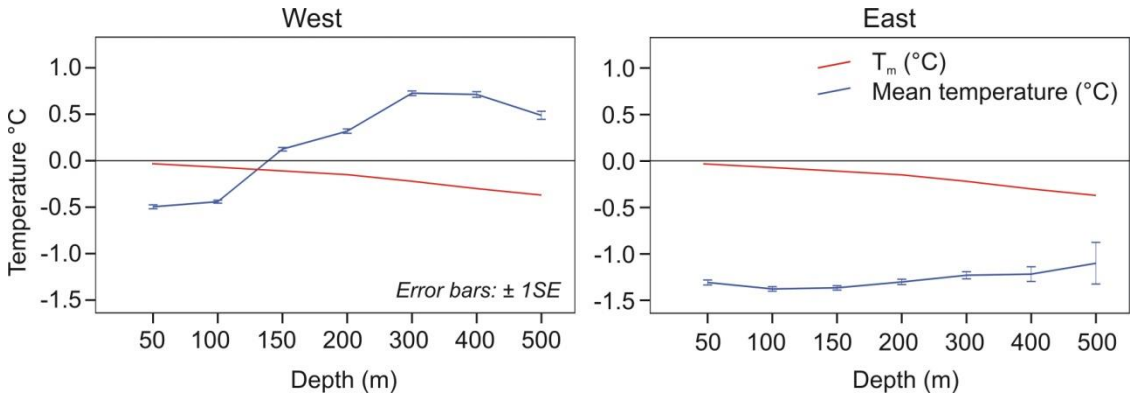

Figure 6.17: Mean ocean temperatures at selected depths (m), by east/west AP.
The Pressure Melting Point (T_m) was calculated for each depth and used as a reference line.

Table 6.4: Mean ocean temperatures at each depth (m), by east/west AP.
The mean values are calculated from the measurements on 5 km grid cell spacing. (Figure 6.17).

Mean Temperatures (°C)		
Depth	West	East
50	-0.44	-1.33
100	-0.41	-1.39
150	0.12	-1.37
200	0.31	-1.31
300	0.72	-1.24
400	0.71	-1.20
500	0.47	-1.06

When the ocean is separated into the five regions used throughout this study (Figure 6.14a), the NE and E regions have mean ocean temperatures that are at least 1 °C below the T_m at all depths and show little variation (Figure 6.18a). The NW region has mean temperatures closer to, but still below, the T_m at all depths, and also has little variation with depth. The other westerly regions all have mean temperatures either at (W) or below (SW and SSW) the T_m at 50 m and 100 m, but an increase in temperature with depth means that water at 150 m is greater than the T_m. The increase in temperature with depth levels out at 300 m, with highest mean temperatures at +1.5 °C in the SW region. It must be noted that despite using the 5 km regular grid spacing for temperature values, the data quantity varies considerably between regions and depths: the E region in particular has significantly fewer temperature measurements, with less than ten at depths of 400 and 500 m (Figure 6.18b).

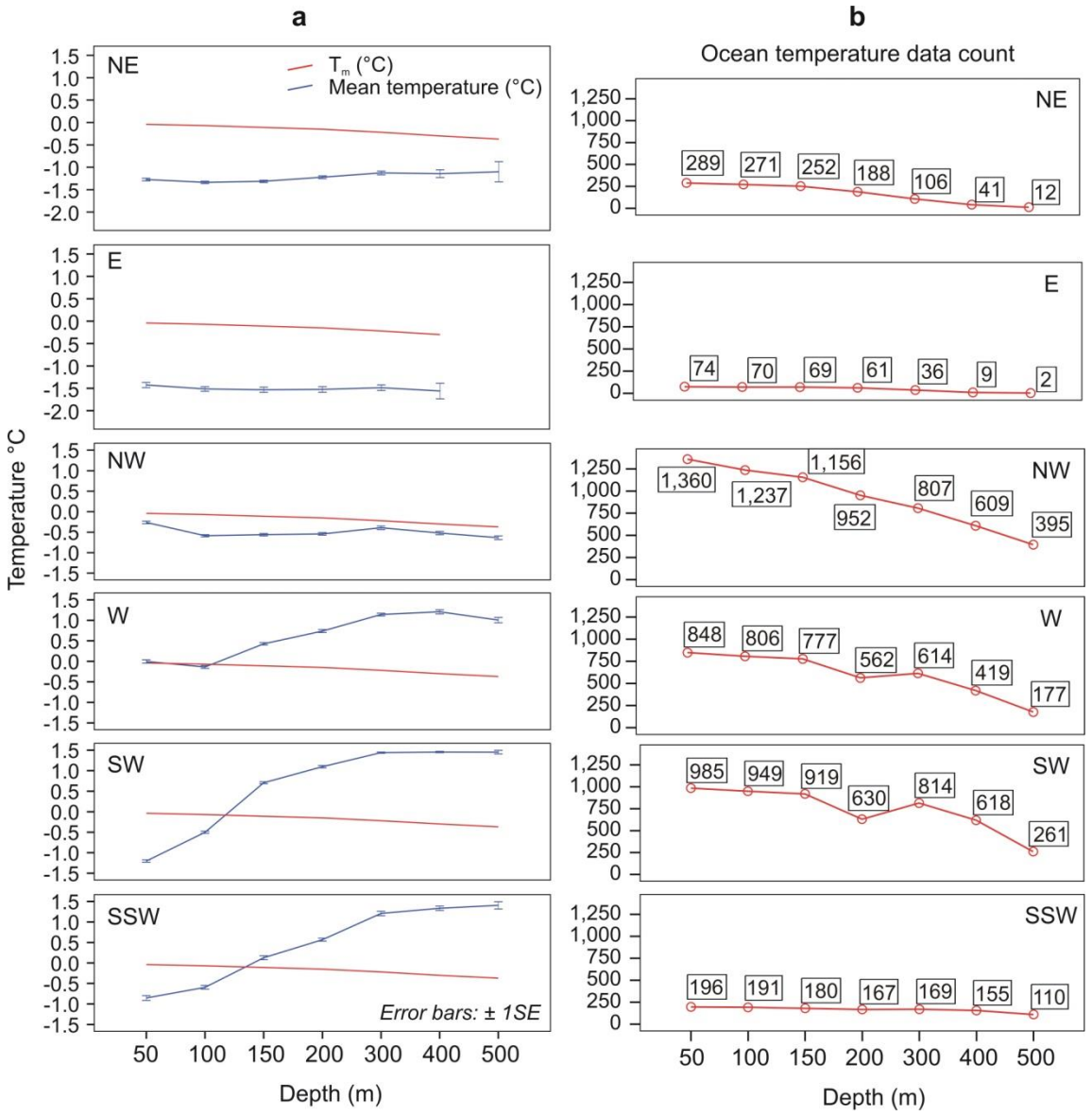

Figure 6.18: Mean ocean temperatures at selected depths, by Regions.
The Pressure Melting Point (T_m) of ice was calculated for each depth and used as a reference line. The numbers of ocean temperature data contributing to the mean values in (**a**), are shown in boxes on (**b**). These must be taken into consideration; for example data in the E region are particularly sparse.

In summary, to the west of the AP the regional patterns reveal a strong north-south temperature gradient that emerges at depths of 150 m and deeper, whereas to the east the temperature remains cold at all depths. Further analysis will consider only the western regions, where the deeper ocean temperatures are above the T_m and can therefore be considered a driver in ice front change. Conversely, ocean water to the east does not

cause melt at the ice front at any depth and therefore can be ruled out as a driver in glacier retreat in this region.

6.3.3.2 Temporal ocean temperature patterns

The ocean to the west of the AP has a distinct temperature gradient with depth in all regions south of 64° S. It has been shown that at 150 m the temperature shifts to warmer than the pressure melting point. These mean values are acquired from all records, which span from 1945 to 2009, and therefore could potentially mask a temperature trend throughout this period.

Dividing the temperature data into individual depth bands and 5-year intervals reduces the data density, resulting in some categories with few measurements. Since the temperature patterns are distinct for shallower and deeper waters, however, the data can be split into two categories, with 150 m used as the dividing point. Hereafter, depths at or below 150 m are termed ‘deep’ and depths of 50 and 100 m are termed ‘shallow’.

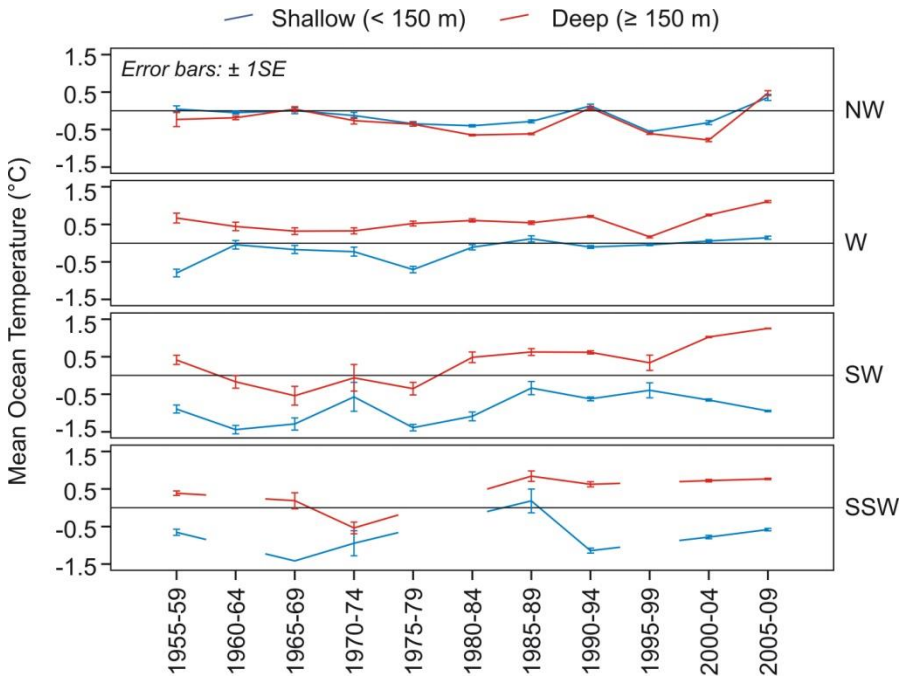

Figure 6.19: Regional mean ocean temperatures by 5-year intervals.
The temperature data are grouped into measurements obtained either above 150 m (termed ‘Shallow’), and at or below 150 m (termed ‘Deep’). The first interval is 1955-59 as earlier temperature records are too sparse for separation into time intervals. The numbers of ocean temperature data contributing to the mean values are shown in Table 6.5.

Table 6.5: Ocean temperature measurement counts.
Data count for temperature measurements in shallow (< 150 m) and deep (at and below 150 m depth) waters in each region (see Figure 6.19).

	NW		W		SW		SSW	
	< 150 m	>= 150 m	< 150 m	>= 150 m	< 150 m	>= 150 m	< 150 m	>= 150 m
1955-59	106	26	109	48	41	40	48	40
1960-64	237	152	49	43	23	24	0	0
1965-69	110	112	65	49	10	5	8	7
1970-74	101	76	56	51	8	7	4	4
1975-79	183	212	84	111	40	37	0	0
1980-84	536	813	100	159	18	24	0	0
1985-89	535	944	103	180	28	39	4	10
1990-94	149	260	365	452	166	273	30	59
1995-99	539	1001	313	502	8	10	0	0
2000-04	138	263	436	651	519	787	193	304
2005-09	323	483	1098	1568	2931	4603	1184	2182

Mean ocean temperatures plotted against 5-year time intervals reveal differences between each of the western regions (Figure 6.19). The mean temperatures in each interval can be considered alongside the data count (Table 6.5) and summarised as follows:

- Temperatures in the NW are largely the same for shallow and deep water and remain close to or below the pressure melting point throughout.
- In the W, differences in temperature between the shallow and deep water become apparent. Deep water is consistently warmer, and there is a notable increase in temperature of deep water since 1995-99.
- In the SW, the temperature difference between shallow and deep water is greater, and an increase in deeper water temperatures is more apparent. The intervals 1965-69, 1970-74 and 1995-99 have 10 data records or fewer, therefore the small spikes in the mean temperature cannot be regarded as wholly representative for the region.
- In the SSW, all intervals between 1960-64 and 1985-89 have 10 data points or fewer, making it difficult to interpret possible trends throughout this period. The two most recent intervals are the most reliable in terms of data quantity and,

whilst shallow and deep water have distinct temperatures, they show a small increase at both depths.

The mean temperatures in 5-year intervals indicate small positive trends in deep water temperatures in the W, SW and SSW regions. Correlation tests between years and ocean temperatures confirm that these correlations do exist, although linear trends are very weak (Table 6.6a and b). The linear regression model results suggest that deep water in the SW has a reasonable correlation with time (r_p = 0.36, significant at <0.01), but with an r^2 of 0.129 there is still considerable variability in the data. The largest increases in temperature occur between 1995-99 and 2005-09 in deep water (Figure 6.19), and in the NW and W this correlation is significant at <0.01, although also with considerable variation in the residuals (r^2 = 0.133 and 0.139, respectively) (Table 6.6c). The peninsula-wide trend has been positive, and dominated by an increase in deep ocean temperature on the western side (r_p = 0.462 and r^2 = 0.213) (Table 6.6a). There is no trend on the eastern side in either deep or shallow water.

Table 6.6: Ocean temperature trends for deep (>= 150 m) and shallow (< 150 m) waters. Pearson's correlation (r_p) and linear regression model (r^2) values for temperature change over time. B are the model slope values where statistical significance < 0.01 (marked with *). Tables **a** and **b** are from all measurements between 1945 to 2009; table **c** is from measurements between 1995 and 2009. Table **a** is temperature change over time surrounding the AP in total, and by east/west regions; tables **b** and **c** are for regions along the west coast only. Most r^2 values are very small, suggesting that there is a large amount of variation in the data, hence the predictive model is not a good fit in all cases.

a **All ocean temperature measurements**

Region	Depth	r_P	r^2	B
Total		0.258*	0.067	0.02
W		0.221*	0.049	0.02
E		0.029	0.001	
W	< 150 m	0.091*	0.008	-0.01
	>= 150 m	0.462*	0.213	0.04
E	< 150 m	0.026	0.001	
	>= 150 m	0.076	0.006	

b **1945 to 2009: 2 depth bins**

Region	Depth	r_P	r^2	B
NW	< 150 m	0.012	0	
	>= 150 m	0.105*	0.011	0.01
W	< 150 m	0.19*	0.036	0.01
	>= 150 m	0.247*	0.061	0.02
SW	< 150 m	0.017	0	
	>= 150 m	0.36*	0.129	0.03
SSW	< 150 m	0.052	0.003	
	>= 150 m	0.074*	0.006	0.01

c **1995 to 2009: 2 depth bins**

Region	Depth	r_P	r^2	B
NW	< 150 m	0.366*	0.134	0.07
	>= 150 m	0.365*	0.133	0.07
W	< 150 m	0.089*	0.008	0.02
	>= 150 m	0.373*	0.139	0.07
SW	< 150 m	0.101*	0.01	-0.04
	>= 150 m	0.166*	0.028	0.04
SSW	< 150 m	0.087*	0.008	0.04
	>= 150 m	0.008	0	

An additional way of visualising temporal trends across the regions is to group temperatures by decadal intervals and consider the values at all depths. The data volume is greater when grouped by decade, and differences in the values can be seen on spatial plots for individual depths, for example at 150 m depth (Figure 6.20). Although data are more sparse prior to the 2000s, a steady increase in temperatures can be seen in the W and SW regions at this depth.

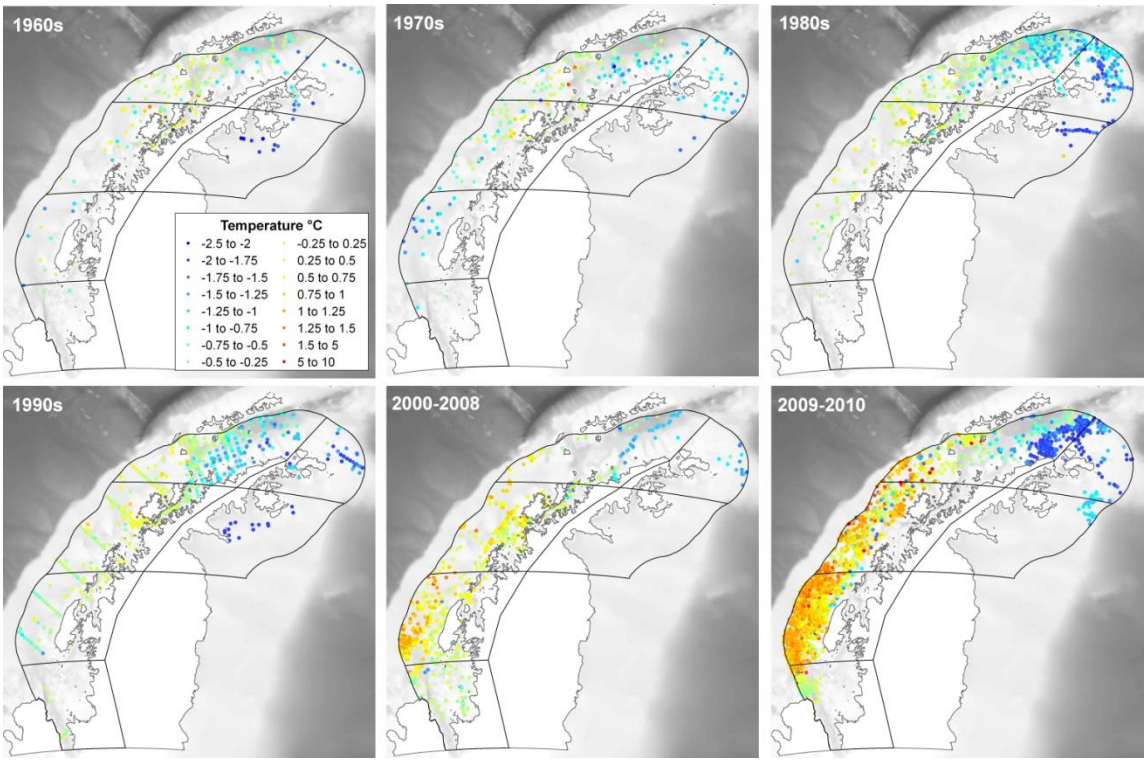

Figure 6.20: Decadal ocean temperatures at 150 m depth.
These plots show all temperature measurements available in the World Oceanographic Database, downloaded by P. Holland (British Antarctic Survey) and collated into decadal intervals. The 2009-10 data are shown separately to illustrate the wealth of data in those years compared to prior intervals.

The mean ocean temperatures per decade plotted by depth bands in a graph matrix (Figure 6.21) show minimal change in the NW and W regions at any depth, and small positive trends in the SW between 100 and 200 m depth. There are insufficient data for years prior to the 2000s in the SSW region (Table 6.7) but small increases can be seen. Since 1945, the correlations between year and temperature are significant at all depths in the W and SW region, although they remain weak in almost all cases (Table 6.8a). The strongest correlations occur in the SW region at 150 m depth ($r^2 = 0.254$), and 200 m (r^2

= 0.221). The slope increase (ß = +0.03 and ß = +0.04) at these depths is greater than the increase for other categories, although clearly this overall trend is minimal. A greater increase in temperature over time occurs between 1995 and 2009 (Table 6.8b), seen in slope values for almost all regions, particularly at depths of 100 m and below. The greatest increase (ß = +0.11), with an r^2 of 0.337 occurred in the W region at 500 m depth. The measurement sample size in the SSW region is too small to produce meaningful trend results. The shallow water in the SW region has decreased in temperature over time, whilst temperatures have increased in all other categories that have significant correlations.

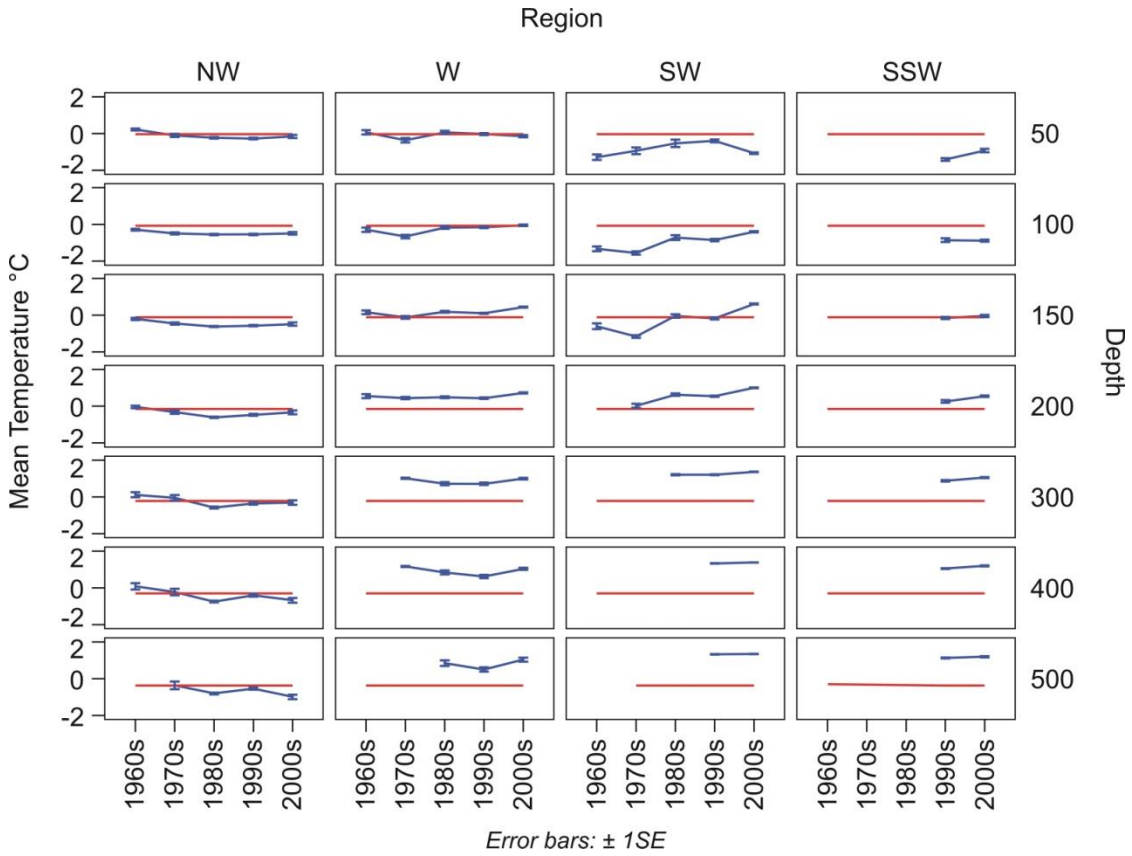

Figure 6.21: Multi-dimensional plots showing mean temperature at specific depths over time. The red lines are the Pressure Melting Point (T_m) at each depth (m). Mean values are removed where the data count is under 10 (with the exception of the SSW region in the 1990s, where the region has a low overall data count). The error bars are ±SE. The ocean temperature data counts contributing to the mean are in Table 6.7.

Table 6.7: Ocean temperature data counts, by region, depth (in metres) and decade. See Figure 6.21.

			NW						SW		
Depth	1960s	1970s	1980s	1990s	2000s	Depth	1960s	1970s	1980s	1990s	2000s
50	191	150	552	364	247	50	18	24	23	87	1777
100	156	134	519	324	214	100	15	24	23	87	1673
150	111	122	479	305	214	150	14	22	23	86	1633
200	95	79	423	291	161	200	11	13	21	79	919
300	29	39	335	259	204	300	2	4	15	56	1457
400	22	30	288	214	125	400	2	4	3	45	1035
500	7	18	232	192	42	500	0	1	1	17	346
			W						SSW		
Depth	1960s	1970s	1980s	1990s	2000s	Depth	1960s	1970s	1980s	1990s	2000s
50	67	74	104	379	804	50	4	2	2	15	704
100	47	66	99	299	730	100	4	2	2	15	673
150	45	61	96	261	712	150	3	2	2	13	650
200	38	47	94	241	406	200	2	2	2	10	568
300	4	26	70	202	617	300	1	0	2	12	614
400	3	19	53	145	371	400	1	0	2	12	450
500	2	9	26	105	113	500	0	0	2	12	204

Table 6.8: Ocean temperature trends at each depth (m), by Region.
Pearson's correlation (r_p) and linear regression model (r^2) values for years and temperatures. B are the model slope values where statistical significance < 0.01 (marked with *). Table **a** is from all measurements between 1945 to 2009; table **b** is from measurements between 1995 and 2009. Most r^2 values are very small suggesting that there is a large amount of variation in the data, hence the predictive model is not a good fit in all cases.

a **1945-2009: individual depths**

Region	Depth	N	r_P	r^2	B	Region	Depth	N	r_P	r^2	B
NW	50	1562	0.007	0		SW	50	1951	0.198*	0.039	-0.02
	100	1399	0.043	0.002			100	1843	0.179*	0.032	0.02
	150	1243	0.129*	0.017	0.01		150	1793	0.504*	0.254	0.04
	200	1057	0.039	0.002			200	1057	0.47*	0.221	0.03
	300	872	0.169*	0.028	0.02		300	1539	0.176*	0.031	0.01
	400	685	0.072	0.005			400	1093	0.123*	0.015	0.01
	500	492	0.08	0.006			500	367	0.086	0.007	
W	50	1488	0.173*	0.03	0.01	SSW	50	751	0.035	0.001	
	100	1296	0.215*	0.046	0.01		100	720	0.079	0.006	
	150	1200	0.298*	0.089	0.02		150	692	0.004	0	
	200	846	0.153*	0.023	0.01		200	601	0.044	0.002	
	300	926	0.24*	0.057	0.02		300	629	0.114*	0.013	0.02
	400	594	0.223*	0.05	0.02		400	465	0.142*	0.02	0.02
	500	257	0.165*	0.027	0.02		500	219	0.126	0.016	

b **1995-2009: individual depths**

Region	Depth	N	r_P	r^2	B	Region	Depth	N	r_P	r^2	B
NW	50	533	.368*	0.135	0.07	SW	50	1781	.251*	0.063	-0.09
	100	467	.380*	0.144	0.06		100	1677	0.03	0.001	
	150	452	.437*	0.191	0.08		150	1637	.263*	0.069	0.06
	200	392	.341*	0.116	0.07		200	923	.235*	0.055	0.04
	300	409	.412*	0.169	0.09		300	1459	.128*	0.016	0.02
	400	296	.249*	0.062	0.05		400	1035	.107*	0.012	0.02
	500	198	0.177	0.031			500	346	0.091	0.008	
W	50	986	.128*	0.016	0.03	SSW	50	704	0.031	0.001	
	100	861	0.036	0.001			100	673	.161*	0.026	0.07
	150	830	0.269*	0.072	0.05		150	650	0.022	0	
	200	524	0.314*	0.099	0.06		200	568	0.066	0.004	
	300	732	0.435*	0.189	0.08		300	614	0.098	0.01	
	400	454	0.463*	0.214	0.10		400	450	.123*	0.015	0.03
	500	181	0.581*	0.337	0.11		500	204	0.1	0.01	

In summary, the temperatures of the ocean deeper than 150 m show signs of increasing, particularly from the 1990s onwards, in all regions along the west coast. These increases are small, however, with much variability in the trends. The strongest warming over the long term has occurred in the SW between 150 and 200 m.

6.3.3.3 Temperature differences between repeat measurements

The ocean temperature patterns are based on a wide variety of measurements across extensive regions, with different levels of coverage between time periods and depths. Although trends can be seen in the data, they should be assessed against trends derived from measurements that are repeated at the same locations.

There are a limited number of measurements for which this is the case; however there are a sufficient number of repeat measurements between the 1990s and 2000s. Since the regional overview showed that this was a period of notable warming, any true trends will be apparent between repeat measurements. For this study, measurements are considered to be repeated if they were collected within a distance of 1 km over more than one year; therefore buffers of 1 km were created around each measurement. Where buffers overlap (i.e. where there are repeated measurements), the mean values were calculated. This was carried out for measurements in the 1990s and separately for the 2000s, resulting in a mean temperature for each decade. The differences between the mean values in the 1990s and 2000s were then calculated at each measurement location. This was carried out for measurements at each depth individually.

There are 242 1990s-2000s difference calculations in total, all of which are in the W and SW regions (Figure 6.22). There is a reasonable distribution of points at each depth, ranging between 14 (at 500 m) and 54 (at 50m) (Table 6.9). The total mean temperature differences reveal a warming at all depths except for at 50m, which has cooled slightly. The greatest warming has occurred between 100 and 200 m, with a maximum difference of +0.65 °C at 150 m. If the W and SW regions are considered separately, there has been a greater increase in temperature at the middle depths (100 to 200 m) in the SW than in the W region (Figure 6.22). In the SW the greatest temperature increase was an average of 0.9 °C at 150 m depth.

These temperature differences between repeat measurements correspond with the regional overall pattern, where greatest warming is occurring at mid-depths (100-200 m), particularly in the south.

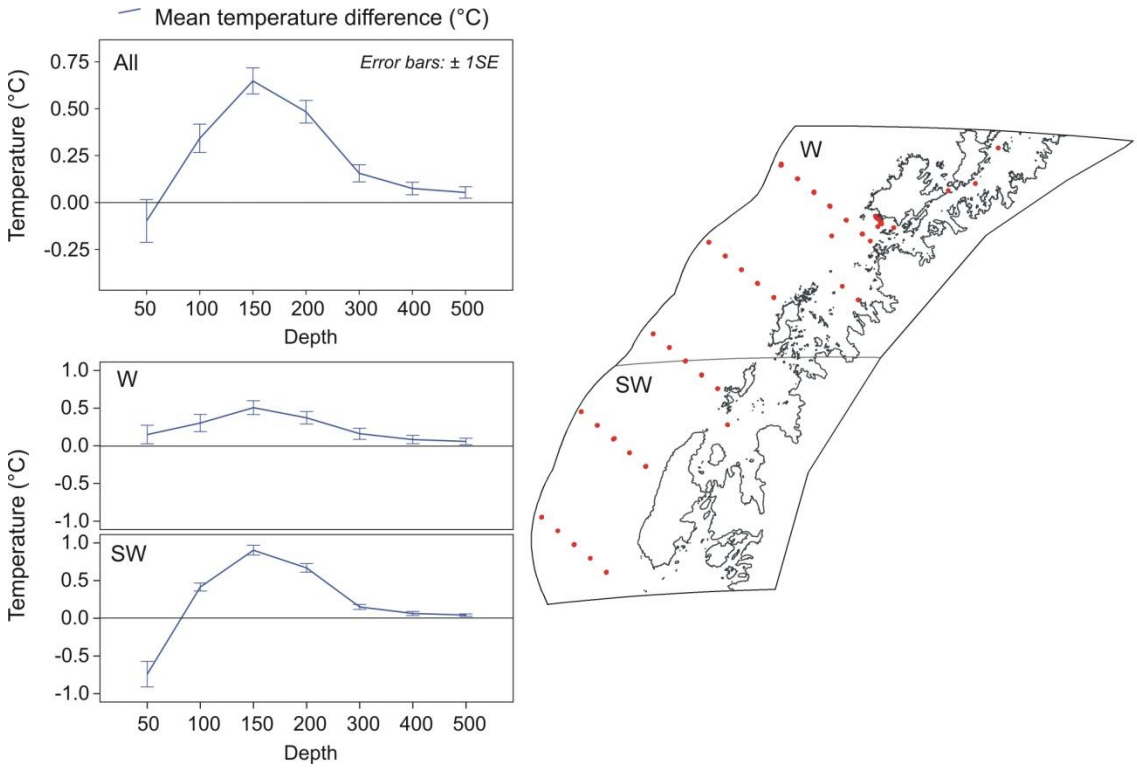

Figure 6.22: Repeat temperature measurements between 1990s-2000s.
Mean ocean temperatures in the 1990s subtracted from mean ocean temperatures in the 2000s, at specific depths (in metres). All repeat measurements are located in the W and SW regions (displayed as points on the map above), and are displayed as totals (top graph), and split by region (lower two graphs).

Table 6.9: Ocean temperature differences between 1990s-2000s, by depth (m).
Temperature differences are calculated from repeat measurements between the 1990s and 2000s, where mean values in the 1990s are subtracted from mean values in the 2000s. Results for W and SW regions are shown separately.

	W		SW		Total	
Depth	Count	Mean	Count	Mean	Count	Mean
50	39	0.15	15	-0.74	54	-0.10
100	27	0.30	15	0.41	42	0.34
150	27	0.51	15	0.90	42	0.65
200	23	0.37	14	0.67	37	0.48
300	19	0.16	13	0.15	32	0.16
400	12	0.08	9	0.06	21	0.07
500	10	0.06	4	0.04	14	0.05
Total	157	0.26	85	0.24	242	0.25

6.3.4 Ocean temperatures close to the coast

Analysis thus far has shown trends in ocean temperature up to 100 km from the AP coast, but ocean temperature trends close to the coast require particular analysis. As is the case with bathymetric measurements, the ocean temperature records are sparse for large stretches of coast. Similarly therefore, a radius of 5km from the glacier front was used to determine mean temperatures for each glacier where recorded temperatures are available; any closer and the number of glaciers with temperature records becomes significantly reduced. Mean temperatures within 5 km of each glacier front were calculated at each depth. The percentage of glaciers with ocean temperature data decreases at each depth; for example at a depth of 500 m there are only 25 glaciers and of these, only 22 have both temperature and bathymetric data (Table 6.10). Out of a total of 696 glaciers along the west coast this is a very small percentage (3.2%).

Table 6.10: Glaciers with ocean temperature and bathymetry measurements within 5 km.

Depth (m)	Temperature records (Glacier Count)	Temperature records %	Temperature and Bathymetry records (Glacier Count)	Temperature and Bathymetry records %
50	172	24.7	151	21.7
100	141	20.3	121	17.4
150	122	17.5	103	14.8
200	118	17.0	99	14.2
300	100	14.4	85	12.2
400	60	8.6	50	7.2
500	25	3.6	22	3.2

By interpolating between ocean temperature measurements, however, the number of glaciers with temperature data is increased and a consistent measure of temperature at each depth is maintained. Data interpolation was not considered necessary for the wide-scale regional analysis since measurements are prolific across these regions. For the coastal region, however, it can be used to attribute the closest available temperatures to each glacier front and hence increase the temperature coverage. An interpolated grid at 5 km cell size was created for each depth by using the TopotoRaster tool in ArcGIS 10.1. The resulting grids in the coastal regions have high correlations between measured and

modelled temperatures (Table 6.11). This is not a valid method for comparing temperatures at separate time intervals, however, as the data are too sparse for reliable interpolation.

Table 6.11: Measurements vs. interpolated grids.
Correlations (r_s) between real ocean temperature measurements and interpolated grid results within 5 km of each glacier front. N is number of glaciers where at least one data point is within 5km of the front. Correlations are based on the mean ocean temperature values within 5km of each ice front.

Depth (m)	N	R_s
50	167	0.88
100	138	0.91
150	119	0.86
200	117	0.93
300	98	0.90
400	59	0.89
500	25	0.92

These ocean temperature data are used in later analyses in relation to glacier frontal behaviour, but an overview of temperatures within 5 km of the coast reveal patterns similar to those for the wider regions (Figure 6.23). In the NW, temperatures are cold (i.e. below the pressure melting point) at all depths; in the W temperatures in shallow water are close to 0 °C with slightly warmer temperatures at depths below 100 m; in the SW there is a distinct shift from cool to warm water at 150 m, becoming warmer with depth; this is similar in the SSW, with even cooler water at 50 and 100 m.

The mean ocean temperature spatial patterns across wide regions are similar to those within 5 km of the coast. Where the bathymetry close to the ice fronts is 150 m or below, the ocean temperatures are sufficiently warm to cause ice melt. Although the measurements close to the ice fronts are too sparse to adequately assess change over time, the wider regions reveal a warming at mid-depths (100 to 200 m), particularly in the SW region. As the majority of bathymetry measurements close to the ice fronts are below mid-depths (Table 6.3), it can be construed that the warming waters are having an effect on driving melt at the ice fronts. An analysis of ice front retreat alongside these ocean temperature patterns is necessary to assess this hypothesis. This, along with

patterns observed in atmospheric temperature changes, is undertaken in the following discussion chapter.

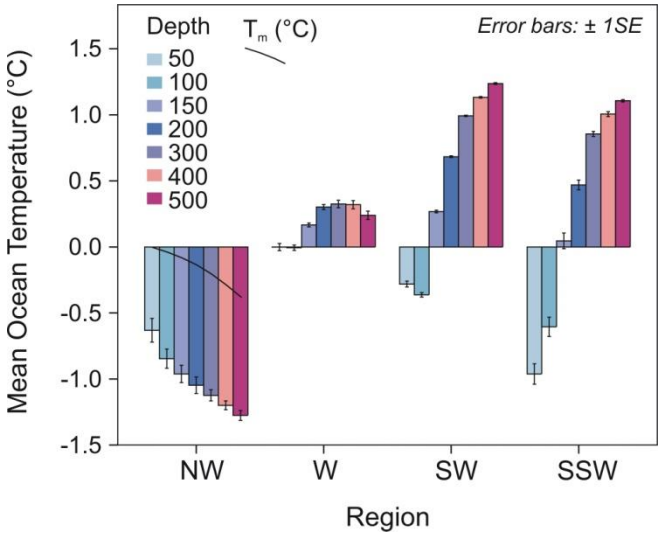

Figure 6.23: Mean ocean temperatures within 5 km of individual glacier fronts (west coast). These mean values are calculated from interpolated grids using all available temperature values at each depth (in metres). Mean temperatures for glaciers in the NW are all below the Pressure Melting Point (T_m).

6.4 Summary

In this chapter the primary regional drivers of glacier front change have been evaluated on a wide-scale and, where data are sufficient, close to the glacier fronts. Atmospheric and ocean temperature data were analysed independently, and regional spatial and temporal patterns have emerged.

6.4.1 Atmospheric patterns

Station records show that the strongest increase in positive degree days over the past half-century has occurred on the east side of the AP. Mean temperatures measured at Esperanza station in the NE are greater than anywhere else on the peninsula and increasing at the fastest rate. An increase, although not as strong, has also occurred at Faraday/Vernadsky station in the W. Further south at Rothera station the mean

temperature is lower than anywhere further north, with a small (but statistically insignificant) increase since the 1960s.

Patterns of mean melt duration between 2000 and 2009 show that glaciers in the NW and parts of the W regions are subject to a longer melt season than elsewhere on the AP. Mean values within 5 km upstream from glacier fronts show there is a correlation between MMD and latitude, whereby the melt season is longest in the NW and shortest in the SW.

Mean surface temperatures obtained from infrared satellite imagery between 1980 and 2008 show a similar overall pattern to that observed in the MMD: temperatures have been greatest in the north (particularly north of 64° S on both sides of the AP) and high along the western coast north of ~65° S. A strong correlation between surface temperature and latitude occurs in the east and weaker in the west; regionally, there is a distinct lowering of mean annual temperatures between the NW (-4.5 °C) and the SSW (-10.5 °C).

Patterns of surface temperature change over time show a peninsula-wide increase since the records began in 1980-84. Mean temperatures within 5 km of glacier fronts show that regional averages have increased at similar rates, and a slight cooling occurred in 1990-94 in all regions.

Surface mass balance results showed there was distinctly greater mean accumulation along the western side than the east between 1980 and 2009. Otherwise, there were no distinct regional differences and no significant trends over time, although notably SMB was almost universally high in 1995-99.

6.4.2 Ocean temperature patterns

Ocean temperature measurements selected from specific depths reveal distinct spatial patterns around the AP. Map plots reveal a largely mixed temperature distribution at depths of 50 and 100 m, with temperatures noticeably cool in the SW and NE regions. At 150 m deep, however, a distinct shift in temperature occurs, with a clear north-south gradient from cool to warm water. This gradient becomes further enhanced with

increasing depth. A distinctly cool region in the NW and NE remains constant at all depths.

Regional mean temperature calculations at each depth confirm this marked difference between the east and west AP: to the east the ocean temperatures are well below the pressure melting point (T_m) at all depths; to the west the ocean becomes warmer with depth, rising above the T_m by 150 m deep. The NW remains below the T_m. at all depths whereas the regions to the south continue to increase in temperature with depth before levelling out at 300 m.

Ocean temperature trends differ between deep (≥ 150 m) and shallow (< 150 m) water in each region, except in the NW where water temperatures at both depths are similar and have changed little since the 1950s. In the W, SW and W regions, deep water is warmer than shallow water during all time intervals and shows an overall increase over time. There are no significantly different temperature changes in any individual time period, but warming of deep water between 2000-04 and 2005-09 is noticeable. When separated by depth bands, the overall greatest increase in ocean temperatures occurred at 150 m in the SW region. This is corroborated by repeat measurement results, which show that between the 1990s and 2000s, the ocean temperature warmed the most at mid-depths (100 m – 200 m) in the SW.

The bathymetry close to the glacier fronts is limited, but where it does exist, there is evidence to suggest that water deeper than 200 m reaches the majority of glacier fronts. Mean water temperatures in the W, SW and SSW regions are greater than the pressure melting point at and deeper than 150 m, making it highly plausible that water at these depths are driving melt at the ice fronts. In addition, temperatures at mid-depths are warming more than at other depths, an increase that is particularly apparent since the 1990s.

6.4.3 Differences between temperature patterns

In this chapter, dissimilarities between the recent AP oceanic and atmospheric temperature patterns have emerged. Perhaps the most obvious difference occurs on the

eastern side of the AP, where air temperatures have been warmer and increasing more rapidly than elsewhere, whereas the ocean temperatures have remained cool at all depths since records began. Similarly, in the distinct region in the north-west, the surface temperatures have increased whilst the ocean has remained cool throughout. A further opposing trend is the north-south gradient along the west coast which exists for both atmospheric and ocean temperatures, but with opposing temperature gradients.

These patterns must be assessed alongside glacier front changes to determine the strength of spatial and temporal correlations, and this is carried out in the following discussion chapter.

Chapter 7

Identifying the principal driver of glacier area changes on the Antarctic Peninsula

7.1 Introduction

Interpreting the behaviour of the numerous glaciological features making up the APIS is critical for recognising responses to local and regional environmental changes (Section 2.2.3). The glacier system is complex and, prior to this study, individual glaciers within it had not been comprehensively mapped. The AP therefore lacked data fundamental to marine glacier studies. The advent of the new DEM with sufficient accuracy and resolution (Chapter 3), plus a consistent method for deriving glacier drainage basin outlines (Section 4.2.3), has resulted in a comprehensive dataset of 1590 glacier drainage basins for the AP between 63° and 70° S. In total, 925 of the glaciers are marine-terminating and, after glacier basins that were once conjoined are merged, the result is 860 glaciers with more than one frontal position record. The level of detail contained in these datasets means the possibilities for glacier-change research in the AP have significantly increased.

The new datasets facilitate research on important unanswered questions in a region that is undergoing rapid climate change. One such question is that on a regional scale, are the glacier front changes occurring primarily due to changes in the atmosphere or the ocean? A better understanding of the many marine-terminating glaciers, which respond rapidly to changes in mass balance, can be a valuable contribution to the debate on the principal driver of ice front changes in the region.

The quantification of changes in both AP glacier area and their regional control factors presented in preceding chapters offers a first opportunity to assess spatial and temporal correlations between the two. The glacier inventory has enabled new research on AP

glacier characteristics and frontal behaviour. In addition, the collation and regional analysis of atmospheric and ocean temperature data means it is now possible to analyse the significance of wide-scale correlations of these controls on glacier front change. This chapter aims to use the new findings to identify the dominant driver of glacier area change on a regional scale. The chapter is divided into two parts: in the first half, the glacier changes and their primary controls are analysed, and, in the second half, these results are discussed in the context of other research in the region.

The first part is structured to address three main questions:

- Can the patterns in area change be explained primarily by local glaciological control factors?
- Do atmospheric patterns show a significant correlation with area changes, either spatially or over time?
- Do ocean temperature patterns show a significant correlation with area changes, either spatially or over time?

The results presented in previous chapters are assimilated to address these questions, beginning with a summary of glacier-change patterns (Section 7.2) followed by a discussion of glaciological controls on observed frontal changes (Section 7.3). These patterns are considered first alongside atmospheric temperature patterns (Section 7.4), and then ocean temperature patterns (Section 7.5). The results are then discussed alongside findings from other research in Antarctica, plus the likely cause and implications of further change (Section 7.6). Definitions of the six regions referred to throughout this chapter can be seen in Figure 6.1.

7.2 AP glacier area-change patterns

The glacier area-change results presented in this study included overall glacier area change from the earliest to latest recorded positions. As discussed in Section 4.5.1, glacier-change temporal studies are inherently complex due to the irregularity and differing accuracies of data records. A new method to maximise the frontal-position data in the AP, while keeping errors to a minimum, resulted in change-rate calculations over

5-year intervals, between 1945 and 2009 (Section 4.5.2). The AP glaciers might be expected to show non-synchronous behaviour due to the mixed population of floating and grounded termini, plus numerous other distinct characteristics. However, spatial patterns and temporal trends have been observed that reveal a regional synchronicity. These can be summarised as follows:

Overall change (Section 5.3.1):

1. There has been overall ice loss since the 1940s and 90.5% of all 860 marine-terminating glaciers have retreated since their earliest records (Section 5.3.1).
2. Primary differences have occurred between the east and west coast: in the east there has been a far greater mean glacier retreat, primarily due to the loss of the large ice shelves (Figure 5.17).
3. A gradient in mean overall ice loss from north to south is present along the west coast (Figure 5.17).
4. Glaciers in a distinct region along the north-west coast (~65° S to the northern tip) have remained stable, or shown small advances, throughout the study period (Figure 5.13 and Figure 5.23).

Temporal trends (Section 5.3.2):

1. There was no clear pattern in retreat until the late 1970s, after which the retreat rates began to increase (Figure 5.21).
2. There was a statistically significant reduction in retreat rates in the late 1980s/early 1990s, observed across a broad range of glacier types (Figure 5.22, Table 5.6).
3. There has been a statistically significant increase in retreat rates since the late 1990s, in all regions except the NW (Figure 5.22, Table 5.6).
4. There has been a southerly migration of increasing retreat rates: glaciers in the W region began retreating in the late 1950s, glaciers in the SW in the late 1960s and glaciers in the SSW in the early 1970s. Glaciers in the W have had small mean change rates throughout, whereas glaciers in the SW and SSW have been retreating at much faster rates, particularly since the late 1990s (Figure 5.25).

Mean differences in area change rates over time have been relatively small, with many glacier fronts defined as 'stable' across several intervals. Over the long-term, however, these trends are significant. The data distribution is suited for interpretation at 5-yearly intervals or longer but, as explained in the methodology in Chapter 4, cannot be considered for short term (i.e. annual) glacier-change analysis.

7.3 Local controls on frontal behaviour

One aim of the study was to establish whether there are particular glacier characteristics that predominate in influencing the patterns of glacier area-changes throughout the region. For example, local glaciological controls may mask any wider regional influence from external controls. The glacier characteristics recorded in this study, namely class-type, basin complexity, frontal-type, basin size, length, geometry, surface elevations, slope and aspect, were therefore assessed alongside the glacier area changes (Section 5.3.1).

Most glacier basin characteristics are strongly inter-dependent and are particularly influenced by the basin area. For example, the data are heavily skewed towards small glaciers: these tend to be short, steep mountain glaciers with low mean elevations, and the majority of these have calving fronts. Large, low-sloping outlet glaciers originating on the plateau are those that tend to have floating fronts. Unsurprisingly these have lost the greatest overall area of ice, but when the influence of glacier size is reduced using relative change, there are no clear differences between glaciers with different characteristics. Multivariate analysis of glacier basin characteristics and area change is not practical (and arguably not profitable), owing to the skewed nature of almost all characteristics and their inter-dependence. The area change results cannot be quantified in such a way as to suit complex analysis alongside characteristics, but a simple test shows that the strongest correlation with absolute overall loss is the outlet width (r_s = +0.56) and with relative overall loss it is mean elevation (r_s = -0.44) (Section 5.3.1). Thus, large (and/or divergent) glaciers that have wide fronts have greater area loss even if there have been minimal changes in their length, and those with a lower mean elevation (e.g. small mountain glaciers) have shown greater change relative to their size.

Although these correlations are statistically significant, they are not strong, which suggests other factors are at play in long-term change. As regards non-scalar characteristics, there are no correlations with overall area change, with the exception of glaciers that have floating fronts; the mean absolute area loss is considerably greater than any other category. The distinct spatial patterns are further evidence that local glacier characteristics are overridden by a wider-regional control.

Overall area change was calculated from first to last recorded positions, which inevitably differs in duration per glacier. Measuring temporal trends, on the other hand, gives a further opportunity to identify disparities in behaviour between glaciers with different attributes. The consistent measure of area change in $km^2 a^{-1}$, calculated in 5-yearly intervals since the 1940s, reveals a comparable trend between glaciers with a wide range of characteristics (Section 5.4). The long-term trend across the AP for all glaciers combined was of largely uniform retreat from the 1940s until the late 1970s, after which there was a statistically significant decrease in retreat rates until the early 1990s, followed by a significant acceleration in retreat. This trend is apparent across many separate variables, with no single predominant glacier characteristic influencing the pattern (Figure 5.25). Since the glaciers are glaciologically distinct yet share similar temporal trends, a common change in external forcing is likely to be driving the area-changes on a regional scale.

7.4 Atmospheric controls on glacier area change

It is well known that the AP has undergone more rapid warming than in any other region in Antarctica (Section 2.3.1). The popular theory that the demise of ice shelves in the region is closely linked to a southerly migration of a thermal limit (Morris & Vaughan, 2003) could also be considered likely to apply to glacier frontal change (Section 2.2.3). It was first suggested that this may not be the case in Cook *et al.* (2005), who noted that the migration from advance to retreat implied a warming more rapid than the maximum seasonal rate of warming and, furthermore, only 75% of the glaciers north of the thermal limit for ice shelves were retreating. This section analyses the new glacier change results

to assess whether it is possible for the regional synchronicity to be related to atmospheric forcing.

7.4.1 Spatial patterns

Chapter 6 (Section 6.2) presented new findings on regional atmospheric patterns derived from several sources: station temperature records; surface-melt from QSCAT satellite data between 2000-09; surface temperatures from infrared satellite imagery between 1980-2008; and surface mass balance between 1980-2009 from modelled data. The main conclusions on mean atmospheric spatial patterns can be summarised as follows (with reference to Figures 6.8 and 6.9):

1. There is a strong peninsula-wide north-south gradient in high-low mean air temperatures observed in all data sources.
2. On the eastern side, close to glacier fronts, the spatial distribution of mean melt duration (MMD) in 2000-09 and mean surface temperature in 1980-2008 are both closely correlated with degrees latitude, i.e. melt duration is shorter and air temperatures are cooler towards the south.
3. On the western side, the north-south air temperature gradient is also present, although with slightly greater variability. Regional means show that mean surface temperatures close to glacier-fronts are highest in the NW and steadily decrease towards the SSW.
4. There is distinctly greater mean surface accumulation along the western side than the east (Figure 6.12).

When these spatial patterns are considered directly alongside regional mean overall glacier change-rates, there are opposing north-south gradients for both MMD (Figure 7.1) and mean surface temperatures (Figure 7.2). These mean temperatures are based on measurements close to the glacier fronts, and yet they seem to have had little effect on glacier front change.

In the west, the mean atmospheric temperature and frontal retreat rates have opposing north-south gradients along the whole coast. Evidently this negative correlation does not

indicate the cause, but these mean values do suggest that atmospheric temperatures are not a strong control on long-term glacier retreat on a regional scale.

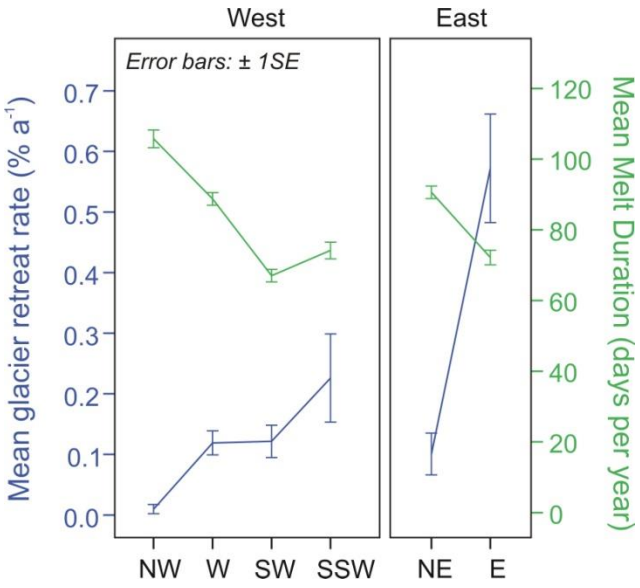

Figure 7.1: Mean melt durations and glacier retreat rates, by Region.
Regional average mean melt durations (days per year) between 2000-09, and mean glacier retreat rates (% a^{-1}) over the same period. The values are associated with individual glaciers: a total of 715 glaciers have MMD values and 263 glaciers have retreat rate calculations between 2000 and 2009.

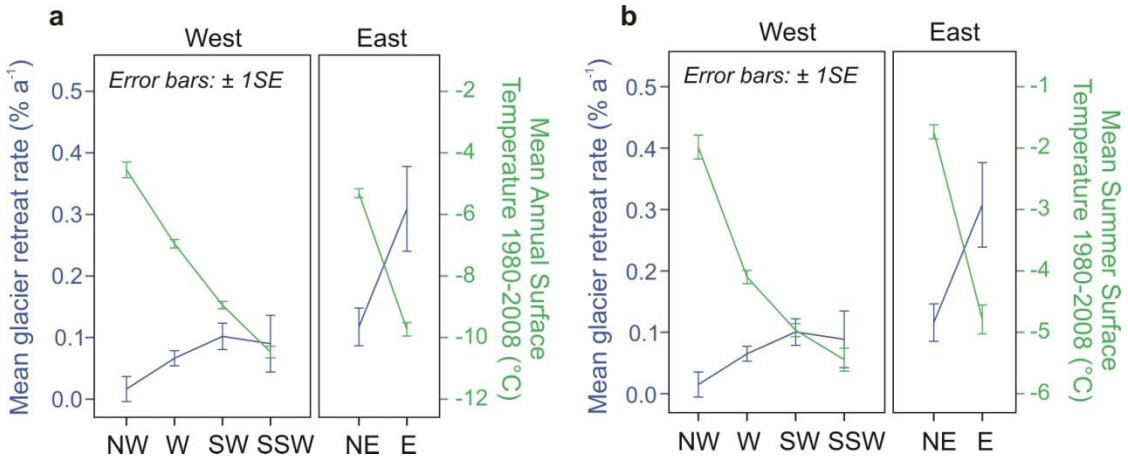

Figure 7.2: Mean surface temperatures and glacier retreat rates, by Region.
Mean surface temperatures between 1980 and 2008 and relative retreat rates over the same period: mean annual surface temperatures (**a**) and mean January-March seasonal temperatures (**b**).

The eastern side has an independent climate regime and yet here too is a negative correlation between glacier retreat rates and surface temperature: the mean surface temperatures in the NE are significantly higher than in the E and yet mean glacier retreat is much lower than in the E (Figure 7.2). In the eastern AP, however, the relationship is complicated by the buttressing effect of ice shelves, resulting in rapid glacier retreat rates after the ice shelves collapsed. The warming atmospheric temperatures in this region are understood to have played a crucial role in these ice shelf break-up events (Section 2.2.3.1) but the direct effect of the atmosphere on the glacier fronts since then is less clear.

The overall peninsula-wide glacier change rates (in % a^{-1}) show little or no correspondence with the MMD (Figure 7.3) or surface temperatures (Figure 7.4). Statistical analyses of trends based on glacier change rates are restricted by the non-uniform scale-distribution of these data. The highly skewed distribution of glacier change rates, and the inclusion of both positive and negative values, has prevented transformation of the data into a meaningful dispersion. Linear regression is usually the best descriptor of the relationship between the variables for normally-distributed data, but in this case non-parametric correlation tests must be used. The Spearman's Rank (r_s) correlation test shows no statistically significant correlations, apart from a small (r_s = -0.187) correlation between glacier change rates in 2000-09 with MMD along the west coast (Table 7.1). This is negative, hence the longer the melt duration the greater the retreat rates. This is only since 2000, however, whereas there are no significant correlations between surface temperatures and glacier changes since 1985.

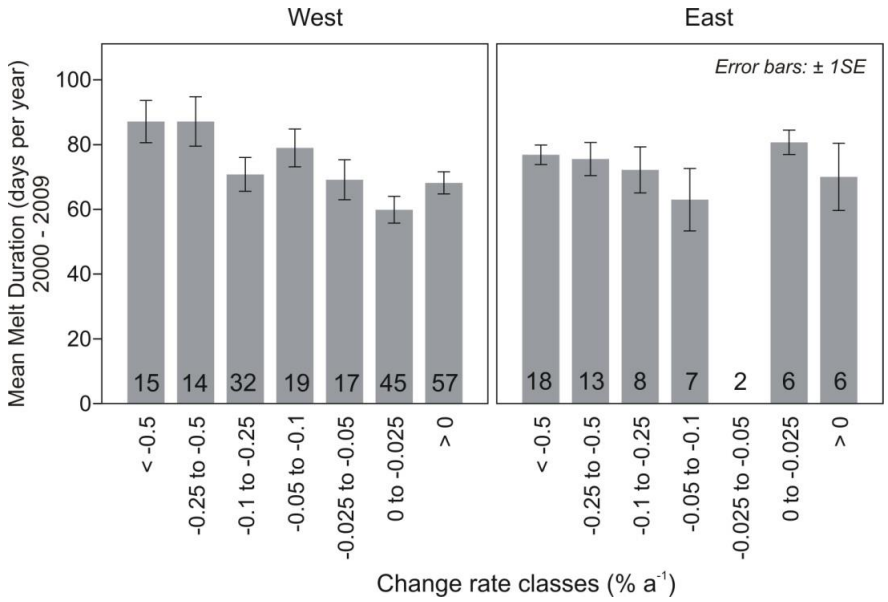

Figure 7.3: Mean melt duration classed by glacier change rates between 2000-09.
The valid numbers of glaciers in each change rate class are shown above the x-axis. In total, 62 glaciers in the east and 201 glaciers in the west have change rate measurements in both intervals 2000-04 and 2005-09.

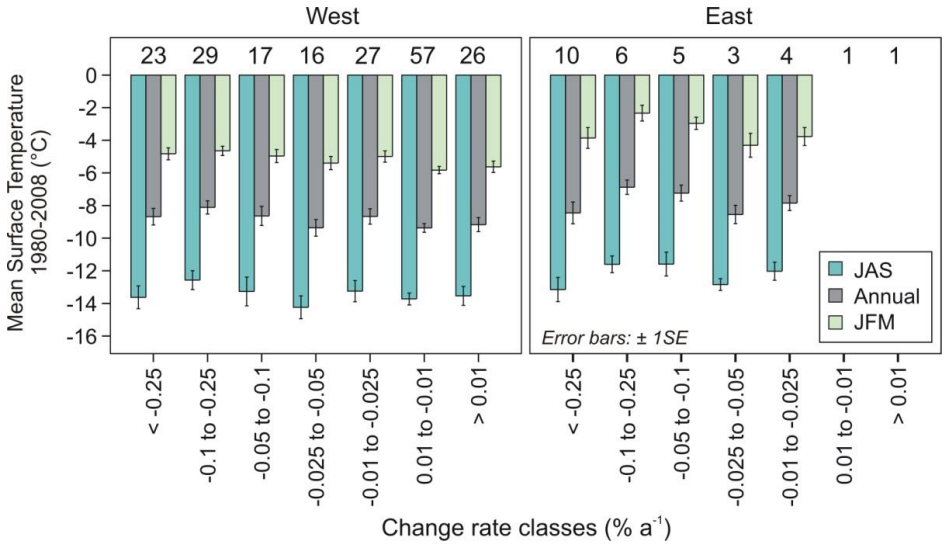

Figure 7.4: Mean surface temperatures classed by glacier change rates.
Mean surface temperatures for glaciers classed by their rates of change between periods 1985-89 and 2005-09. The valid numbers of glaciers in each change rate class are shown along the upper x-axis. The surface temperature values are mean annual, winter (JAS) and summer (JFM).

Table 7.1: Correlations between mean surface temperatures, MMD and glacier change. Spearman's Rank (r_s) correlations for Mean Melt Duration (MMD), Surface Temperature (ST), July-Aug-Sept (JAS) and Jan-Feb-Mar (JFM) with glacier changes rates over the same periods for which there is data: MMD (2000-09) and ST (1980-2008). Glacier count is shown alongside region name. Correlations marked with * are significant at the 0.01 level.

	All: 263	West: 199	East: 62
	r_s	r_s	r_s
MMD	-0.207*	-0.187*	-0.067
Mean ST (Annual)	0.007	-0.042	-0.167
Mean ST (JAS)	-0.083	-0.135	-0.204
Mean ST (JFM)	-0.147	0.072	-0.117

7.4.2 Temporal patterns

The large availability of temporal surface temperature data has enabled analysis of changes over time close to the glacier fronts (Section 6.2.3.3). Regional mean surface temperatures and accumulation were calculated at 5-yearly intervals for all glaciers with these data, and patterns can be summarised as follows (see Figures 6.10 to 6.13):

1. There has been a peninsula-wide increase in surface temperature since the records began in 1980.
2. Regional average surface temperatures close to glacier fronts have steadily increased at comparable rates.
3. There was a slight cooling in the interval 1990-94, in all regions.
4. The period 1995-99 had above average temperatures throughout the AP.
5. Increase in mean surface temperatures in the NW, NE and E has decelerated since 2000-04 whereas further south, temperatures have continued to rise.
6. There have been no statistically significant regional trends in surface mass balance although, most notably, it was almost universally high in 1995-99.

Comparisons alongside changes in mean glacier change rates (% a^{-1}) reveal opposing regional trends with mean annual and summer surface temperatures (Figure 7.5). Glaciers in the western side of the AP have regionally distinct trends; for example, glaciers in the NW have shown minimal change since the 1980s, and there are consecutively greater scales of retreat towards the south (Figure 7.5a). Equal but opposite

to this are the mean annual and summer surface temperatures, which have consecutively cooler regional temperatures from north to south (Figure 7.5b). The same pattern is true for the eastern side. Mean surface temperatures remain below 0 °C in all regions both annually, and in summer-only, for all epochs. These values do not indicate whether or not melt takes place (since PDD values are the only true measure of surface melt) but they indicate regions in which melt is more likely to have occurred. Hence, surface melt close to ice fronts is most likely to have occurred in the NW and NE, and yet these two regions have the lowest retreat rates in all intervals.

Regarding temporal anomalies, surface temperature anomalies from the mean indicate that annual temperatures were lower during the interval 1990-94 in all four regions in the west, and in both regions in the east (Figure 7.5c). This is not apparent in the summer temperatures. This decrease in temperature is negligible, however, and does not alter the gradual increase in temperatures that takes place in all regions, or the overall distinct regional differences (Figure 7.5b). The universal increase in surface temperatures from 1995-99 onwards occurred at the time when glacier retreat increased in most regions, although this association does not occur in the NW. The increase in surface temperature was not significantly greater than the mean and it would therefore have minimal impact in regions where the mean summer temperatures are well below 0 °C.

The temporal trends in SMB are not straightforward and no statistically significant regional long-term trend has occurred. Much variation has occurred across the temporal intervals, but one epoch in which surface accumulation was universally greater than the mean was during the late 1990s. This is not reflected in the glacier-front changes at this time when, in fact, retreat rates were increasing.

The conclusion from these results is that there are no spatial or temporal patterns that suggest that atmospheric forcing is having a regional impact on glacier front changes. The regional synchronicity that is taking place in AP glacier front behaviour therefore cannot be interpreted as simply as the atmospheric thermal limit of viability that exists for ice shelves.

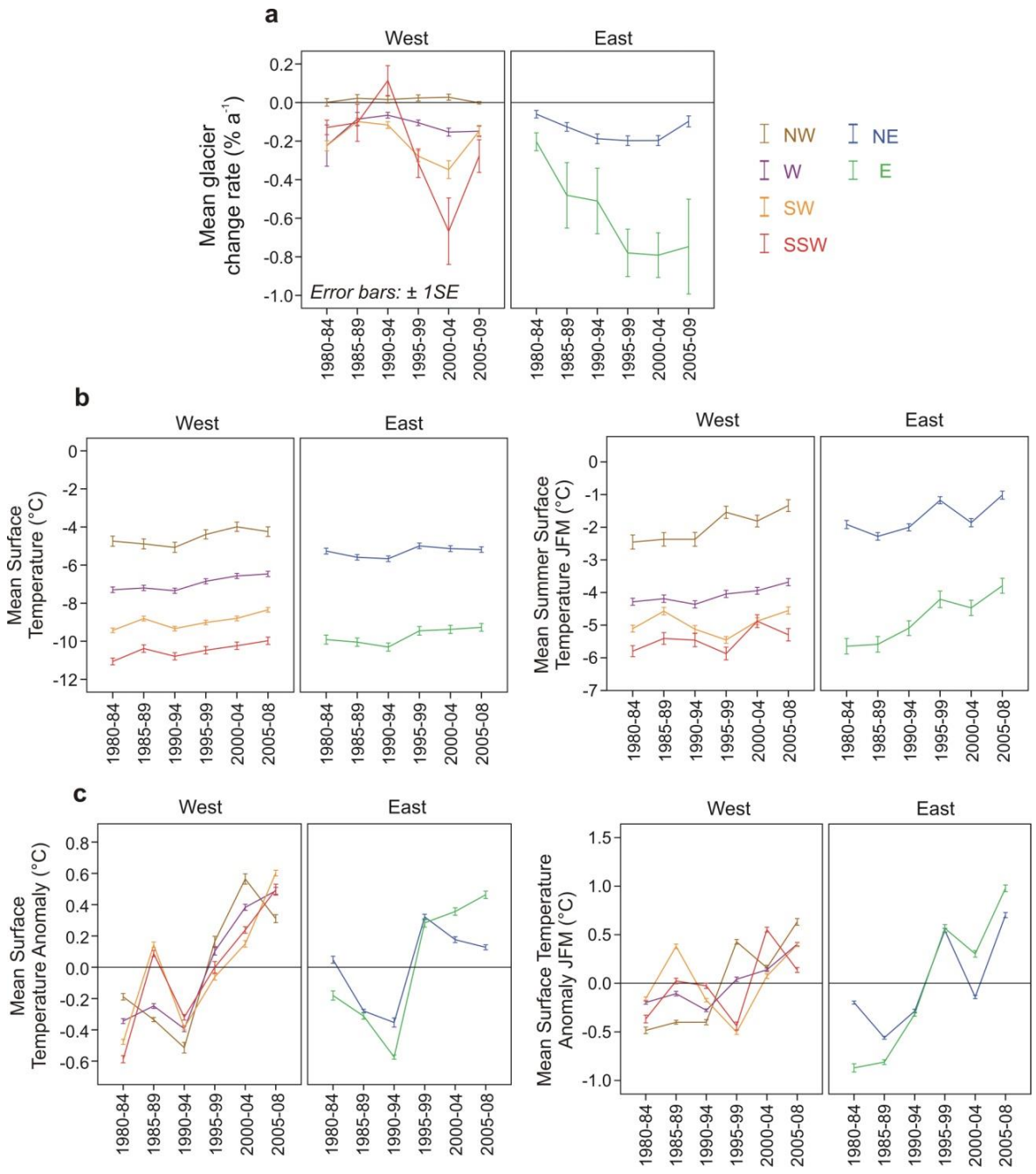

Figure 7.5: Temporal patterns for glacier change rates and surface temperatures.
Glacier change rates in 5-yr intervals from 1980-84 to 2005-09 (**a**) and changes in mean surface temperatures over the same time period (**b**). Anomalies from the mean surface temperatures show periods that are cooler/warmer than the average (**c**). Surface temperature measurements are within 5-km of glacier fronts and are the mean values for all glaciers in each region. Error bars are ± SE.

7.5 Ocean temperature controls on glacier area change

The question of ocean temperatures being a principal driver of glacier front change is addressed by first summarising the main findings from Chapter 6 (Section 6.3) on spatial and temporal patterns in ocean temperatures. These results are then tested in relation to glacier-changes by addressing the following questions:

- What are the ocean depths and temperatures like close to the ice fronts?
- How well does the spatial distribution of overall long-term glacier front change correlate with regional mean ocean temperatures?
- Are short-term rates of glacier change synchronous with temporal changes in ocean temperature?

7.5.1 Wide-scale patterns in ocean temperature

East and West:

1. Primary differences in mean ocean temperature have been between the oceans to the east and west of the AP: the waters at all depths off the east coast have been cooler than those to the west (Figure 6.17; Figure 7.6).
2. The mean (1945-2009) ocean temperatures to the west of the AP increase rapidly with depth, to a maximum of +0.72 °C at 300 m. To the east, there is a slight increase with depth to a maximum of -1.06 °C at 500 m (Table 6.4).
3. To the west, mean ocean temperatures are above the pressure melting point of ice (T_m) at 150 m depth and deeper; to the east, water is cooler than the T_m at all depths (Figure 6.18).
4. There has been a statistically significant overall increase in ocean temperature surrounding the AP, although the correlation is weak (r_p = 0.258). The correlation is dominated by an increase in deep (<= 150 m) ocean temperature on the western side (r_p = 0.462) (Table 6.6).

The oceans to the east and west of the AP have distinct oceanic regimes, separated by the barrier of the AP landmass. The eastern side is dominated by cold deep waters

originating from the Weddell Sea sub-polar Gyre, whereas the western sea is fed from the south by the Antarctic Circumpolar Current (Section 2.3.2). The Weddell Sea has remained well below the pressure melting point of ice throughout the period of interest in this study and so is not considered further in relation to glacier front changes.

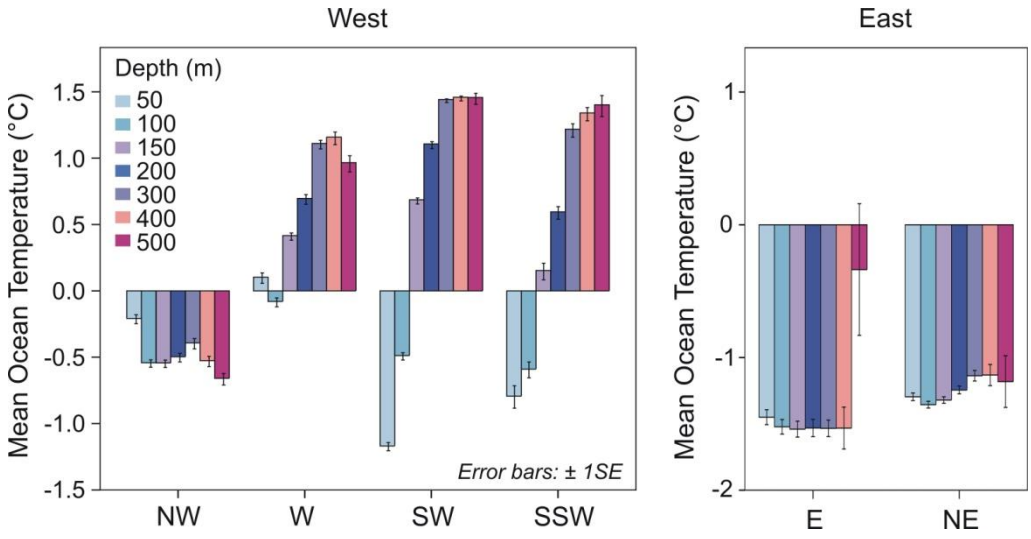

Figure 7.6: Regional mean ocean temperatures.
Mean (1945-2009) ocean temperatures at each depth across regions up to 100 km from the coast. The region mean values are based on measurements averaged onto 5 km grids for each depth.

The western ocean temperatures however are substantially warmer and are now considered in more detail.

Western regions:

1. In the west, there is a clear north-south gradient from cool to warm water, which becomes enhanced with increasing depth (Figure 6.18).
2. Water in the NW region remains below the T_m at all depths. There has been little overall change since the 1950s (Figures 6.16, 6.18) but there has been a weak warming trend since the 1990s (Table 6.6).
3. Regions further south have cool shallow ocean temperatures, but temperatures rise above the T_m at 150 m and below; there are significant (although weak) temperature increases since the 1950s, particularly in the W and SW (Figure 6.19, Table 6.6).

4. There has been an increase in the rate of deep water warming between 1995-99 and 2005-09 in the NW, W and SW. In the SSW there are too few measurements prior to the 2000s for valid comparisons to be made (Figure 6.19, Table 6.6).
5. The greatest increase in ocean temperatures occurred at mid-depths (100-200 m) in the SW region between the 1990s and 2000s (Figure 6.22, Table 6.8).

7.5.2 Coastal bathymetry and near-shore ocean temperatures

The mean (1945-2009) ocean temperature pattern to the west of the AP can be displayed using isobathytherms: although temperatures are mixed at shallower depths, the spatial differences in temperature become more distinct at depths of ~200 m and the distribution remains similar below this depth. The isotherms at 300 m depth and the overall change rates for all glaciers show a clear regional unity (Figure 7.7). The distinct cool ocean region in the NW has a close spatial correspondence with the region of stable/advancing glaciers. This stretches from the northern tip of the AP southwards between the mainland and Brabant and Anvers Islands (Figure 2.1), to approximately 65° S. The spatial correlation is apparent on a wide regional scale, but it is necessary to establish whether the glacier fronts are exposed to these waters.

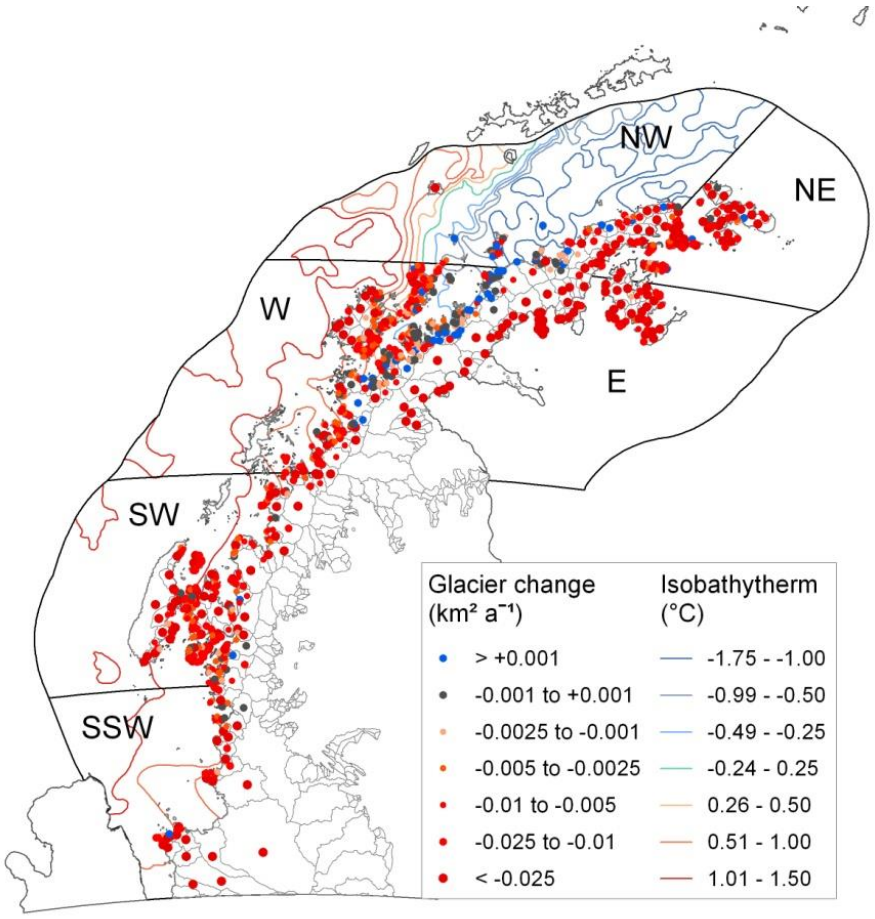

Figure 7.7: Ocean temperatures and overall glacier change: spatial patterns.
The cold water region in the north-west was distinct at all depths: isotherms at 300 m depth show the spatial similarity between mean ocean temperatures at -0.25 C and glaciers that have shown overall advance or stability.

As discussed in Chapter 6 (Section 6.3.4), ocean temperature measurements close to shore are limited, but interpolated grids allow mean temperatures to be calculated within 5 km of the glacier fronts. When mean ocean temperatures closer to shore are plotted, the patterns observed in ocean temperatures up to 100 km offshore (Figure 7.6) are maintained (Figure 7.8). Within 5 km of the glacier fronts, the mean ocean temperatures show a similar spatial pattern to the wide regional pattern although glaciers in the NW and W regions have cooler mean temperatures (since warmer water to the west is excluded) (Figure 7.8a). The mean temperatures remain much the same when glaciers with a bathymetry measurement below 400 m in depth are considered independently (Figure 7.8b).

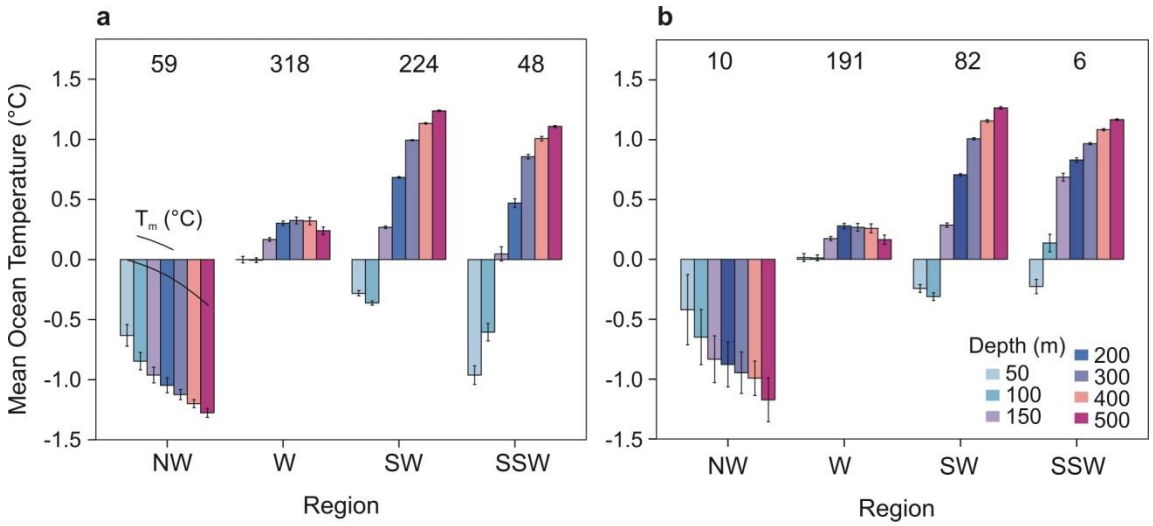

Figure 7.8: Regional mean ocean temperatures, close to shore (west coast).
Ocean temperature graphs: mean temperatures (1945-2009) within 5 km of glacier fronts. Mean temperatures for all glaciers (**a**), and for only glaciers with bathymetry measurements deeper than 400 m within 5 km of their fronts (**b**). The mean values are calculated from interpolated grids from all available temperature values. Mean temperatures for glaciers in the NW are all below the Pressure Melting Point (T_m). The numbers of glaciers contributing to the mean are along the upper x-axis on both graphs.

Chapter 6 (Section 6.3.2) explains that bathymetry measurement coverage close to glacier fronts is far from comprehensive: 74% of glaciers have a measurement within 5 km of their fronts, 45% within 2 km and 30% within 1 km (Table 6.2). These glaciers have a wide spatial distribution and calculations show that the minimum depths for these glaciers are -511, -386 and -321 metres within 5 km, 2 km and 1 km, respectively. Taken further, glacier counts reveal that 81% of all glaciers with more than two bathymetric measurements have minimum depths of 200 m or below within 1 km of their fronts (Table 6.3). From these results it cannot be inferred with certainty that water at these depths directly reaches the ice interface. However, these are the most detailed bathymetric data available and give the best insight as to depths close to the glacier fronts.

The presence of numerous bathymetric troughs extending from the coast to as far as the edge of the continental shelf strengthens the hypothesis that deep ocean waters reach coastal regions. These palaeo-ice streams (discussed in Chapter 2 – Section 2.2.1) are sufficiently deep to allow south-eastwards passage from deeper ocean regions (such as Bransfield Strait) towards the mainland. One such passage is the strait between Brabant

and Anvers Islands (Figure 2.1). Many glaciers are situated where these deep troughs extend from the mainland, where depths reach below 500 m close to the coast.

Ice thickness data at the ice fronts are uncertain and, until these become available, grounding line mapping remains approximate. In the present study, further analysis of interactions between ocean temperature and ice fronts is based on the hypothesis that water at 200 m or below does reach the majority of ice fronts on a broad regional scale. Detailed analysis on glacier front change and ocean temperatures on a more local scale however would require precise bathymetric and ice thickness data, which are currently available for only a few glaciers.

7.5.3 Correlations between ocean temperature and overall glacier change

Spatial patterns have revealed similarities between mean ocean temperatures and long-term glacier area change. Further tests can be undertaken to determine how well they are correlated, i.e. are mean ocean temperatures (1945-2009) directly related to the scale of change?

Whereas glacier changes showed little or no correspondence with the atmospheric surface temperatures (Figure 7.4), a clear correlation with west AP ocean temperatures is observed (Figure 7.9). The mean ocean temperatures are based on measurements acquired throughout the study period (1945-2009). Glaciers that have retreated the most have the highest mean ocean temperatures near their fronts, and glaciers that have remained stable or advanced have the coolest mean ocean temperatures. There is a steady gradient between the two extremes. This correlation is independent from the spatial distribution along the AP.

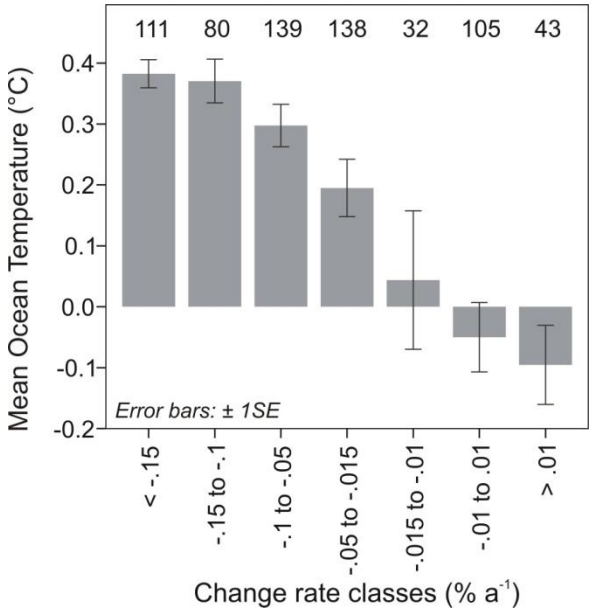

Figure 7.9: Mean ocean temperatures classed by glacier change rate.
Mean (1945-2009) ocean temperature within 5 km of glacier fronts classed by glacier change rates (west coast glaciers). Ocean records are from measurements spanning between 1945 and 2009 and glacier change rates are from earliest to latest records per glacier. The valid numbers of glaciers in each change rate class are shown along the upper x-axis.

When temperatures at each depth are segregated, the relationship becomes plainer still (Figure 7.10a). The largest retreat category has the highest ocean temperatures at all depths below 100 m. Temperatures at all depths from 150 m and below display the same correlation with change rates: highest temperatures correlate with greatest retreat, and *vice versa*. At the two shallowest depths (50 m and 100 m) there is no relationship with change rate classes, suggesting that water at these depths has had little impact on melt at the glacier fronts. A further test is where only glaciers with a minimum bathymetry of deeper than 400 m are considered (Figure 7.10b). Greater certainty that deep water reaches these 299 glaciers means that the results are more robust: the same trend is observed, with only small differences present in the two shallow water categories.

The relationship may be heavily influenced by one region more than another, and so the regions can be considered independently. This is restricted by the number of glaciers within each change rate category however; only the W region has a sufficient number of glaciers within each change rate category for an even comparison of temperatures at each depth.

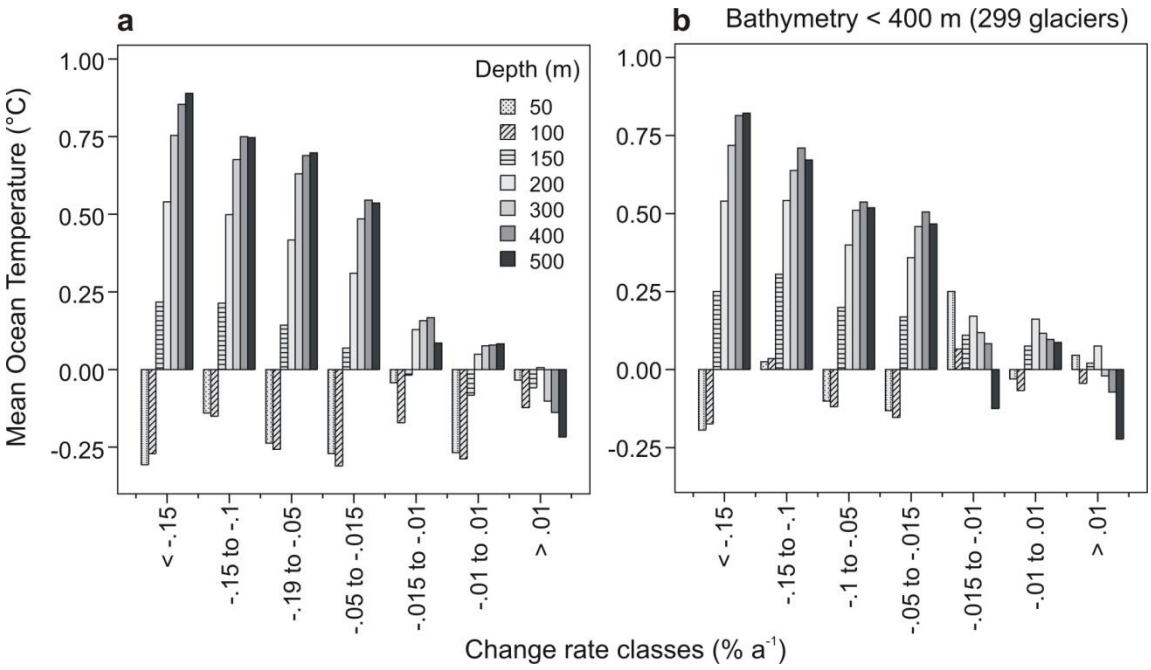

Figure 7.10: Same as Figure 7.9, separated by depth.
Mean ocean temperatures at each depth (within 5 km of glacier fronts) are shown in each change rate class (**a**). The same figure is shown for only glaciers with depths lower than 400 m within 5 km of their fronts (**b**).

If the other regions are grouped there is a good distribution across all categories. The results for the W region show the presence of a correlation between change rate and ocean temperature, although the trend only becomes clear at depths of 300 m and below (Figure 7.11a). The other regions combined, on the other hand, show the correlation is strong at depths of 150 m and below (Figure 7.11b), with a greater scale of mean temperatures at each depth than in the W region, in all change-rate categories. These regional differences suggest there may be additional spatial controls on the scale of retreat, but the correlation with ocean temperatures remains present.

So far, only relative change rates have been considered, since the hypothesis is that ocean temperature is the primary control for glacier area change rates rather than total area of ice loss. If absolute area loss is considered, the correlation can also be seen (Figure 7.12a and b). In this case, the distinction between temperatures at particular depths is less clear, but the correlation is present at 150 m and below in the W region (Figure 7.12a). The gradient is less apparent in the grouped regions (Figure 7.12b) due to the difference in scale between cool temperatures shallower than 150 m in all change rate categories, and

warm temperatures deeper than 300 m. The absolute change rate per glacier is strongly dependent on the basin size and yet the correlation with ocean temperatures still exists.

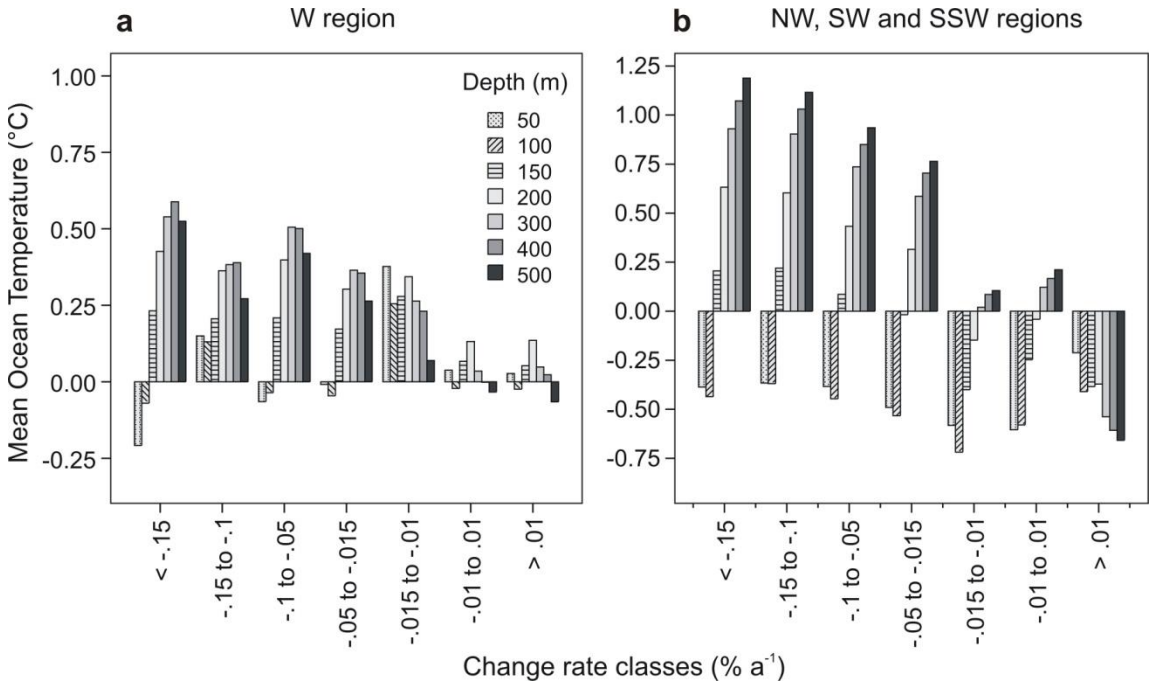

Figure 7.11: Mean ocean temperatures classed by glacier change rate, for separate regions. Mean ocean temperatures at each depth (within 5 km of glacier fronts) by relative change rate classes (% a^{-1}) for glaciers within the 'W' region (**a**) and NW, SW and SSW regions combined (**b**).

As explained in Section 7.5.1, the skewed nature of the glacier change rates prevents linear regression analysis, but when the data are tested by rank order, they reveal strong correlations. Spearman's Rank (r_s) correlation between relative change rates and mean temperatures becomes stronger with depth: there is no correlation at 50 and 100 m, but at 150 m and deeper, the correlations are statistically significant (at <0.01) (Table 7.2). The correlation strengthens from -0.28 at 150 m, to a maximum of -0.4 at 400 m. This corroborates the results where ocean temperatures were shown to have a gradient across change-rate categories (Figures 7.10 to 7.12). The correlations are negative, meaning the warmer the ocean temperatures the greater the retreat rates. The conclusion can be made therefore that glacier area change rates have a significant correlation with mean ocean temperatures at 150 m and deeper, which becomes stronger with depth.

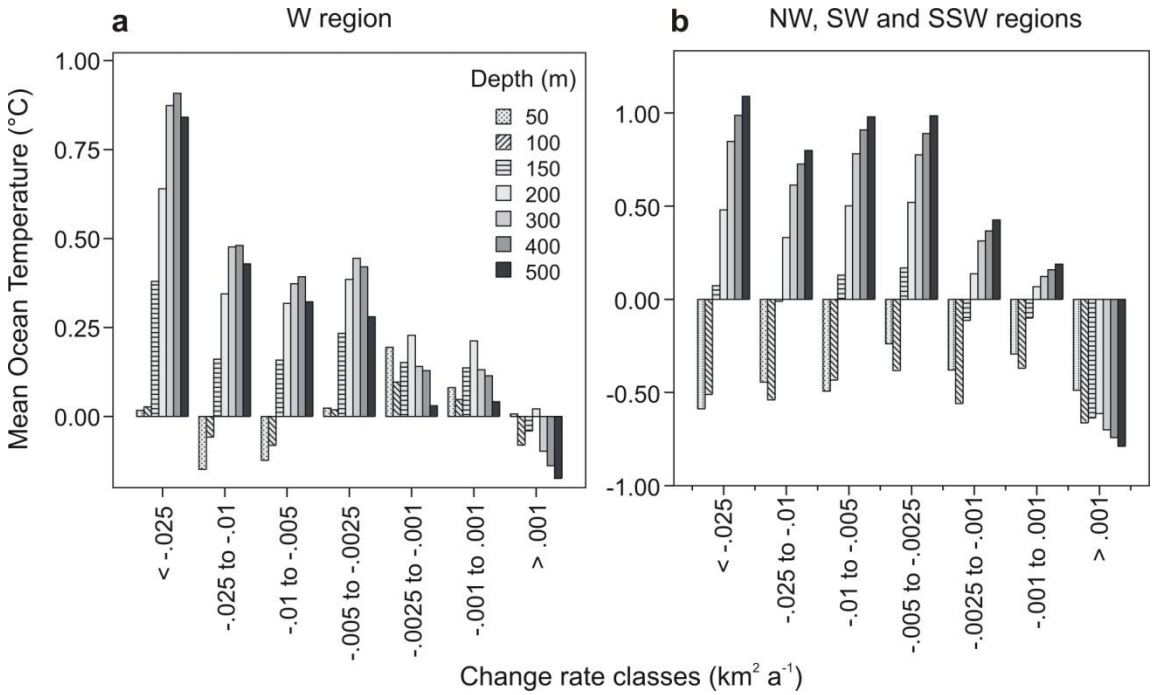

Figure 7.12: Same as Figure 7.11, for absolute area change rates ($km^2\ a^{-1}$).
Mean ocean temperatures at each depth (within 5 km of glacier fronts) by area change rate classes ($km^2\ a^{-1}$) for glaciers within the 'W' region (**a**) and NW, SW and SSW regions (**b**).

Table 7.2: Correlations between ocean temperatures and glacier change rates.
Spearman's Rank (r_s) correlations between mean relative change rates and mean ocean temperature at each depth. Correlations marked with * are significant at the 0.01 level.

Western AP: 648 glaciers

Depth	r_s
50	0.099
100	0.037
150	-0.277*
200	-0.359*
300	-0.383*
400	-0.402*
500	-0.391*

The r_s values, when separated by region, show that this correlation is true in the W and SW regions, but there is no significant correlation in the NW or SSW (Table 7.3). It is likely that the results for these regions are affected by the small range of ocean temperatures at each depth; for example, temperatures in the NW are cool at all depths, and in the SSW the deeper ocean temperatures are warm throughout the region. The correlation results are therefore most meaningful when applied to glaciers across the whole region, with a wide range of glacier change rates and temperatures at each depth.

Table 7.3: Same as Table 7.2, by Region.
Spearman's Rank (r_s) correlations between mean relative change rates and mean ocean temperature at each depth, by region. Glacier count is shown alongside region name. Correlations marked with * are significant at the 0.01 level.

	NW: 59	W: 317	SW: 224	SSW: 48
Depth	r_s	r_s	r_s	r_s
50	0.127	0.099	-0.012	0.03
100	0.115	0.003	-0.006	0.238
150	0.176	-0.285*	-0.071	0.24
200	0.201	-0.359*	-0.244*	0.211
300	0.098	-0.339*	-0.203*	0.308
400	0.067	-0.363*	-0.222*	0.182
500	0.05	-0.357*	-0.184*	0.274

7.5.4 Temporal synchroneity of ocean temperature and glacier change rates

7.5.4.1 Western AP temporal patterns

Results have shown that, along the western AP, long-term glacier area changes have a significant correlation with ocean temperatures at 150 m and deeper. The mean ocean temperatures (1945-2009) are below the pressure melting point of ice at 50 and 100 m, and rise above it at 150 m and below, corroborating the theory that the 'deep' ocean is driving glacier front retreat. This is further strengthened by the results for the distinct region in the NW, where glaciers have shown minimal frontal change and the mean ocean temperatures (1945-2009) at all depths are below the melting point.

These results suggest that the ocean is a strong driver of frontal change over the long-term. A subsequent question is whether ocean temperature fluctuations also control glacier area change over the short term. Chapter 5 (Section 5.3.3) presented glacier change rates in 5-yearly intervals and one principal finding was a shift towards greater rates of retreat from 1995-99 onwards, visible in all coastal regions except in the NW (summarised in Figure 7.13). This pattern is the same for both absolute and relative change rates. Furthermore, there was a universal reduction in glacier retreat in the late 1980s/early 1990s and a southerly migration of retreat rates (summarised in Figure 7.14a). The main questions to address therefore are whether ocean temperatures at 150 m and deeper have: a) warmed significantly since the late 1990s; b) universally cooled during the late 1980s/early 1990s; c) whether there is a southerly migration in warming ocean temperatures; and d) remained below the T_m in the NW region throughout the study period.

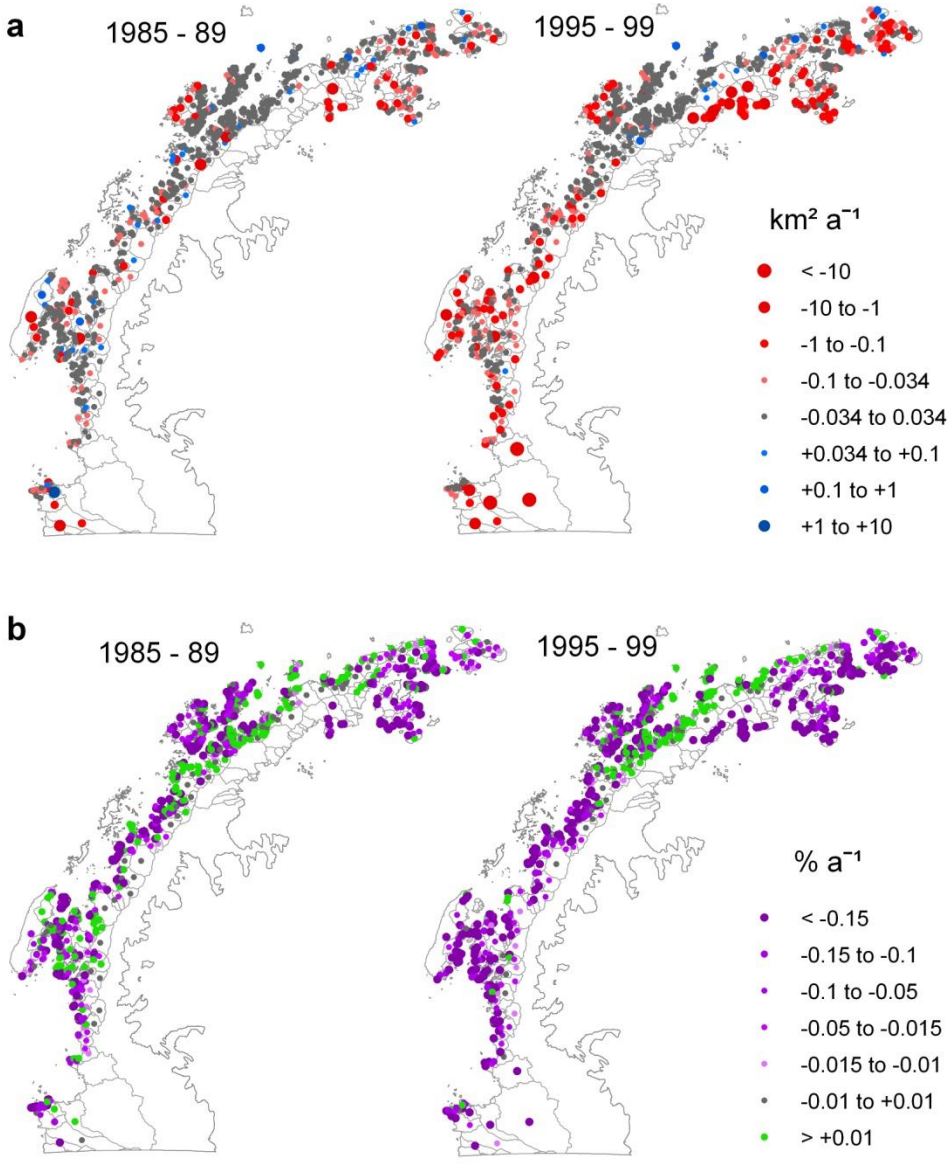

Figure 7.13: Spatial distribution of glacier change rates in 1985-89 and 1995-99. Change rates in $km^2\ a^{-1}$ (**a**) and $\%\ a^{-1}$ (**b**), for two time periods. The spatial distribution of those in retreat shifts and by 1995-99 almost all glaciers are in retreat, except for those along the north-west coast, which remain stable throughout.

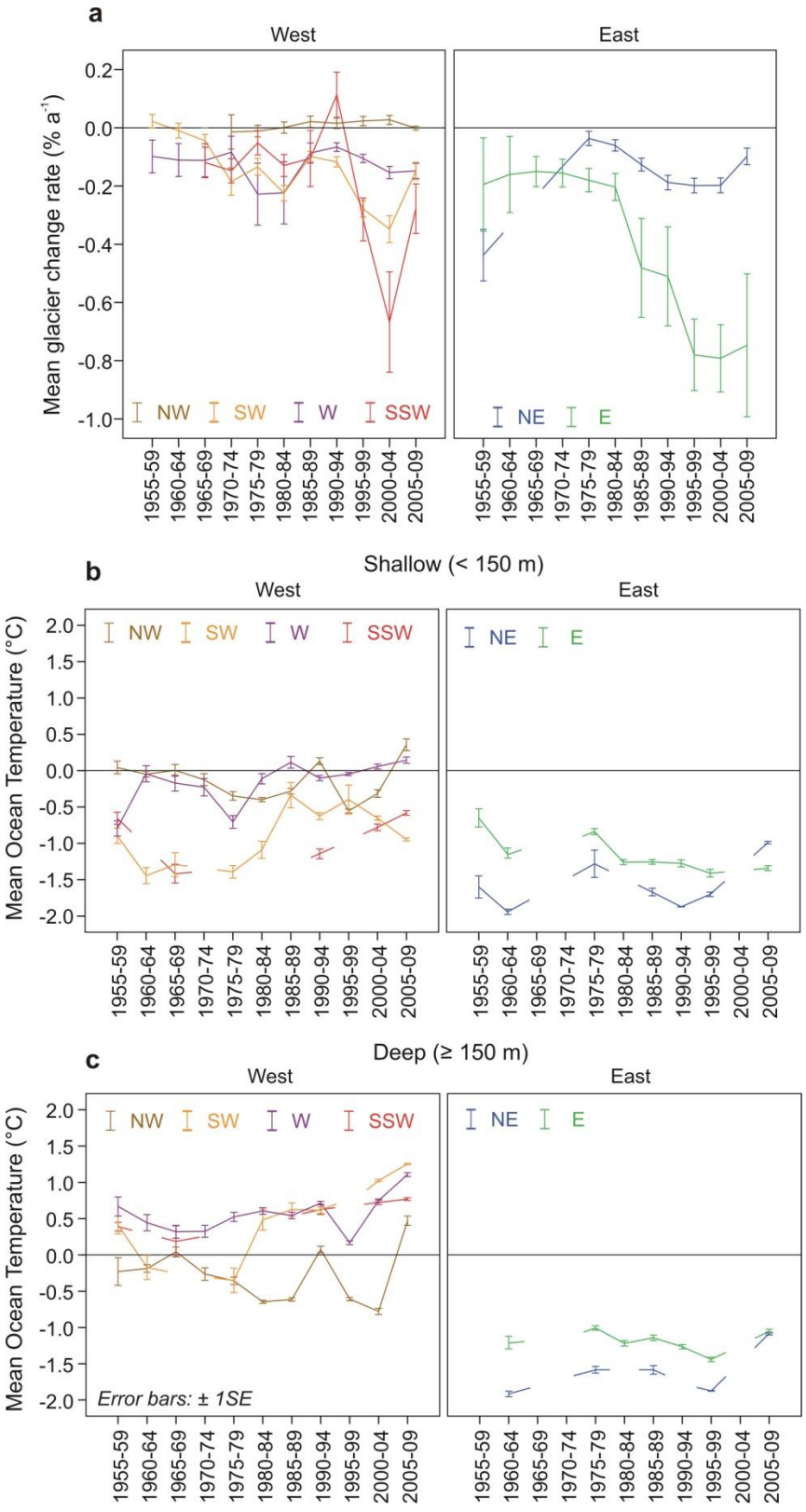

Figure 7.14: Temporal patterns for glacier change rates and ocean temperatures.
Mean deep/shallow ocean temperatures across 5-yearly intervals since 1955-59, by Region. Error bars are ± SE.

The ocean temperature results presented in Chapter 6, showed no statistically significant trend in shallow (i.e. 50 m and 100 m) water temperatures since 1945 (Figure 7.14b and Table 6.6) and these have remained close to or below the pressure melting point throughout. The deep ocean temperatures in the NW have indeed remained below or close to the T_m since the 1950s, until 2005-09. In the W and SW regions the deep ocean has a statistically significant increase in temperature over time, but the r^2 of 0.061 and 0.129, respectively, show there is much variation in the data and therefore the trend is weak (Figure 7.14c and Table 6.6).

Regarding the universal reduction in glacier retreat rates in the late 1980s/early 1990s, there are too few ocean measurements between neighbouring time periods to identify significant temperature differences. Mean regional values show there may have been a period of cooler ocean temperatures during the late 1990s in the W region (Figure 7.14c). However, there are insufficient ocean data during the late 1990s in the SW and SSW regions to determine whether this temperature decrease occurred universally and whether this trend was significant.

A greater number of measurements in recent years mean that confidence in results since the late 1990s is markedly improved. These data reveal a steeper increase in mean deep ocean temperatures in all regions to the west of the AP between the late 1990s and 2009 (Section 6.3.3.2) (Figure 6.22 and Figure 7.14c). Temperature differences between repeat measurements in the W and SW confirmed this to be the case, particularly at depths between 100 and 200 m (Figure 6.23). An increase in glacier retreat rates has occurred throughout the AP since the late 1990s (except in the NW) so there is a concurrence with mean deep ocean temperatures for this period. Deep ocean temperatures in the NW region have remained below the T_m until 2000-04, after which it has risen above the T_m. There was no corresponding change in glacier area in 2005-09 (Figure 7.14c) but is possible that greater retreat may have occurred since then.

7.5.4.2 Sample region temporal patterns

The mean ocean temperature calculations over time have so far been based on all measurements up to 100 km offshore. The calculation of temperature changes close to glacier fronts presents a greater challenge. Although interpolated grids enabled spatial analysis of temperatures at each depth close to the glacier fronts, these were mean values of all measurements between 1945 and 2009. Measurements become significantly sparser when separated into time intervals, particularly prior to the 1990s, meaning that interpolating data on a time interval basis is not a viable option.

The W region contains a greater number of measurements close to the shore than other regions, but even so, temperatures cannot be assigned to individual glaciers for meaningful results (Figure 7.15). The region contains a wide range of temperature measurements at each depth and straddles the boundary between the cold water to the north and warm water to the south. There are too few temperature measurements close to shore in the southern section however to make analysing the impact of short-term change on each side of the boundary viable. More temperature measurements close to shore are key to further research on short-term trends.

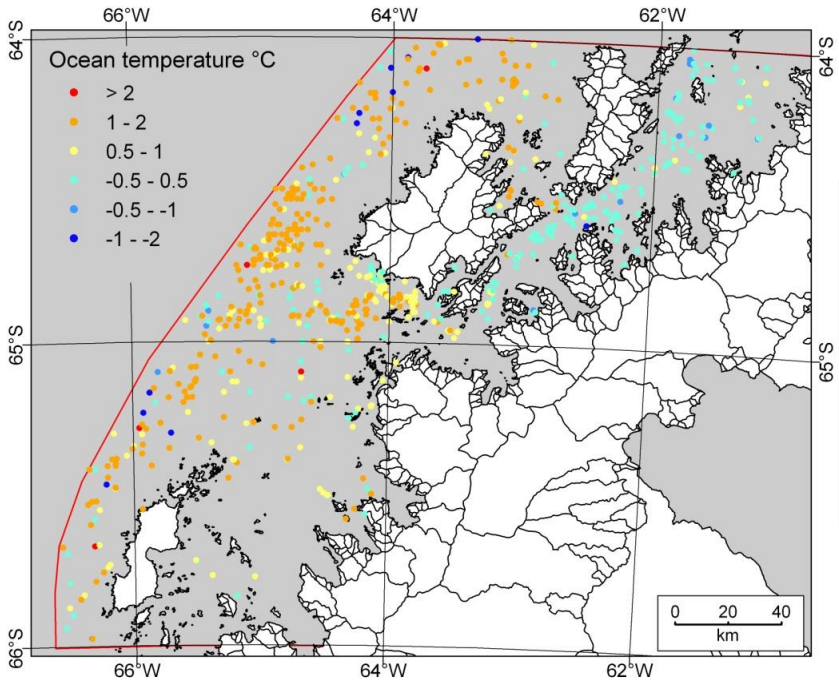

Temperature Measurement Count

	< 150 m	≥ 150 m
1960-64	28	23
1965-69	41	29
1970-74	22	21
1975-79	12	14
1980-84	40	65
1985-89	39	72
1990-94	191	175
1995-99	282	436
2000-04	228	349
2005-09	169	240

Figure 7.15: Sample region – illustrating ocean temperature data spatial distribution.
All ocean temperatures in the W Region, constrained to within approx. 30 km of the coast.

7.6 Glacier-Ocean interactions in the Antarctic Peninsula

This study has revealed that along the western edge of the AP, the glacier front changes have a clear correlation with ocean temperatures. A spatial pattern has emerged showing a distinct region in the NW where glaciers have remained stable or advanced, and deep ocean waters are below the pressure melting point of ice. A statistically significant correlation is present throughout the rest of the western AP between glacier change rates and ocean temperatures at depths at and below 150 m. Furthermore, there has been a shift towards greater glacier retreat since the 1990s, alongside an increase in ocean warming. The implication is that the ocean temperatures are outweighing the atmospheric control factors on glacier-front changes along the western AP.

The theory that ocean temperatures are having a significant impact on glacier behaviour on the AP has not been addressed before and requires a more in-depth discussion. This section first discusses existing knowledge on ice-ocean interactions in West Antarctica, where a strong coupling between ocean temperature and ice front changes has been found. The new findings are then discussed in this context, followed by conclusions on the likely causes of the warm ocean temperatures and the implications for glaciers this region.

7.6.1 Ice-Ocean interactions in West Antarctica

7.6.1.1 Amundsen Sea Embayment

One of the most popularly researched regions in Antarctica in recent years is the Amundsen Sea Embayment (ASE), which drains one third of the West Antarctic Ice Sheet and contains glaciers that are among the fastest flowing in Antarctica (Rignot *et al.*, 2011a). The region has been considerably out of balance since the first satellite radar interferometry measurements in the 1990s (Rignot, 1998). The glaciers have been accelerating and thinning, and their grounding lines have been retreating at a rate of 1 km a^{-1}, one of the fastest retreat rates in the world (MacGregor *et al.*, 2012; Mouginot *et al.*,

2014; Rignot *et al.*, 2014). Mass flux measurements from all the glaciers in the ASE were recently combined, using Landsat feature tracking and satellite radar interferometry, spanning the past 41 years (Mouginot *et al.*, 2014). It was found that the total ice discharge has increased by 77% since 1973, and half of this increase occurred between 2003 and 2009. Further papers published recently state that the grounding lines of the six principal glaciers in the ASE retreated between 1992-2011 and show no sign of abating (Rignot *et al.*, 2014), and that early-stage collapse has begun (Joughin *et al.*, 2014).

It is now widely acknowledged that the intrusion of warm Circumpolar Deep Water (CDW) onto the West Antarctic continental shelf causes increased melt rates at the base of these glaciers and ice shelves, a retreat of ice sheet grounding lines and increased ice sheet discharge (e.g. Rignot & Jacobs, 2002; Shepherd *et al.*, 2004; Pritchard *et al.*, 2009; Pritchard *et al.*, 2012; Rignot *et al.*, 2013). The oceanic influence on the Amundsen Sea ice shelves is determined by the properties and circulation of the CDW that floods the network of deep, glacially carved troughs (Jenkins *et al.*, 2010). Upper water column properties indicate that the CDW flowing into the sub-ice shelf cavities are responsible for the high melt rates. Indeed, a general ocean circulation model predicts that total ice shelf basal melt increases quadratically as the ocean close to the ice front warms (Holland *et al.*, 2008).

The Abbot Ice Shelf, to the east of the ASE, produces a large volume of meltwater and the presence of warm CDW and thermocline waters beneath the ice shelf have recently been inferred (Cochran *et al.*, 2014). A trough extends across the continental shelf, allowing southward passage of warm deep water. The CDW was detected at depths below 400 m, and the overlying thermocline is > 1 °C above freezing at depths up to ~200-250 m (Cochran *et al.*, 2014). At these depths, water has access to and from the ice shelf cavity, and can rapidly melt thicker inflowing ice. At the far west side of the WAIS, ocean variability is also contributing to the basal melt rate near the ice front of Ross Ice Shelf, where a strong annual cycle has been related to seasonal provision of warm water to the ice base (Arzeno *et al.*, 2014).

Ice shelf melt rates around Antarctica are highly heterogeneous, ranging from ~0.1 m a^{-1} for the large ice shelves to >10 m a^{-1} for some of the small ice shelves in the ASE. These

large values occur where the warm CDW intrudes across the ice shelf and then under the ice shelves (Pritchard *et al.*, 2012). Small melt rates occur where thermal forcing is small (i.e. the water is cold) and other sources of ocean currents such as tides become important (e.g. Mueller *et al.*, 2012). This is the case for the Larsen Ice Shelf along the eastern AP.

7.6.1.2 Bellingshausen Sea

To the east of the Amundsen Sea (AS) lies the Bellingshausen Sea (BS), which extends from Abbot Ice Shelf along the west side of the Antarctic Peninsula (location in Figure 2.6). Oceanographically the BS is similar to the AS and markedly different from other embayed seas around Antarctica (Holland *et al.*, 2010). The BS continental shelf is flooded by CDW, which originates from the Antarctic Circumpolar Current (ACC), and the temperature maximum occurs at the depth of the shelf break. The north-easterly flow of the ACC means that pulses of warm CDW appear centred on bathymetric depressions in Marguerite Bay and in the many smaller troughs that occur further north (Holland *et al.*, 2010). The oceanographic setting of the western AP is described in more detail in Section 2.3.2.1.

A number of recent studies concur that the ice shelves in the south-west AP show evidence of increasing basal melt. A study based on satellite radar altimetry missions between 1978 and 2003 showed that all ice shelves on the AP showed a net surface lowering, but the fastest rates occurred close to the fronts of Stange, Wilkins and George VI ice shelves (locations in Figure 2.2), implying increasing basal melt caused by warming ocean temperatures near the fronts (Section 2.2.3.1) (Fricker & Padman, 2012). The authors proposed that surface lowering on the Larsen C Ice Shelf, on the other hand, is driven primarily by firn compaction. Further evidence that the south-west AP ice shelves are susceptible to ocean warming was found by Rignot *et al.* (2013), who estimated melt rates and mass balance of all Antarctic ice shelves for 2007-08. Basal melt was found to outweigh calving flux rates, and half of the melt was found to come from the 10 small ice shelves situated in the AS and BS, which includes George VI, Wilkins, Bach and Stange ice shelves (Rignot *et al.*, 2013). These were observed to be sensitive to ocean warming and circulation strength.

Evidence of ice shelf basal melt increase in the south-west of the AP was backed up by Holland *et al.* (2010), whose ocean and sea-ice model suggests that melting beneath George VI Ice Shelf may have been causing thinning for decades. In another study, retreat rates of the southern front of the ice shelf were found to have increased following periods of warm-water upwelling in the BS and, coupled with grounding line retreat, it is thought that the thinning southern extent is increasingly susceptible to ongoing oceanic warming (Holt *et al.*, 2013).

7.6.2 Ice-ocean interactions along the west Antarctic Peninsula

The studies discussed above concur that basal melt is causing increased thinning of ice shelves in the south-west AP. The ice shelves mentioned so far are all situated just south of the present study region. North of George VI Ice Shelf, in Marguerite Bay, the ocean temperatures have been found to be warmer than further south (Holland *et al.*, 2010). Indeed, the newly studied ocean temperature data reveal that warm deep ocean temperatures are present as far north as Anvers Island. Ocean temperatures are affecting ice shelves to the south, but this study shows, for the first time, that warm ocean waters are also influencing the marine-terminating glaciers further north. The new results give evidence that the ocean temperature at 150 m and deeper is a principal driver of glacier front changes along the western AP coast.

Existing research on ice-ocean interactions in this region is limited, largely because there are fewer ice shelves. The Wordie Ice Shelf, situated in Marguerite Bay, disintegrated in a series of break-ups in the 1970s and 1980s, and by 1992 there was little more than a few disconnected and retreating glacier tongues remaining (Cook & Vaughan, 2010). The popular understanding is that the retreat was triggered by the warming trend in the mean annual air temperatures since the 1970s (Vaughan, 1993) and indeed it was situated north of the position of the thermal limit of viability in 2000 (Morris & Vaughan, 2003). Interestingly, however, the retreat has not yet been considered in the context of warming ocean temperatures in the region.

The two small ice shelves situated north of Marguerite Bay: Jones, which had disappeared by 2003, and Müller, which still remains, have not yet been studied

alongside recent ocean temperature data. This could offer new insight as to their behaviour and, in particular, why Müller Ice Shelf remains even though it is north of the atmospheric limit of viability. Domack *et al.* (1995) first proposed that an influx of cold CDW to the fjord during the Little Ice Age may have explained its stability at this time, but more recent ocean data have not yet been examined.

Findings from studies on tidewater glaciers in Greenland give insight as to the processes that may be taking place along the western coast of the AP. An ice model has suggested that tidewater glaciers adjust extremely rapidly to changing boundary conditions at the calving terminus (Nick *et al.*, 2009). The synchroneity between AP glacier changes and ocean temperatures indicates that this may be taking place on a regional scale in the AP. A further model has shown that marine-terminating glaciers are most sensitive to melting at the glacier grounding line (O'Leary & Christoffersen, 2013). It showed that frontal melt near the base is a strong driver of calving, and therefore water temperatures near the bed of the glacier are critically important to ice front change. Although the depth of grounding lines in the AP are uncertain, it may explain why the deeper waters (150 m and below) in this study are those that have greatest influence on driving frontal change. It is of key importance to establish the depth of grounding lines and the sub-glacial topography for predicting rates of change.

It must be noted that sea-ice is not considered to have an influence on glacier frontal change along the western AP on the timescales being considered in this study. In northern Greenland, sea-ice has been found to influence calving events on a seasonal timescale. For example, during winter, mélange forms within fjords and suppresses calving rates (Amundson *et al.*, 2010). The geography of the western AP, however, means there are few bays where sea-ice is constrained to produce sufficient force on the glacier fronts, and the majority of the coastline is exposed to open water during summer months.

7.6.3 Causes of ocean warming in the west AP

The primary origin of the warm ocean water is a topic of current research and several theories have been proposed. As discussed in Section 2.3.2.1, changes in the CDW are thought to be consistent with a southward shift of the ACC (Gille, 2008). Some climate models suggest that the ACC shifts in response to the southwards shift of the westerly winds that are driven by enhanced greenhouse forcing and the positive trend in the SAM (Turner *et al.*, 2009). Other research has agreed that a combination of decadal warming of the CDW and an acceleration of its on-shelf flow has been linked to stronger winds and an intensification of the SAM (Martinson *et al.*, 2008). Indeed, the most recent research has found that subsurface warming and circulation changes of coastal waters have been due to poleward shifting winds (Spence *et al.*, 2014). Their model shows that a poleward wind shift at the latitudes of the AP can produce an intense warming of subsurface coastal waters that exceeds 2 °C at 200-700 m depth. The coastal warming response to projected SAM wind trends was a weakened north-south pressure gradient, a decrease in speed of coastal waters and the upwelling of the boundary between cold fresh surface water and the warmer layer below (Spence *et al.*, 2014). The authors suggest that anthropogenically induced wind changes can therefore dramatically increase the temperature of ocean water at ice sheet grounding lines. The "upwelling" and "downwelling" of the boundary layer observed near the Wilkins Ice Shelf was also considered to be in response to local winds (pers comm from L. Padman, in Cochran *et al.*, 2014).

An alternative suggestion by Holland *et al.* (2008) is that warm CDW reaching the base of the ice shelves in the ASE is not necessarily due to a heat input to the ocean, but may rather be caused by a shift in ocean circulation. In Holland *et al.* (2010), the authors theorise that the melt rate beneath George VI Ice Shelf in the BS contains interannual variability that could be connected to the variation in sea-ice conditions to the south of the ice shelf. The authors suggest that rather than fluctuations in transport of warm CDW, as observed in models of the AS, the main supply of heat to the ice shelf base in the BS is water mass transformations induced by water surface processes that occur offshore. The

model of the BS however did not take into account the important effects of ocean variability emanating from the ACC.

Changes in CDW are coupled with changes in the west AP climate. A recent increase in CDW upwelling along the west AP has been associated with increased winter SSTs, reduced sea-ice extent and duration, and greater ENSO variability (Martinson *et al.*, 2008). The summer temperature of the near-surface ocean in the west AP has risen, due to trends in atmospheric circulation, temperatures and changes in sea-ice, which has acted as positive feedback in sustaining the atmospheric warming (Meredith *et al.*, 2010). The ENSO ocean-atmosphere mode of variability (Section 2.3.3) has a profound effect on the conditions in the BS. Following ENSO events, the coastal AP shows a clear response to the strengthening low pressure centre over the Amundsen-Bellingshausen Seas, with significantly increased atmospheric and oceanic temperatures (Shevenell *et al.*, 2011). Furthermore, when ENSO is in phase with the Southern Annular Mode (SAM) the effects are amplified. This was the case in the early 1990s, which helps to explain the wind-driven sea-ice decreases in the ocean to the west of the AP (Stammerjohn *et al.*, 2008) (Section 2.3.3).

7.6.4 Implications of a warming ocean

The connection between glacier retreat and warm ocean temperatures to the west of the AP has significant implications. The southwards shift in the ACC, the resulting intrusion of warm CDW onto the continental shelf, plus the coupled atmosphere-ocean changes, mean the increased contribution of glaciers to sea-level rise is a primary concern.

As discussed above, the ice shelves extending into the Amundsen and Bellingshausen Seas have undergone rapid change in recent years. A total of 59% increase in the rate of mass loss into the AS and BS between 1992 and 2006 was estimated from radar interferometry and climate modelling (Rignot *et al.*, 2008). Research has shown that basal melt has been the primary cause of increased thinning, the retreat of grounding lines and increased ice sheet discharge. There is growing concern that the WAIS is becoming increasingly unstable, particularly where the ocean water interacts with the grounding lines (e.g. Pritchard *et al.*, 2012; Rignot *et al.*, 2014).

Ice shelves and large floating glacier tongues are well understood to be influenced by ocean temperatures, but with no large ice shelves remaining along the west AP north of 70° S, the extent to which the ocean has had an effect on the glacierized coast has been largely overlooked. The ocean north of George VI Ice Shelf is currently warmer than in regions to the south, where ice shelf basal melt is causing thinning and mass loss (Holland *et al.*, 2010). The results from the present study offer a first insight as to the interactions that are taking place in the region to the north.

This study has shown that the warm ocean waters have an impact not only on large floating glaciers but also on those that are small, grounded, or with a wide range of other characteristics. Since the earliest glacier position records (on average, 1958), 90.5% of glaciers on the AP have retreated. The ocean temperatures below 150 m have consistently been above the pressure melting point since the 1950s (apart from in the NW). This is one result that indicates that warmer oceans may have been causing retreat since the 1950s. It is not yet clear when the ocean reached temperatures sufficient to cause glacier retreat but regional mean temperatures suggests this was prior to the earliest ocean temperature records used in this study (1950s). The retreat has not been consistent throughout the past 50 years, but neither has the ocean temperature increase. The glaciers began to show accelerated retreat from the late 1990s onwards, which corresponded with a mean ocean temperature increase in all regions.

The overall greatest increase in ocean temperatures occurred at 150 m in the SW region. This is corroborated by repeat measurement results, which show that between the 1990s and 2000s, the ocean temperature warmed the most at mid-depths (100 m – 200 m) in the SW. As discussed above, it is highly probable that a thermal expansion of the CDW to the south (i.e. a raising of the thermocline) is the reason for warming at these depths. The majority of glaciers are understood to have bathymetry deeper than 200 m at their fronts, therefore temperatures at these depths will have an effect on the grounding lines. As yet, the grounding line positions are not known for all glaciers, but the behavioural pattern from the large sample size suggests that temperatures at these depths have had a glaciological effect for some time.

Rignot & Jacobs (2002) found that ocean thermal forcing has a strong positive correlation with melt rates, such that a 1 °C increase in ocean temperatures increases basal melt rates by ~10 m a^{-1}. Additionally, the latest research from modelled ocean warming scenarios shows that a poleward wind shift at the same latitudes as the AP can produce an intense warming of subsurface coastal waters that exceed 2 °C at 200-700 m depth (Spence *et al.*, 2014). If ocean warming continues, there will be an increase in mass loss not only from ice shelves, but from the numerous smaller glacier features that line the west coast of the AP.

The wider implication of further glacier retreat and resultant mass loss is the increasing contribution to sea-level rise. One study showed that a 12% speed up of glaciers that occurred from 1996-2006, alongside enhanced melt and net accumulation, resulted in an estimated mass loss of 7 ± 4 Gt a^{-1} in 1996 and 13 ± 7 Gt a^{-1} in 2006 from the west AP glaciers alone (Rignot *et al.*, 2008). Mass balance reconciliation for the whole AP (extended to 74° S) indicated that the APIS was close to balance in the 1990s but there has been a significant mass loss since then, which may have reached as high as 36 ± 10 Gt a^{-1} in 2005-10 (Shepherd *et al.*, 2012) (discussed in Section 2.2.2.1). In ~2005, the AP was estimated to be contributing to global sea-level rise through enhanced glacier melt and acceleration at a rate of 16 ± 0.06 mm a^{-1} (Pritchard & Vaughan, 2007). The new research results indicate that the glaciers are retreating at a faster rate than they were before the late 1990s and, with persistent warm deep ocean temperatures, this is set to continue.

Enhanced glacier retreat from warming oceans will have additional implications, one of which is an increase in the quantity of freshwater in coastal waters. The southward flow of the AP Coastal Current is thought to be partly driven by freshwater being released from land, so acceleration in flow of the current is likely (Meredith *et al.*, 2013) (Section 2.3.2.1). This will have implications for local climate and regional ecosystems. This is already the case, where melting glaciers have opened up new bays in which phytoplankton blooms have occurred (Peck *et al.*, 2010). The authors proposed that this acts as a negative carbon feedback mechanism. Furthermore, a study has proposed that increasing basal ice melt could cause sea-ice expansion, where the meltwater accumulates in a surface layer and shields surface water from warmer deeper waters

(Bintanja *et al.*, 2013). This may be the case elsewhere in Antarctica, but there has been sea-ice reduction off the west AP coast since the 1960s, considered due to increasing winter surface temperatures (Turner & Overland, 2009).

A final consideration is the region off the north-west coast of the AP, where glaciers have remained stable or in some cases have advanced. The ocean temperatures in this region have remained below the pressure melting point since the earliest records. These waters are fed by the Weddell Sea and are known as the Bransfield Strait Surface Water (Figure 2.6), which has a very different ocean circulation pattern than the seas to the south (discussed in Section 2.3.2.2). The shape of the Weddell Sea embayment results in a sub-polar gyre, where Warm Deep Water flows south and cold, freshwater from the continent is transported northward. Temperatures along the east coast are cold at all depths, and although a small warming has occurred since the 1970s (Robertson *et al.*, 2002), the ocean remains too cold to induce glacier retreat. The water circulates westwards around the northern tip of the AP extending to Anvers Island, which encompasses the region that has the most stable glacier fronts. This region is unlikely to change in the near future as water remains significantly colder than water along the west coast to the south.

7.7 Summary

This chapter aimed to bring together results produced in earlier chapters to determine whether there is a dominant driver of glacier front changes on the AP. This has been addressed by considering the new glacier front change results in relation to each potential driver of change, followed by discussing ice-ocean interactions in the AP in the context of current research.

Answers to the questions laid out in Section 7.1 can be summarised as follows:

- Can the patterns in area change be explained primarily by local glaciological control factors?

The 860 marine-terminating glaciers have an extensive range of characteristics, many of which are inter-related and depend heavily on the basin area. Frontal behaviours are unlikely to display a common pattern between glaciers with such distinct characteristics.

The regional and temporal trends in glacier front behaviour are statistically significant, however, suggesting that the glacier fronts are responding to an external regional control factor.

- Do atmospheric patterns show a significant correlation with area changes, either spatially or over time?

There are no spatial or temporal patterns that suggest that atmospheric controls are having a regional impact on glacier front changes along the west coast. The eastern side is complicated by the dominance of ice shelf behaviour, which is thought to be primarily driven by atmospheric temperatures.

- Do ocean temperature patterns show a significant correlation with area changes, either spatially or over time?

i) What are the ocean depths and temperatures like close to the ice fronts?

Bathymetric measurements close to shore are relatively limited, but where they do exist along the west coast, 81% have minimum depths below 200 m within 1 km of their fronts. The mean depth for all glaciers with bathymetric data within 1 km is 321 m. Many deep bathymetric troughs are present, facilitating passage of water from deeper offshore regions.

ii) How well does the spatial distribution of overall long-term ice front change correlate with regional mean ocean temperatures?

Ocean temperatures at 150 m and deeper off the west coast of the AP increase in three dimensions: with depth, from north-south and over time. Spatial patterns between mean deep ocean temperatures and long-term overall glacier change are clear. In particular, the distinct NW region where glaciers have shown minimal change has remained below the T_m at all ocean depths. Correlations between ocean temperatures and long-term glacier change rates throughout the region are statistically significant at 150 m and below, and increase in strength with depth. These correlations are strongest in the W and SW: weaker correlations in the NW and SSW may be explained by the lower temperature gradients between depths in these regions. The correlation results are strong when

applied to glaciers across the whole region, with a wide range of glacier change rates and temperatures at each depth.

iii) Do the glacier short-term rates of change correlate with temporal changes in ocean temperature?

The acquisition of further temporal data is necessary to establish the significance of any short-term temporal correlations that may exist. Most notably, however, the deep ocean to the west has warmed since the late 1990s at a time when there was widespread acceleration in retreat of glaciers throughout the same region.

- What are the causes and implications of the ocean-glacier interactions?

Temperature differences between repeat measurements revealed that greatest warming is occurring at mid-depths (100-200 m), particularly in the SW. Understanding the cause of this warming requires further research, but based on research in other regions around Antarctica, a likely explanation is a thickening of the warm Circumpolar Deep Water to the south (Holland *et al*., 2010). This raising of the thermocline is causing warming at depths that can have a significant glaciological effect. Basal melt is understood to be the main driver of grounding line retreat in the Amundsen Sea Embayment, which is causing rapid ice mass loss from this region of West Antarctica (Holland *et al*., 2010, Walker *et al*., 2007; Thoma *et al*., 2008). A better understanding of the ocean warming to the west of the AP is essential, since evidence now suggests it is highly likely to be the main driver behind glacier retreat in this region.

Chapter 8

Summary and Conclusions

8.1 Thesis summary

The motivation behind this research was to improve knowledge on glaciers of the Antarctic Peninsula, both in terms of their glaciological characteristics and their long-term frontal behaviour, in order to advance glacier research in a region where glaciers have been distinctly under studied. The numerous glaciological features are known to respond rapidly to changes in environmental conditions and can therefore provide a valuable insight into changes in past conditions. The ultimate objective is that these results will help to improve predictions of how glacier mass will change given future climate scenarios and the contribution of the APIS to future sea level.

The APIS glacier system is well-known to be complex and difficult to access; hence there have been few individual glacier mass balance studies carried out in the region. This research was facilitated by closely examining a number of both untapped and newly created resources. There are many gaps in knowledge on glaciers in the region, so the first aim was to produce a benchmark dataset on which further glaciological studies can be based. This entailed producing a DEM with an accuracy and resolution suitable for mapping glacier morphological features in the region, followed by delineation of individual glacier units within the ice sheet. These two new datasets have already proved to be valuable resources for research outside this study. All regional glacier studies require essential information about the glacier characteristics, and here the DEM and glacier basin outlines have been used to produce fundamental details for the first time. This has enabled a descriptive summary of glacier types in the region, which is necessary for understanding their behaviour. An existing resource for the Antarctic Peninsula that had previously not been fully analysed was the *Coastal-Change and Glaciological Maps of Antarctica* dataset. This extensive coverage of historical ice front positions provides

crucial insight into long-term glacier front behaviour. For the present research the dataset was geo-corrected and brought up-to-date and, with the availability of new glacier outlines, it became possible to investigate the changes in extent of all marine-terminating glaciers on the AP.

Spatial patterns were identified for glacier area changes from the earliest to the most recent positions. Temporal analysis was more challenging due to the inconsistencies of data records between glaciers. However, a method was developed in which the frontal positions were analysed on a 5-year interval basis. Temporal patterns in area change rates emerged, across a wide range of glacier types, and also regionally. These statistically significant spatial and temporal patterns indicate that there is an external control factor that currently outweighs local glaciological controls on glacier extent.

The succeeding aim was to identify the primary regional driver of glacier area change. The popular understanding is that the AP ice shelves are controlled primarily by an atmospheric thermal limit, therefore the latest atmospheric data was scrutinised for spatial and temporal patterns in relation to glacier front changes over the same period. Subsequently, all available ocean temperature measurements at a range of depths between 50 and 500 m were analysed in the same way. The results and existing knowledge on controls on ice front changes in neighbouring regions were then discussed.

8.2 Conclusions

8.2.1 The new AP DEM and glacier drainage basins

DEMs provide a readily accessible and valuable data source for measuring glacier characteristics in regions that are difficult to access. Whereas most regions of the globe have reliable and high resolution DEM coverage, most of the Antarctic has been limited to DEMs derived from relatively low resolution radar imagery. While this may be sufficient for the gentle slopes of the Antarctic interior, the available data are unsuitable for the steep-sided coastal regions and small glaciers that constitute the AP. The release of ASTER GDEM in 2009 offered a potential solution to the lack of elevation data, and with a grid size of ~20 m it opened up an opportunity for glacier mapping in the AP. It

was realised however that ASTER GDEM has fundamental errors on snow-covered surfaces, making it unusable for much of the APIS. At the outset of the present study a novel method was developed in which the regions with large errors were replaced with a smooth surface derived from selected GDEM surface contours, resulting in a new 100-m DEM for the region 63° – 70° South (Chapter 3). The method and results were published in Cook *et al.* (2012). Absolute vertical accuracies taken from ICESat tracks from across the varied terrain show that the new DEM has a mean vertical error of -4 m, with an RMSE of ±25 m. For the first time, a DEM with sufficient coverage, accuracy and resolution exists for mapping the glaciers on the AP.

A consistent method for deriving glacier drainage basin outlines was subsequently developed (Section 4.2.3), resulting in a complete dataset of 1590 AP glacier drainage basins. These have been assigned certain variables to define their characteristics and were applied to each glacier either manually (in the case of non-scalar variables such as primary classification and front-type) or automatically (such as elevation details derived from the DEM) (Section 4.3). The individual glacier basins have details including class-type, basin complexity, frontal-type, basin size, length, geometry, surface elevations, slope and aspect. The dataset opens up many possibilities for further glacier research in the region, and many more details can be added as these become available (for example, ice thickness and bed topography). Furthermore, information on glacier dynamics (such as flow rates and changes in surface elevation) can be attributed, and it can be used for continued monitoring of future positions of glacier fronts.

The glaciers in the database not only have many essential attributes, but they also contain information on past glacier front changes (Section 4.4). In total, 925 of the glaciers are marine-terminating and, after glacier basins that were once conjoined were merged, the result is 860 glaciers with more than one positional record. These historical positions have been associated with each basin to enable area-change calculations. The DEM and resulting glacier inventory, their characteristics and area-changes are fundamental to furthering glacier-change research in the region.

8.2.2 Spatial and temporal patterns of glacier area change

The issue of uneven data distribution in between glaciers is encountered in all long-term glacier studies but here a new method has been developed to keep inaccuracies and over-interpretation to a minimum. The data are too infrequent to enable analysis of short-term (e.g. annual) change but for studying longer-term changes an interval of 5 years was considered to be most suitable. Absolute and relative area changes were calculated relative to the basin areas in 2000-04 and, in addition, area change rates calculated between each date gave a consistent measure of change across all intervals. Overall changes, from the earliest to latest positions, were calculated for all glaciers so that spatial distribution and the scale of long-term advance and retreat can be established. The conclusions regarding patterns in overall change can be summarised as follows:

Overall change:

- There has been overall ice loss since the 1940s and 90.5% of all 860 marine-terminating glaciers have retreated since their earliest records.
- Primary differences have occurred between the east and west coast: in the east there has been a far greater mean glacier retreat, primarily due to the loss of the large ice shelves.
- A gradient in mean overall ice loss from north to south is present along the west coast.
- Glaciers in a distinct region along the north-west coast (~65° S to the northern tip) have remained stable, or shown small advances, throughout the study period. This is true for both absolute area change ($km^2\ a^{-1}$) and relative area change (% a^{-1}).

There is a mixed population of glacier types throughout the AP, with no spatial bias in the distribution of glacier attributes. The presence of these distinct regional patterns in overall area change therefore suggests that there is an external control factor influencing long-term glacier front behaviour in the AP. Temporal trends in change-rates indicates this further, summarised as follows:

Temporal trends:

- There was no clear pattern in retreat until the late 1970s, after which the retreat rates began to increase.
- There was a statistically significant reduction in retreat rates in the late 1980s/early 1990s, observed across a broad range of glacier types.
- There has been a statistically significant increase in retreat rates since the late 1990s, in all regions except the NW.
- There has been a southerly migration of increasing retreat rates: glaciers in the W region began retreating in the late 1950s, glaciers in the SW in the late 1960s and glaciers in the SSW in the early 1970s. Glaciers in the W have had small mean change rates throughout, whereas glaciers in the SW and SSW have been retreating at much faster rates, particularly since the late 1990s.

The large number of glaciers, each with individual characteristics, would make a universal trend in glacier front change unlikely under normal mass balance conditions. Area change rates were calculated for glaciers with different characteristics in order to establish whether synchroneity occurred between glacier types. It was found that 'floating front' is a characteristic that has a significantly greater scale of change than any other characteristic. The temporal trends that occurred, however, were identified in glaciers spanning a wide range of different attributes, indicating a common change in external forcing rather than the overriding influence of particular glacier characteristics. Many of these results are published in Cook *et al.* (2014).

8.2.3 Drivers of glacier area change

The primary external controls of atmospheric temperature and ocean temperature on glacier change have been analysed using data with regional coverage. Atmospheric patterns were obtained from station temperature records; surface-melt from QSCAT satellite data between 2000-09; surface temperature data from infrared satellite imagery between 1980-2008; and surface mass balance from modelled output between 1980-2009. Ocean temperature patterns were derived from measurements acquired between 1940 and 2009 at a range of depths between 50 and 500 m, accessed from the World Oceanographic Database.

Atmospheric temperatures

This study has found that there have been no obvious correlations between peninsula-wide atmospheric patterns and glacier area changes since the earliest records. Indeed, on the west coast, mean surface temperature and frontal retreat rates have opposing north-south gradients. Temperature records reveal lowest melt duration and coolest surface temperatures in the south, and longest melt duration and highest surface temperatures in the north. One clear disparity is the region of greatest glacier frontal stability (i.e. north of Anvers Island), which has had consistently higher surface temperatures than any other region further south, and has undergone considerable variation in surface temperature over time. In the east, ice shelf collapse has caused the glaciers that fed them to retreat, which has significantly affected the scale of glacier change in this region. Trends in surface temperature throughout the AP suggest a general warming from the late 1990s onwards, but the distinct regional differences remain and so it is unlikely that they affect ice fronts where the mean summer temperatures are well below 0 °C. The AP glaciers might be expected to show either non-synchronous behaviour (due to the mixed population of floating and grounded termini), or to show a response similar to that of ice shelves in the same region. What is clear, however, is that there is regional synchroneity taking place and it is not universally related to atmospheric forcing.

Ocean temperatures

The oceans surrounding the AP have distinct regimes, where the Weddell Sea to the east is dominated by cold waters and the Bellingshausen Sea to the west is substantially warmer. The eastern waters have remained well below the pressure melting point of ice (T_m) throughout the study period and therefore cannot be considered a driver of melt at the glacier fronts. To the west, however, there are distinct temperature patterns and regional correlations with glacier change, identified here for the first time. There is a clear north to south progression from cool to warm water, which becomes enhanced with increasing depth. The latitudinal temperature gradient at depths of 150 m and below has a close spatial correspondence with overall glacier change rates. These waters have been above the pressure melting point throughout. Water in the distinct region in the NW however has remained below the T_m, and, correspondingly, the glacier fronts have

remained stable or shown slight advances. Aside from spatial correlations, the ocean temperatures at 150 m and below have statistically significant correlations with overall glacier change rates, i.e. glaciers that have shown the greatest retreat have been subject to the warmest ocean temperatures. Temporal trends show there have been weak temperature increases since the 1950s, and a stronger rate of warming since the late 1990s: glacier retreat began to accelerate around this time. Ocean temperature measurements close to the coast are too sparse to be able to draw conclusions about the existence of short-term relationships, but this is clearly an area for further research.

It can be concluded that long-term glacier front changes in the west AP have a statistically significant correlation with ocean temperatures at 150 m and below. Greatest warming has occurred at mid-depths (100-200 m), especially in the SW. Research elsewhere indicates that this is likely due to a raising of the thermocline, caused either by the influx of warmer CDW to the continental shelf or due to a shift in ocean circulation (Holland *et al.*, 2010). The warm water is channelled from the outer shelf to the glacier fronts along the many bathymetric troughs that intersect the shelf to the west. Until now, the significance of the ocean in driving glacier front changes along the west coast of the AP has not been recognised. Since glacier front changes are closely coupled to changes in other glacier dynamics (such as glacier acceleration, feeding back into further thinning and greater ice discharge), continuing retreat could imply a significant contribution to sea level rise. This study has given insight as to the value of measuring changes in glacier extent, the urgency required for continued glacier monitoring, plus the necessity for further analysis of ice-ocean interactions in the region.

8.3 Suggestions for further work

The research in this thesis has covered the broad topic of changes in extent of all marine-terminating glaciers on the AP, using a full range of historical records for ice front positions. These data and results open up opportunities for further analysis and there are a number of ways that the research can be continued. As explained in the Introduction chapter, most of the glaciers on the AP have been little researched, and there is clearly much still to be discovered. A few suggestions are outlined here.

8.3.1 Short-term trends

Analysis of glacier front changes at a finer temporal resolution is necessary for understanding the short-term response of glaciers to environmental conditions. The pentadal intervals at which the glacier-change analysis has been based, is at too broad a time-span to identify patterns that might have occurred between individual years. For example, as discussed in Chapter 2 (Section 2.3.1), the Southern Annular Mode is the principal mode of variability in the Southern Hemisphere Circulation, and it began a positive phase shift in the 1960s. The years with a particularly high SAM index were identified as 1981, 1982 and 2000 and those with a low SAM index as 1985 and 1992 (Marshall, 2003). However, inter-annual signals are not recognised in the averaged pentadal surface temperature, ocean temperature or SMB records. It has not been possible in this study to assess short-term response of glaciers to the SAM, but the dataset can be used as a base for future work on annual changes. The lack of available imagery prior to the early 2000s means that measuring annual cycles over the long-term is limited. The increasing frequency of imagery since then however does mean that this can be calculated for recent years. Many glaciers in the new dataset have frontal positional records at 2-yearly intervals since 2000 and these could be used for further research.

8.3.2 Individual glacier behaviour

Regional patterns have been identified but the glacier inventory and frontal-change results offer resources for glacier studies on a local scale. The behaviour of each glacier is distinct and not all glaciers conform to the regional trends. Examples include glaciers that have displayed locally unusual behaviour, such as surging glaciers. One possibility of a surging-type glacier was identified in north-east Adelaide Island, which advanced by over 10 km during the 1960s.

Research with a focus on individual embayments where data on boundary conditions are more plentiful is recommended. An example is shown in Figure 8.1, where bathymetry tracks reach close to the ice fronts of several glaciers, and neighbouring glaciers have displayed different frontal behaviour. The bathymetry data, together with the ice front

records, can enable more detailed analysis of how glaciers in close proximity are affected by variations in ocean temperature. In a recent study in Greenland for example, a strong link was found between the grounding line depth and rates of mass loss for two neighbouring glaciers (Porter *et al.*, 2014).

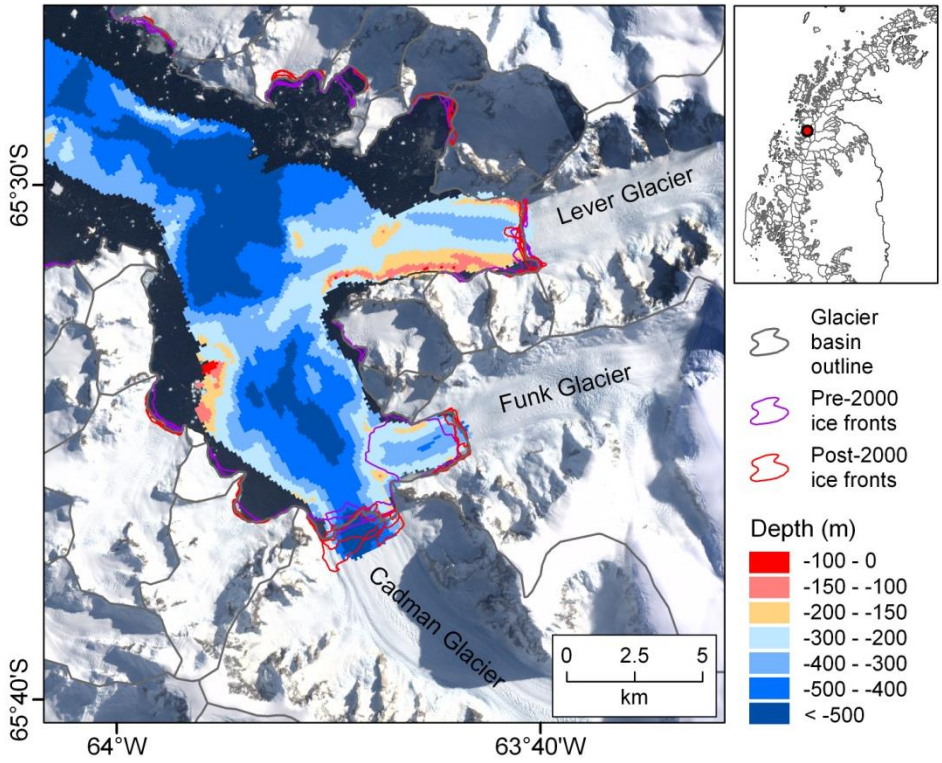

Figure 8.1: Glaciers and bathymetry in Beascochea Bay (location shown on inset). Funk Glacier was at its most advanced in 1968 where it may have been grounded on the shallower ocean bed. Since then the glacier has retreated through a deeper channel and has been relatively stable since 1989. Cadman Glacier, which has bathymetry deeper than 500 m at its front, has had an active ice front and overall retreat from 1968 to 2009. Lever Glacier has remained stable and appears to be grounded in shallower water.

8.3.3 Additional boundary conditions

The research in this thesis has been restricted to boundary conditions where data are available. As the availability increases, new data can be added to the glacier dataset. These include information on the sub-glacial topography and ice thickness, as well as glacier dynamics such as changes in flow rates and surface elevation. Data for this region

are developing rapidly, with the focus mainly on changes in the past decade. Ocean temperature measurements since 2009 have been plentiful and so identifying correlations in recent years is a topic that requires research. These combined datasets will help to significantly improve understanding the variability in glacier retreat in recent years.

8.3.4 Modelling future contribution to sea level

The results from this research can be used to improve predictions of likely future changes of marine-terminating glaciers and their contribution to sea-level rise given particular climate scenarios. Quantifying future mass changes on the AP has been restricted since the dynamic behaviour at the glacier termini has been poorly understood. Since changes at the glacier fronts are closely coupled with glacier acceleration, thinning and ice discharge, the new area-change results provide improved details on ice dynamics for marine boundary conditions used in ice flow models. A computation of the contribution of the APIS to sea level up to 2200 was recently undertaken, based on ice fluxes from surface velocities, altimetry and surface mass balance (Barrand *et al.*, 2013a). The authors suggest that the inclusion of the AP glacier drainage basins, and a better understanding of grounding line movement and retreat, will improve future projections. These modelled results also depend on good meteorological models: the latest oceanic and atmospheric temperature data presented in this study can also contribute to improving regional warming scenarios.

References

AMUNDSON, J.M., FAHNESTOCK, M., TRUFFER, M., BROWN, J., LÜTHI, M.P. & MOTYKA, R.J. 2010. Ice mélange dynamics and implications for terminus stability, Jakobshavn Isbræ, Greenland: *Journal of Geophysical Research: Earth Surface (2003–2012)*, **115**, F1.

ARBLASTER, J.M., MEEHL, G.A. & KAROLY, D.J. 2011. Future climate change in the Southern Hemisphere: Competing effects of ozone and greenhouse gases: *Geophysical Research Letters*, **38**.

ARENDT, A., BOLCH, T., COGLEY, J., GARDNER, A., HAGEN, J., HOCK, R., KASER, G., PFEFFER, W., MOHOLDT, G. & PAUL, F. 2012. Randolph Glacier Inventory [v2. 0]: A Dataset of Global Glacier Outlines. Global Land Ice Measurements from Space, Boulder Colorado, USA: *Digital Media*.

ARIGONY-NETO, J., SIMÕES, J.C. & BREMER, U.F. 2004. Implementation of the Admiralty Bay Geographic Information System, King George Island, Antarctica: *Pesq Antart Bras*, **4**, 187-190.

ARNDT, J.E., SCHENKE, H.W., JAKOBSSON, M., NITSCHE, F.O., BUYS, G., GOLEBY, B., REBESCO, M., BOHOYO, F., HONG, J., BLACK, J., GREKU, R., UDINTSEV, G., BARRIOS, F., REYNOSO-PERALTA, W., TAISEI, M. & WIGLEY, R. 2013. The International Bathymetric Chart of the Southern Ocean (IBCSO) Version 1.0—A new bathymetric compilation covering circum-Antarctic waters: *Geophysical Research Letters*, **40**, 12, 3111-3117.

ARZENO, I.B., BEARDSLEY, R.C., LIMEBURNER, R., OWENS, B., PADMAN, L., SPRINGER, S.R., STEWART, C.L. & WILLIAMS, M.J. 2014. Ocean variability contributing to basal melt rate near the ice front of Ross Ice Shelf, Antarctica: *Journal of Geophysical Research: Oceans*.

ASTERGDEM-VALIDATIONTEAM 2011. ASTER Global Digital Elevation Model Version 2 – Summary of Validation Results: http://www.jspacesystems.or.jp/ersdac/GDEM/ver2Validation/Summary.GDEM2.validation.report.final.pdf.

ASTERGDEM-VALIDATIONTEAM, METI/ERSDAC, NASA/LPDAAC & USGS/EROS 2009. ASTER GDEM Validation Summary Report: http://www.jspacesystems.or.jp/ersdac/GDEM/E/image/ASTERGDEM.ValidationSummaryReport.Ver1.pdf.

BAHR, D.B., MEIER, M.F. & PECKHAM, S.D. 1997. The physical basis of glacier volume-area scaling: *Journal of Geophysical Research-Solid Earth*, **102**, B9, 20355-20362.

BAMBER, J.L., GOMEZ-DANS, J.L. & GRIGGS, J.A. 2009. A new 1 km digital elevation model of the Antarctic derived from combined satellite radar and laser data - Part 1: Data and methods: *Cryosphere*, **3**, 1, 101-111.

BANWELL, A.F., MACAYEAL, D.R. & SERGIENKO, O.V. 2013. Breakup of the Larsen B Ice Shelf triggered by chain reaction drainage of supraglacial lakes: *Geophysical Research Letters*, **40**, 22, 5872-5876.

BARLETTA, V.R., SABADINI, R. & BORDONI, A. 2008. Isolating the PGR signal in the GRACE data: impact on mass balance estimates in Antarctica and Greenland: *Geophysical Journal International*, **172**, 1, 18-30.

BARRAND, N.E., HINDMARSH, R., ARTHERN, R.J., WILLIAMS, R.C., MOUGINOT, J., SCHEUCHL, B., RIGNOT, E., LIGTENBERG, S.R.M., VAN DEN BROEKE, M.R., EDWARDS, T.L., COOK, A.J. & SIMONSEN, S.B. 2013a. Computing the volume response of the Antarctic Peninsula ice sheet to warming scenarios to 2200: *Journal of Glaciology*, **59**, 215, 1-13.

BARRAND, N.E., VAUGHAN, D.G., STEINER, N., TEDESCO, M., MUNNEKE, P.K., VAN DEN BROEKE, M.R. & HOSKING, J.S. 2013b. Trends in Antarctic Peninsula surface melting conditions from observations and regional climate modeling: *Journal of Geophysical Research-Earth Surface*, **118**, 1, 315-330.

BARRY, R.G. 2006. The status of research on glaciers and global glacier recession: a review: *Progress in Physical Geography*, **30**, 3, 285-306.

BAS, SPRI & WCMC 1993. Antarctic digital database user's guide and reference manual, Cambridge, Scientific Committee on Antarctic Research.

BENN, D.I., WARREN, C.R. & MOTTRAM, R.H. 2007. Calving processes and the dynamics of calving glaciers: *Earth-Science Reviews*, **82**, 3, 143-179.

BENTLEY, M.J., FOGWILL, C.J., KUBIK, P.W. & SUGDEN, D.E. 2006. Geomorphological evidence and cosmogenic Be-10/Al-26 exposure ages for the Last Glacial Maximum and deglaciation of the Antarctic Peninsula Ice Sheet: *Geological Society of America Bulletin*, **118**, 9-10, 1149-1159.

BENTLEY, M.J., HODGSON, D.A., SMITH, J.A., COFAIGH, C.O., DOMACK, E.W., LARTER, R.D., ROBERTS, S.J., BRACHFELD, S., LEVENTER, A., HJORT, C., HILLENBRAND, C.D. & EVANS, J. 2009. Mechanisms of Holocene palaeoenvironmental change in the Antarctic Peninsula region: *Holocene*, **19**, 1, 51-69.

BENTLEY, M.J., HODGSON, D.A., SUGDEN, D.E., ROBERTS, S.J., SMITH, J.A., LENG, M.J. & BRYANT, C. 2005. Early Holocene retreat of the George VI Ice Shelf, Antarctic Peninsula: *Geology*, **33**, 3, 173-176.

BERTHIER, E., SCAMBOS, T.A. & SHUMAN, C.A. 2012. Mass loss of Larsen B tributary glaciers (Antarctic Peninsula) unabated since 2002: *Geophysical Research Letters*, **39**, L13501, 1 - 6.

BINDSCHADLER, R., CHOI, H., WICHLACZ, A., BINGHAM, R., BOHLANDER, J., BRUNT, K., CORR, H., DREWS, R., FRICKER, H., HALL, M., HINDMARSH, R., KOHLER, J., PADMAN, L., RACK, W., ROTSCHKY, G., URBINI, S., VORNBERGER, P. & YOUNG, N. 2011a. Getting around Antarctica: new high-resolution mappings of the grounded and freely-floating boundaries of the Antarctic ice sheet created for the International Polar Year: *Cryosphere*, **5**, 3, 569-588.

BINDSCHADLER, R., VAUGHAN, D.G. & VORNBERGER, P. 2011b. Variability of basal melt beneath the Pine Island Glacier ice shelf, West Antarctica: *Journal of Glaciology*, **57**, 204, 581-595.

BINDSCHADLER, R., VORNBERGER, P., FLEMING, A., FOX, A., MULLINS, J., BINNIE, D., PAULSEN, S.J., GRANNEMAN, B. & GORODETZKY, D. 2008. The Landsat Image Mosaic of Antarctica: *Remote Sensing of Environment*, **112**, 12, 4214-4226.

BINTANJA, R., VAN OLDENBORGH, G., DRIJFHOUT, S., WOUTERS, B. & KATSMAN, C. 2013. Important role for ocean warming and increased ice-shelf melt in Antarctic sea-ice expansion: *Nature Geoscience*.

BJØRK, A.A., KJÆR, K.H., KORSGAARD, N.J., KHAN, S.A., KJELDSEN, K.K., ANDRESEN, C.S., LARSEN, N.K. & FUNDER, S. 2012. An aerial view of 80 years of climate-related glacier fluctuations in southeast Greenland: *Nature Geoscience*, **5**, 6, 427-432.

BJÖRNSSON, H. 1986. Delineation of glacier drainage basins on western Vatnajökull: *Ann. Glaciol*, **8**, 19-21.

BLISS, A., HOCK, R. & COGLEY, J.G. 2013. A new inventory of mountain glaciers and ice caps for the Antarctic Periphery: *Annals of Glaciology*, **54**, 63, 8.

BOLCH, T., MENOUNOS, B. & WHEATE, R. 2010. Landsat-based inventory of glaciers in western Canada, 1985-2005: *Remote Sensing of Environment*, **114**, 1, 127-137.

BÖNING, C.W., DISPERT, A., VISBECK, M., RINTOUL, S. & SCHWARZKOPF, F.U. 2008. The response of the Antarctic Circumpolar Current to recent climate change: *Nature Geoscience*, **1**, 12, 864-869.

BOX, J.E. & DECKER, D.T. 2011. Greenland marine-terminating glacier area changes: 2000-2010: *Annals of Glaciology*, **52**, 59, 91-98.

BRACHFELD, S., DOMACK, E., KISSEL, C., LAJ, C., LEVENTER, A., ISHMAN, S., GILBERT, R., CAMERLENGHI, A. & EGLINTON, L.B. 2003. Holocene history of the Larsen-A Ice Shelf constrained by geomagnetic paleointensity dating: *Geology*, **31**, 9, 749-752.

BRAUN, M. & GOSSMANN, H. 2002. Glacial changes in the areas of Admiralty Bay and Potter Cove, King George Island, maritime Antarctica, Geoecology of Antarctic Ice-Free Coastal Landscapes, Springer, 75-89.

BRAUN, M., HUMBERT, A. & MOLL, A. 2009. Changes of Wilkins Ice Shelf over the past 15 years and inferences on its stability: *Cryosphere*, **3**, 1, 41-56.

BRAUN, M., SIMOES, J.C., VOGT, S., BREMER, U.F., BLINDOW, N., PFENDER, M., SAURER, H., AQUINO, F.E. & FERRON, F.A. 2001. An improved topographic database for King George Island: compilation, application and outlook: *Antarctic Science*, **13**, 1, 41-52.

BRENNER, A.C., DIMARZIO, J.R. & ZWALLY, H.J. 2007. Precision and accuracy of satellite radar and laser altimeter data over the continental ice sheets: *Ieee Transactions on Geoscience and Remote Sensing*, **45**, 2, 321-331.

BURGESS, D.O. & SHARP, M.J. 2004. Recent changes in areal extent of the Devon Ice Cap, Nunavut, Canada: *Arctic Antarctic and Alpine Research*, **36**, 2, 261-271.

BURGESS, D.O., SHARP, M.J., MAIR, D.W., DOWDESWELL, J.A. & BENHAM, T.J. 2005. Flow dynamics and iceberg calving rates of Devon Ice Cap, Nunavut, Canada: *Journal of Glaciology*, **51**, 173, 219-230.

CALVET, J., SELLES, D. & CORBERA, J. 1999. Fluctuations in the length of the Livingston (South Shetland Islands) ice cap between 1956 and 1996: *ACTA GEOLOGICA HISPANICA*, **34**, 4, 365-374.

CARR, J.R., STOKES, C.R. & VIELI, A. 2013. Recent progress in understanding marine-terminating Arctic outlet glacier response to climatic and oceanic forcing: Twenty years of rapid change: *Progress in Physical Geography*, **37**, 4, 436-467.

CAZENAVE, A., DOMINH, K., GUINEHUT, S., BERTHIER, E., LLOVEL, W., RAMILLIEN, G., ABLAIN, M. & LARNICOL, G. 2009. Sea level budget over 2003–2008: A reevaluation from GRACE space gravimetry, satellite altimetry and Argo: *Global and Planetary Change*, **65**, 1, 83-88.

CHEN, J.L., WILSON, C.R., BLANKENSHIP, D. & TAPLEY, B.D. 2009. Accelerated Antarctic ice loss from satellite gravity measurements: *Nature Geoscience*, **2**, 12, 859-862.

COCHRAN, J.R., JACOBS, S.S., TINTO, K.J. & BELL, R.E. 2014. Bathymetric and oceanic controls on Abbot Ice Shelf thickness and stability: *The Cryosphere*, **8**, 3, 877-889.

COGLEY, J.G. 2009. Geodetic and direct mass-balance measurements: comparison and joint analysis: *Annals of Glaciology*, **50**, 50, 96-100.

COGLEY, J.G., HOCK, R., RASMUSSEN, L.A., ARENDT, A.A., BAUDER, A., BRAITHWAITE, R.J., JANSSON, P., KASER, G., MÖLLER, M., NICHOLSON, L. & ZEMP, M. 2011. Glossary of Glacier Mass Balance and Related Terms: *IHP-VII Technical Documents in Hydrology No. 86*, **IACS Contribution No. 2**.

COMISO, J.C. 2000. Variability and trends in Antarctic surface temperatures from in situ and satellite infrared measurements: *Journal of Climate*, **13**, 10, 1674-1696.

COOK, A.J., FOX, A.J., VAUGHAN, D.G. & FERRIGNO, J.G. 2005. Retreating glacier fronts on the Antarctic Peninsula over the past half-century: *Science*, **308**, 541-544.

COOK, A.J., MURRAY, T., LUCKMAN, A., VAUGHAN, D.G. & BARRAND, N.E. 2012. A new 100-m Digital Elevation Model of the Antarctic Peninsula derived from ASTER Global DEM: methods and accuracy assessment: *Earth System Science Data*, **4**, 129 - 142.

COOK, A.J. & VAUGHAN, D.G. 2010. Overview of areal changes of the ice shelves on the Antarctic Peninsula over the past 50 years: *Cryosphere*, **4**, 1, 77-98.

COOK, A.J., VAUGHAN, D.G., LUCKMAN, A. & MURRAY, T. 2014 (In Press). A new Antarctic Peninsula glacier basin inventory and observed area changes since the 1940s: *Antarctic Science*, **Special Issue**.

COOPER, A.P.R. 1997. Historical observations of Prince Gustav Ice Shelf: *Polar Record*, **33**, 285-294.

CZIFERSZKY, A., FLEMING, A. & FOX, A. 2010. An assessment of ASTER elevation data over glaciated terrain on Pourquoi Pas Island, Antarctic Peninsula, *in* Gibbs, S., ed., Elevation Models for Geoscience, Geological Society Special Publications.

DAVIES, B.J., CARRIVICK, J.L., GLASSER, N.F., HAMBREY, M.J. & SMELLIE, J.L. 2012. Variable glacier response to atmospheric warming, northern Antarctic Peninsula, 1988-2009: *Cryosphere*, **6**, 5, 1031-1048.

DE ANGELIS, H. & SKVARCA, P. 2003. Glacier surge after ice shelf collapse: *Science*, **299**, 5612, 1560-1562.

DIMARZIO, J., BRENNER, A.C., SCHUTZ, B., SHUMAN, C.A. & ZWALLY, H.J. 2007. GLAS/ICESat 500m laser altimetry digital elevation model of Antarctica, *in* NSIDC, ed.: Boulder, Colorado, USA, Digital Media.

DOAKE, C.S.M. & VAUGHAN, D.G. 1991. Rapid disintegration of Wordie Ice Shelf in response to atmospheric warming: *Nature*, **350**, 328-330.

DOMACK, E., DURAN, D., LEVENTER, A., ISHMAN, S., DOANE, S., MCCALLUM, S., AMBLAS, D., RING, J., GILBERT, R. & PRENTICE, M. 2005. Stability of the Larsen B ice shelf on the Antarctic Peninsula during the Holocene epoch: *Nature*, **436**, 7051, 681-685.

DOMACK, E.W., ISHMAN, S.E., STEIN, A.B., MCCLENNEN, C.E. & JULL, A.J.T. 1995. Late Holocene advance of Muller Ice Shelf, Antarctic Peninsula: sedimentological, geochemical and palaeontological evidence: *Antarctic Science*, **7**, 159-170.

DOMACK, E.W., LEVENTER, A., ROOT, S., RING, J., WILLIAMS, E., CARLSON, D., HIRSHORN, E., WRIGHT, W., GILBERT, R. & BURR, G. 2003. Marine sedimentary record of natural environmental variability, *in* Domack, E., Leventer, A., Burnett, A., Bindschadler, R., Convey, P., and Kirby, M., eds., Antarctic Peninsula Climate Variability: Historical and Paleoenvironmental Perspectives. Antarctic Research Series, 79, Volume 79: Washington, DC, AGU, 61-68.

DREWRY, D.J. 1983, The surface of the Antarctic Ice Sheet: Scott Polar Research Institute.

DUPONT, T.K. & ALLEY, R.B. 2005. Assessment of the importance of ice-shelf buttressing to ice-sheet flow: *Geophysical Research Letters*, **32**, L04503, doi:10.1029/2004GL022024.

EINEDER, M., JABER, W.A., FLORICIOIU, D., ROTT, H., YAGUE-MARTINEZ, N. & IEEE 2011. Glacier Flow and Topography Measurements with TerraSAR-X and TanDEM-X, New York, Ieee, 2011 Ieee International Geoscience and Remote Sensing Symposium, 3835-3838 p.:

ESRI 1991. Environmental Systems Research Institute: *ARC/INFO User's Guide: Cell-based Modeling with GRID, Redlands, California.*

EVANS, J., PUDSEY, C.J., OCOFAIGH, C., MORRIS, P. & DOMACK, E. 2005. Late Quaternary glacial history, flow dynamics and sedimentation along the eastern margin of the Antarctic Peninsula Ice Sheet: *Quaternary Science Reviews*, **24**, 5-6, 741-774.

FAHRBACH, E., HOPPEMA, M., ROHARDT, G., SCHRÖDER, M. & WISOTZKI, A. 2004. Decadal-scale variations of water mass properties in the deep Weddell Sea: *Ocean Dynamics*, **54**, 1, 77-91.

FARINOTTI, D., HUSS, M., BAUDER, A., FUNK, M. & TRUFFER, M. 2009. A method to estimate the ice volume and ice-thickness distribution of alpine glaciers: *Journal of Glaciology*, **55**, 191, 422-430.

FERRIGNO, G.J., COOK, A.J., FOLEY, M.K., WILLIAMS, R.S., SWITHINBANK, C., FOX, A., THOMSON, W.J. & SIEVERS, J. 2006, Coastal-Change and Glaciological Map of the

Trinity Peninsula Area and South Shetland Islands, Antarctica: 1843–2001, U.S. Geological Survey Geologic Investigations Series Map I-2600-A (map sheet, text).
FERRIGNO, G.J., COOK, A.J., MATHIE, M.A., WILLIAMS, R.S., SWITHINBANK, C., FOLEY, M.K., FOX, A., THOMSON, W.J. & SIEVERS, J. 2008, Coastal-change and glaciological map of the Larsen Ice Shelf area, Antarctica: 1940–2005, U.S. Geological Survey Geologic Investigations Series Map I–2600–B, (map sheet, text).
FERRIGNO, G.J., COOK, A.J., MATHIE, M.A., WILLIAMS, R.S., SWITHINBANK, C., FOLEY, M.K., FOX, A., THOMSON, W.J. & SIEVERS, J. 2009, Coastal-change and glaciological map of the Palmer Land area, Antarctica: 1947–2009, U.S. Geological Survey Geologic Investigations Series Map I–2600–C (map sheet, text).
FOX, A. & CZIFERSZKY, A. 2008. Unlocking the time-capsule of historic aerial photography to measure volume changes in Antarctic Peninsula glaciers over a fifty-year period.: *Photogrammetric Enginneering and Remote Sensing*, **23**, 121, 51-68.
FOX, A.J. 1995. Using multiple data sources to enhance photogrammetry for mapping Antarctic terrain: *Polar Research*, **14**, 3, 317-327.
FOX, A.J. & COOPER, A.P.R. 1998. Climate-change indicators from archival aerial photography of the Antarctic Peninsula: *Annals of Glaciology*, **27**, 636-642.
FRETWELL, P., PRITCHARD, H.D., VAUGHAN, D.G., BAMBER, J.L., BARRAND, N.E., BELL, R., BIANCHI, C., BINGHAM, R.G., BLANKENSHIP, D.D., CASASSA, G., CATANIA, G., CALLENS, D., CONWAY, H., COOK, A.J., CORR, H.F.J., DAMASKE, D., DAMM, V., FERRACCIOLI, F., FORSBERG, R., FUJITA, S., GIM, Y., GOGINENI, P., GRIGGS, J.A., HINDMARSH, R.C.A., HOLMLUND, P., HOLT, J.W., JACOBEL, R.W., JENKINS, A., JOKAT, W., JORDAN, T., KING, E.C., KOHLER, J., KRABILL, W., RIGER-KUSK, M., LANGLEY, K.A., LEITCHENKOV, G., LEUSCHEN, C., LUYENDYK, B.P., MATSUOKA, K., MOUGINOT, J., NITSCHE, F.O., NOGI, Y., NOST, O.A., POPOV, S.V., RIGNOT, E., RIPPIN, D.M., RIVERA, A., ROBERTS, J., ROSS, N., SIEGERT, M.J., SMITH, A.M., STEINHAGE, D., STUDINGER, M., SUN, B., TINTO, B.K., WELCH, B.C., WILSON, D., YOUNG, D.A., XIANGBIN, C. & ZIRIZZOTTI, A. 2013. Bedmap2: improved ice bed, surface and thickness datasets for Antarctica: *The Cryosphere*, **7**, 1, 375-393.
FREY, H. & PAUL, F. 2012. On the suitability of the SRTM DEM and ASTER GDEM for the compilation of topographic parameters in glacier inventories: *International Journal of Applied Earth Observation and Geoinformation*, **18**, 480-490.
FRICKER, H.A. & PADMAN, L. 2012. Thirty years of elevation change on Antarctic Peninsula ice shelves from multimission satellite radar altimetry: *Journal of Geophysical Research: Oceans (1978–2012)*, **117**, C2.
GANTERT, S., RIEGLER, G., TEUFEL, F., LANG, O., PETRAT, L., KOPPE, W. & HERRMANN, J. TerraSAR-X, TanDEM-X, TerraSAR-X2 and their applications, *in* Proceedings Synthetic Aperture Radar (APSAR), 2011 3rd International Asia-Pacific Conference on26-30 Sept. 2011 2011, 1-4.
GARDELLE, J., BERTHIER, E. & ARNAUD, Y. 2012. Impact of resolution and radar penetration on glacier elevation changes computed from DEM differencing: *Journal of Glaciology*, **58**, 208, 419-422.
GILLE, S.T. 2002. Warming of the Southern Ocean since the 1950s: *Science*, **295**, 5558, 1275-1277.
GILLE, S.T. 2008. Decadal-scale temperature trends in the Southern Hemisphere ocean: *Journal of Climate*, **21**, 18.
GIOVINETTO, M.B. & BENTLEY, C.R. 1985. Surface balance in ice drainage systems of Antarctica: *Antarctic Journal of the United States*, **20**, 6-13.
GLASSER, N.F., SCAMBOS, T.A., BOHLANDER, J., TRUFFER, M., PETTIT, E. & DAVIES, B.J. 2011. From ice-shelf tributary to tidewater glacier: continued rapid recession, acceleration and

thinning of Rohss Glacier following the 1995 collapse of the Prince Gustav Ice Shelf, Antarctic Peninsula: *Journal of Glaciology*, **57**, 203, 397-406.
GLIMS & NSIDC 2005, updated 2012. Global Land Ice Measurements from Space (GLIMS) Glacier Database: Boulder, CO USA, National Snow and Ice Data Center.
GORDON, A.L., VISBECK, M. & COMISO, J.C. 2007. A Possible Link between the Weddell Polynya and the Southern Annular Mode: *Journal of Climate*, **20**, 11.
GREGORY, J.M., WHITE, N.J., CHURCH, J.A., BIERKENS, M.F.P., BOX, J.E., DEN BROEKE, M.R., COGLEY, J.G., FETTWEIS, X., HANNA, E., HUYBRECHTS, P., KONIKOW, L.F., LECLERCQ, P.W., MARZEION, B., OERLEMANS, J., TAMISIEA, M.E., WADA, Y., WAKE, L.M. & DE WAL, R.S.W. 2013. Twentieth-Century Global-Mean Sea Level Rise: Is the Whole Greater than the Sum of the Parts?: *Journal of Climate*, **26**, 13, 4476-4499.
GUNTER, B., URBAN, T., RIVA, R., HELSEN, M., HARPOLD, R., POOLE, S., NAGEL, P., SCHUTZ, B. & TAPLEY, B. 2009. A comparison of coincident GRACE and ICESat data over Antarctica: *Journal of Geodesy*, **83**, 11, 1051-1060.
HAEBERLI, W. & HOELZLE, M. 1995. Application of inventory data for estimating characteristics of and regional climate-change effects on mountain glaciers: A pilot study with the European Alps, Annals of Glaciology, Vol 21, 1995: Proceedings of the International Symposium on the Role of the Cryosphere in Global Change, 206-212 p.:
HARANGOZO, S. 2000. A search for ENSO teleconnections in the west Antarctic Peninsula climate in austral winter: *International Journal of Climatology*, **20**, 6, 663-679.
HARDY, R.J., BAMBER, J.L. & ORFORD, S. 2000. The delineation of drainage basins on the Greenland ice sheet for mass-balance analyses using a combined modelling and geographical information system approach: *Hydrological Processes*, **14**, 11-12, 1931-1941.
HEROY, D.C. & ANDERSON, J.B. 2005. Ice-sheet extent of the Antarctic Peninsula region during the Last Glacial Maximum (LGM) - Insights from glacial geomorphology: *Geological Society of America Bulletin*, **117**, 11-12, 1497-1512.
HEROY, D.C. & ANDERSON, J.B. 2007. Radiocarbon constraints on Antarctic Peninsula Ice Sheet retreat following the Last Glacial Maximum (LGM): *Quaternary Science Reviews*, **26**, 25-28, 3286-3297.
HOCK, R., DE WOUL, M., RADIC, V. & DYURGEROV, M. 2009. Mountain glaciers and ice caps around Antarctica make a large sea-level rise contribution: *Geophysical Research Letters*, **36**, L07501, 1 - 5.
HODGSON, D.A., BENTLEY, M.J., ROBERTS, S.J., SMITH, J.A., SUGDEN, D.E. & DOMACK, E.W. 2006. Examining Holocene stability of Antarctic Peninsula ice shelves: *Eos, Transactions American Geophysical Union*, **87**, 31, 305-308.
HOELZLE, M., HAEBERLI, W., DISCHL, M. & PESCHKE, W. 2003. Secular glacier mass balances derived from cumulative glacier length changes: *Global and Planetary Change*, **36**, 4, 295-306.
HOLLAND, P.R., CORR, H.F., VAUGHAN, D.G., JENKINS, A. & SKVARCA, P. 2009. Marine ice in Larsen ice shelf: *Geophysical Research Letters*, **36**, 11.
HOLLAND, P.R., JENKINS, A. & HOLLAND, D.M. 2008. The response of ice shelf basal melting to variations in ocean temperature: *Journal of Climate*, **21**, 11, 2558-2572.
HOLLAND, P.R., JENKINS, A. & HOLLAND, D.M. 2010. Ice and ocean processes in the Bellingshausen Sea, Antarctica: *Journal of Geophysical Research-Oceans*, **115**.
HOLLAND, P.R. & KWOK, R. 2012. Wind-driven trends in Antarctic sea-ice drift: *Nature Geoscience*, **5**, 12, 872-875.
HOLT, T.O., GLASSER, N.F., QUINCEY, D.J. & SIEGFRIED, M. 2013. Speedup and fracturing of George VI Ice Shelf, Antarctic Peninsula: *The Cryosphere*, **7**, 797-816.
HORWATH, M. & DIETRICH, R. 2009. Signal and error in mass change inferences from GRACE: the case of Antarctica: *Geophysical Journal International*, **177**, 3, 849-864.

HOWAT, I.M. & EDDY, A. 2011. Multi-decadal retreat of Greenland's marine-terminating glaciers: *Journal of Glaciology*, **57**, 203, 389-396.

HOWAT, I.M., JOUGHIN, I., FAHNESTOCK, M., SMITH, B.E. & SCAMBOS, T.A. 2008. Synchronous retreat and acceleration of southeast Greenland outlet glaciers 2000-06: ice dynamics and coupling to climate: *Journal of Glaciology*, **54**, 187, 646-660.

HUGHES, T. 1975. The West Antarctic ice sheet: Instability, disintegration, and initiation of ice ages: *Reviews of Geophysics*, **13**, 4, 502-526.

HULBE, C.L., SCAMBOS, T.A., YOUNGBERG, T. & LAMB, A.K. 2008. Patterns of glacier response to disintegration of the Larsen B ice shelf, Antarctic Peninsula: *Global and Planetary Change*, **63**, 1, 1-8.

HUSS, M. & FARINOTTI, D. 2014. A high-resolution bedrock map for the Antarctic Peninsula: *The Cryosphere Discuss.*, **8**, 1, 1191-1225.

HUTCHINSON, M.F. 1989. A new procedure for gridding elevation and stream line data with automatic removal of spurious pits: *Journal of Hydrology*, **106**, 3-4, 211-232.

HVIDEGAARD, S.M., SORENSEN, L.S. & FORSBERG, R. 2012. ASTER GDEM validation using LiDAR data over coastal regions of Greenland: *Remote Sensing Letters*, **3**, 1, 85-91.

INGOLFSSON, O., HJORT, C. & HUMLUM, O. 2003. Glacial and climate history of the Antarctic Peninsula since the Last Glacial Maximum: *Arctic Antarctic and Alpine Research*, **35**, 2, 175-186.

IPCC 2007. Summary for Policymakers., *in* Solomon, S., D. Qin, M. Manning, Z. Chen, M. Marquis, K.B. Averyt, M.Tignor, and H.L. Miller, eds., Climate Change 2007: The Physical Science Basis Contribution of Working Group I to the Fourth Assessment Report of the Intergovernmental Panel on Climate Change: Cambridge, United Kingdom and New York, USA, Cambridge University Press.

IPCC 2013. Summary for Policymakers, *in* Stocker, T.F., Qin, D., Plattner, G.-K., Tignor, M., Allen, S.K., Boschung, J., Nauels, A., Xia, Y., Bex, V., and Midgley, P.M., eds., Climate Change 2013: The Physical Science Basis. Working Group I to the Fifth Assessment Report of the Intergovernmental Panel on Climate Change: Cambridge, United Kingdom and New York, NY, USA., Cambridge University Press.

IVINS, E.R., WATKINS, M.M., YUAN, D.N., DIETRICH, R., CASASSA, G. & RULKE, A. 2011. On-land ice loss and glacial isostatic adjustment at the Drake Passage: 2003-2009: *Journal of Geophysical Research-Solid Earth*, **116**.

JANSEN, D., KULESSA, B., SAMMONDS, P., LUCKMAN, A., KING, E. & GLASSER, N.F. 2010. Present stability of the Larsen C ice shelf, Antarctic Peninsula: *Journal of Glaciology*, **56**, 198, 593-600.

JENKINS, A., DUTRIEUX, P., JACOBS, S.S., MCPHAIL, S.D., PERRETT, J.R., WEBB, A.T. & WHITE, D. 2010. Observations beneath Pine Island Glacier in West Antarctica and implications for its retreat: *Nature Geosci*, **3**, 7, 468-472.

JEZEK, K.C. 1999. Glaciological properties of the Antarctic ice sheet from RADARSAT-1 synthetic aperture radar imagery, Annals of Glaciology, Volume 29, 286-290.

JISKOOT, H., CURRAN, C.J., TESSLER, D.L. & SHENTON, L.R. 2009. Changes in Clemenceau Icefield and Chaba Group glaciers, Canada, related to hypsometry, tributary detachment, length-slope and area-aspect relations: *Annals of Glaciology*, **50**, 53, 133-143.

JOHNSON, J.S., BENTLEY, M.J., ROBERTS, S.J., BINNIE, S.A. & FREEMAN, S. 2011. Holocene deglacial history of the northeast Antarctic Peninsula - A review and new chronological constraints: *Quaternary Science Reviews*, **30**, 27-28, 3791-3802.

JOUGHIN, I., SMITH, B.E. & MEDLEY, B. 2014. Marine Ice Sheet Collapse Potentially Under Way for the Thwaites Glacier Basin, West Antarctica: *Science*, **344**, 6185, 735-738.

KÄÄB, A., HUGGEL, C., PAUL, F., WESSELS, R., RAUP, B., KIEFFER, H. & KARGEL, J.S. 2002a. Glacier monitoring from ASTER imagery: accuracy and applications: *EARSeL eProceedings No.2*, 43-53.

KÄÄB, A., PAUL, F., MAISCH, M., HOELZLE, M. & HAEBERLI, W. 2002b. The new remote-sensing-derived Swiss glacier inventory: II. First results, *in* Winther, J.G., and Solberg, R., eds., Annals of Glaciology, Vol 34, 2002, Volume 34: Cambridge, Int Glaciological Soc, 362-366.

KARGEL, J.S., ABRAMS, M.J., BISHOP, M.P., BUSH, A., HAMILTON, G., JISKOOT, H., KÄÄB, A., KIEFFER, H.H., LEE, E.M. & PAUL, F. 2005. Multispectral imaging contributions to global land ice measurements from space: *Remote Sensing of Environment*, **99**, 1, 187-219.

KERVYN, M., ERNST, G.G.J., GOOSSENS, R. & JACOBS, P. 2008. Mapping volcano topography with remote sensing: ASTER vs. SRTM: *International Journal of Remote Sensing*, **29**, 22, 6515-6538.

KIENHOLZ, C., RICH, J., ARENDT, A. & HOCK, R. 2014. A new method for deriving glacier centerlines applied to glaciers in Alaska and northwest Canada: *The Cryosphere*, **8**, 2, 503-519.

KING, J.C. 1994. Recent climate variability in the vicinity of the Antarctic Peninsula: *International Journal of Climatology*, **14**, 357-369.

KING, J.C., ANDERSON, P.S., VAUGHAN, D.G., MANN, G.W. & MOBBS, S.D. 2004. Wind-Borne redistribution of snow across an Antarctic ice rise: *Journal of Geophysical Research*, **109**, D11, D11104 doi:11110.11029/12003JD004361.

KING, J.C. & HARANGOZO, S.A. 1998. Climate change in the western Antarctic Peninsula since 1945: observations and possible causes: *Annals of Glaciology*, **27**, 571-575.

KING, M.A., BINGHAM, R.J., MOORE, P., WHITEHOUSE, P.L., BENTLEY, M.J. & MILNE, G.A. 2012. Lower satellite-gravimetry estimates of Antarctic sea-level contribution: *Nature*, **491**, 7425, 586-589.

KING, M.A., MAKINSON, K. & GUDMUNDSSON, G.H. 2011a. Nonlinear interaction between ocean tides and the Larsen C Ice Shelf system: *Geophysical Research Letters*, **38**, 8.

KING, M.A., PADMAN, L., NICHOLLS, K., CLARKE, P.J., GUDMUNDSSON, G.H., KULESSA, B. & SHEPHERD, A. 2011b. Ocean tides in the Weddell Sea: New observations on the Filchner-Ronne and Larsen C ice shelves and model validation: *Journal of Geophysical Research: Oceans (1978–2012)*, **116**, C6.

KLINCK, J.M., HOFMANN, E.E., BEARDSLEY, R.C., SALIHOGLU, B. & HOWARD, S. 2004. Water-mass properties and circulation on the west Antarctic Peninsula Continental Shelf in Austral Fall and Winter 2001: *Deep Sea Research Part II: Topical Studies in Oceanography*, **51**, 17, 1925-1946.

KORONA, J., BERTHIER, E., BERNARD, M., REMY, F. & THOUVENOT, E. 2009. SPIRIT. SPOT 5 stereoscopic survey of Polar Ice: Reference Images and Topographies during the fourth International Polar Year (2007-2009): *Isprs Journal of Photogrammetry and Remote Sensing*, **64**, 2, 204-212.

KULESSA, B., JANSEN, D., LUCKMAN, A.J., KING, E.C. & SAMMONDS, P.R. 2014. Marine ice regulates the future stability of a large Antarctic ice shelf: *Nature communications*, **5**.

KUNZ, M., KING, M.A., MILLS, J.P., MILLER, P.E., FOX, A.J., VAUGHAN, D.G. & MARSH, S.H. 2012. Multi-decadal glacier surface lowering in the Antarctic Peninsula: *Geophysical Research Letters*, **39**, L19502, 1 - 5.

KURTZ, N. & MARKUS, T. 2012. Satellite observations of Antarctic sea ice thickness and volume: *Journal of Geophysical Research: Oceans (1978–2012)*, **117**, C8.

LECLERCQ, P., OERLEMANS, J., BASAGIC, H., BUSHUEVA, I., COOK, A. & LE BRIS, R. 2014. A data set of worldwide glacier length fluctuations: *The Cryosphere*, **8**, 2, 659-672.

LECLERCQ, P.W., OERLEMANS, J. & COGLEY, J.G. 2011. Estimating the Glacier Contribution to Sea-Level Rise for the Period 1800-2005: *Surveys in Geophysics*, **32**, 4-5, 519-535.

LECLERCQ, P.W., WEIDICK, A., PAUL, F., BOLCH, T., CITTERIO, M. & OERLEMANS, J. 2012. Brief communication "Historical glacier length changes in West Greenland": *Cryosphere*, **6**, 6, 1339-1343.

LEE, D.S., STOREY, J.C., CHOATE, M.J. & HAYES, R.W. 2004. Four years of Landsat-7 on-orbit geometric calibration and performance: *Geoscience and Remote Sensing, IEEE Transactions on*, **42**, 12, 2786-2795.

LEE, T., HOBBS, W.R., WILLIS, J.K., HALKIDES, D., FUKUMORI, I., ARMSTRONG, E.M., HAYASHI, A.K., LIU, W.T., PATZERT, W. & WANG, O. 2010. Record warming in the South Pacific and western Antarctica associated with the strong central-Pacific El Nino in 2009-10: *Geophysical Research Letters*, **37**.

LENAERTS, J.T.M., VAN DEN BROEKE, M.R., VAN DE BERG, W.J., VAN MEIJGAARD, E. & MUNNEKE, P.K. 2012. A new, high-resolution surface mass balance map of Antarctica (1979-2010) based on regional atmospheric climate modeling: *Geophysical Research Letters*, **39**.

LEWIS, S.M. & SMITH, L.C. 2009. Hydrologic drainage of the Greenland Ice Sheet: *Hydrological Processes*, **23**, 14, 2004-2011.

LI, X., HOLLAND, D.M., GERBER, E.P. & YOO, C. 2014. Impacts of the north and tropical Atlantic Ocean on the Antarctic Peninsula and sea ice: *Nature*, **505**, 7484, 538-542.

LIGTENBERG, S.R.M., VAN DE BERG, W.J., VAN DEN BROEKE, M.R., RAE, J.G.L. & VAN MEIJGAARD, E. 2013. Future surface mass balance of the Antarctic ice sheet and its influence on sea level change, simulated by a regional atmospheric climate model: *Climate Dynamics*, **41**, 3-4, 867-884.

LIU, H., JEZEK, K., LI, B. & ZHAO, Z. 2001. Radarsat Antarctic Mapping Project Digital Elevation Model version 2: *National Snow and Ice Data Center*, **v2**.

LIU, H.X., JEZEK, K.C. & LI, B. 1999. Development of Antarctic DEM by integrating cartographic and remotely sensed data: A GIS-based approach.: *Journal of Geophysical Research*, **104**, B10, 23199-23213.

LIVINGSTONE, S.J., Ó COFAIGH, C., STOKES, C.R., HILLENBRAND, C.-D., VIELI, A. & JAMIESON, S.S.R. 2012. Antarctic palaeo-ice streams: *Earth-Science Reviews*, **111**, 1–2, 90-128.

LODWICK, G.D. & PAINE, S.H. 1985. A Digital Elevation Model of the Barnes Ice-Cap Derived from Landsat MSS Data: *Photogrammetric Engineering and Remote Sensing*, **51**, 12, 1937-1944.

MACFERRIN, M., ABDALATI, W. & SCAMBOS, T.A. In review. Summary of ASTER GDEM 1 and 2 errors on the Greenland Ice Sheet, with recommendations for scientific use: *Remote Sensing of Environment*.

MACGREGOR, J.A., CATANIA, G.A., MARKOWSKI, M.S. & ANDREWS, A.G. 2012. Widespread rifting and retreat of ice-shelf margins in the eastern Amundsen Sea Embayment between 1972 and 2011: *Journal of Glaciology*, **58**, 209, 458-466.

MARSHALL, G.J. 2002. Analysis of recent circulation and thermal advection change in the northern Antarctic Peninsula: *International Journal of Climatology*, **22**, 12, 1557-1567.

MARSHALL, G.J. 2003. Trends in the southern annular mode from observations and reanalyses: *Journal of Climate*, **16**, 4134-4143.

MARSHALL, G.J. 2009. On the annual and semi-annual cycles of precipitation across Antarctica: *International Journal of Climatology*, **29**, 15, 2298-2308.

MARSHALL, G.J., ORR, A., VAN LIPZIG, N.P.M. & KING, J.C. 2006. The impact of a changing Southern Hemisphere Annular Mode on Antarctic Peninsula summer temperatures: *Journal of Climate*, **19**, 20, 5388-5404.

MARTINSON, D.G., STAMMERJOHN, S.E., IANNUZZI, R.A., SMITH, R.C. & VERNET, M. 2008. Western Antarctic Peninsula physical oceanography and spatio-temporal variability: *Deep-Sea Research Part II -Topical Studies in Oceanography*, **55**, 18-19, 1964-1987.

MASSON, V., VIMEUX, F., JOUZEL, J., MORGAN, V., DELMOTTE, M., CIAIS, P., HAMMER, C., JOHNSEN, S., LIPENKOV, V.Y., MOSLEY-THOMPSON, E., PETIT, J.R., STEIG, E.J., STIEVENARD, M. & VAIKMAE, R. 2000. Holocene climate variability in Antarctica based on 11 ice-core isotopic records: *Quaternary Research*, **54**, 3, 348-358.

MAYEWSKI, P.A., MEREDITH, M.P., SUMMERHAYES, C.P., TURNER, J., WORBY, A., BARRETT, P.J., CASASSA, G., BERTLER, N.A.N., BRACEGIRDLE, T., GARABATO, A.C.N., BROMWICH, D., CAMPBELL, H., HAMILTON, G.S., LYONS, W.B., MAASCH, K.A., AOKI, S., XIAO, C. & VAN OMMEN, T. 2009. State of the Antarctic and Southern Ocean Climate System: *Reviews of Geophysics*, **47**.

MCNABB, R. & HOCK, R. 2014. Alaska tidewater glacier terminus positions, 1948–2012: *Journal of Geophysical Research: Earth Surface*, **119**, 2, 153-167.

MEEHL, G.A., STOCKER, T.F., COLLINS, W.D., FRIEDLINGSTEIN, P., GAYE, A.T., GREGORY, J.M., KITOH, A., KNUTTI, R., MURPHY, J.M., NODA, A., RAPER, S.C.B., WATTERSON, I.G., WEAVER, A.J. & ZHAO, Z.-C. 2007. Global Climate Projections, *in* Solomon, S., Qin, D., Manning, M., Z. Chen, M. Marquis, Averyt, K.B., Tignor, M., and Miller, H.L., eds., Climate Change 2007: The Physical Science Basis. Contribution of Working Group I to the Fourth Assessment Report of the Intergovernmental Panel on Climate Change Cambridge, United Kingdom and New York, NY, USA, Cambridge University Press, 749-845.

MERCER, J.H. 1978. West Antarctic ice sheet and CO2 greenhouse effect: a threat of disaster: *Nature*, **271**, 321-325.

MEREDITH, M.P. & KING, J.C. 2005. Rapid climate change in the ocean west of the Antarctic Peninsula during the second half of the 20th century: *Geophysical Research Letters*, **32**, L19604, 1 - 5.

MEREDITH, M.P., VENABLES, H.J., CLARKE, A., DUCKLOW, H.W., ERICKSON, M., LENG, M.J., LENAERTS, J.T.M. & VAN DEN BROEKE, M.R. 2013. The Freshwater System West of the Antarctic Peninsula: Spatial and Temporal Changes: *Journal of Climate*, **26**, 5, 1669-1684.

MEREDITH, M.P., WALLACE, M.I., STAMMERJOHN, S.E., RENFREW, I.A., CLARKE, A., VENABLES, H.J., SHOOSMITH, D.R., SOUSTER, T. & LENG, M.J. 2010. Changes in the freshwater composition of the upper ocean west of the Antarctic Peninsula during the first decade of the 21st century: *Progress in Oceanography*, **87**, 1, 127-143.

MILES, B., STOKES, C., VIELI, A. & COX, N. 2013. Rapid, climate-driven changes in outlet glaciers on the Pacific coast of East Antarctica: *Nature*, **500**, 7464, 563-566.

MILES, G.M., MARSHALL, G.J., MCCONNELL, J.R. & ARISTARAIN, A.J. 2008. Recent accumulation variability and change on the Antarctic Peninsula from the ERA40 reanalysis: *International Journal of Climatology*, **28**, 11, 1409-1422.

MOHOLDT, G., NUTH, C., HAGEN, J.O. & KOHLER, J. 2010. Recent elevation changes of Svalbard glaciers derived from ICESat laser altimetry: *Remote Sensing of Environment*, **114**, 11, 2756-2767.

MOON, T. & JOUGHIN, I. 2008. Changes in ice front position on Greenland's outlet glaciers from 1992 to 2007: *Journal of Geophysical Research-Earth Surface*, **113**, F2.

MORRIS, E.M. & MULVANEY, R. 2004. Recent variations in surface mass balance of the Antarctic Peninsula ice sheet: *Journal of Glaciology*, **50**, 169, 257-267.

MORRIS, E.M. & VAUGHAN, D.G. 1994. Snow surface temperatures in West Antarctica: *Antarctic Science*, **6**, 4, 529-535.

MORRIS, E.M. & VAUGHAN, D.G. 2003. Spatial and temporal variation of surface temperature on the Antarctic Peninsula and the limit of viability of ice shelves, *in* Domack, E., Leventer, A., Burnett, A., Bindschadler, R., Convey, P., and Kirby, M., eds., Antarctic Peninsula Climate Variability: Historical and Paleoenvironmental Perspectives., Volume Antarctic Research Series, 79: Washington, DC, AGU, 61-68.

MOUGINOT, J., RIGNOT, E. & SCHEUCHL, B. 2014. Sustained increase in ice discharge fromthe Amundsen Sea Embayment, West Antarctica, from1973 to 2013: *Geophysical Research Letters*, **41**, 5, 1576-1584.

MUELLER, R., PADMAN, L., DINNIMAN, M., EROFEEVA, S., FRICKER, H. & KING, M. 2012. Impact of tide topography interactions on basal melting of Larsen C Ice Shelf, Antarctica: *Journal of Geophysical Research: Oceans (1978–2012)*, **117**, C5.

MÜLLER, F., CAFLISCH, T. & MÜLLER, G. 1977. Instructions for the compilation and assemblage of data for a world glacier inventory.: Temporal Technical Secretariat for the World Glacier Inventory (TTS/WGI).

MULVANEY, R., ABRAM, N.J., HINDMARSH, R.C.A., ARROWSMITH, C., FLEET, L., TRIEST, J., SIME, L.C., ALEMANY, O. & FOORD, S. 2012. Recent Antarctic Peninsula warming relative to Holocene climate and ice-shelf history: *Nature*, **489**, 7414, 141-204.

NICHOLLS, K.W., ØSTERHUS, S., MAKINSON, K., GAMMELSRØD, T. & FAHRBACH, E. 2009. Ice-ocean processes over the continental shelf of the southern Weddell Sea, Antarctica: A review: *Reviews of Geophysics*, **47**, 3.

NICK, F.M., VIELI, A., HOWAT, I.M. & JOUGHIN, I. 2009. Large-scale changes in Greenland outlet glacier dynamics triggered at the terminus: *Nature Geosci*, **2**, 2, 110-114.

NUTH, C. & KÄÄB, A. 2011. Co-registration and bias corrections of satellite elevation data sets for quantifying glacier thickness change: *Cryosphere*, **5**, 1, 271-290.

O'LEARY, M. & CHRISTOFFERSEN, P. 2013. Calving on tidewater glaciers amplified by submarine frontal melting: *The Cryosphere*, **7**, 1, 119-128.

OERLEMANS, J., DYURGEROV, M. & DE WAL, R. 2007. Reconstructing the glacier contribution to sea-level rise back to 1850: *Cryosphere*, **1**, 1, 59-65.

PARK, B.-K., CHANG, S.-K., YOON, H.I. & CHUNG, H. 1998. Recent retreat of the ice cliffs on King George Island, South Shetland Islands, Antarctic Peninsula: *Annals of Glaciology*, **27**, 633-635.

PAUL, F. 2010. The influence of changes in glacier extent and surface elevation on modeled mass balance: *Cryosphere*, **4**, 4, 569-581.

PAUL, F. & ANDREASSEN, L.M. 2009. A new glacier inventory for the Svartisen region, Norway, from Landsat ETM plus data: challenges and change assessment: *Journal of Glaciology*, **55**, 192, 607-618.

PAUL, F., BARRY, R.G., COGLEY, J.G., FREY, H., HAEBERLI, W., OHMURA, A., OMMANNEY, C.S.L., RAUP, B., RIVERA, A. & ZEMP, M. 2009. Recommendations for the compilation of glacier inventory data from digital sources: *Annals of Glaciology*, **50**, 53, 119-126.

PAUL, F., KÄÄB, A., MAISCH, M., KELLENBERGER, T. & HAEBERLI, W. 2002. The new remote-sensing-derived swiss glacier inventory: I. Methods, *in* Winther, J.G., and Solberg, R., eds., Annals of Glaciology, Vol 34, 2002, Volume 34: Cambridge, Int Glaciological Soc, 355-361.

PAUL, F. & SVOBODA, F. 2009. A new glacier inventory on southern Baffin Island, Canada, from ASTER data: II. Data analysis, glacier change and applications: *Annals of Glaciology*, **50**, 53, 22-31.

PECK, L.S., BARNES, D.K.A., COOK, A.J., FLEMING, A.H. & CLARKE, A. 2010. Negative feedback in the cold: ice retreat produces new carbon sinks in Antarctica: *Global Change Biology*, **16**, 9, 2614-2623.

PORTER, D.F., TINTO, K.J., BOGHOSIAN, A., COCHRAN, J.R., BELL, R.E., MANIZADE, S.S. & SONNTAG, J.G. 2014. Bathymetric control of tidewater glacier mass loss in northwest Greenland: *Earth and Planetary Science Letters*, **401**, 40-46.

PRITCHARD, H. & VAUGHAN, D.G. 2007. Widespread acceleration of tidewater glaciers on the Antarctic Peninsula *Journal of Geophysical Research*, **112**, F03S29, doi:10.1029/2006JF000597.

PRITCHARD, H.D., ARTHERN, R.J., VAUGHAN, D.G. & EDWARDS, L.A. 2009. Extensive dynamic thinning on the margins of the Greenland and Antarctic ice sheets: *Nature*, **461**, 971 - 975.

PRITCHARD, H.D., LIGTENBERG, S.R.M., FRICKER, H.A., VAUGHAN, D.G., VAN DEN BROEKE, M.R. & PADMAN, L. 2012. Antarctic ice-sheet loss driven by basal melting of ice shelves: *Nature*, **484**, 7395, 502-505.

PUDSEY, C.J. & EVANS, J. 2001. First survey of Antarctic sub-ice shelf sediments reveals mid-Holocene ice shelf retreat: *Geology*, **29**, 9, 787-790.

PUDSEY, C.J., MURRAY, J.W., APPLEBY, P. & EVANS, J. 2006. Lee shelf history from petrographic and foraminiferal evidence, Northeast Antarctic Peninsula: *Quaternary Science Reviews*, **25**, 17-18, 2357-2379.

RABASSA, J., SKVARCA, P., BERTANI, L. & MAZZONI, E. 1982. Glacier inventory of James Ross and Vega Islands, Antarctic Peninsula: *Annals of Glaciology*, **3**, 260-264.

RACOVITEANU, A.E., MANLEY, W.F., ARNAUD, Y. & WILLIAMS, M.W. 2007. Evaluating digital elevation models for glaciologic applications: An example from Nevado Coropuna, Peruvian Andes: *Global and Planetary Change*, **59**, 1-4, 110-125.

RADIC, V. & HOCK, R. 2010. Regional and global volumes of glaciers derived from statistical upscaling of glacier inventory data: *Journal of Geophysical Research-Earth Surface*, **115**.

RADIC, V. & HOCK, R. 2011. Regionally differentiated contribution of mountain glaciers and ice caps to future sea-level rise: *Nature Geoscience*, **4**, 2, 91-94.

RAMILLIEN, G., LOMBARD, A., CAZENAVE, A., IVINS, E.R., LLUBES, M., REMY, F. & BIANCALE, R. 2006. Interannual variations of the mass balance of the Antarctica and Greenland ice sheets from GRACE: *Global and Planetary Change*, **53**, 3, 198-208.

RAU, F., KARGEL, J.S. & RAUP, B. 2006. The GLIMS Glacier Inventory of the Antarctic Peninsula: *The Earth Observer*, **18**, 6, 9-11.

RAU, F., MAUZ, F., DE ANGELIS, H., JANA, R., NETO, J.A., SKVARCA, P., VOGT, S., SAURER, H. & GOSSMANN, H. 2004. Variations of glacier frontal positions on the northern Antarctic Peninsula: *Annals of Glaciology*, **39**, 525-530.

RAU, F., MAUZ, F., VOGT, S., KHALSA, S.J.S. & RAUP, B. 2005. Illustrated GLIMS Glacier Classification Manual Version 1.0: *GLIMS Regional Center 'Antarctic Peninsula'*.

RAUP, B., KÄÄB, A., KARGEL, J.S., BISHOP, M.P., HAMILTON, G., LEE, E., PAUL, F., RAU, F., SOLTESZ, D., KHALSA, S.J.S., BEEDLE, M. & HELM, C. 2007. Remote sensing and GIS technology in the global land ice measurements from space (GLIMS) project: *Computers & Geosciences*, **33**, 1, 104-125.

REES, W.G. 2012. Assessment of ASTER global digital elevation model data for Arctic research: *Polar Record*, **48**, 244, 31-39.

REUTER, H.I., NELSON, A., STROBL, P., MEHL, W. & JARVIS, A. 2009. A First Assessment of ASTER GDEM tiles for Absolute Accuracy, Relative Accuracy and Terrain Parameters, New York, IEEE, 2009 IEEE International Geoscience and Remote Sensing Symposium, Vols 1-5, 3665-3668 p.:

REYNOLDS, J. 1981. The distribution of mean annual temperatures in the Antarctic Peninsula: *British Antarctic Survey Bulletin*, **54**, 123-133.

RICHARD, Y., ROUAULT, M., POHL, B., CRETAT, J., DUCLOT, I., TABOULOT, S., REASON, C.J.C., MACRON, C. & BUIRON, D. 2013. Temperature changes in the mid- and high- latitudes of the Southern Hemisphere: *International Journal of Climatology*, **33**, 8, 1948-1963.

RIGNOT, E. 1998. Fast recession of a West Antarctic Glacier: *Science*, **281**, 549-551.

RIGNOT, E., BAMBER, J.L., VAN DEN BROEKE, M.R., DAVIS, C., LI, Y., VAN DE BERG, W.J. & VAN MEIJGAARD, E. 2008. Recent Antarctic ice mass loss from radar interferometry and regional climate modelling: *Nature Geoscience*, **1**, 2, 106-110.

RIGNOT, E., CASASSA, G., GOGINENI, P., KRABILL, W., RIVERA, A. & THOMAS, R. 2004. Accelerated ice discharge from the Antarctic Peninsula following the collapse of Larsen B ice shelf: *Geophysical Research Letters*, **31**, L18401, doi:10.1029/2004GL020679.

RIGNOT, E., CASASSA, G., GOGINENI, S., KANAGARATNAM, P., KRABILL, W., PRITCHARD, H., RIVERA, A., THOMAS, R. & VAUGHAN, D. 2005. Recent ice loss from the Fleming and other glaciers,Wordie Bay, West Antarctic Peninsula: *Geophysical Research Letters*, **32**, L07502, doi:10.1029/2004GL021947.

RIGNOT, E. & JACOBS, S. 2002. Rapid bottom melting widespread near Antarctic Ice Sheet Grounding lines: *Science*, **296**, 2020-2023.

RIGNOT, E., JACOBS, S., MOUGINOT, J. & SCHEUCHL, B. 2013. Ice-Shelf Melting Around Antarctica: *Science*, **341**, 6143, 266-270.

RIGNOT, E., MOUGINOT, J., MORLIGHEM, M., SEROUSSI, H. & SCHEUCHL, B. 2014. Widespread, rapid grounding line retreat of Pine Island, Thwaites, Smith, and Kohler glaciers, West Antarctica, from 1992 to 2011: *Geophysical Research Letters*.

RIGNOT, E., MOUGINOT, J. & SCHEUCHL, B. 2011a. Ice Flow of the Antarctic Ice Sheet: *Science*, **333**, 6048, 1427-1430.

RIGNOT, E., VELICOGNA, I., VAN DEN BROEKE, M., MONAGHAN, A. & LENAERTS, J. 2011b. Acceleration of the contribution of the Greenland and Antarctic ice sheets to sea level rise: *Geophysical Research Letters*, **38**, 5.

ROBERTSON, R., VISBECK, M., GORDON, A.L. & FAHRBACH, E. 2002. Long-term temperature trends in the deep waters of the Weddell Sea: *Deep Sea Research Part II: Topical Studies in Oceanography*, **49**, 21, 4791-4806.

ROQUET, F., WUNSCH, C., FORGET, G., HEIMBACH, P., GUINET, C., REVERDIN, G., CHARRASSIN, J.-B., BAILLEUL, F., COSTA, D.P., HUCKSTADT, L.A., GOETZ, K.T., KOVACS, K.M., LYDERSEN, C., BIUW, M., NOST, O.A., BORNEMANN, H., PLOETZ, J., BESTER, M.N., MCINTYRE, T., MUELBERT, M.C., HINDELL, M.A., MCMAHON, C.R., WILLIAMS, G., HARCOURT, R., FIELD, I.C., CHAFIK, L., NICHOLLS, K.W., BOEHME, L. & FEDAK, M.A. 2013. Estimates of the Southern Ocean general circulation improved by animal-borne instruments: *Geophysical Research Letters*, **40**, 23, 6176-6180.

ROSS 1847. A voyage of discovery and research in the southern and Antarctic regions, during the years 1839-43, John Murray, **2 volumes**: London.

ROTT, H., MULLER, F., NAGLER, T. & FLORICIOIU, D. 2011. The imbalance of glaciers after disintegration of Larsen-B ice shelf, Antarctic Peninsula: *Cryosphere*, **5**, 1, 125-134.

ROTT, H., RACK, W. & NAGLER, T. Increased export of grounded ice after the collapse of northern Larsen Ice Shelf, Antarctic Peninsula, observed by Envisat ASAR, *in* Proceedings Geoscience and Remote Sensing Symposium, 2007. IGARSS 2007. IEEE International2007, IEEE, 1174-1176.

ROTT, H., RACK, W., NAGLER, T. & SKVARCA, P. 1998. Climatically induced retreat and collapse of northern Larsen Ice Shelf, Antarctic Peninsula: *Annals of Glaciology*, **27**, 86-92.

ROTT, H., RACK, W., SKVARCA, P. & DE ANGELIS, H. 2002. Northern Larsen Ice Shelf, Antarctica: further retreat after collapse: *Annals of Glaciology*, **34**, 277-282.

ROTT, H., SKVARCA, P. & NAGLER, T. 1996. Rapid collapse of Northern Larsen Ice Shelf, Antarctica: *Science*, **271**, 788-792.

SCAMBOS, T., HULBE, C. & FAHNESTOCK, M. 2003. Climate-induced ice shelf disintegration in the Antarctic Peninsula, *in* Domack, E., Leventer, A., Burnett, A., Bindschadler, R., Convey, P., and Kirby, M., eds., Antarctic Peninsula Climate Variability: Historical and Paleoenvironmental Perspectives. Antarctic Research Series, 79, Volume 79: Washington, DC, AGU, 79-92.

SCAMBOS, T.A., BERTHIER, E., HARAN, T., SHUMAN, C.A., COOK, A.J., LIGTENBERG, S.R.M. & BOHLANDER, J. 2014. Detailed ice loss pattern in the northern Antarctic Peninsula:

widespread decline driven by ice front retreats: *The Cryosphere Discuss.*, **8**, 3, 3237-3261.

SCAMBOS, T.A., BERTHIER, E. & SHUMAN, C.A. 2011. The triggering of subglacial lake drainage during rapid glacier drawdown: Crane Glacier, Antarctic Peninsula: *Annals of Glaciology*, **52**, 59, 74-82.

SCAMBOS, T.A., BOHLANDER, J.A., SHUMAN, C.A. & SKVARCA, P. 2004. Glacier acceleration and thinning after ice shelf collapse in the Larsen B embayment, Antarctica: *Geophysical Research Letters*, **31**, 18, L18402.

SCAMBOS, T.A., HULBE, C., FAHNESTOCK, M. & BOHLANDER, J. 2000. The link between climate warming and break-up of ice shelves in the Antarctic Peninsula: *Journal of Glaciology*, **46**, 154, 516-530.

SCIENTIFIC COMMITTEE ON ANTARCTIC RESEARCH 2005. The Antarctic digital database, Version-4.1 http://www.add.scar.org/.

SHEPHERD, A., IVINS, E.R., GERUO, A., BARLETTA, V.R., BENTLEY, M.J., BETTADPUR, S., BRIGGS, K.H., BROMWICH, D.H., FORSBERG, R., GALIN, N., HORWATH, M., JACOBS, S., JOUGHIN, I., KING, M.A., LENAERTS, J.T.M., LI, J., LIGTENBERG, S.R.M., LUCKMAN, A., LUTHCKE, S.B., MCMILLAN, M., MEISTER, R., MILNE, G., MOUGINOT, J., MUIR, A., NICOLAS, J.P., PADEN, J., PAYNE, A.J., PRITCHARD, H., RIGNOT, E., ROTT, H., SORENSEN, L.S., SCAMBOS, T.A., SCHEUCHL, B., SCHRAMA, E.J.O., SMITH, B., SUNDAL, A.V., VAN ANGELEN, J.H., VAN DE BERG, W.J., VAN DEN BROEKE, M.R., VAUGHAN, D.G., VELICOGNA, I., WAHR, J., WHITEHOUSE, P.L., WINGHAM, D.J., YI, D., YOUNG, D. & ZWALLY, H.J. 2012. A Reconciled Estimate of Ice-Sheet Mass Balance: *Science*, **338**, 6111, 1183-1189.

SHEPHERD, A., WINGHAM, D., PAYNE, T. & SKVARCA, P. 2003. Larsen ice shelf has progressively thinned: *Science*, **302**, 5646, 856-859.

SHEPHERD, A., WINGHAM, D.J. & RIGNOT, E. 2004. Warm ocean is eroding West Antarctic Ice Sheet: *Geophysical Research Letters*, **31**, L23402, doi:10.1029\2004GL021106.

SHEVENELL, A.E., INGALLS, A.E., DOMACK, E.W. & KELLY, C. 2011. Holocene Southern Ocean surface temperature variability west of the Antarctic Peninsula: *Nature*, **470**, 7333, 250-254.

SHI, H.-L., LU, Y., DU, Z.-L., JIA, L.-L., ZHANG, Z.-Z. & ZHOU, C.-X. 2011. Mass change detection in Antarctic ice sheet using ICESat block analysis techniques from 2003~ 2008: *Diqiu Wuli Xuebao*, **54**, 4, 958-965.

SHUMAN, C.A., BERTHIER, E. & SCAMBOS, T.A. 2011. 2001-2009 elevation and mass losses in the Larsen A and B embayments, Antarctic Peninsula: *Journal of Glaciology*, **57**, 204, 737-754.

SHUMAN, C.A., ZWALLY, H.J., SCHUTZ, B.E., BRENNER, A.C., DIMARZIO, J.P., SUCHDEO, V.P. & FRICKER, H.A. 2006. ICESat Antarctic elevation data: Preliminary precision and accuracy assessment: *Geophysical Research Letters*, **33**, 7.

SIEVERS, J., GRINDEL, A. & MEIER, W. 1989. Digital satellite image mapping of Antarctica, **59**, 33.

SIMMONDS, I. 2003. Modes of atmospheric variability over the Southern Ocean: *Journal of Geophysical Research: Oceans (1978–2012)*, **108**, C4, SOV 5-1-SOV 5-30.

SIMOES, J.C., BREMER, U.F., AQUINO, F.E. & FERRON, F.A. 1999. Morphology and variations of glacial drainage basins in the King George Island ice field, Antarctica, *in* Jacka, T.H., ed., Annals of Glaciology, Vol 29, 1999, Volume 29: Cambridge, Int Glaciological Soc, 220-224.

SKVARCA, P. 1993. Fast recession of the Northern Larsen Ice Shelf monitored by space images: *Annals of Glaciology*, **17**, 317-321.

SKVARCA, P., RACK, W., ROTT, H. & DONANGELO, T.I.Y. 1999. Climatic trend and the retreat and disintegration of ice shelves on the Antarctic Peninsula: an overview: *Polar Research*, **18**, 2, 151-157.

SKVARCA, P., ROTT, H. & NAGLER, T. 1995. Satellite imagery, a baseline for glacier variation study on James Ross Island, Antarctica: *Annals of Glaciology*, **21**, 1, 291-296.

SMITH, A.M., VAUGHAN, D.G., DOAKE, C.S.M. & JOHNSON, A.C. 1998. Surface lowering of the ice ramp at Rothera Point, Antarctic Peninsula, in response to regional climate change: *Annals of Glaciology*, **27**, 113-118.

SMITH, D.A. & KLINCK, J.M. 2002. Water properties on the west Antarctic Peninsula continental shelf: a model study of effects of surface fluxes and sea ice: *Deep Sea Research Part II: Topical Studies in Oceanography*, **49**, 21, 4863-4886.

SMITH, J.A., BENTLEY, M.J., HODGSON, D.A. & COOK, A.J. 2007. George VI Ice Shelf: past history, present behaviour and potential mechanisms for future collapse: *Antarctic Science*.

SMITH, J.A., HILLENBRAND, C.D., PUDSEY, C.J., ALLEN, C.S. & GRAHAM, A.G.C. 2010. The presence of polynyas in the Weddell Sea during the Last Glacial Period with implications for the reconstruction of sea-ice limits and ice sheet history: *Earth and Planetary Science Letters*, **296**, 3-4, 287-298.

SMITH, R.C. & STAMMERJOHN, S.E. 2001. Variations of surface air temperature and sea-ice extent in the western Antarctic Peninsula region: *Annals of Glaciology*, **33**, 493-500.

SPENCE, P., GRIFFIES, S.M., ENGLAND, M.H., HOGG, A.M., SAENKO, O.A. & JOURDAIN, N.C. 2014. Rapid subsurface warming and circulation changes of Antarctic coastal waters by poleward shifting winds: *Geophysical Research Letters*, 2014GL060613.

STAMMERJOHN, S.E., MARTINSON, D.G., SMITH, R.C. & IANNUZZI, R.A. 2008. Sea ice in the western Antarctic Peninsula region: Spatio-temporal variability from ecological and climate change perspectives: *Deep Sea Research Part II: Topical Studies in Oceanography*, **55**, 18, 2041-2058.

STEIG, E.J., SCHNEIDER, D.P., RUTHERFORD, S.D., MANN, M.E., COMISO, J.C. & SHINDELL, D.T. 2009. Warming of the Antarctic ice-sheet surface since the 1957 International Geophysical Year: *Nature*, **457**, 7228, 459-464.

STINEMAN, R.W. 1980. A Consistently Well-Behaved Method of lnterpolation: *Creative Computing*, 54-57.

STRELIN, J.A., SONE, T., MORI, J., TORIELLI, C.A. & NAKAMURA, T. 2006. New data related to holocene landform development and climatic change from James Ross Island, Antarctic Peninsula, Antarctica: Contributions to Global Earth Sciences, 455-459 p.:

SVOBODA, F. & PAUL, F. 2009. A new glacier inventory on southern Baffin Island, Canada, from ASTER data: I. Applied methods, challenges and solutions: *Annals of Glaciology*, **50**, 53, 11-21.

TEDESCO, M. & MONAGHAN, A.J. 2009. An updated Antarctic melt record through 2009 and its linkages to high-latitude and tropical climate variability: *Geophysical Research Letters*, **36**.

TENNANT, C., MENOUNOS, B., WHEATE, R. & CLAGUE, J. 2012. Area change of glaciers in the Canadian Rocky Mountains, 1919 to 2006: *The Cryosphere*, **6**, 6, 1541-1552.

THOMAS, E.R., MARSHALL, G.J. & MCCONNELL, J.R. 2008. A doubling in snow accumulation in the western Antarctic Peninsula since 1850: *Geophysical Research Letters*, **35**, L01706.

TOUTIN, T. 2008. ASTER DEMs for geomatic and geoscientific applications: a review: *International Journal of Remote Sensing*, **29**, 7, 1855-1875.

TURNER, J. 2004. The El Niño–Southern Oscillation and Antarctica: *International Journal of Climatology*, **24**, 1, 1-31.

TURNER, J., BINDSCHADLER, R., CONVEY, P., DI PRISCO, G., FAHRBACH, E., GUTT, J., HODGSON, D., MAYEWSKI, P. & SUMMERHAYES, C. 2009. Antarctic climate change and the environment.

TURNER, J., COLWELL, S.R. & HARANGOZO, S. 1997. Variability of precipitation over the coastal western Antarctic Peninsula from synoptic observations: *Journal of Geophysical Research*, **102**, 13999-14007.

TURNER, J., COLWELL, S.R., MARSHALL, G.J., LACHLAN-COPE, T.A., CARLETON, A.M., JONES, P.D., LAGUN, V., REID, P.A. & IAGOVKINA, S. 2005a. Antarctic climate change during the last 50 years: *International Journal of Climatology*, **25**, 3, 279-294.

TURNER, J., LACHLAN-COPE, T., COLWELL, S. & MARSHALL, G.J. 2005b. A positive trend in western Antarctic Peninsula precipitation over the last 50 years reflecting regional and Antarctic-wide atmospheric circulation changes, *in* Hamilton, G., ed., Annals of Glaciology, Vol 41, 2005, Volume 41: Cambridge, Int Glaciological Soc, 85-91.

TURNER, J., LACHLAN-COPE, T., THOMAS, J.P. & COLWELL, S.R. 1995. The synoptic origins of precipitation over the Antarctic Peninsula: *Antarctic Science*, **7**, 3, 327-337.

TURNER, J., LACHLAN-COPE, T.A., MARSHALL, G.J., MORRIS, E.M., MULVANEY, R. & WINTER, W. 2002. Spatial variability of Antarctic Peninsula net surface mass balance: *Journal of Geophysical Research-Atmospheres*, **107**, D13.

TURNER, J. & OVERLAND, J. 2009. Contrasting climate change in the two polar regions: *Polar Research*, **28**, 2, 146-164.

VAN DEN BROEKE, M. 2005. Strong surface melting preceded collapse of Antarctic Peninsula ice shelf: *Geophysical Research Letters*, **32**, L12815, doi:10.1029/2005GL0223247.

VAN DEN BROEKE, M., VAN DE BERG, W.J. & VAN MEIJGAARD, E. 2006. Snowfall in coastal West Antarctica much greater than previously assumed: *Geophysical Research Letters*, **33**, 2.

VAN DEN BROEKE, M.R. 2000. On the interpretation of Antarctic temperature trends: *Journal of Climate*, **13**, 3885-3889.

VAN DER VEEN, C.J. 2007. Fracture propagation as means of rapidly transferring surface meltwater to the base of glaciers: *Geophysical Research Letters*, **34**, 1.

VAN LIPZIG, N., KING, J., LACHLAN-COPE, T. & VAN DEN BROEKE, M. 2004. Precipitation, sublimation, and snow drift in the Antarctic Peninsula region from a regional atmospheric model: *Journal of Geophysical Research: Atmospheres (1984–2012)*, **109**, D24.

VAUGHAN, D.G. 1993. Implications of the break-up of Wordie Ice Shelf, Antarctica for sea level: *Antarctic Science*, **5**, 4, 403-408.

VAUGHAN, D.G. 2006. Recent trends in melting conditions on the Antarctic Peninsula and their implications for ice-sheet mass balance: *Arctic, Antarctic and Alpine Research*, **38**, 1, 147-152.

VAUGHAN, D.G. & BAMBER, J.L. Delineation of Antarctic Ice-Drainage Basins, *in* Proceedings Chapman Conference on West Antarctic Ice Sheet, Maine, USA, 1999/// 1999, AGU.

VAUGHAN, D.G., BAMBER, J.L., GIOVINETTO, M., RUSSELL, J. & COOPER, A.P.R. 1999. Reassessment of net surface mass balance in Antarctica: *Journal of Climate*, **12**, 933-945.

VAUGHAN, D.G. & DOAKE, C.S.M. 1996. Recent atmospheric warming and retreat of ice shelves on the Antarctic Peninsula: *Nature*, **379**, 328-331.

VAUGHAN, D.G., MARSHALL, G.J., CONNOLLEY, W.M., PARKINSON, C.L., MULVANEY, R., HODGSON, D.A., KING, J.C., PUDSEY, C.J. & TURNER, J. 2003. Recent rapid regional climate warming on the Antarctic Peninsula: *Climatic Change*, **60**, 243-274.

VELICOGNA, I. 2009. Increasing rates of ice mass loss from the Greenland and Antarctic ice sheets revealed by GRACE: *Geophysical Research Letters*, **36**, 19.

VELICOGNA, I. & WAHR, J. 2006. Measurements of time-variable gravity show mass loss in Antarctica: *Science*, **311**, 5768, 1754-1756.
VIELI, A., PAYNE, A.J., SHEPHERD, A. & DU, Z. 2007. Causes of pre-collapse changes of the Larsen B ice shelf: Numerical modelling and assimilation of satellite observations: *Earth and Planetary Science Letters*, **259**, 3-4, 297-306.
WALLACE, M.I., MEREDITH, M.P., BRANDON, M.A., SHERWIN, T.J., DALE, A. & CLARKE, A. 2008. On the characteristics of internal tides and coastal upwelling behaviour in Marguerite Bay, west Antarctic Peninsula: *Deep Sea Research Part II: Topical Studies in Oceanography*, **55**, 18, 2023-2040.
WEERTMAN, J. 1973. Theory of fatigue crack growth based on a BCS crack theory with work hardening: *International Journal of Fracture*, **9**, 2, 125-131.
WENDT, J., RIVERA, A., WENDT, A., BOWN, F., ZAMORA, R., CASASSA, G. & BRAVO, C. 2010. Recent ice-surface-elevation changes of Fleming Glacier in response to the removal of the Wordie Ice Shelf, Antarctic Peninsula: *Annals of Glaciology*, **51**, 55, 97-102.
WGMS 1989. World Glacier Inventory - Status 1988: *IAHS (ICSI) / UNEP / UNESCO*, 458.
WGMS & NSIDC 2012. World Glacier Inventory (Dataset): Zurich, Switzerland; Boulder CO, USA.
WHITE, W.B. & PETERSON, R.G. 1996. An Antarctic circumpolar wave in surface pressure, wind, temperature and sea-ice extent, **380**, 699-702.
WILLIAMS JR, R. & FERRIGNO, J. 1998. Coastal-change and Glaciological Maps of Antarctica (USGS Fact Sheet, FS-050-98): *US Geological Survey, Reston, VA, 2pp*.
WILLIAMS, R.S., FERRIGNO, J.G., SWITHINBANK, C., LUCCHITTA, B.K. & SEEKINS, B.A. 1995. Coastal-Change and Glaciological Maps of Antarctica: *Annals of Glaciology*, **21**, Proceedings of the International Symposium on the Role of the Cryosphere in Global Change, 284-290.
WINGHAM, D.J., RIDOUT, A.J., SCHARROO, R., ARTHERN, R.J. & SCHUM, C.K. 1998. Antarctic elevation change from 1992 to 1996: *Science*, **282**, 456-458.
WINGHAM, D.J., SHEPHERD, A., MUIR, A. & MARSHALL, G.J. 2006. Mass balance of the Antarctic ice sheet: *Philosophical Transactions of the Royal Society A: Mathematical, Physical and Engineering Sciences*, DOI: 10.1098/rsta.2006.1792.
ZEMP, M., HOELZLE, M. & HAEBERLI, W. 2009. Six decades of glacier mass-balance observations: a review of the worldwide monitoring network: *Annals of Glaciology*, **50**, 50, 101-111.
ZWALLY, H.J., COMISO, J.C., PARKINSON, C.L., CAVALIERI, D.J. & GLOERSEN, P. 2002a. Variability of Antarctic sea ice 1979-1998: *Journal of Geophysical Research-Oceans*, **107**, C5, art. no.-3041.
ZWALLY, H.J., GIOVINETTO, M., JUN LI, CONEJO, H.G., BECKLEY, M.A., BRENNER, A.C., SABA, J.L. & DONGHUI YI 2005. Mass changes of the Greenland and Antarctic ice sheets and shelves and contributions to sea-level rise: 1992 - 2002: *Journal of Glaciology*, **51**, 175, 509-527.
ZWALLY, H.J., SCHUTZ, B., ABDALATI, W., ABSHIRE, J., BENTLEY, C., BRENNER, A., BUFTON, J., DEZIO, J., HANCOCK, D., HARDING, D., HERRING, T., MINSTER, B., QUINN, K., PALM, S., SPINHIRNE, J. & THOMAS, R. 2002b. ICESat's laser measurements of polar ice, atmosphere, ocean, and land: *Journal of Geodynamics*, **34**, 3-4, 405-445.
ZWALLY, H.J., SCHUTZ, R., BENTLEY, C., BUFTON, J., HERRING, T., MINSTER, J., SPINHIRNE, J. & THOMAS, R. 2003. GLAS/ICESat L2 Antarctic and Greenland Ice Sheet Altimetry Data: *Digital Media*.

APPENDIX – Chapter 1

Relevant papers published prior to undertaking the PhD:

COOK, A.J., FOX, A.J., VAUGHAN, D.G. & FERRIGNO, J.G. 2005. Retreating glacier fronts on the Antarctic Peninsula over the past half-century: *Science*, 308, 541-544.

COOK, A.J. & VAUGHAN, D.G. 2010. Overview of areal changes of the ice shelves on the Antarctic Peninsula over the past 50 years: *Cryosphere*, 4, 1, 77-98.

FERRIGNO, G.J., COOK, A.J., FOLEY, M.K., WILLIAMS, R.S., SWITHINBANK, C., FOX, A., THOMSON, W.J. & SIEVERS, J. 2006, Coastal-Change and Glaciological Map of the Trinity Peninsula Area and South Shetland Islands, Antarctica: 1843–2001, U.S. Geological Survey Geologic Investigations Series Map I-2600-A (map sheet, text).

FERRIGNO, G.J., COOK, A.J., MATHIE, M.A., WILLIAMS, R.S., SWITHINBANK, C., FOLEY, M.K., FOX, A., THOMSON, W.J. & SIEVERS, J. 2008, Coastal-change and glaciological map of the Larsen Ice Shelf area, Antarctica: 1940–2005, U.S. Geological Survey Geologic Investigations Series Map I–2600–B, (map sheet, text).

FERRIGNO, G.J., COOK, A.J., MATHIE, M.A., WILLIAMS, R.S., SWITHINBANK, C., FOLEY, M.K., FOX, A., THOMSON, W.J. & SIEVERS, J. 2009, Coastal-change and glaciological map of the Palmer Land area, Antarctica: 1947–2009, U.S. Geological Survey Geologic Investigations Series Map I–2600–C (map sheet, text).

PECK, L.S., BARNES, D.K.A., COOK, A.J., FLEMING, A.H. & CLARKE, A. 2010. Negative feedback in the cold: ice retreat produces new carbon sinks in Antarctica: *Global Change Biology*, **16**, 9, 2614-2623.

SMITH, J.A., BENTLEY, M.J., HODGSON, D.A. & COOK, A.J. 2007. George VI Ice Shelf: past history, present behaviour and potential mechanisms for future collapse: *Antarctic Science*.

Papers published from research undertaken during the PhD:

COOK, A.J., MURRAY, T., LUCKMAN, A., VAUGHAN, D.G. & BARRAND, N.E. 2012. A new 100-m Digital Elevation Model of the Antarctic Peninsula derived from ASTER Global DEM: methods and accuracy assessment: *Earth System Science Data*, 4, 129 - 142.

COOK, A.J., VAUGHAN, D.G., LUCKMAN, A. & MURRAY, T. 2014. A new Antarctic Peninsula glacier basin inventory and observed area changes since the 1940s: *Antarctic Science*, Special Issue (In Press).

BARRAND, N.E., HINDMARSH, R., ARTHERN, R.J., WILLIAMS, R.C., MOUGINOT, J., SCHEUCHL, B., RIGNOT, E., LIGTENBERG, S.R.M., VAN DEN BROEKE, M.R., EDWARDS, T.L., COOK, A.J. & SIMONSEN, S.B. 2013. Computing the volume response of the Antarctic Peninsula ice sheet to warming scenarios to 2200: *Journal of Glaciology*, 59, 215, 1-13.

FRETWELL, P., PRITCHARD, H.D., VAUGHAN, D.G., BAMBER, J.L., BARRAND, N.E., BELL, R., BIANCHI, C., BINGHAM, R.G., BLANKENSHIP, D.D., CASASSA, G., CATANIA, G., CALLENS, D., CONWAY, H., COOK, A.J., CORR, H.F.J., DAMASKE, D., DAMM, V.,

FERRACCIOLI, F., FORSBERG, R., FUJITA, S., GIM, Y., GOGINENI, P., GRIGGS, J.A., HINDMARSH, R.C.A., HOLMLUND, P., HOLT, J.W., JACOBEL, R.W., JENKINS, A., JOKAT, W., JORDAN, T., KING, E.C., KOHLER, J., KRABILL, W., RIGER-KUSK, M., LANGLEY, K.A., LEITCHENKOV, G., LEUSCHEN, C., LUYENDYK, B.P., MATSUOKA, K., MOUGINOT, J., NITSCHE, F.O., NOGI, Y., NOST, O.A., POPOV, S.V., RIGNOT, E., RIPPIN, D.M., RIVERA, A., ROBERTS, J., ROSS, N., SIEGERT, M.J., SMITH, A.M., STEINHAGE, D., STUDINGER, M., SUN, B., TINTO, B.K., WELCH, B.C., WILSON, D., YOUNG, D.A., XIANGBIN, C. & ZIRIZZOTTI, A. 2013. Bedmap2: improved ice bed, surface and thickness datasets for Antarctica: *The Cryosphere*, 7, 1, 375-393.

LECLERCQ, P., OERLEMANS, J., BASAGIC, H., BUSHUEVA, I., COOK, A. & LE BRIS, R. 2014. A data set of worldwide glacier length fluctuations: *The Cryosphere*, 8, 2, 659-672.

SCAMBOS, T.A., BERTHIER, E., HARAN, T., SHUMAN, C.A., COOK, A.J., LIGTENBERG, S.R.M. & BOHLANDER, J. 2014. Detailed ice loss pattern in the northern Antarctic Peninsula: widespread decline driven by ice front retreats: *The Cryosphere Discuss.*, 8, 3, 3237-3261.

APPENDIX – Chapter 2

Appendix 2.1:

Summary of Antarctic Ice Sheet mass balance research studies and the time period for which estimates were made (from Shepherd et al., 2012).

Each estimate included the APIS, although the region was not always defined as a separate ice mass. The reconciled estimate however does distinguish the East, West and Antarctic Peninsula Ice Sheets. The estimated mass balance change (in gigatonnes year^{-1}) between 1992 and 2011 for Greenland is –142 ± 49, East Antarctica +14 ± 43, West Antarctica –65 ± 26 and the Antarctic Peninsula –20 ± 14. Abbreviations: Radar Altimetry (RA); Laser Altimetry (LA); Input Output Model (IOM); grounded ice (*); floating ice (†).

Study	Technique	Survey Period	Gt a^{-1}
(Wingham *et al.*, 1998)	RA	1992 - 1996	-60 ± 76
(Zwally *et al.*, 2005)	RA	1992 – 2001	-30.3 ± 12.1 *
(Zwally et al., 2005)	RA	1992 – 2001	47.8 ± 14.8 †
(Ramillien *et al.*, 2006)	Gravimetry	2002 – 2005	- 40 ± 32
(Velicogna & Wahr, 2006)	Gravimetry	2002 – 2005	-137 ± 72
(Wingham *et al.*, 2006)	RA	1992 – 2003	27 ± 29
(Rignot *et al.*, 2008)	IOM	1996	-112 ± 91
(Rignot et al. 2008)	IOM	2000	-138 ± 92
(Rignot et al.2008)	IOM	2006	-196 ± 92
(Barletta *et al.*, 2008)	Gravimetry	2003 – 2007	-171± 39
(Cazenave *et al.*, 2009)	Gravimetry	2003 – 2007	-198 ± 22
(Chen *et al.*, 2009)	Gravimetry	2002 – 2009	-190 ± 77
(Chen et al. 2009)	Gravimetry	2002 – 2005	- 144 ± 58
(Chen et al. 2009)	Gravimetry	2006 – 2009	- 220 ± 89
(Gunter *et al.*, 2009)	LA	2003 – 2007	-25 ± 1 to -101 ± 2.5
(Gunter et al. 2009)	Gravimetry	2003 – 2007	- 77.5 ± 13.5 to -83 ± 9
(Horwath & Dietrich, 2009)	Gravimetry	2002 - 2008	-109 ± 48
(Velicogna, 2009)	Gravimetry	2002 – 2006	-104
(Velicogna 2009)	Gravimetry	2006 - 2009	-246
(Velicogna 2009)	Gravimetry	2002- 2009	-143 ± 73
(Rignot *et al.*, 2011b)	IOM & Gravimetry	2006	-200 ± 150
(Shi *et al.*, 2011)	LA	2003 – 2008	-77.5 ± 4.5

Appendix 2.2:

Description of mass balance measurements used in reconciling the total mass balance for the Antarctic Ice Sheet by Shepherd et al. (2012)

Data sources used to produce ice sheet mass estimates of the AIS have included satellite altimetry, interferometry and gravimetry data sets. The first AIS mass balance estimate was made by Wingham *et al.* (1998), based on Radar Altimetry (RA) measurements for the period 1992-1996, and subsequent RA studies have used European Remote-sensing Satellites ERS-1 and ERS-2, and Envisat 35-day repeat satellite RA observations between May 1992 and September 2003 (e.g. Zwally *et al.*, 2005; Wingham *et al.*, 2006). The more recent introduction of Laser Altimetry (LA) from ICESat (Ice, Cloud, and Land Elevation Satellite), acquired between September 2003 and November 2008, has enabled precise along-track repeat measurements at high resolution, although the tracks are widely separated in some regions and sparsely sampled in time (e.g. Gunter *et al.*, 2009).

The Input-Output Method (IOM) for estimating mass balance "quantifies the difference between glacier mass gained through snowfall and lost by sublimation and meltwater runoff and the discharge of ice into the ocean" (Shepherd *et al.*, 2012). The approach has the advantage of allowing changes in surface mass balance (SMB) and ice dynamics to be studied for individual glacier drainage basins. Although earlier IOM studies used SMB derived from interpolation of sparse ground observations, regional atmospheric climate models are now used because they provide predictions at high temporal and spatial resolution. Mass balance estimates based on the IOM method for the years 1996, 2000 and 2006 by Rignot *et al.* (2008) have been included in the reconciled mass estimate of the AIS. It was estimated that mass losses specifically for the Antarctic Peninsula increased by 140%, reaching 60 ± 46 Gt a^{-1} by 2006 (Rignot *et al.*, 2008).

More recent estimations of AIS mass fluctuations have been based on gravitational data obtained from The Gravity Recovery and Climate Experiment (GRACE) satellite, launched in 2002, which measures changes in Earth surface gravitational attraction. This is a revolutionary method for measuring ice mass change as it provides regional averages that do not require interpolative techniques, and mass fluctuations can be measured directly and at monthly temporal sampling. However, a key challenge has been to

distinguish fluctuations in ice-sheet mass from changes in the underlying crust and mantle. This is achieved by using models of Glacial Isostatic Adjustment (GIA), which, in the case of the AIS, has led to significant adjustments (King *et al.*, 2012; Shepherd *et al.*, 2012). The improvement of both methods has been an active research topic and significant advances have been made since the first mass estimates from GRACE.

APPENDIX – Chapter 3

Appendix 3.1:

Sample ICESat tracks in the region 66°- 68° S, transecting the new DEM, used in accuracy assessments (Section 3.6.1.1). In the map, the purple areas (with a transparency and hence different shading according to elevation) are the erroneous regions that have been edited to produce the New DEM. The ICESat track numbers relate to the following data downloaded from NSIDC (Zwally *et al.*, 2003):

GLA06_0144: XYGLA06_531_2121_002_0144_3_01_0001 (17/10/2007)

GLA06_0167: XYGLA06_531_2121_002_0167_3_01_0001 (19/10/2007)

GLA06_0286: XYGLA06_531_2121_002_0286_3_01_0001 (27/10/2007)

GLA06_0382: XYGLA06_531_2121_002_0382_3_01_0001 (02/11/2007)

GLA06_0405: XYGLA06_531_2121_002_0405_3_01_0001 (04/11/2007)

The profiles illustrate relative differences between each DEM to show how the data compares at different locations, elevations, topography and steepness of slope. The profile for track GLA06_0144 is illustrated in Figure 3.7 in Chapter 3 and definitions of the DEM dataset acronyms are in Table 3.1.

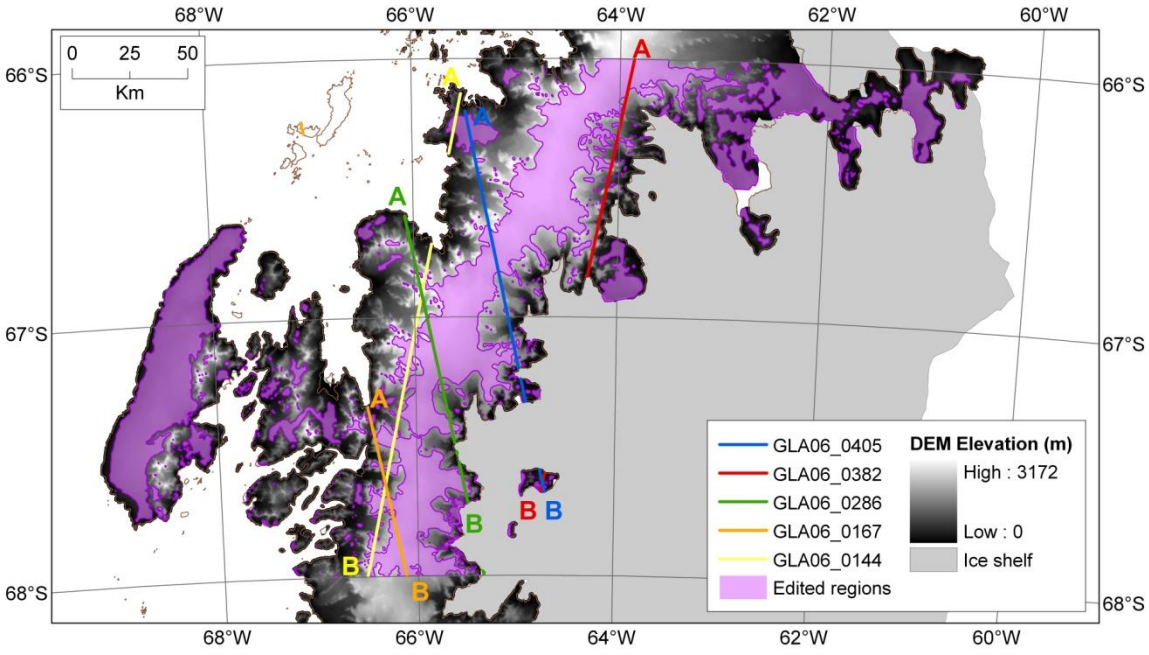

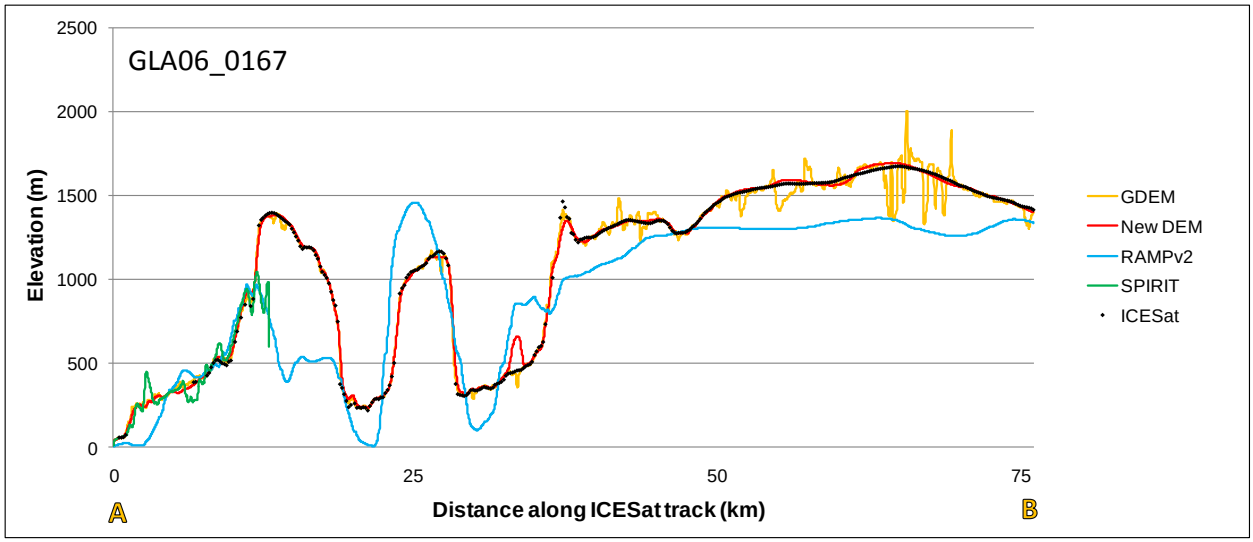
GLA06_0167
Elevation (m)
2500
2000
1500
1000
500
0
0
25
50
75
A
Distance along ICESat track (km)
B
GDEM
New DEM
RAMPv2
SPIRIT
ICESat

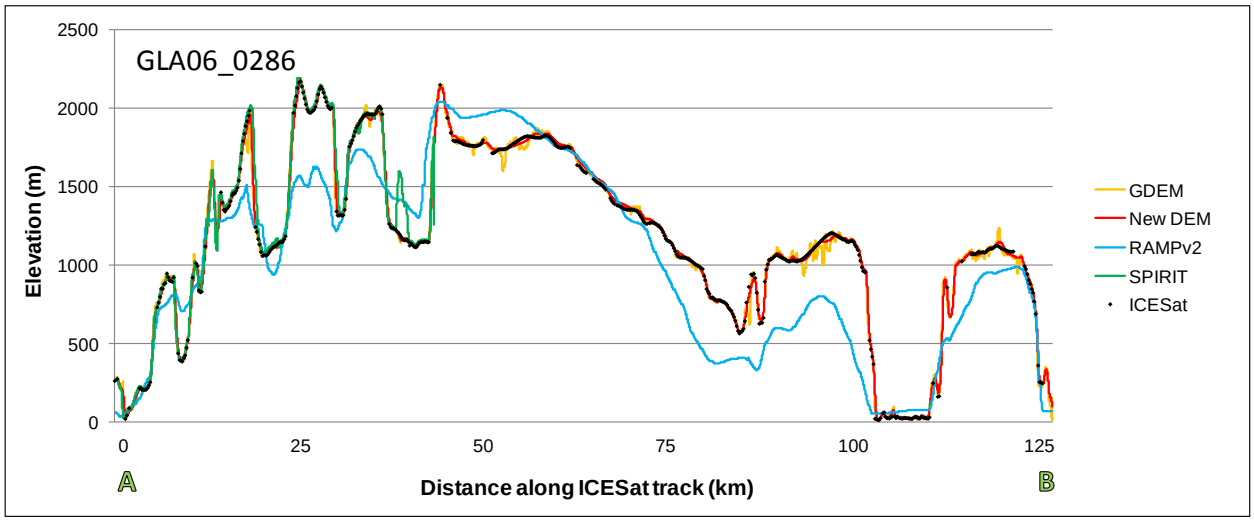
GLA06_0286
Elevation (m)
2500
2000
1500
1000
500
0
0
25
50
75
100
125
A
Distance along ICESat track (km)
B
GDEM
New DEM
RAMPv2
SPIRIT
ICESat

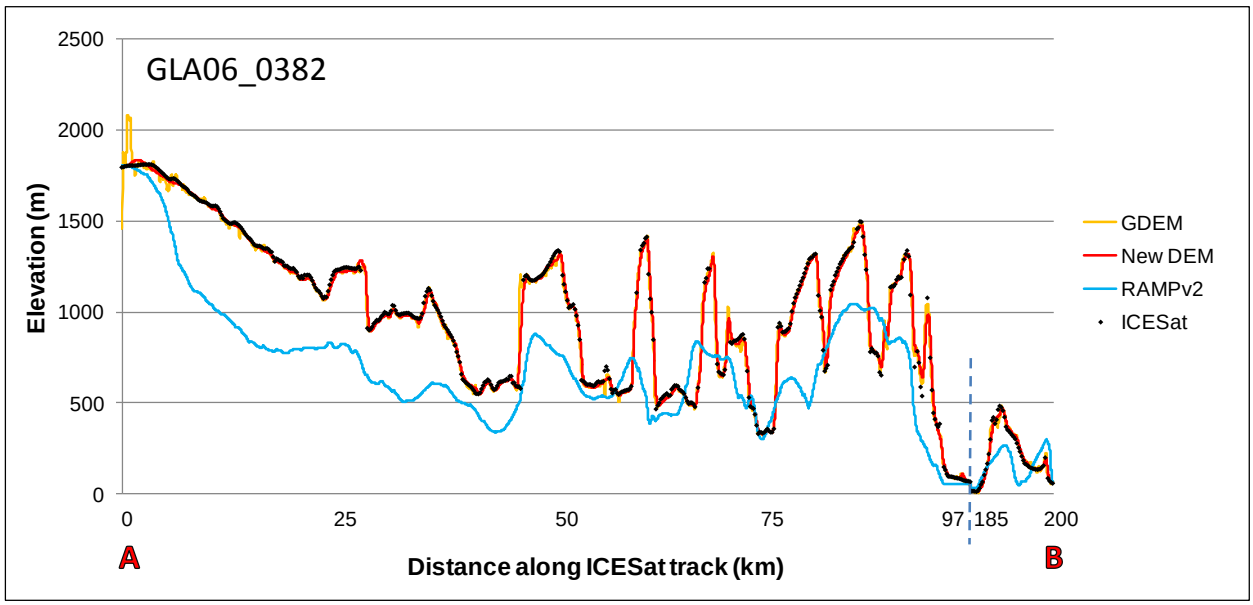
GLA06_0382
Elevation (m)
2500
2000
1500
1000
500
0
0
25
50
75
97
185
200
A
Distance along ICESat track (km)
B
GDEM
New DEM
RAMPv2
ICESat

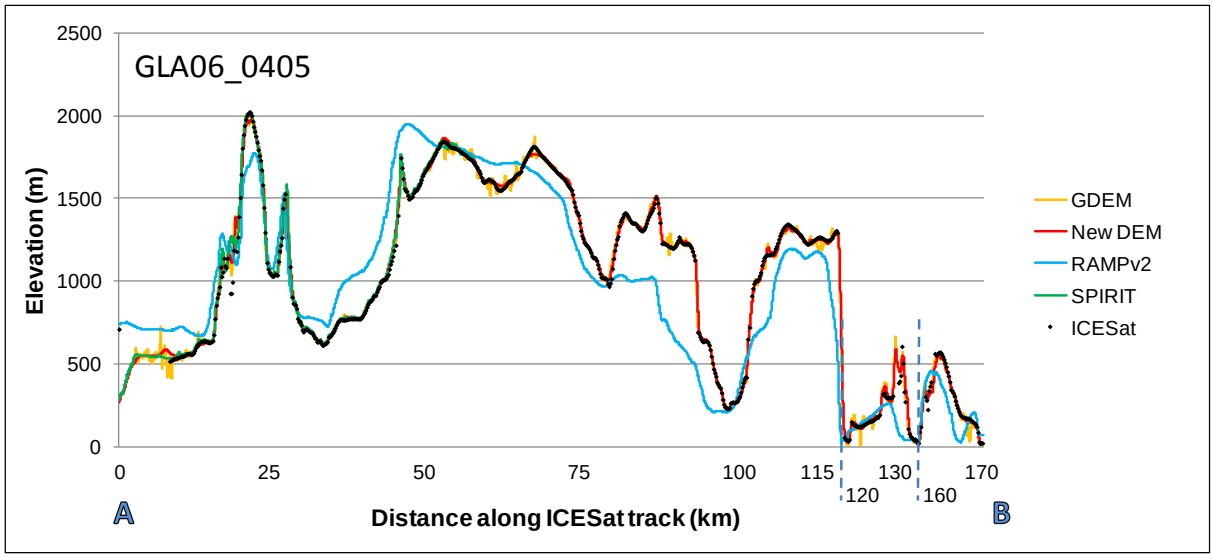
GLA06_0405
2500
2000
1500
1000
500
0
Elevation (m)
0
25
50
75
100
115
120
130
160
170
A
B
Distance along ICESat track (km)
GDEM
New DEM
RAMPv2
SPIRIT
ICESat

APPENDIX – Chapter 4

Appendix 4.1:

Definitions of Nominal classifications

Definitions of Nominal parameters obtained from the Global Land Ice Measurements from Space (GLIMS) Classification Manual (Rau *et al*., 2005) and the Glossary of Glacier Mass Balance (Cogley *et al.*, 2011). The category numbers conform to those in GLIMS classification system.

Primary classification (Class):

- 2 - Ice-field: ice covering mountainous terrain, not thick enough to overwhelm surrounding topography, and where flow is not radial or dome shaped. This may include low-lying areas where ice divides are not clearly detectable. Flow is influenced by underlying topography. It can include an ice mass that has flow features visible but does not qualify as an outlet glacier or an ice cap.
- 3 - Ice-cap: dome shaped ice mass with approximately radial flow, which largely obscures bedrock and where the profile is even/regular. The ice mass is unconstrained by topography. It can include a low-relief, radial ice mass with little flow that originates from mountains. Large islands that are covered in ice are defined as an ice-cap, even if topography may imply ice-field.
- 4 - Outlet glacier: glacier (usually of valley glacier form) that drains an ice sheet, ice field or ice cap. It follows local topographic depressions. The catchment area may not be clearly delineated. These are larger than mountain glaciers, flow features are clearly visible and the ice velocity tends to be greater than the surrounding ice mass. Includes ice draining from icefield/ice caps that have had floating tongues in the past.
- 6 - Mountain glacier: the glacier adheres to mountain sides and is any shape, often located in a cirque/niche. The terminus is often constrained within a bay, has clear ‘pinning points’ at the edge of the drainage basin and has flow features visible. The accumulation region is not on a broad plateau and has clearly definable catchment.
- 10 - Small ice-covered island: the island is between 1 – 5 km long/wide, and the majority is ice-covered. This is not a GLIMS glacier type, but was added as such features are prevalent close to the Antarctic Peninsula
- 0 - Uncertain/Misc

Form:

- 1 - Compound basins: more than one compound basin that merge together.
- 2 - Compound basin: more than one accumulation basin feeding one glacier system. In many cases on the AP separate glacier entities coalesce to form a single glacier at the terminus.
- 3 - Simple basin: glacier is fed from one single accumulation area.
- 0 - Uncertain/Misc

Front:

- 4 - Calving: tidewater, sufficiently extending into sea to produce icebergs.
- 10 - Calving/Piedmont: occurs in unconstrained topographic areas, with expanding glacier fronts or from an ice field. These have steeper-sloped calving fronts than lobed glacier fronts and flow is not radial.
- 12 - Calving/lobed: initial stage of tongue formation, part of an ice cap or ice field with a radial margin, and is grounded. The front has a lower slope angle than a piedmont front.
- 13 - Ice-shelf nourishing: tributaries of an ice shelf.
- 14 – Floating: the terminus is floating in the sea and an approximate grounding line may be detectable. The grounding line is not clearly identifiable for many marine-terminating glaciers on the AP so the term 'floating' was only assigned in cases where it was considered to be unambiguous. These decisions were based on the positions of the ASAID grounding line, combined with interpretation from surface features visible on the LIMA.
- 20 - Land-terminating: the terminus is behind the LIMA coastline
- 0 - Uncertain/Misc

Confidence:

Due to the subjective nature of nominal categorisation, a degree of confidence in decisions made was assigned to each glacier. One value was assigned to summarise the overall confidence in allocation of *Class*, *Form* and *Front* attributes:

- 1 – Confident about all (*Class*, *Form* and *Front*) classification types
- 2 – Confident about some aspects of classification but not others
- 3 – Unsure/guess as to all aspects of classification

Appendix 4.2:

Sample region with glacier basin primary classifications marked.

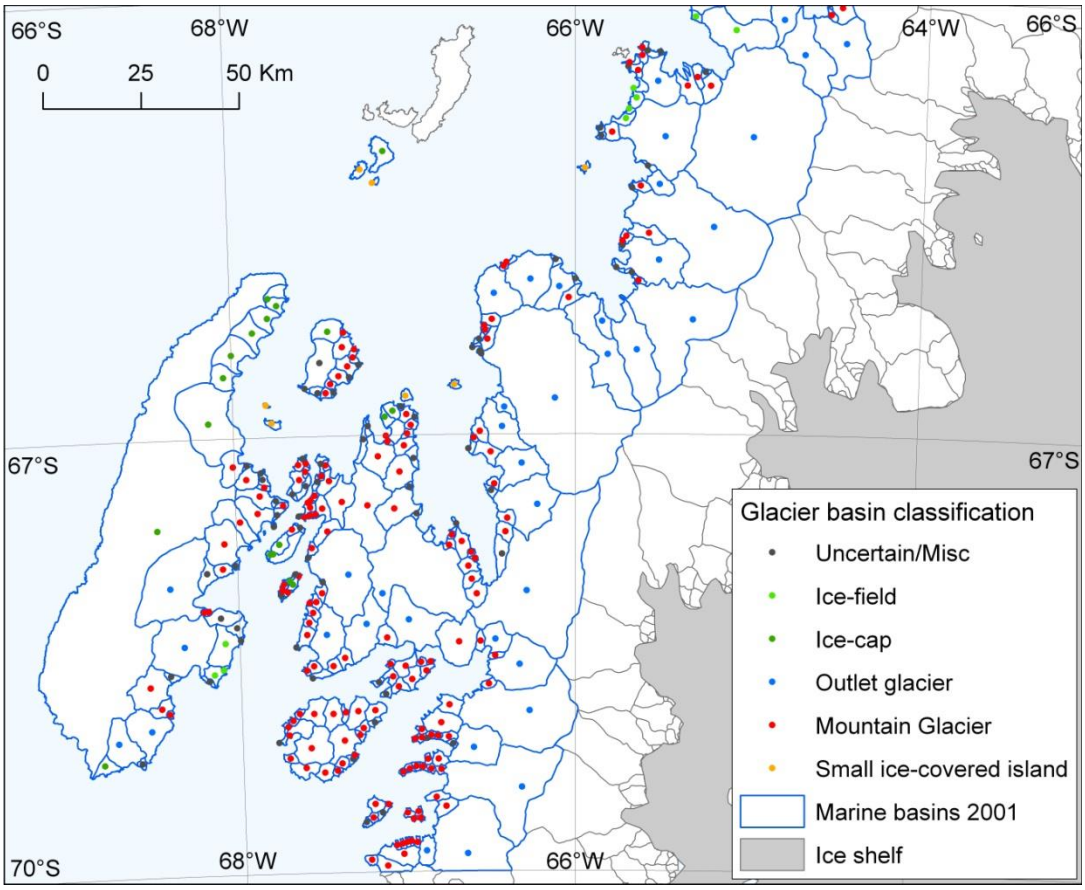

Appendix 4.3:

Source Material used for the Coastal-Change and Glaciological Maps of the Antarctic Peninsula project.

In total over 2000 aerial photographs and over 100 satellite images were used.

Year	Source-type
1843-1950	Historical maps and documents, from BAS[1] archives
1940	US Antarctic Service Expedition oblique aerial photographs
1947	RARE[2] vertical and oblique aerial photographs
1956-57	FIDASE[3] vertical aerial photographs (1:27,000)
1964-69	USA TMA[4] vertical (1:38,000) and oblique aerial photographs
1972-79, 1986, 1989, 1991, 1999	British Royal Navy vertical (1:12,000; 1:24,000) aerial photographs
1962, 1986, 1989, 1990-95, 1997, 1999, 2001	BAS[1] vertical (1:20,000 to 1:30,000) aerial photographs
1989	IfAG[5] vertical (1:70,000) aerial photographs
2001	BAS[1] hand-held oblique camera, from Twin Otter
1963	Corona Satellite images
1975	Kosmos KATE200 mosaic (obtained from article by Skvarca, 1994)
1986, 1988-90	IfAG[5] mosaic satellite image (Landsat 4/5)
1986, 1989	Landsat 4/5 images
1973-74, 1977-79	Landsat 1/2/3 images
1997	RADARSAT Antarctic Mosaic
2000-2002	Landsat 7 ETM+ images

[1] British Antarctic Survey
[2] Ronne Antarctic Research Expedition
[3] Falkland Island and Dependencies Aerial Survey Expedition
[4] United States of America Trimetrogon Antarctica
[5] Institut für Angewandte Geodäsie

Appendix 4.4:

Methodology for digitisation of source material in Coastal-Change and Glaciological Maps of Antarctica project

IFAG mosaic

The Institute für Angewandt Geodäsie (IfAG) Landsat TM image mosaic was used as the image base onto which the coastlines were mapped for each of the three output maps of the Antarctic Peninsula (I–2600–A, –B, and –C). This mosaic was determined to be the most geodetically accurate image base available of the AP. It was created using 62 control points from the BAS geodetic-control network of the area adjusted in 1985. Conventional block-adjustment techniques were used (Sievers and others, 1989). The accuracy was calculated by A.P.R. Cooper, BAS, to be ± 150 m (Cooper, oral commun., 2001).
The coastline on the image mosaic was digitized and assigned a reliability of 1. Because the IfAG mosaic was used as the map base, the accuracy of all other data sources was assigned relative to the accuracy of the IfAG mosaic. For those parts of the rock coastline that were hidden in shadow, or in areas obscured by cloud, the IfAG mosaic was used in conjunction with Falkland Islands and Dependencies Aerial Survey Expedition (FIDASE) photographs and the Antarctic Digital Database (ADD).

Vertical Aerial Photography

Vertical aerial photographs were by far the most common data source used, and the reliability was generally high. When it was possible to digitize the ice front or ice wall accurately from the photographs, the ice front or ice wall was assigned a reliability of 1. In other cases, for example where features were obscured to a greater or lesser degree by clouds, the information was given a reliability rating of 2. Frequently, there were no permanent features visible or present on the background image or the photograph, so that positioning of the ice front or ice wall was difficult or impossible. In such cases, the ice front or ice wall either was not drawn at all, or was assigned a reliability of 3 if it could be placed with reasonable confidence. In cases of reliability 2 or 3, the reliability rating chosen is explained in the comment field.

Oblique Aerial Photography

Oblique aerial photographs were always given a reliability of 2 or 3. Although it was difficult to accurately define scale or distance from oblique aerial photographs, it was still possible to position the coastline relative to other features. If the ice front or ice wall could be clearly seen, was in the foreground, and could be positioned relative to fixed features, it was drawn with a reliability of 2. If it was obscured by cloud, or if the photograph was grainy, or if the coast was in the background of the photograph, it was

assigned a reliability of 3. Often a coastline was positioned by using a combination of oblique aerial photographs from different directions or in conjunction with vertical aerial photographs; in these cases it was possible to give a reliability of 1 or 2.

Landsat images and overlays

The initial analysis of glaciological features and coastal change began with annotation of glaciological features by Charles Swithinbank on maps or transparent overlays of the enlarged Landsat images. The resulting images and overlays were later transferred to BAS to be combined digitally with the other sources of information.
In the BAS Mapping and Geographic Information Centre (MAGIC), each satellite image was incorporated into the digital database using a series of nine artificial control points that could be identified on the IfAG image mosaic. The arcs (line segments) were digitized following, for the most part, the glaciological annotations made by Charles Swithinbank. Because they were digitized at scale 1:500,000, they were given a reliability of 2 or 3.

RADARSAT

Individual RADARSAT images having a pixel resolution of 25 m were used for the project. Because of geodetic position errors and layover problems associated with the high-relief terrain of the Antarctic Peninsula, the coastline digitized from these images had an offset of features ranging from 500 m to 3 km when compared to the IfAG mosaic. Where possible, the RADARSAT coastline was corrected using the more reliable areas of rock coastline, allowing some areas of ice shelf and outlet-glacier fronts to be included in the dataset with a reliability of 2 or 3. The majority of RADARSAT coastline, however, has been omitted from this project until the offset problem has been solved.

Landsat 7 ETM+ images

The Landsat 7 ETM+ images were imported digitally and reprojected. Where necessary, an image was registered and rectified. Once correctly positioned, the ice-coast areas were digitized on-screen at large-scale and assigned a reliability of 1 or 2.

Documents

Many paper maps and written documents show the ice coast pre-aerial photography, dating back to 1843. Although such sources of data are usually too inaccurate to meet the scientific objectives of this project, the coastlines revealed on these historical maps and charts give a qualitative idea of the approximate position of the ice front. Some maps were able to provide a position of the ice front when used in conjunction with aerial

photographs. Other maps were published at a large enough scale (for example, 1:100,000) to make them useable, and they were assigned a reliability of 3.

Appendix 4.5:

Source Material Reliability Ratings

Coastline accuracies are based on assignation of a reliability rating to each record. This method was developed for the *Coastal-Change and Glaciological Maps of Antarctica* project and the source material for each region is outlined in full in Ferrigno *et al.* (2006, 2008, and 2009). The error values associated with each reliability ratings represent an upper error margin. Data with reliability ratings greater than 3 are in the original Coastal-Change dataset but are omitted from the area-change inventory produced for the present study. All coastlines digitized for years since 2000 have ratings 1 or 2.

Reliability 1 (within 60 m)

Accurately digitized from:

- Vertical aerial photographs that have adequate rock features for positioning
- Satellite imagery digitised directly on-screen (good quality, geo-referenced imagery). This includes the Landsat TM images making up the IfAG mosaic, and Landsat 7 ETM+ images.

Reliability 2 (within 150 m)

Interpreted from:

- Vertical aerial photographs where the images are grainy, or the coastline is slightly obscured by cloud
- Near-oblique airphotos, where the ice coastline is clearly visible, in the foreground and with adequate permanent features visible
- Hardcopy Landsat MSS/TM images interpreted on a digitizing table, where the coast is clearly visible
- Digital RADARSAT images registered to the IfAG mosaic.

Reliability 3 (within 300 m)

Interpreted from:

- Vertical or oblique airphotos in which there are few or no reference features visible. Vertical photos could be linked back to the nearest permanent feature, and obliques showed rock features in the background.
- Far-oblique airphotos, in which the coastline is in the distance, or is poorly visible (due to graininess or over-exposure of the photograph, cloud, or difficulty in interpretation caused by sea-ice).
- Satellite images in which some features are poorly geo-referenced but still show useful coastline data
- Non-georeferenced large-scale maps, and sketch maps.

Reliability 4 (within 600 m)

Interpreted from:

- Non-georeferenced large-scale (1:200,000 or larger) historical maps where the inaccuracy is probably greater than the coastal change (where the accuracy of known rock features is highly questionable).
- Non-georeferenced small-scale (1:500,000) historical maps.
- Very generalised maps of areas for which no other information is available.

Reliability 5 (within 1 km)

Coastline based on interpretation from written descriptions. Such descriptions can give a good indication of the location of an ice front (in general terms) but not the shape. They are useful because they show where the ice front may have been, before the introduction of primary cartographic data.

Appendix 4.6:

The marine-terminating glaciers have the following attributes:

Glacier basin attributes

Attribute	Desciption
ID	Glacier basin ID
MaxDB	Single or Multiple basin
MDB_ID	Multiple basin ID
Name	
AJC_name	Unofficial name
Class	Primary classification
Form	Form
Front	Front type
Confidence	Attribute confidence rating
Basins	Number of basins in 2000-02
Area_Km2	Basin area in 2000-02
Lat	Latitude (polygon centroid)
Long	Longitude (polygon centroid)
E_W	East/West AP
Mainl_Isl	Situated on Mainland or Island
Degree	Latitudinal degree band
Region	Region (NE, E, NW, W, SW or SSW)
Z_Min	Minimum elevation
Z_Max	Maximum elevation
Z_Mean	Mean elevation
SLength	Surface length along centreline
Min_Slope	Minimum slope
Max_Slope	Maximum slope
Avg_Slope	Mean slope
MaxFlow	Maximum flow length
Wo	Width at outlet
Wb	Mean basin width
DegConv	Degree of convergence
Min_Vel	Minimum velocity
Max_Vel	Maximum velocity
Mean_Vel	Mean velocity

Area change attributes:

Area-change Attributes	Description
First_year	
Last_year	
First_Last	Number of years
First_Area	
Last_Area	
Total_diff	Area difference (km^2)
Prcnt_diff	Percent difference (%)
Total_rate	$Km^2\ a^{-1}$
Prcnt_rate	%/yr
Num_dates	Number of records
Area_1945	Area (5-year intervals)
" "	
Area_2010	
Prcnt_1945	Area percentage (5-yr intervals)
" "	
Prcnt_2010	
Areadiff_1945	Area difference from 2000-02
" "	
Areadiff_2010	
Date45_49	Record date (5-yr intervals)
" "	
Date_2010	
Year45_49	Record year (5-yr intervals)
" "	
Year_2010	
Rely45_49	Record reliability (5-yr intervals)
" "	
Rely_2010	
wpyr45_49	Change rate per year (km^2/yr)
" "	
wpyr2010	
wpyr45prcn	Percent rate per year (%/yr)
" "	
wpyr10prcn	

Temperature data attributes:

Temperature data	Within 5 km upstream
MMD_Count	Valid MMD data (2000-09)
MMD_Min	Minimum MMD
MMD_Max	Maximum MMD
MMD_Mean	Mean MMD
MeanTemp	Mean Surface Temp (1981-2008)
MnTmp_AMJ	Mean Temp Apr-June
MnTmp_JAS	Mean Temp Jul-Sept
MnTmp_JFM	Mean Temp Jan-Mar
MnTmp_OND	Mean Temp Oct-Dec
TmpAnm8184	Temperature Anomaly 1981-84
" "	" "
TmpAnm0508	Temperature Anomaly 2005-08
JASAnm8184	Temp Anomaly Jul-Sept 1981-84
" "	" "
JASAnm0508	Temp Anomaly Jul-Sept 2005-08
JFMAnm8184	Temp Anomaly Jan-Mar 1981-84
" "	" "
JFMAnm0508	Temp Anomaly Jan-Mar 2005-08
MnTempCalc_8184	Mean Temp 1981-84
" "	" "
MnTempCalc_0508	Mean Temp 2005-08
MnTempJFMCalc_8184	Mean Temp Jan-Mar 1981-84
" "	" "
MnTempJFMCalc_0508	Mean Temp Jan-Mar 1981-84

Ocean data attributes:

Ocean data	Within 5 km offshore
OceanTemp_Mean	Mean ocean temperature
MnTemp50	Mean temperature, 50 m depth
CntTemp50	Data count, 50 m depth
" "	" "
MnTemp500	Mean temp. 500 m depth
CntTemp500	Data count, 500 m depth
MnTemp_50grd	Interpolated temp., 50 m depth
CntTmp50mgrd	Interpolated data count, 50 m depth
" "	" "
MnTemp_500grd	Interpolated temp., 500 m depth
CntTmp500grd	Interpolated data count, 500 m depth
Bathy5km_Mean	Mean bathymetry within 5 km
Bathy5km_Min	Min " "
Bathy5km_Max	Max " "
Bathy5km_Count	Data count " "

Bathymetry as above, within 2 and 1 km from glacier front

APPENDIX – Chapter 5

Appendix 5.1:

All glacier basins on the AP (n = 1590): Size class, Class and Front summary table

		Size class (km^2)								
		< 5	5 - 10	10 - 20	20 - 50	50 - 100	100 - 200	200 - 500	> 500	Total
Class	Uncertain/Misc	272	63	27	16	5	1	1	0	385
	Ice-field	3	12	18	27	10	5	2	0	77
	Ice-cap	36	29	44	59	35	21	9	1	234
	Outlet glacier	2	8	17	37	41	49	58	28	240
	Mountain glacier	175	147	110	91	20	7	1	0	551
	Small island	79	16	7	0	1	0	0	0	103
	Total	567	275	223	230	112	83	71	29	
Front	Uncertain/Misc	335	65	31	12	0	1	0	0	444
	Calving	189	152	114	105	50	31	25	6	672
	Calving/Piedmont	6	10	21	22	9	6	4	0	78
	Calving/Lobed	2	3	7	16	4	7	1	1	41
	Ice-shelf nourishing	34	36	43	55	35	21	28	12	264
	Floating	0	6	5	17	14	17	13	10	82
	Land-terminating	1	3	2	3	0	0	0	0	9
	Total	567	275	223	230	112	83	71	29	

Appendix 5.2:

All glacier basins on the AP (n = 1590): Class, Form and Front classification summary table

Class	Form	Front							
		Uncert /Misc	Calving	Calving/ Piedmont	Calving/ Lobed	Ice-shelf nourish	Floating	Land-term.	Total
Uncertain/ Misc	Uncert/Misc	290	40	7	1	37	2	0	377
	Comp. basins	0	0	0	0	0	0	0	0
	Comp. basin	0	1	0	0	0	0	0	1
	Simple basin	0	6	0	0	0	0	1	7
	Total	290	47	7	1	37	2	1	385
Ice-field	Uncert/Misc	5	7	53	1	4	7	0	77
	Comp. basins	0	0	0	0	0	0	0	0
	Comp. basin	0	0	0	0	0	0	0	0
	Simple basin	0	0	0	0	0	0	0	0
	Total	5	7	53	1	4	7	0	77
Ice-cap	Uncert/Misc	54	60	16	39	59	4	2	234
	Comp. basins	0	0	0	0	0	0	0	0
	Comp. basin	0	0	0	0	0	0	0	0
	Simple basin	0	0	0	0	0	0	0	0
	Total	54	60	16	39	59	4	2	234
Outlet glacier	Uncert/Misc	0	34	1	0	17	8	0	60
	Comp. basins	0	16	0	0	16	15	0	47
	Comp. basin	0	48	1	0	16	22	0	87
	Simple basin	0	37	0	0	4	5	0	46
	Total	0	135	2	0	53	50	0	240
Mountain glacier	Uncert/Misc	3	82	0	0	24	7	1	117
	Comp. basins	0	1	0	0	1	0	0	2
	Comp. basin	0	39	0	0	18	4	1	62
	Simple basin	3	301	0	0	54	8	4	370
	Total	6	423	0	0	97	19	6	551
Small island	Uncert/Misc	89	0	0	0	14	0	0	103
	Comp. basins	0	0	0	0	0	0	0	0
	Comp. basin	0	0	0	0	0	0	0	0
	Simple basin	0	0	0	0	0	0	0	0
	Total	0	0	0	0	0	0	0	0
Total (Class)	Uncert/Misc	441	223	77	41	155	28	3	968
	Comp. basins	0	17	0	0	17	15	0	49
	Comp. basin	0	88	1	0	34	26	1	150
	Simple basin	3	344	0	0	58	13	5	423
Total (All)		444	672	78	41	264	82	9	1590

Appendix 5.3:

Number and area coverage of marine-terminating glacier basins (n = 892) on the AP, by glacier size class

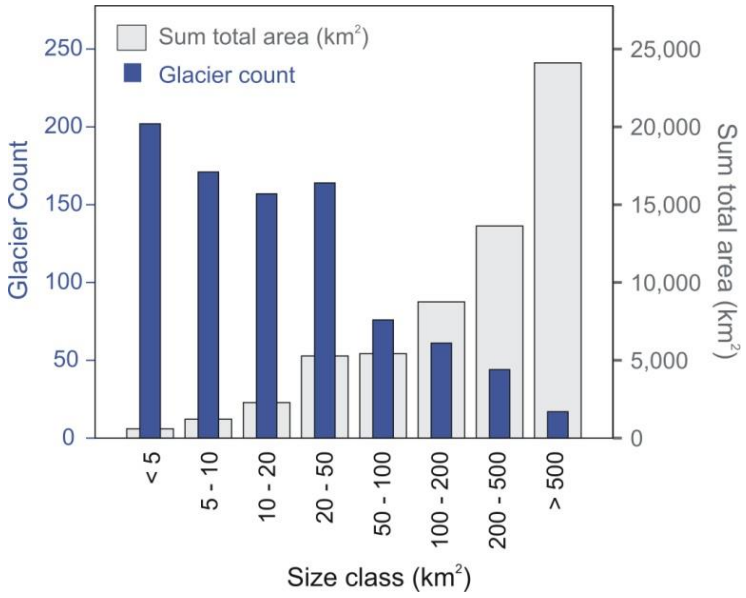

Appendix 5.4:

Marine-terminating glacier basins on the AP (n = 892): Class, Form and Front classification summary table

Marine-terminating

Class	Form	Front					
		Uncert /Misc	Calving	Calving/ Piedmont	Calving/ Lobed	Floating	Total
Uncertain/Misc	Uncert/Misc	1	34	5	1	2	45
	Comp. basins	0	0	0	0	0	0
	Comp. basin	0	1	0	0	0	1
	Simple basin	0	6	0	0	0	6
	Total	1	41	5	1	2	52
Ice-field	Uncert/Misc	3	7	50	1	7	68
	Comp. basins	0	0	0	0	0	0
	Comp. basin	0	0	0	0	0	0
	Simple basin	0	0	0	0	0	0
	Total	3	7	50	1	7	68
Ice-cap	Uncert/Misc	35	56	15	35	4	145
	Comp. basins	0	0	0	0	0	0
	Comp. basin	0	0	0	0	0	0
	Simple basin	0	0	0	0	0	0
	Total	35	56	15	35	4	145
Outlet glacier	Uncert/Misc	0	33	1	0	8	42
	Comp. basins	0	16	0	0	15	32
	Comp. basin	0	49	1	0	21	74
	Simple basin	0	37	0	0	5	42
	Total	0	135	2	0	49	190
Mountain glacier	Uncert/Misc	3	77	0	0	7	87
	Comp. basins	0	1	0	0	0	1
	Comp. basin	0	39	0	0	4	43
	Simple basin	3	294	0	0	8	305
	Total	6	411	0	0	19	436
Total (Class)	Uncert/Misc	42	207	71	37	28	387
	Comp. basins	0	17	0	0	15	33
	Comp. basin	0	89	1	0	25	118
	Simple basin	3	337	0	0	13	353
Total (All)	Total	45	650	72	37	81	892

Appendix 5.5:

Change-rate glacier counts within each latitudinal degree

	Latitudinal Degree (°S)							
	63 - 64	64 - 65	65 - 66	66 - 67	67 - 68	68 - 69	69 - 70	Total
1945 - 49	17	17	12	36	42	21	0	145
1950 - 54	29	28	12	36	36	0	0	141
1955 - 59	29	64	52	53	85	0	0	283
1960 - 64	0	60	50	28	86	0	0	224
1965 - 69	0	59	50	32	101	23	3	268
1970 - 74	12	107	2	47	92	26	11	297
1975 - 79	103	106	0	43	94	26	12	384
1980 - 84	103	109	0	43	94	26	12	387
1985 - 89	138	282	80	74	128	27	18	747
1990 - 94	145	282	80	54	102	24	18	705
1995 - 99	146	298	81	54	102	25	19	725
2000 - 04	147	311	87	55	109	26	19	754
2005 - 09	36	107	47	26	41	15	10	282
2010	32	105	46	25	40	13	10	271

Appendix 5.6:

Box plots showing all glacier change-rates. For each interval, the thick dark line in the box centre is the median value; the box represents 50% of the data; the whiskers are the limits of data not considered as outliers; the back circles are outliers and the coloured stars are extreme outliers. Plot **a.** is all glaciers in $km^2\ a^{-1}$, on a logarithmic scale, demonstrating the large dispersion of the data. Plot **b.** is a closer look at values close to the median. The peach coloured strip is the band where glaciers are considered to be stable: this is based on a test on the 'annual cycle' of glacier fronts in the region, and should be regarded as an estimate. Plot **c**. is the glacier change rate relative to the basin size, in $\%\ a^{-1}$.

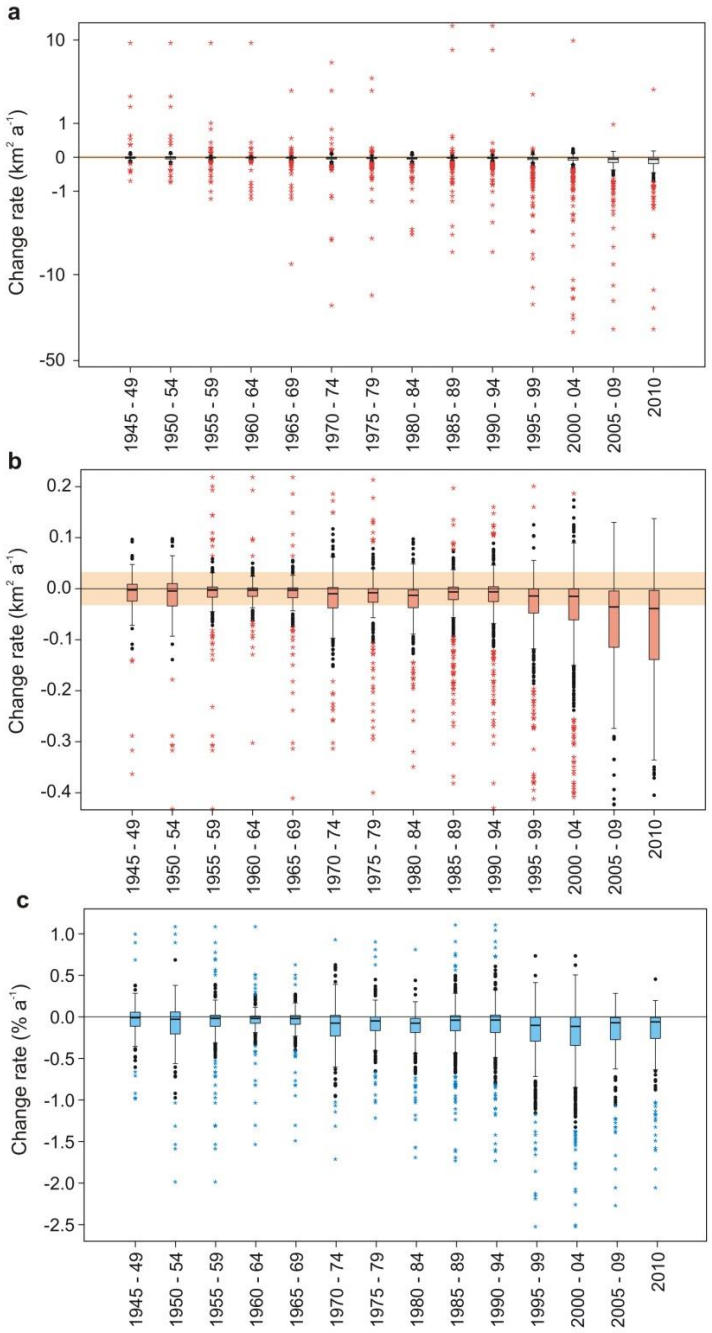

Appendix 5.7:

Wilcoxon signed rank tests on statistical significance of differences in area change rates (% a^{-1}) between epochs for each region. Numbers highlighted in red are significant at < 0.05 level. These results relate to the region definitions and trends shown in Figure 5.25.

Wilcoxon Signed Ranks Tests: Regions

NE	N	Mean	Std. Dev	Pair	Z	Sig. (2-tailed)
1945 - 49	17	-0.30	0.22	1950 - 54 - 1945 - 49	-1.342a	0.18
1950 - 54	29	-0.43	0.48	1955 - 59 - 1950 - 54	-1.342a	0.18
1955 - 59	29	-0.44	0.48			
1960 - 64	0	.	.			
1965 - 69	0	.	.			
1970 - 74	1	-0.13	.			
1975 - 79	67	-0.04	0.20	1980 - 84 - 1975 - 79	-1.782a	0.075
1980 - 84	68	-0.06	0.16	1985 - 89 - 1980 - 84	-2.949a	0.003
1985 - 89	88	-0.13	0.21	1990 - 94 - 1985 - 89	-3.779a	0
1990 - 94	98	-0.19	0.25	1995 - 99 - 1990 - 94	-3.265a	0.001
1995 - 99	99	-0.20	0.25	2000 - 04 - 1995 - 99	-.943b	0.346
2000 - 04	99	-0.20	0.26	2005 - 09 - 2000 - 04	-2.191b	0.028
2005 - 09	22	-0.10	0.13	2010 - 2005 - 09	-1.372b	0.17
2010	18	-0.07	0.19			

W	N	Mean	Std. Dev	Pair	Z	Sig. (2-tailed)
1945 - 49	20	0.21	1.24	1950 - 54 - 1945 - 49	.000a	1
1950 - 54	20	0.21	1.24	1955 - 59 - 1950 - 54	-2.223b	0.026
1955 - 59	101	-0.10	0.57	1960 - 64 - 1955 - 59	-2.223b	0.026
1960 - 64	92	-0.11	0.54	1965 - 69 - 1960 - 64	-.070b	0.944
1965 - 69	92	-0.11	0.54	1970 - 74 - 1965 - 69	-.279b	0.78
1970 - 74	90	-0.08	0.52	1975 - 79 - 1970 - 74	-.327b	0.744
1975 - 79	85	-0.23	0.98	1980 - 84 - 1975 - 79	-.606c	0.544
1980 - 84	85	-0.22	0.98	1985 - 89 - 1980 - 84	-4.116c	0
1985 - 89	319	-0.09	0.62	1990 - 94 - 1985 - 89	-2.688c	0.007
1990 - 94	319	-0.07	0.27	1995 - 99 - 1990 - 94	-5.079b	0
1995 - 99	320	-0.11	0.26	2000 - 04 - 1995 - 99	-5.007b	0
2000 - 04	324	-0.15	0.38	2005 - 09 - 2000 - 04	-1.310b	0.19
2005 - 09	103	-0.15	0.26	2010 - 2005 - 09	-1.211b	0.226
2010	100	-0.13	0.21			

E	N	Mean	Std. Dev	Pair	Z	Sig. (2-tailed)
1945 - 49	9	-0.04	0.10	1950 - 54 - 1945 - 49	-.365a	0.715
1950 - 54	20	-0.14	0.53	1955 - 59 - 1950 - 54	-.365a	0.715
1955 - 59	15	-0.19	0.62	1960 - 64 - 1955 - 59	.000b	1
1960 - 64	18	-0.16	0.55	1965 - 69 - 1960 - 64	.000b	1
1965 - 69	17	-0.15	0.21	1970 - 74 - 1965 - 69	.000b	1
1970 - 74	19	-0.16	0.21	1975 - 79 - 1970 - 74	-.764a	0.445
1975 - 79	21	-0.18	0.18	1980 - 84 - 1975 - 79	-.639a	0.523
1980 - 84	24	-0.20	0.23	1985 - 89 - 1980 - 84	-1.248c	0.212
1985 - 89	43	-0.48	1.11	1990 - 94 - 1985 - 89	-1.657a	0.097
1990 - 94	43	-0.51	1.12	1995 - 99 - 1990 - 94	-2.486a	0.013
1995 - 99	59	-0.78	0.94	2000 - 04 - 1995 - 99	-1.775c	0.076
2000 - 04	74	-0.79	0.99	2005 - 09 - 2000 - 04	-4.038c	0
2005 - 09	51	-0.75	1.75	2010 - 2005 - 09	-2.735c	0.006
2010	51	-0.66	1.76			

SW	N	Mean	Std. Dev	Pair	Z	Sig. (2-tailed)
1945 - 49	78	0.08	0.33	1950 - 54 - 1945 - 49	.000a	1
1950 - 54	72	0.08	0.34	1955 - 59 - 1950 - 54	-1.743b	0.081
1955 - 59	138	0.02	0.27	1960 - 64 - 1955 - 59	-1.236b	0.217
1960 - 64	114	-0.01	0.27	1965 - 69 - 1960 - 64	-.457b	0.647
1965 - 69	133	-0.04	0.25	1970 - 74 - 1965 - 69	-3.073b	0.002
1970 - 74	139	-0.18	0.56	1975 - 79 - 1970 - 74	-.886c	0.376
1975 - 79	137	-0.13	0.33	1980 - 84 - 1975 - 79	-3.688b	0
1980 - 84	137	-0.22	0.31	1985 - 89 - 1980 - 84	-7.141c	0
1985 - 89	202	-0.10	0.25	1990 - 94 - 1985 - 89	-3.683b	0
1990 - 94	156	-0.12	0.22	1995 - 99 - 1990 - 94	-9.430b	0
1995 - 99	156	-0.28	0.35	2000 - 04 - 1995 - 99	-2.654b	0.008
2000 - 04	164	-0.35	0.59	2005 - 09 - 2000 - 04	-.706b	0.48
2005 - 09	67	-0.15	0.25	2010 - 2005 - 09	-4.925b	0
2010	65	-0.18	0.28			

NW	N	Mean	Std. Dev	Pair	Z	Sig. (2-tailed)
1945 - 49	0	.	.	1950 - 54 - 1945 - 49		
1950 - 54	0	.	.	1955 - 59 - 1950 - 54		
1955 - 59	0	.	.	1960 - 64 - 1955 - 59		
1960 - 64	0	.	.	1965 - 69 - 1960 - 64		
1965 - 69	0	.	.	1970 - 74 - 1965 - 69		
1970 - 74	11	-0.01	0.20	1975 - 79 - 1970 - 74	.000a	1
1975 - 79	36	-0.01	0.12	1980 - 84 - 1975 - 79	-.535b	0.593
1980 - 84	35	0.00	0.12	1985 - 89 - 1980 - 84	-.273b	0.785
1985 - 89	50	0.02	0.14	1990 - 94 - 1985 - 89	-.134b	0.893
1990 - 94	47	0.02	0.13	1995 - 99 - 1990 - 94	-.511b	0.609
1995 - 99	47	0.02	0.11	2000 - 04 - 1995 - 99	-.408b	0.683
2000 - 04	48	0.03	0.11	2005 - 09 - 2000 - 04	-.094c	0.925
2005 - 09	14	0.00	0.02	2010 - 2005 - 09	-1.601b	0.109
2010	14	0.01	0.03			

SSW	N	Mean	Std. Dev	Pair	Z	Sig. (2-tailed)
1945 - 49	21	-0.06	0.24	1950 - 54 - 1945 - 49		
1950 - 54	0	.	.	1955 - 59 - 1950 - 54		
1955 - 59	0	.	.	1960 - 64 - 1955 - 59		
1960 - 64	0	.	.	1965 - 69 - 1960 - 64		
1965 - 69	26	-0.12	0.27	1970 - 74 - 1965 - 69	-1.604a	0.109
1970 - 74	37	-0.15	0.25	1975 - 79 - 1970 - 74	-2.171a	0.03
1975 - 79	38	-0.05	0.26	1980 - 84 - 1975 - 79	-.672b	0.502
1980 - 84	38	-0.13	0.23	1985 - 89 - 1980 - 84	-.730b	0.465
1985 - 89	45	-0.11	0.65	1990 - 94 - 1985 - 89	-2.484a	0.013
1990 - 94	42	0.11	0.50	1995 - 99 - 1990 - 94	-4.340b	0
1995 - 99	44	-0.32	0.49	2000 - 04 - 1995 - 99	-3.024b	0.002
2000 - 04	45	-0.67	1.16	2005 - 09 - 2000 - 04	-.848a	0.397
2005 - 09	25	-0.28	0.42	2010 - 2005 - 09	-3.910b	0
2010	23	-0.36	0.49			

Appendix 5.8:

Glacier counts for mean rates of change values shown in Figure 5.26.

	Basin area	
	> 15 km^2	< 15 km^2
1945 - 49	75	70
1950 - 54	70	71
1955 - 59	136	147
1960 - 64	111	113
1965 - 69	142	126
1970 - 74	155	142
1975 - 79	224	160
1980 - 84	226	161
1985 - 89	359	388
1990 - 94	348	357
1995 - 99	366	359
2000 - 04	388	366
2005 - 09	238	44
2010	232	39

	Class	
	Outlet	Mountain
1945 - 49	38	69
1950 - 54	34	59
1955 - 59	58	150
1960 - 64	50	126
1965 - 69	64	145
1970 - 74	74	157
1975 - 79	102	165
1980 - 84	103	166
1985 - 89	160	370
1990 - 94	157	333
1995 - 99	167	335
2000 - 04	178	351
2005 - 09	149	103
2010	148	97

	Front	
	Grounded	Floating
1945 - 49	116	8
1950 - 54	104	10
1955 - 59	220	22
1960 - 64	177	22
1965 - 69	214	23
1970 - 74	246	16
1975 - 79	299	15
1980 - 84	302	15
1985 - 89	576	49
1990 - 94	533	49
1995 - 99	537	60
2000 - 04	555	71
2005 - 09	201	63
2010	192	63

	Geometry	
	Convergent	Divergent
1945 - 49	86	59
1950 - 54	78	63
1955 - 59	174	109
1960 - 64	138	86
1965 - 69	163	104
1970 - 74	174	122
1975 - 79	224	158
1980 - 84	226	159
1985 - 89	435	306
1990 - 94	416	282
1995 - 99	427	291
2000 - 04	452	295
2005 - 09	224	52
2010	217	48

	Max Flow Velocity	
	< 25 m/yr	> 25 m/yr
1945 - 49	38	53
1950 - 54	29	36
1955 - 59	73	79
1960 - 64	58	63
1965 - 69	71	85
1970 - 74	61	95
1975 - 79	77	128
1980 - 84	78	128
1985 - 89	176	213
1990 - 94	158	205
1995 - 99	166	217
2000 - 04	178	228
2005 - 09	60	150
2010	57	147

	Mean Slope	
	< 20 %	> 20 %
1945 - 49	96	49
1950 - 54	97	44
1955 - 59	156	127
1960 - 64	114	110
1965 - 69	145	123
1970 - 74	158	139
1975 - 79	236	147
1980 - 84	239	147
1985 - 89	405	338
1990 - 94	395	305
1995 - 99	414	306
2000 - 04	434	315
2005 - 09	210	72
2010	204	67

	Surface Length	
	< 5 km	> 5 km
1945 - 49	70	75
1950 - 54	73	68
1955 - 59	144	139
1960 - 64	108	116
1965 - 69	121	147
1970 - 74	144	153
1975 - 79	169	214
1980 - 84	170	216
1985 - 89	386	357
1990 - 94	350	350
1995 - 99	352	368
2000 - 04	357	392
2005 - 09	34	248
2010	29	242

	Mean Aspect	
	E to SE	SW to W
1945 - 49	23	38
1950 - 54	28	37
1955 - 59	56	74
1960 - 64	45	58
1965 - 69	51	62
1970 - 74	59	77
1975 - 79	88	96
1980 - 84	90	96
1985 - 89	139	200
1990 - 94	134	187
1995 - 99	143	187
2000 - 04	146	194
2005 - 09	47	70
2010	43	67